University of Strathclyde

Department of Electronic and Electrical Engineering

INVESTIGATION OF THE CUMULATIVE IMPACT OF ALKALINE ELECTROLYSERS ON ELECTRICAL POWER SYSTEMS

by

MAHDI KIAEE

A thesis submitted in partial fulfilment of the requirements for the

degree of Doctor of Philosophy

February 2016

COPYRIGHT STATEMENT

Signed: Mahdi Kiaee 

Date: 02/02/2016

ACKNOWLEDGEMENTS:

I would like to thank my academic supervisors Professor David Infield, Professor Andrew Cruden, and Professor Graham Ault for their help, guidance, encouragement, support and patience during my PhD project.

This work, as part of the SUPERGEN project on 'Delivery of Sustainable Hydrogen (DoSH2, Grant Reference: EP/G01244X/1)', was supported by Engineering and Physical Sciences Research Council (EPSRC) in the UK.

I would also like to thank the management and the staff of NEL Hydrogen Company (especially: Dr Petr Chladek, Dr Hans Jörg Fell, Mr Iain Alexander Russell and Mr Oddmund Wallevik) for their kind help and support for the collection of operational data from their electrolyser at the Porsgrunn Research Park in Norway and also for helping me to have a better understanding of the operation and characteristics of their commercial pressurised and atmospheric alkaline electrolysers.

I would also like to thank my research colleagues, Dr Tamunosaki G. Douglas and Dr Daniel Chade who helped me to have a better understanding of the design and the electrochemistry of alkaline electrolysers.

I also thank Dr Yuchao Ma for helping me to become familiar with the models of electric power systems. I would also like to thank Dr Amitava Roy for his constructive comments about my work, and also Dr Sikai Huang for providing me with some information about vehicle fuel consumptions. I would also like to thank Dr Rebecca Carter, Dr Ammar Zaher, Dr Maria Carla Di Vincenzo who helped me in learning how to work with LabVIEW and data acquisition systems. I would also like to thank Dr Lei Wu for providing me with the estimation of GB wind power generation capacity in 2020. I convey my thanks to Ms Jennifer MacKenzie, Ms Sadie Smart, Ms Carol Sheridan, and Ms Linzi Wylie for all the secretarial support during the project. Finally, I must admit that reaching this stage in my life would not have been possible without the invaluable support from my family and friends.

CONTENTS

LIST OF FIGURES

LIST OF TABLES

NOMENCLATURE

A	Ampere
AC	Alternating Current
ADC	Analogue to Digital Converter
AED	The aggregate electrolysis demand (GW)
$ANED$	The aggregate nominal electrolysis demand (GW)
ANM	Active Network Management
ANonED	The aggregate non-electrolysis demand (GW)
$ASDL$	Aggregate Station Demand Limit (MW)
B	The set of bus numbers within the network
Bar(g)	Gauge pressure, i.e., pressure in bars above ambient or atmospheric pressure
BESS	Battery Energy Storage System
BEV	Battery Electric Vehicle
BOP	Balance of Plant
C	Coulomb
C_{DP}	The conversion factor used to change the amount of energy in a litre of diesel into the amount of energy in a litre of petrol
C_{Gal}	The coefficient used to change a US gallon to litre
C_i	Cost function coefficients

CAES	Compressed Air Energy Storage
$Capital$	The capital cost of an electrolyser in £/MW
CCS	Carbon Capture and Storage
CHP	Combined Heat and Power
$Cost_{Storage}$	The cost of hydrogen storage in billion pounds
D	Load damping constant
DAQ	Data acquisition
DC	Direct Current
DDC	Dynamic Demand Control
D_{El}^{t}	The aggregate electrolyser demand excluding the grid and compressor losses at each time interval (GW)
D_{ElComp}^{t}	The aggregate demand from electrolysers and compressors including the losses they add on the system (GW)
D_{EVs}^{t}	The aggregate EV demand including all of the additional losses that they cause on the system(GW)
D_{i}^{t}	The amount of demand (excluding the demand of electrolysers) in MW on bus 'i' of the last feeder (from bus 53 to bus 77) at the current time step t
DH_2	The daily amount of hydrogen in kg needed for all the HFCVs vehicles if they replace all of the vehicles on roads in the UK
$D(s)$	Transfer function of the frequency detection system
°C	Degree Centigrade

D_N^t	The aggregate electricity demand on the UK power system excluding the demand from EVs and hydrogen stations (GW)
$\Delta E_{Loss}\%$	The percentage reduction in the total energy loss on the distribution network during the simulation
$\Delta f\%$	The percentage of the frequency change in the system
$\Delta\omega_r$	The change in the rotor speed in per unit
ΔP_e	The total load change in the system in per unit
$\Delta P_G\%$	The percentage of the power output change of the generator
ΔP_L	The change in load as a result of the change in non-frequency sensitive load in per unit
ΔP_m	The total mechanical power change in the system in per unit
DER	Distributed Energy Resources
DG	Distributed Generator
DISCOs	Distribution companies
DNO	Distribution Network Operator
DSM	Demand Side Management
E_{El}^{kg}	The energy needed to produce a kg of hydrogen with the electrolyser (kWh/kg)
E_{HHV}	The Higher Heating Value (HHV) of hydrogen. The energy needed to produce 1 Nm^3 of hydrogen when the efficiency of the electrolysis is 100% (3.5 kWh/Nm^3).

$E_{\kappa EVs}^{Total}$	The total energy needed per year in TWh to supply all EVs if only $(100-\kappa\%)$ of the vehicles on road get replaced by them
$E_{\kappa FCVs}^{Total}$	The total energy needed per year in TWh for HFCVs if only $\kappa\%$ of vehicles on road become replaced by HFCVs
E_{Loss}	Total energy loss during the simulation (MWh)
E_{Loss}^{With}	The total energy loss on the distribution network in the system with electrolysers (MWh)
$E_{Loss}^{Without}$	The total energy loss on the distribution network in the system without electrolysers (MWh)
E_{Solar}	The total solar energy delivered to the grid during the simulated year (TWh)
E_{St}	The total energy delivered to all of the stations during the simulation (MWh)
E_{St}^{Day}	The energy needed to be supplied to each station for hydrogen production and compression every day (MWh)
E_{Wind}	The total wind energy delivered to the grid during the simulated year (TWh)
$ECOM$	Extra capital, operational and maintenance cost (£/h)
EHV	Extra High Voltage
ELD_{ij}^{t}	The demand of 'i'th active electrolyser located at 'j'th active filling station (MW)
$Excess_{H_2}\%$	The percentage of the excess hydrogen produced during a year
f	The power system frequency (Hz)

f_{NL}	The steady state frequency of the generating unit at no load (Hz)
f_{FL}	The steady state frequency of the generating unit at full load (Hz)
f_0	The nominal or rated frequency of the power system (Hz)
F	The Faraday constant (96485.30 C/mol)
F_{HP}	Fraction of total turbine power generated by high pressure stage
F_{LP}	Fraction of total turbine power generated by low pressure section
FCDM	Frequency Control Using Demand Management
FITs	Feed-In-Tariffs
FES	Flywheel Energy Storage
FFPP	Fossil Fuel Power Plant
GA	Genetic Algorithm
GB	Great Britain
GB SQSS	The Great Britain Security and Quality of Supply Standard
GW	Gigawatt power
GWh	Gigawatt hour energy
$H2P_{ij}^{t}$	Hydrogen produced by 'i'th active electrolyser located at 'j'th active hydrogen filling station (kg)
HARI	Hydrogen and Renewable Integration
HFCV	Hydrogen Fuel Cell Vehicle

HV	High Voltage
Hz	Hertz
i	The DC current of the cells (A)
$\left\|I_{ij}^{t}\right\|$	The magnitude of current (A) flowing between bus 'i' and 'j' of the power system in the time interval of 't'
$\left\|I_{ij}^{Lim}\right\|$	The limit for the current magnitude (A) flowing between bus 'i' and 'j' of the power system
ICE	Internal Combustion Engine
IESO	Independent Electricity System Operator
I_j	The amplitude of the jth ($j \neq 1$) harmonic of the signal. I_1 is the amplitude of the fundamental.
I_{min}	The minimum current acceptable by the cell stack (A)
INAED	Initial Nominal Aggregate Electrolysis Demand (GW)
ISO	Independent System Operators
kg	Kilogram
K_I	Integral control gain
KOH	Potassium Hydroxide used as the electrolyte in the electrolyser and more commonly known as lye
kW	Kilowatt power
kWh	Kilowatt hour energy
L_{Diesel}	The amount of daily diesel consumption for the vehicles on road in the UK in litres

L_{Petrol}	The amount of daily petrol consumption for the vehicles on road in the UK in litres
LA	Lead Acid
LEL	Lower Explosion Limit
LFC	Load Frequency Control
LFDD	Low Frequency Demand Disconnection
LHV	Lower Heating Value of hydrogen (33 kWh/Kg)
$Life$	The lifetime of an electrolyser in years
Li-on	Lithium ion
LNG	Liquefied Natural Gas
M	Inertia constant (s)
M_{H_2}	The mass of hydrogen gas produced (kg)
mA/cm^2	Milli-ampere per square centimetre
mm WG	Millimetres, water gauge
mol	Mole
MW	Megawatt power
MWh	Megawatt hour energy
n	The number of electrons (2) transferred per hydrogen molecule produced during the electrolysis
N_C	The number of cells connected in series in the cell stack

N_{El}^{EST}	The number of electrolysers at each station
N_{SS}	The total number of solar sites in the UK 2050 scenarios
$NAEL_j^t$	The number of active electrolysers at active filling station 'j' at each time interval 't'
NaS	Sodium Sulphur
NAS^t	The number of active stations at the current time interval of 't'
NB	The number of branches on the power system
NDP	The number of data points during the simulation (e.g. if the simulation is carried out for a duration of 24 hours with time interval of 1 hour, then NDP=24)
NGET	National Grid Electricity Transmission
NiCd	Nickel Cadmium
NiMH	Nickel Metal Hybrid
NiO	Nickel oxide
Nm^3	Normal Cubic Metre
Nm^3/h	Normal Cubic Metre per hour
NREL	National Renewable Energy Laboratory
NS	The total number of filling stations
$\eta_{Bch}\%$	The efficiency of the batteries during charge in an EV (%)
$\eta_{Bdis}\%$	The efficiency of batteries during discharge in an EV (%)
$\eta_{Comp}\%$	The efficiency of the hydrogen compressors (%)

$\eta_{Diesel}\%$	The average efficiency of diesel cars (%)
$\eta_{El}\%$	The efficiency of hydrogen production by electrolysers (%)
$\eta_{EV}^{System}\%$	The efficiency of the system with EVs from after the grid electricity generation point to the wheels (%)
$\eta_{f}\%$	The Faraday efficiency (%)
$\eta_{FC}\%$	The efficiency of fuel cells (%)
$\eta_{FCV}\%$	The efficiency of hydrogen fuel cell vehicles (%)
$\eta_{FCV}^{System}\%$	The efficiency of the system with hydrogen fuel cell vehicles from after the grid electricity generation point to the wheels (%)
$\eta_{ij}^{t}\%$	The efficiency of the 'i'th active electrolyser in the 'j'th active station in percentage (%)
$\eta_{IM}\%$	The efficiency of the inverter and electric motor together in an EV or a FCV (%)
$\eta_{gb}\%$	The efficiency of the gear box in an EV or FCV (%)
$\eta_{grid}\%$	The average efficiency of the electrical power system to transfer electricity from the point of generation to the point of consumption (%)
$\eta_{Petrol}\%$	The average efficiency of petrol cars (%)
$\eta_{Rec}\%$	The efficiency of the rectifier to charge the batteries of an EV (%)
$\eta_{V.E.Stack}\%$	The voltage efficiency of the cell stack (%)
NW	The total number of wind farms placed within the network

OLTC	On-load tap changing
OM	The annual operational and maintenance cost of an electrolyser in £/MW/year
OPF	Optimal Power Flow
OSZ_i	The optimal size of station 'i' in MW which is determined by the maximum demand of each station during a year simulation
P_{BOP}	The electrolyser Balance of Plant power requirement (W)
P_{EL}	The electric demand of each electrolyser (W)
PEM	Proton Exchange Membrane
PLC	Programmable Logic Controller
P_{FCVs}^{Total}	The total power needed to supply all of the stations (GW)
P_{FPP}^{t}	The total aggregate power generation from conventional FFPPs (GW)
$P_{Loss_i}^{t}$	The amount of power loss (MW) on branch 'i' of the power system at the time interval 't'
$P_{Min.El}$	The minimum operational load of the electrolyser plant to work properly in normal hydrogen production mode (W)
$P_{Min.Stack}$	The minimum operational load of the electrolyser cell stack (W)
$P_{N.El}$	The nominal demand of the electrolyser plant (W)
$P_{Nuclear}^{t}$	The total aggregate nuclear power generation (GW)

P_{Solar}^{t}	The total aggregate solar power generation (GW) within the system at time interval 't'
P_{Wind}^{t}	The total aggregate wind power generation (GW) within the system at time interval 't'
PHS	Pumped Hydro Storage
PS_{i}^{t}	The power output (kW) from solar site 'i' at time interval 't'
PSB	Polysulphide Bromide
pu	Per unit
PV	Photo-Voltaic
R	Speed droop characteristic
R_{EVFCVs}	The ratio showing how much the system with EVs is more efficient than the system with HFCVs
RE	Renewable Energy
RMS	Root Mean Square
ROCs	Renewable Obligation Certificates
s	Second as the unit of time. It also represents the complex number frequency in transfer functions.
S_{FFPP}	The aggregate size of FFPPs needed to balance the system (GW)
S_{ij}^{t}	The complex power flow (MVA) between bus 'i' and 'j' of the network in the current time interval of 't'

$\left\|S_{ij}^{t}\right\|$	The apparent power (MVA) between bus 'i' and 'j' of the power system in the current time interval of 't'
$\left\|S_{ij}^{Lim}\right\|$	The apparent power limit (MVA) between bus 'i' and 'j' of the power system
SC	Super-Capacitor
SD_i^t	The demand (MW) from station 'i' during the current time interval of 't'
SHETL	Scottish Hydro Electric Transmission Limited
SMR	Steam Methane Reformation
SOEC	Solid Oxide Electrolysis Cells
SPT	Scottish Power Transmission
$S_{A.El}$	The aggregate size of electrolysers (GW)
S_S	The total aggregate installed solar power capacity (GW) in each UK 2050 scenario
S_{St}	The initial size of each station (MW)
$S_{Storage}$	The total size of hydrogen storage needed in the UK in million kg
St	Hydrogen Station
STOR	Short Term Operating Reserve
$Surplus(t)$	The surplus wind generation (MW)
S_W^i	Size of i^{th} wind farm (MW)
SMES	Superconducting Magnetic Energy Storage

t	The current time interval number in the simulations
t	Metric tonne
T	The simulation time interval in hours.
T_{CH}	Time constant of main inlet volumes and steam chest (s)
T_d	Time constant of the frequency detection system (s)
T_G	Governor time constant (s)
$TH2P$	The total hydrogen produced in metric tonne (**t**)
THD	Total Harmonic Distortion (%)
TIC_i	The total installed solar capacity (kW peak) at solar site 'i'
T_{RH}	Time constant of re-heater (s)
$TLB_{Prob}\%$	The probability of thermal limit violations (%)
TLB_t	The function indicating whether there has been any thermal limit violation within the grid at time interval 't'
TSO	Transmission System Operator
UKGDS	United Kingdom Generic Distribution System
$UF_{El}\%$	The utilisation factor of electrolysers (%)
$UF_{FFPP}\%$	The utilisation factor of aggregate FFPP capacity (%)
UG	Underground
UPS	Uninterruptible Power Supply
V	Volt

$\lvert V_i^t \rvert$	The magnitude of voltage on bus 'i' of the power system in pu in the current time interval of 't'
$\lvert V_i^{Min} \rvert$	The minimum limit for the voltage magnitude on bus 'i' of the power system (pu)
$\lvert V_i^{Max} \rvert$	The maximum limit for the voltage magnitude on bus 'i' of the power system (pu)
V_{min}	The voltage (V) of the stack when the cells have minimum current
V_{Stack}	The DC voltage of the cell stack (V)
$VB_{Prob}\%$	The probability of voltage constraint violation (%)
V_{Thn}	Thermo-neutral voltage (V)
VB_t	The function that indicates whether there has been any voltage violation within the grid at time interval 't'
VRB	Vanadium Redox Battery
W	Watt (unit of power)
$\bar{W}$	The average wind power during the simulation (GW)
W_i^t	The output of wind farm 'i' in MW at the current time step t
W_N	The wind power capacity within the system (GW)
$WPen$	The wind power penetration
YC_{H_2}	The amount of hydrogen consumption (kg) by HFCVs during the simulated year

YP_{H_2}	The amount of hydrogen produced (kg) by electrolysers during the simulated year
ZnBr	Zinc Bromine

ABSTRACT

Hydrogen could be the best candidate fuel for our future, especially in the transportation sector. It could be generated using water electrolysers running with power from carbon-free, renewable resources, since this is zero emission at the point of use, and so can help transition from the energy infrastructure available today into an energy world with a growing renewable electricity supply.

This work models a highly distributed electrolyser system e.g. an urban hydrogen filling station network, and explores the Demand Side Management (DSM) potential of these electrolysers to improve the performance of the power system operating under the impact of intermittent renewable power generation.

A comprehensive literature review has been carried out on the hydrogen economy, electrolysers and the potential role of storage devices in power systems. Three main areas related to alkaline electrolysers working within power systems were identified for further exploration.

- Potential role of electrolysers in the existing distribution networks to increase the integrated wind power capacity
- Potential role of electrolysers to stabilise the frequency of the power system
- Potential role of electrolysers to absorb any surplus, carbon free, generation within the UK electricity network

The first item of archival value within this work is the identification, presentation and discussion of electrolyser characteristics which are relevant to the introduction of an acceptable control strategy to integrate such electrolyser loads within the power system and thus provide improved performance of the network when exposed to the highly time variable energy supply from renewable sources. Two types of electrolyser made by NEL Hydrogen are detailed: atmospheric and pressurised. Their characteristics are reported in this thesis using the results from experiments designed by the author. In addition, an experiment has also been carried out on a PEM electrolyser available at Strathclyde University to compare its results with the characteristics of the commercial alkaline units.

Second, a novel algorithm for sizing, placing and control of electrolysis based hydrogen filling stations operating within radial distribution networks has been proposed and its performance is assessed using a United Kingdom Generic Distribution System (*UKGDS)* case study. The controller objective is to dispatch alkaline electrolysers appropriately to increase the amount of integrated wind power capacity and reduce the grid losses within the network while satisfying the network constraints and respecting the electrolyser characteristics.

In addition, a *MATLAB Simulink* model has been developed to investigate the impact of alkaline electrolysers as dynamically controlled loads for the stabilisation of system frequency in the case of a sudden loss of generation and also when the power system has high penetrations of wind power. The electrolysers are controlled according to a droop control strategy. A novel approach to determine the aggregate nominal electrolysis demand for frequency stability purposes has also been proposed in this work, and the financial viability of the proposed strategy to control electrolysers has been assessed.

Finally, several scenarios have been modelled to investigate the role of electrolysers to absorb surplus power and produce hydrogen for the fuel cell vehicles in the UK in the year 2050. Different wind, solar and nuclear power generation capacities have been considered. On the demand side, different penetration levels of electric vehicles and hydrogen fuel cell cars have been modelled. The results are discussed and analysed.

Keywords: Alkaline electrolysers, Renewable power, Active Network Management, Distribution network, Power system stability, Hydrogen economy, Power system losses, Demand side management, Load Frequency Control, Energy storage.

1 INTRODUCTION AND BACKGROUND

1.1 Hydrogen as an energy vector

The amount of fossil fuels available on earth is finite, and therefore, it is very likely that they will become more expensive in the future [1]. Due to the problem of pollution from fossil fuels and also an increase in oil prices, there has been an effort to diversify our energy supply, especially in the transportation sector, and to use cleaner fuels [2]. Alternative fuels such as ethanol, biodiesel, gasoline or methane are proposed for future transportation use, but those fuels are not available everywhere, and most of them need a different engine technology to operate efficiently. In addition, many of these proposed fuels still pollute the environment when used in vehicles. However, hydrogen can be a universal fuel because it can be produced from all of these feed stocks as well as many others [2], and it is the most abundant element in the world [3], so it could be utilised as a suitable storage and transmission vector for energy, and there is a strong case [4, 5] that hydrogen could become the major energy carrier in the near future, especially for transport [6, 7]. The result of this change could increase energy and economic security and reduce environmental impacts, such as CO_2 emissions. However, it should be noted that hydrogen is not available in pure form in nature, and it needs to be extracted from other composites to be used as a carbon free fuel.

Hydrogen can be produced from a wide variety of feedstocks with a wide variety of processes, so every region in the world would be able to produce most of their own hydrogen requirement and satisfy their energy needs. Therefore, another advantage of developing a hydrogen economy is that by producing and using hydrogen in a country, money and jobs will be kept from being exported [2].

Each year, about 50 million tons of hydrogen is used globally [4], and most of this hydrogen is used as a chemical to make fertilizer and to purify gasoline, rather than as a fuel. Hydrogen has applications in different industries such as food, chemical, steel, electronic, glass, power, polysilicon, renewable energy and transport industries. Currently most of the hydrogen produced today is made from natural gas [4]. Even if

all of the hydrogen produced today was utilised to satisfy energy needs, it could only provide 2% of the total demand, so the current hydrogen production is not able to fulfil world energy demand [8]. It is possible to obtain hydrogen using energy from renewable or nuclear generators [9], however, there are still some problems with the cost, safety and waste products of nuclear power stations [10].

Electrolysers supplied with electric power from renewable energy sources could be utilised to provide carbon-free hydrogen for future hydrogen filling stations supplying Hydrogen Fuel Cell Vehicles (HFCVs), or Internal Combustion Engines (ICEs) modified to burn hydrogen. The reverse reaction to water electrolysis takes place in hydrogen fuel cells, where hydrogen could also be used in fuel cells to produce electricity and give it back to the power system. This introduces the possible use of hydrogen as a form of electricity storage, where it is stored between electrolysis and fuel cell plants, for example.

Power generating combustion engines can be altered to work with hydrogen without significant issues [11]. Hydrogen engines are easily available in the market today for both stationary and transport applications. They are cheaper and more reliable than fuel cells, but they have lower efficiencies [11]. Fuel cells can achieve efficiencies of up to 60%, but hydrogen internal combustion engines have an efficiency of around 20%. However, if hydrogen ICEs are operated frequently in part load condition, then their average efficiency could be reduced to 17% [12].

Fuel Cell Vehicles (FCVs), which work with hydrogen gas rather than gasoline, could significantly reduce harmful emissions from the transportation sector. Hydrogen gas is fed into the fuel cell and converted into electricity and used to power an electric drive system [4], so a fuel cell has a higher efficiency than thermal engines, which have limited efficiency due to Carnot-cycle limitations. However, in practice, electrical resistances and kinetic over-voltages at the electrodes reduce the efficiency of a fuel cell significantly [11].

Some of the advantages of the development of hydrogen as a fuel for vehicles are listed below:

- The efficiency of fuel cells vehicles is about two or three times greater than the efficiency of conventional vehicles.
- Fuel cell vehicles could help in reduction of air pollution, particularly in urban areas, as they do not produce any carbon dioxide at the point of use, and they just produce water vapour.
- With production of hydrogen from many energy resources, such as natural gas, nuclear or coal, renewable electricity, waste, biomass or even directly from sunlight, the supply for our future transport energy could be secured.
- Fuel cell vehicles have very quiet propulsion, so the noise in urban areas would significantly reduce if we use them instead of conventional internal combustion engine vehicles.
- It could help us to become independent of oil and gas resources for transport use [4].

Figure 1.1 illustrates the difference between the useful specific energy (energy per unit of mass) of current deep discharge lead-acid (Pb-A) batteries, nickel metal hydride (NiMH), advanced lithium-ion (Li-ion) batteries and the US ABC (Advanced Battery Consortium) goal with the specific energy of a PEM fuel cell system which contains compressed hydrogen storage tanks with two pressures of 35 MPa (350 bar) and 70 MPa (700 bar) with fibre-wrapped composite tanks [13]. Obviously, the systems operating with hydrogen have much higher energy density in comparison to the battery systems.

Economic, social and policy issues will impact the utilisation of electrified vehicles for future transportation [14]. A successful transition to a hydrogen economy needs a significant production and distribution fuelling infrastructure and a proper strategy for utilisation of available renewable power [4]. There are many hydrogen filling stations operating in the world, and some of these use local electrolysers to produce the hydrogen on site [15].

There is also the possibility of selling the oxygen gas produced in the electrolysis process. This could increase the financial return benefits from system operation, as the oxygen could be used in a variety of industries such as power plants, steel industry,

welding industries, chemical industry, water treatment, medical applications, combustion efficiency enhancement and metal processing.

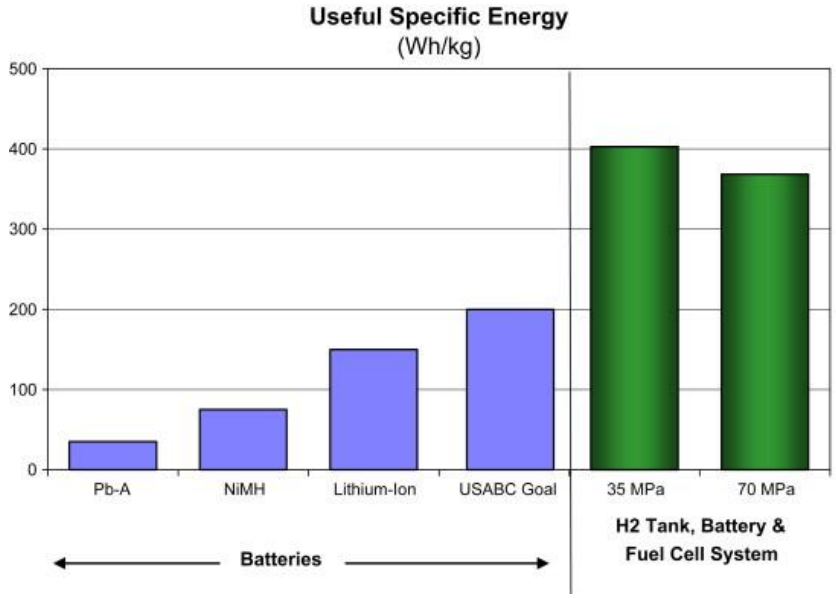

Figure 1.1 Comparison between the useful specific energy of hydrogen and fuel cell systems and various battery systems [13]

Low cost wind power can be produced in areas with good annual wind speeds, aided by the price of commercial wind turbines being significantly reduced during the past decade [16]. The global capacity to generate wind power is continuously increasing, and the main issue arising from this increase is that the power systems might not be able to absorb the renewable power generated at all times due to lack of demand or network constraints. Large integration of wind power into the electricity market has been hampered due to the highly variable characteristic of wind power. There might be occasions when the operators must curtail some of the generated wind power to avoid any imbalance in the electric power system. However, at such times electrolysers could be utilised to absorb the 'excess' electricity, which probably has a cheaper price. It is possible to optimise the existing power system capacity by utilising some electrolysis plants close to wind farms, and running electrolysers to use up some of the variable renewable power from wind farms. This means that, in the future, hydrogen production and storage could help to increase the penetration of wind power in the grid. This hydrogen could also be used to inject electricity back into the grid during

the time that there is low wind power generation or when there is a peak in demand using fuel cells connected to the power system. It is also possible to sell hydrogen in the market. In that case, the market price of hydrogen and electricity will determine the time to run the electrolyser. Therefore, water electrolysis by wind power has a good chance to become the best economical solution for large scale hydrogen production in the future [8].

Renewable systems based on hydrogen as an energy carrier will be especially useful in areas with access to abundant renewable energy resources that suffer from problems of producing enough electricity from fossil fuelled power generators or with insufficient grid infrastructure. There are many people around the world who live in islanded areas without any connection to the main electrical grid. Normally, fuel prices are also high in these isolated communities, hence if there is enough capacity to produce renewable energy in those isolated islands, then hydrogen production and storage systems could help in providing uninterruptible power for such communities provided that the hydrogen technology becomes cost-effective. The stored hydrogen can be used to generate power in a fuel cell or a hydrogen combustion engine when the power output from the renewable sources in the system is not sufficient to satisfy the demand. It is also possible to use the hydrogen in vehicles as a fuel and supply electricity to isolated loads in stand-alone systems simultaneously.

In isolated power systems, hydrogen storage is also useful in cases where there is a weak electrical connection point between the hydrogen system and the main grid, so the system is not able to export all of the renewable power available, e.g. during windy times. When the wind power available is higher than the demand and the export capacity of the grid connection point, the excess power could be converted into hydrogen and stored. In Norway, for example, the best windy locations are often found in sparsely populated coastline areas where the grid normally has long distribution feeders with limited capacity, and the electrolyser can use the excess wind power. In such systems, the designers can achieve much better overall system efficiency by optimising the hydrogen production and consumption and also the import and export rate of electricity by considering the electricity market prices and the cost of grid losses [11].

In addition, in areas with no electrical infrastructure and no electricity consumption, or in areas where grid connection of wind turbines is not considered to be economically or technically viable, hydrogen could be produced from wind power and consumed by fuel cell vehicles [11].

Electrolysers, fuel cells and storage tanks normally have a modular configuration, and this flexibility in the sizing of hydrogen systems is an advantage in comparison to other energy storage systems. Hydrogen electricity storage systems have a round trip efficiency of much less than 50% [11]. Low round trip efficiency, in this particular application, and a high cost of hydrogen systems are some of the reasons that have hampered their commercialisation so far [11].

1.2 Clean future vehicles

About 22% of the UK carbon dioxide emission is due to the emissions from the road transportation sector [17]. There are a number of primary alternatives, such as battery electric vehicles or fuel cell vehicles, available for our clean future transport, which can replace the conventional petrol or diesel ICE vehicles. Hydrogen is more likely to enter into the transport sector rather than the electricity sector in the near future.

Battery electric cars do not emit greenhouse gases at the point of use, but they have a number of problems which are mentioned below:

- Their driving range is normally lower than petrol or diesel ICE vehicles.
- It takes a significant time to recharge them.
- They have higher weight than typical petrol or diesel ICE vehicles.
- Their price is more than that of normal petrol or diesel ICE vehicles [10].

Thomas [13] has assessed the primary transportation alternatives to find which one is the best for future transport. His work compares the benefits of the replacement of conventional gasoline cars with other options such as hybrid electric vehicles, or all-electric vehicles powered by batteries or fuel cells. It concludes that to achieve goals of 80% reduction in greenhouse gases (compared to 1990 levels) in the light duty

transportation sector, and to become mostly independent of imported oil in transportation sector, most of the light duty vehicle fleet must be converted to all-electric vehicles, which would be powered by either batteries or fuel cells. It also shows that, for vehicles with ranges of greater than 160 km, fuel cell vehicles are better than battery powered vehicles in terms of mass, volume, cost, initial greenhouse gas reductions, refuelling time, life cycle costs and well-to-wheels energy efficiency using natural gas or biomass as the source for the hydrogen production [13].

Here, a comparison is made between fuel cell electric vehicles and advanced lithium ion battery electric vehicles.

- A fuel cell weighs less than batteries in a battery electric vehicle with the same travel range.
- A fuel cell takes up less space on the vehicle.
- A fuel cell costs less than batteries, and this results in a lower cost of the vehicle and lower life-cycle costs [13].
- Battery technology must be improved to facilitate the widespread adoption of Battery Electric Vehicles (BEVs). Batteries have relatively low energy density, meaning that they have to be designed in large and heavy sizes to enable a car to travel a reasonable long distance. This also increases the cost of the batteries installed in a car [14]. On the other hand, energy density is not an important issue in FCEVs to achieve a reasonably long travel distance (e.g. up to 300 miles) because they can have a larger gas storage tank to achieve longer travel ranges [14].
- A fuel cell requires less well-to-wheels natural gas or biomass energy to run the vehicle compared to BEVs being supplied by electricity generated from such resources.
- A fuel cell generates less greenhouse gases if the hydrogen is produced from natural gas.
- A fuel cell vehicle takes much less time to refuel [13]. It takes only a few minutes to refuel a hydrogen tank, but fully charging a battery may

take a couple of hours, depending on the battery technology and the limitation imposed by the local electrical power system [14].

- Even if battery electric vehicles become easily available, then the local electrical supply system may not still be able to provide such power for fast charging of long range battery electric vehicles [13].
- Hydrogen fuel cell electric vehicles have superiority over battery electric vehicles due to the nature of hydrogen which could be stored for a long period of time. This capability can reduce the problem with daily and seasonal variability of renewable power generation and the demand for hydrogen or electricity [13].

On the other hand,

- Batteries have a higher round trip energy efficiency in comparison to hydrogen storage technologies if hydrogen is produced from electrical energy.
- Battery electric vehicles have better initial access to recharging capability [13].

To increase the travel range of a fuel cell vehicle, its hydrogen tank needs to slightly get larger, but the extra mass would be negligible. On the other hand, the mass of a battery electric vehicle increases significantly when attempting to increase its travel range by adding heavy batteries, and therefore the efficiency of battery electric vehicles will be significantly lower if they were able to achieve long travel ranges [13].

Offer et al. [14] have also compared battery EVs, HFCVs and hydrogen fuel cell plug-in hybrid vehicles. Qualitative comparisons between technologies and infrastructural requirements, and also quantitative comparisons of the lifecycle cost of the power train over 100,000 miles were undertaken, accounting for capital and fuel costs. They concluded that HFCVs could have a part to play in future road transport, but the best platform for integration of fuel cells is the BEV using an on-board fuel cell range extender. Batteries have high efficiency and hydrogen fuel cells have higher peak power and could be recharged faster, so these two technologies can be combined in a hybrid system to complement each other in a battery/hydrogen hybrid system which

also has better economics than either battery or fuel cell vehicle alone. However, Offer et al. [14] concluded that for a car travelling only within a city, the BEV solution may be the cheapest option, however the battery size should be minimised.

If hydrogen for HFCVs is produced by the current electrical grid in the UK, or if the BEVs are to be charged from the same grid, then the greenhouse gas emission implications will be serious due to the fact that most of the electrical power generated in the UK comes from fossil fuels which produce carbon emissions [13]. The total amount of carbon dioxide emissions resulting from deployment of BEVs depends on the mixture of power generation technologies in the electrical network utilised for recharging batteries [14]. If the hydrogen is produced from natural gas, then the amount of emission as a result of using HFCVs would be smaller than the amount of emissions from charging BEVs from the current UK power system [13].

Thomas [13] shows that, on a full-cycle well-to-wheels basis for the vehicles with a travel range of more than 400 km, HFCVs would use from 22% to 48% less energy than a BEVs if the hydrogen is produced from natural gas [13]. This superiority in the well-to-wheels energy efficiency of HFCVs in comparison to BEVs is due to the higher efficiency of converting natural gas to hydrogen compared to converting natural gas to electricity in power plants [13]. The process of converting natural gas to hydrogen is around 75% efficient, but the natural gas combined cycle power plants have the efficiency of approximately 48% for electricity production [13]. The average efficiency of a fuel cell system is approximately 52% in converting hydrogen to electricity, while battery systems have a typical efficiency as high as 90% in delivering electricity to the motor [13]. However, if we consider the full system's well-to-wheel efficiency, then the efficiency of HFCVs is higher due to the greater conversion efficiency of natural gas to hydrogen and the fact that the BEVs are heavier than the HFCVs for a given range [13]. In vehicles with ranges smaller than 400 km, the paper concludes that using renewable electricity directly to charge EV batteries would be more efficient than converting that electricity to hydrogen for a HFCV because the overall efficiency of a battery system is higher than a hydrogen system [13]. However, even if both of the vehicles are powered with wind energy, a HFCV would have a lower life cycle cost in comparison to the BEVs [13].

It is true that there are some costs for the electrolyser, hydrogen pipelines, compressors and hydrogen storage if HFCVs are to be widely used, but the total incremental HFCV cost plus the costs of extra wind power generation installation would be less than the incremental costs of a BEV plus the added costs of the charging system for each BEV [13]. Thomas et al. concludes that society would spend 53% less implementing a system of powering HFCVs from wind rather than implementing a wind-to-BEV pathway, assuming both vehicles were designed to travel 400 km [13]. In addition, the analysis by Offer et al. [14] shows that in 2030 HFCVs could achieve lifecycle costs equal to conventional gasoline vehicles. However, the fuel tank in a HFCV is bigger than the fuel tank of a gasoline vehicle with the same travelling range because hydrogen tanks do not have as good a volumetric energy density as gasoline tanks.

Currently, there are many companies such as Hyundai, Toyota, Honda and BMW making HFCVs. It is expected that the mass production of HFCVs will reduce their price [14].

1.3 Hydrogen storage

Hydrogen can be stored in different forms such as compressed gas, cryogenic liquid, or in solid media/materials such as metal hydrides and carbon materials [11]. It can also be chemically stored in the form of liquid carriers such as methanol, ammonia. The most common method of hydrogen storage is to use pressurised storage tanks.

Ozaki et al. [18] have compared different hydrogen storage technologies for large scale energy storage considering facility construction costs, the utility expense, and the ground area required for construction and operation of each technology. The technologies that they examined consist of compressed or liquefied gas, metal hydride technology, and clathrate hydrate. Their results show that the hydrate-based storage requires the minimum ground area and annual costs if the cool energy generated by adjacent liquefied natural gas (LNG) facilities is available to produce hydrate. Otherwise, the high pressure gas storage system has the minimum annual costs as the

hydrate production process would require significant energy for its refrigeration system [18].

Hydrogen compression is commonly achieved by using piston or centrifugal compressors; however, due to the low density of hydrogen, several stages of compression are needed if the pressure difference between the input and the output of the compressor is significant [11]. Hydrogen storage systems with higher pressures have higher overall energy density, but pressurising hydrogen to very high levels will need a significant amount of energy, which will increase the operational cost of the system. The optimal hydrogen storage pressure could be selected based on a trade-off between extra investment cost due to the size of hydrogen storage, and the increased investment and operating cost of hydrogen compression system [12].

Underground storage could be a good option for future large scale hydrogen storage because it is estimated to be about twice as cheap as storage in pressurised cylinders [11]. The efficiencies of hydrogen storage devices are typically between 88% and 95% [19]. In a mature hydrogen economy, where there exists a proper hydrogen pipeline system, a significant amount of hydrogen could also be stored in the pipeline network [13] through 'line packing' process which is done by packing more gas into the pipeline by increasing the pressure.

A detailed list of hydrogen storage challenges and the technical targets to be met, in addition to a guide for the development of hydrogen storage technologies, are presented in the hydrogen storage section of the Fuel Cell Technologies Office Multi-Year Research, Development, and Demonstration Plan [20].

1.4 Hydrogen Production methods

Hydrogen could be produced from many different feedstocks such as natural gas, coal, renewable energy sources or nuclear power using water electrolysis. Currently around 96% of hydrogen is produced from fossil fuels [8]. The proportions of hydrogen produced from different resources are mentioned below.

- 48% of the hydrogen in the market is obtained from natural gas steam reforming
- 30% from naphtha reforming
- 18% from coal gasification
- 4% from other sources such as electricity

Holladay et al. have reviewed the technologies related to hydrogen production [2], and the current different ways to produce hydrogen are listed below, with the detailed description for each of these methods to be found in [2].

- Fuel processing
    - Hydrocarbon reforming
        - Steam reforming
        - Partial oxidation
        - Auto-thermal reforming
        - Preferential oxidation and water-gas-shift
    - Desulfurization
    - Pyrolysis
    - Plasma reforming
    - Aqueous phase reforming
    - Ammonia reforming
- Non-reforming hydrogen production
    - Hydrogen from biomass
        - Biomass gasification
        - Biological hydrogen
            - Direct photolysis
            - Dark fermentation
            - Photo-fermentative processes
            - Microbial electrolysis cells
            - Multi-stage integrated process
            - Water-gas-shift
- Hydrogen from water
    - Electrolysis

        - Alkaline electrolyser.
        - Proton exchange membrane electrolyser
        - Solid oxide electrolysis cells
    - Thermo chemical water splitting
    - Photo electrolysis

Reforming and gasification are the most mature technologies for hydrogen production. However, water electrolysis powered by renewable energy is a near-term, low-emission technology for hydrogen production [2]. Hydrogen produced with electricity has normally a higher purity than the hydrogen produced with fossil fuels [10].

1.4.1 Steam methane reforming

Steam Methane Reforming (SMR) is a fossil fuel based hydrogen production method, and it is one of the most mature and efficient ways to produce hydrogen. There are many large-scale SMR plants around the globe producing more than 9,000 kg of hydrogen per day in a single plant. This makes those plants very cost effective. The total efficiency of large SMR plants is about 65% to 70%. The main problem with SMR is the amount of carbon dioxide produced in the process. The hydrogen produced in large centralised plants should be distributed to local hydrogen filling stations via pipelines or pressurised cylinders transported with trucks, which are both costly [10].

Currently, hydrogen production from hydrocarbons is cheaper than hydrogen production from electricity, but fossil resources are limited, and hydrogen production using them also produces significant carbon dioxide [11]. For example, hydrogen production by natural gas produces 10 kg of carbon dioxide for each kilogram of hydrogen produced [8]. Separation and capture of the carbon dioxide resulting from hydrogen production with fossil fuels can reduce the pollution from the process significantly, but there are still some issues associated with carbon capture and storage technology and its costs [8].

Due to the low cost of hydrogen production from fossil fuels, it is expected that they will remain the main source for hydrogen production in the short to medium term, but

a sustainable hydrogen economy cannot rely on fossil fuels, so hydrogen production from renewable resources must be considered more seriously if the hydrogen economy were to contribute to future energy systems. Hydrogen could be produced using several renewable energy resources such as biomass (e.g. bioethanol steam reforming and biomass gasification), solar or wind power [8].

1.4.2 Hydrogen production with water electrolysis

An alternative hydrogen production method is to use an electrolyser. The electrolyser is a mature technology to produce hydrogen with high purity, and it could be used for clean, onsite hydrogen production from renewable resources. An electrolyser splits water into its components of hydrogen and oxygen gases, using a DC electric current. There are two electrodes used in an electrolysis process: one with a negative charge is called the cathode and hydrogen is produced on it; the other one with positive charge is called the anode and oxygen is produced on it.

There are three types of electrolyser which are in common development at present:

- Alkaline electrolysers
- Proton Exchange Membrane electrolysers (PEM)
- Solid Oxide Electrolysis Cells (SOEC) [2]

Alkaline electrolysers are currently more popular than the other types mainly because of their lower costs [2], however SOEC electrolysers are more efficient than the other types, but they have not been sufficiently developed for commercial use yet. PEM electrolysers are also more efficient than alkaline electrolysers, however, they suffer from higher costs. Among the three types of electrolysers, the alkaline ones are the most developed, and cost less than the other two types of electrolysers, but they are not as efficient as PEM or SOEC electrolysers [2]. Due to their lower capital costs and mature commercial status (2.1 MW alkaline electrolysers are readily available) alkaline electrolysers will be the focus of the work within this thesis.

Some of the advantages of onsite production of hydrogen from electrolysers are listed below:

- As it does not require the hydrogen to be shipped in tankers or otherwise transported to site, the overall hydrogen supply and production is less costly if considering the costs of hydrogen transport.
- The process will not produce any local carbon dioxide or other pollutants. However, these might be produced at coal or gas fired power stations if the electricity is provided by such plants.
- Electrolysers could use excess wind or solar energy in response to fluctuations in wind or solar input or consumer demand, and they could also use the extra power from the grid during off-peak times, all leading to improved grid operation, especially, with high penetrations of renewable power generation [2].

If the cost of natural gas increases in future, then hydrogen production from renewable energy could become more economically attractive than hydrogen production from natural gas, especially if carbon dioxide and other pollutant emissions are included in the analysis [2].

To fairly compare the hydrogen production by SMR and electrolysis, a number of factors, which are listed below, should be considered.

- The amount of carbon dioxide emissions in the future grid per kWh of electricity on a dynamic basis, and also the amount of CO_2 emissions from the SMR process.
- The capital, operational and maintenance costs of SMR and electrolysis plants.
- The price of methane in the future.
- The dynamic electricity tariff for dynamically controlled electrolysers.
- The electrolysers can help to increase the penetration of wind power on the system and consequently help decarbonise the power system, so the benefits of this decarbonisation should also be considered in any analysis.

The above factors are not clearly predictable at the moment. In addition, conducting a comprehensive techno-economic comparison of these two methods for a future hydrogen economy is beyond the scope of this PhD work.

1.4.2.1 Alkaline electrolysers

To increase the conductivity of water and consequently decrease the losses in the electrolysis process, Potassium Hydroxide (KOH) solution is used instead of pure water, and such electrolysers are called Alkaline Electrolysers. Most of the alkaline electrolysers use electrolyte with a KOH weight concentration of 20-30% with water to achieve the optimal conductivity. Typical operating temperatures and pressures of alkaline electrolysers are 70 to 100°C and 1 to 30 bar, respectively [21].

The reactions on the cathode and anode and also the overall reaction of alkaline electrolysers are provided below:

Anode reaction: $2OH^- \rightarrow \frac{1}{2}O_2 + H_2O + 2e^-$ (1.1)

Cathode reaction: $2H_2O + 2e^- \rightarrow H_2 + 2OH^-$ (1.2)

Overall reaction: $H_2O \rightarrow H_2 + \frac{1}{2}O_2$ (1.3)

From Equation 1.3, it is clear that the volume of hydrogen produced in the water electrolysis process is double the volume of oxygen produced. Figure 1.2 shows a diagram of a simple one cell alkaline electrolyser [21]. It shows how the ions pass through the diaphragm from one cell compartment to the other part of the cell and how the gases are produced on the electrodes. The electrodes are separated by a diaphragm that separates the product gases and facilitates the transportation of the hydroxide ions from one electrode to the other. Many of these cells are attached together in a modular configuration to make a larger electrolyser with a higher rate of hydrogen production.

Two types of cell designs exist for alkaline electrolysers: monopolar or bipolar. In the monopolar design, the electrodes are either directly connected to the negative or positive points of the power supply, meaning the cells have a parallel electrical connection [21]. On the other hand, in the bipolar design the electrolysis cells are

connected in series electrically and geometrically. The bipolar electrolyser stacks are therefore more compact than the monopolar designs. Figure 1.3 shows these two different cell configurations. Due to the compactness of the bipolar system, the current paths in the electrical wires and electrodes are shorter, so the losses due to the internal ohmic resistance of the electrolyte are less than the losses in the monopolar system. This therefore implies that electrolysers with a bipolar configuration have a higher efficiency. On the other hand, monopolar electrolysers are typically less costly to manufacture because they have a simpler configuration. Most of the commercial alkaline electrolysers available in the market have bipolar configuration [21].

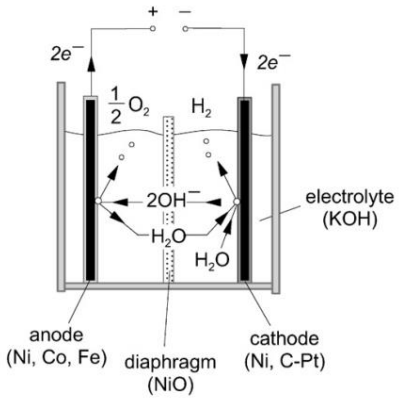

Figure 1.2 A simple diagram of an alkaline electrolyser [21]

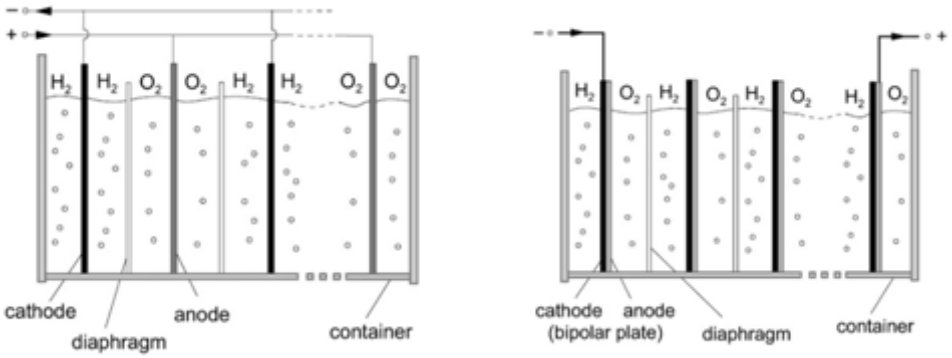

Figure 1.3 Monopolar (left) and bipolar (right) design of electrolysers [21]

According to Faraday's law, the hydrogen production rate of an electrolyser cell stack is directly proportional to the transfer rate of electrons at the electrodes [21]. The ratio between the actual and theoretical amount of hydrogen produced in an electrolysis cell stack is called the Faraday (Current) efficiency, where losses are caused by parasitic

currents in the gas ducts. By decreasing cell current densities, the parasitic currents will increase due to an increase in the proportion of electrolyte in the cells which decreases the electrical resistance in the cells [21].

The amount of hydrogen production in a bipolar electrolysis cell stack is directly proportional to the current passing through that stack. If a constant current of 'i' is applied to the cell during a time slot of 't', then the amount of hydrogen produced by the stack made of several cells connected in series could be estimated from Equation 1.4 [22]:

$$M_{H_2} = \eta_f * N_C * \frac{i*t*2.01}{F*n*1000} \quad (1.4)$$

where

M_{H_2} The mass of hydrogen gas produced (kg)

η_f The Faraday efficiency

N_C The number of cells connected in series in the cell stack

t The duration of time in which the current 'i' is applied to the stack (s)

i The DC current to the cells (A)

F The Faraday constant (96485.30 C/mol)

n The number of electrons (2) transferred per hydrogen molecule produced during the electrolysis.

Most of the electrolyser manufacturers have adopted a zero-gap configuration design due to an improvement in the efficiency of the electrolysis process. In the zero-gap cell design, the electrode materials are pressed onto either side of the diaphragm, so that the hydrogen and oxygen gases are forced to leave at the rear the of electrodes [21].

The most common cathode material in alkaline electrolysers is nickel with a catalytic coating, such as platinum. The anode electrode is commonly made of nickel or copper metals coated with metal oxides, such as manganese, tungsten or ruthenium [2].

The membrane of an alkaline electrolyser is very thin (less than 0.5mm) resulting in a low electrical resistance. Asbestos diaphragms which were being used in early alkaline units have been replaced by new composite materials, e.g. polysulfones or oxide-ceramics containing Nickel Oxide (NiO) or alkaline-earth metal titanates [8].

Hydrogen molecules are much smaller than oxygen ones, so it is much easier for hydrogen gas to leak into oxygen compartments. Due to this concern, electrolyser manufacturers include sensors to measure the content of hydrogen in the oxygen stream, and the inclusion of sensors to measure the oxygen content in the hydrogen is normally optional.

The electrical equivalent circuit of an electrolysis cell could be shown as in the diagram in Figure 1.4. This diagram consists of the following parts which could change due to variations in the operational conditions [10].

- The battery, E, represents the reversible voltage of the cell.
- The R_{Ohm} resistor represents the Ohmic over-potential of the cell.
- The R_{act} resistor represents the activation over-potential of the cell.
- A capacitor representing the impact of double layer capacitance.

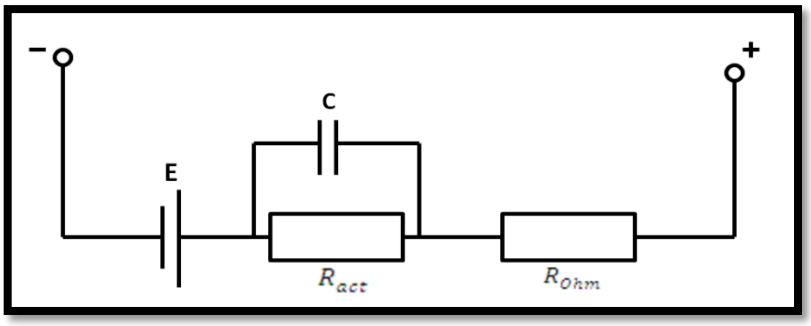

Figure 1.4 Electrical circuit equivalent of an electrolysis cell

The minimum voltage needed for water electrolysis at 25°C and 1atm is called the reversible voltage and is equal to 1.23V. A change in the current of the cell does not affect its reversible voltage, but the reversible voltage is a function of the cell operating temperature and pressure, and it increases rapidly with an increase in pressure of the system at any temperature [10].

The components that carry electricity into the cells for hydrogen production naturally have some finite resistance, and the resulting electrical losses reduce the efficiency of the electrolysis process. The losses due to the resistance of such components are called Ohmic losses, and the increase in the cell voltage that result from such losses is called Ohmic over-potential. The Ohmic resistance of the cell is equal to the sum of the Ohmic resistances of the cell components, including the bipolar plates, current collectors, electrodes, and electrolyte layer between the electrodes and diaphragm. The Ohmic resistance also changes with temperature. The diaphragm of these electrolysis units should have low electrical resistance (e.g. 9×10^{-5} Ω [10]) to help minimise the energy loss in the hydrogen production process [21]. Gas bubbles at the electrode surfaces can also add to the Ohmic over-potential in the cells [10]. It is claimed that the coverage of the electrode surfaces by gas bubbles directly adds to the electrical resistance of the whole system by reducing the contact area between the electrolyte and the electrode surface, blocking the electron transfer, and increasing the Ohmic losses [23]. The bubbles effectively reduce the active area of the electrodes while they adhere to their surface.

The losses in the electrolysis process that result specifically from electrode kinetics are called activation losses, and the increase in the cell voltage as a result of such losses is called activation over-potential. Ohmic and activation over-potentials change with respect to a change in the current of the cell stack, with the activation over-potential of the cells increasing logarithmically with respect to the increase in the cell current density.

Due to the over-potentials explained above, the voltage of the cell increases if there is an increase in the current density of an electrolysis cell. The relationship between the cell voltage versus the current density, for a typical alkaline electrolyser at a high (80°C) and low (20°C) operational temperature, is shown in Figure 1.5 [21].

The actual minimum voltage that should be applied to an electrolysis cell to start the electrolysis process, without any heat exchange with the environment, is called thermo-neutral voltage [24]. When alkaline electrolysers work with a reasonable current density (100–300 mA/cm^2 [2]) to satisfy the hydrogen production demand, their activation and ohmic over-potentials cause an increase in the voltage of each cell,

and the electrolysis voltage will go above the theoretical thermo-neutral voltage of 1.48V. The amount of increase depends on both activation and ohmic over-potentials of the cells, and the voltage can normally reach up to 1.8V-2V in each cell [10]. The voltage needed for the electrolysis process to achieve the same rate of hydrogen production can also increase as a result of corrosion of the electrodes during the life of electrolyser.

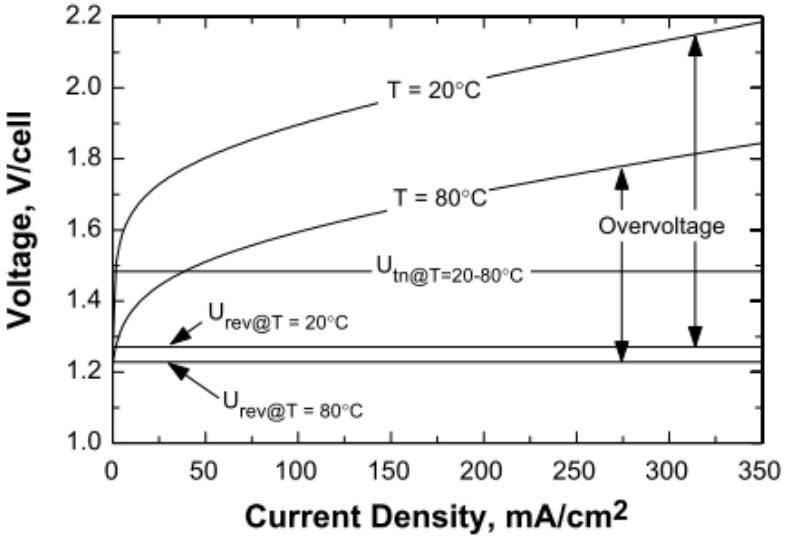

Figure 1.5 Typical I/V curve of an electrolysis cell at a high and low temperature [21]

Due to the logarithmic relationship between the activation over-potential and the current of the cells (explained in more details in [10]), when the current of the cells is high, the voltage change is mainly affected by the change in the Ohmic over-potential, but at low current densities, the activation over-potential mainly affects the cell voltage, and the Ohmic over-potential contributes less to a change in cell voltage at low current densities.

When the cell current density is above a certain limit (e.g. typically more than 75 mA/cm^2 in Figure 1.5), its voltage and current have an approximately linear relationship because the electrolyser behaviour is then mainly governed by the Ohmic electric resistances of the electrolyte, electrodes, and membranes [8].

In literature [21, 24], mostly the term thermo-neutral voltage (V_{Thn}) is used as a reference voltage to calculate the efficiency of electrolysers. As explained in [24], the

efficiency could be calculated based on the thermo-neutral voltage, which is the actual minimum voltage that has to be applied to the electrolysis cell, below which the electrolysis is endothermic and above which it is exothermic. At standard conditions (25ºC and 1bar pressure), the thermo-neutral voltage is equal to 1.48V [21]. The efficiency of the electrolyser is inversely proportional to the stack potential [8]. The energy efficiency can be calculated by dividing the thermo-neutral by the voltage of the cell [21]. In current densities of close to zero, the cells have a very high voltage efficiency, near to 100%. When the input power of the electrolyser increases, the current and voltage of the stack increase. This means that the efficiency of the stack decreases with increasing load, but at the same time the amount of hydrogen production increases due to an increase in the current through the stack [8].

If the applied alkaline electrolysis cell voltage goes above the thermo-neutral voltage of 1.48V, then there will be some heat generation in the cell, which increases the temperature of the electrolysis, but at voltages below the thermo-neutral voltage, additional heat has to be supplied to the cell to split water [8]. At higher temperatures the cell over-voltages decrease due to the reduction in Ohmic resistances, resulting in higher efficiency of the electrolysis process [8]. For example, if the electrolysis temperature increases from 375 K to 1050 K (i.e. in SOEC), then the combined thermal and electrical energy requirements for the electrolysis process will approximately decrease by 35% [2]. However, the overall efficiency will increase only if the heat energy is freely available as the waste product of another process.

Alkaline electrolysers must have a proper thermal management system to maintain their operational temperature within the acceptable limits. Such accurate thermal management is necessary to have a safe and efficient system. Operation of the electrolyser at unacceptable temperatures can increase the corrosion rate and damage the electrodes and membranes, leading to a decrease in the lifetime of the electrolyser [8]. In addition, at higher temperatures, the amount of water vaporisation increases significantly. Hence, if the system is working at high current densities with good thermal insulation, then to keep the operational temperature constant, it will be necessary to remove heat from the stack due to the significant heat produced within the cells.

Reduction of the voltage of cells decreases the energy consumption of the electrolyser, so the cost of hydrogen production will reduce. An increase in the nominal current density of the electrolyser reduces the capital investment costs of manufacturing alkaline electrolyser. However, increasing the nominal current density of the electrolyser leads to higher electrode over-potentials and consequently lower efficiency. In addition, the Ohmic resistance in the electrolyte increases with increasing current due to a rise in the amount of gas bubbles [21].

The electrodes in an alkaline solution must be resistant to corrosion and have good electric conductivity and catalytic properties, as well as acceptable structural integrity. Depending on the design of the system, the electrode might corrode if the hydrogen production is stopped as the electrolyte (KOH solution) is very corrosive. In that case, the electrodes should be polarised to minimise their corrosion. To polarize the electrodes, a current must be passed through them during standby or shutdown mode [11]. The other solution to the corrosion problem is to remove the electrolyte from the cells when the system does not produce significant hydrogen for long periods [11], i.e. 'drain' the system.

The thermo-neutral voltage for water electrolysis does not change noticeably if the system pressure increases while the temperature is below 1000°C. This is an advantage of pressurised electrolysis, but the electrolyser has to have perfect gas leakage insulation which is difficult to achieve in commercial alkaline electrolysers [10].

At a temperature of 25°C and pressure of 1atm, the heat generated in the formation of liquid water reaction is 39 kWh per kg of hydrogen produced. This value is called the Higher Heating Value (HHV) of hydrogen and is defined as the amount of heat generated by burning one kilogram of hydrogen at 25°C after the products of the reaction have returned to 25°C. The heat of formation of steam is 33 kWh/Kg of hydrogen which is the Lower Heating Value (LHV) of hydrogen [25].

Liquid water is normally electrolysed to produce hydrogen, so the amount of energy needed to produce hydrogen from water is 39 kWh/kg or 3.5 kWh/Nm^3 if the efficiency of electrolysis is assumed to be 100%. To calculate the energy efficiency of

a particular electrolyser, this value should be divided by the actual energy consumed by the unit for production of a kilogram of hydrogen [25].

1.4.2.2 PEM electrolysers

In Proton Exchange Membrane (PEM) electrolysers the electrolyte is a solid positive ion-conducting membrane (e.g. Nafion [8]), unlike the corrosive KOH solution in alkaline units. The hydrogen ions pass through the membrane.

As shown in Equations 1.5 and 1.6, hydrogen is produced by supplying water to the anode where it is decomposed into oxygen, hydrogen ions, and electrons [26]. The hydrogen ions pass through the proton-conductive membrane from the anode to the cathode side and form hydrogen [25]. The electrons exit the cell from the anode via the external power supply circuit. At the cathode the electrons and hydrogen ions are recombined to produce hydrogen gas.

Anode reaction: $2H_2O \rightarrow 4H^+ + O_2 + 4e^-$ (1.5)

Cathode reaction: $4H^+ + 4e^- \rightarrow 2H_2$ (1.6)

Overall reaction: $2H_2O \rightarrow 2H_2 + O_2$ (1.7)

PEM-based electrolysers typically use Platinum black (Pt black), iridium, ruthenium, and rhodium as electrode catalysts. They also have Nafion membranes, which separate the electrodes and act as gas separators [2].

A comparison is made here between PEM and alkaline electrolysers:

- PEM technology is fairly expensive in comparison to alkaline electrolysers because PEM electrolysers have expensive metal catalysts [27] and a polymer membrane [11]. Alkaline electrolysers have much cheaper membranes and electrodes and consequently a much cheaper price.
- The impurity of gases is higher in alkaline electrolysers in comparison to PEM units.

- PEM-type electrolysers have been developed mainly at small scale due to the significant cost of development of large-scale ones. On the other hand, alkaline units have lower capital costs and can produce hydrogen within a wide range of nominal production rates [25].
- PEM electrolysers have a more limited lifetime of around 2000-5000 hours in comparison to alkaline electrolysers, which can normally work for 10-15 years.
- PEM systems are more compact and safer than alkaline systems because they do not use Potassium Hydroxide and separators.
- PEM electrolysers do not need a gas separation unit.
- PEM units have low ionic resistances, so they can achieve high current densities of more than 1600 mA/cm^2 when the typical current density of alkaline electrolysers is only 100–300 mA/cm^2 [2]. As a result, PEM electrolysers are lighter than alkaline units with the same rating.
- PEM units can achieve a high operational pressure of 20 MPa without using any mechanical compressor [8].
- PEM electrolysers have faster response rates to a control signal to change their load because they have solid polymer electrolyte instead of a circulating electrolyte [28].
- PEM electrolysers have a shorter start-up period, and they also have a wider operational range of 5%–100% of their rated load, so they may prove to be more suitable for wind-hydrogen systems than alkaline electrolysers due to this greater flexibility and operation range [28]. This is particularly true for small to medium range (50–250 kW) electrolysers.

The main disadvantage of the PEM electrolysers is the uncertainty about their lifetime [12] and cost.

1.4.2.3 High temperature electrolysers

Another electrolysis system, which uses high temperature (800-1000ºC [29]) water vapour to produce hydrogen, is called the Solid Oxide Electrolysis Cell (SOEC). It can increase the efficiency of water electrolysis significantly because the electrical energy

needed decreases at high temperatures, but SOECs are still at their early development stages [8]. SOECs need costly materials due to the operational conditions at high temperatures. They also need an additional heat source, unlike normal alkaline electrolysers [2].

Although high temperature electrolysis consumes less electrical energy, it demands the input of a considerable amount of heat/thermal energy to maintain the required temperature, so if there is some extra heat available from some plants that produce heat as a by-product (e.g. heat from thermal power plants), then it could be used for electrolysis, thereby lowering energy consumption, and this will help reduce the overall hydrogen production cost.

The total efficiency of the high temperature electrolysis depends on the operating temperature and the thermal source. The efficiency of SOECs can reach very high values of around 90% if it is calculated based on only the electrical energy input of the cells. However, if the energy consumed by the thermal source to create the heat for electrolysis is included in the efficiency calculations, then the total efficiency can drop significantly [2].

1.5 Electrolysers: market review

Currently, there are many companies producing electrolysers that are commercially available in the market. Table 1.1 contains the name of some of these major electrolyser manufacturers and the type of electrolysers they produce. This table also shows the energy consumption, operational pressure and the hydrogen production rate of those electrolysers [30-38]. These electrolysers should be able to work efficiently with an acceptable lifetime while operating with fluctuating wind power.

Table 1.1 List of electrolysers in the market [30-38]

Name of electrolyser/ manufacturer	Nominal load	Hydrogen production rate	Type	Operating pressure	Operational range	Energy consumption (kWh/Nm^3)
HPac 10/ ITM POWER	3.5 kW	0.6 Nm^3/h	PEM	15 bar (g)	N/A	5.0
HPac 40/ ITM POWER	11 kW	2.4 Nm^3/h	PEM	15 bar (g)	N/A	4.8
NEL A/ NEL Hydrogen	Up to 2.1 MW	10 to 500 Nm^3/h	Alkaline	1 bar	20%- 100%	4.1 to 4.35 ± 0.1
NEL P.60/ NEL Hydrogen	300 kW	60 Nm^3/h	Alkaline	15 bar (g)	10%-100%	4.9
HySTAT™-10-10 Elementary type/ Hydrogenics	100 kVA	10 Nm^3/h	Alkaline	10 bar (g)	25%-100%	4.9
HySTAT™-15-10 Elementary type/ Hydrogenics	120 kVA	15 Nm^3/h	Alkaline	10 bar (g)	25%-100%	4.9
HySTAT™-10-25 Elementary type/ Hydrogenics	100 kVA	10 Nm^3/h	Alkaline	25 bar (g)	25%-100%	4.9
HySTAT™-10-10 V type/ Hydrogenics	100+35 kVA	10 Nm^3/h	Alkaline	10 bar (g)	25%-100%	5.4
HySTAT™-15-10 V type/ Hydrogenics	120+35 kVA	15 Nm^3/h	Alkaline	10 bar (g)	25%-100%	5.4
HySTAT™-30-10 V type/ Hydrogenics	240+35 kVA	30 Nm^3/h	Alkaline	10 bar (g)	25%-100%	5.2

HySTAT™-45-10 V type/ Hydrogenics	360+35 kVA	45 Nm^3/h	Alkaline	10 bar (g)	25%-100%	5.2
HySTAT™-60-10 V type/ Hydrogenics	480+35 kVA	60 Nm^3/h	Alkaline	10 bar (g)	25%-100%	5.2
HyLYZER®- 1 Nm3/h /Hydrogenics	10 kW	1 Nm^3/h	PEM	0-7.9 bar(g)	0-100%	6.7
HyLYZER®- 2 Nm3/h /Hydrogenics	20 kW	2 Nm^3/h	PEM	0-7.9 bar(g)	0-100%	6.7
PureH2 electrolyser 2/ pure ENERGY	15 kW	2.66 Nm^3/h	Alkaline	Up to 12 bar	20%- 100%	5.6
PureH2 electrolyser 4/ pure ENERGY	22.3 kW	4 Nm^3/h	Alkaline	Up to 12 bar	20%- 100%	5.57
PureH2 electrolyser 5/ pure ENERGY	30.5 kW	5.3 Nm^3/h	Alkaline	Up to 12 bar	20%- 100%	5.75
PureH2 electrolyser 6/ pure ENERGY	38 kW	6.66 Nm^3/h	Alkaline	Up to 12 bar	20%- 100%	5.7
PureH2 electrolyser 8/ pure ENERGY	49.5 kW	8.66 Nm^3/h	Alkaline	Up to 12 bar	20%- 100%	5.71
PureH2 electrolyser 10/ pure ENERGY	58 kW	10.66 Nm^3/h	Alkaline	Up to 12 bar	20%- 100%	5.44
PureH2 electrolyser 16/ pure ENERGY	81 kW	16 Nm^3/h	Alkaline	Up to 12 bar	20%- 100%	5
PureH2 electrolyser 21/ pure ENERGY	108 kW	21.33 Nm^3/h	Alkaline	Up to 12 bar	20%- 100%	5

PureH2 electrolyser 32/ pure ENERGY	175 kW	32 Nm^3/h	Alkaline	Up to 12 bar	20%- 100%	5.46
PureH2 electrolyser 42/ pure ENERGY	213 kW	42.63 Nm^3/h	Alkaline	Up to 12 bar	20%- 100%	5
HOGEN® S10/ Proton Onsite	4 kVA	0.265 Nm^3/h	PEM	13.8 bar (g)	0-100%	6.7
HOGEN® S20/ Proton Onsite	8 kVA	0.53 Nm^3/h	PEM	13.8 bar (g)	0-100%	6.7
HOGEN® S40/ Proton Onsite	12 kVA	1.05 Nm^3/h	PEM	13.8 bar (g)	0-100%	6.7
HOGEN® H2m/ Proton Onsite	22 kVA	2 Nm^3/h	PEM	15 bar (g)	0-100%	7.3
HOGEN® H4m/ Proton Onsite	40 kVA	4 Nm^3/h	PEM	15 bar (g)	0-100%	7
HOGEN® H6m/ Proton Onsite	58 kVA	6 Nm^3/h	PEM	15 bar (g)	0-100%	6.8
HOGEN® C10/ Proton Onsite	100 kVA	10 Nm^3/h	PEM	30 bar (g)	0-100%	6.2
HOGEN® C20/ Proton Onsite	200 kVA	20 Nm^3/h	PEM	30 bar (g)	0-100%	6
HOGEN® C30/ Proton Onsite	250 kVA	30 Nm^3/h	PEM	30 bar (g)	0-100%	5.8
Hydrofiller 15 /Avālence	2 kW	0.34 Nm^3/h	Alkaline	Up to 450 bar	N/A	5
Hydrofiller 50 /Avālence	7 kW	1.38 Nm^3/h	Alkaline	Up to 450 bar	N/A	5
Hydrofiller 85 /Avālence	12 kW	2.31 Nm^3/h	Alkaline	Up to 450 bar	N/A	5

Hydrofiller 175 /Avālence	25 kW	4.6 Nm^3/h	Alkaline	Up to 450 bar	N/A	5
AGE /AccaGen	Up to 500 kW	Up to 150 Nm^3/h	Alkaline	50 bar	10-100%	5
BAMAG /ELT	Up to 1.5 MW	3 to 330 Nm^3/h	Alkaline	1 bar	25%-100%	4.3 – 4.6
LURGI/ELT	Up to 3.2 MW	100 to 760 Nm^3/h	Alkaline	30 bar	25%-100%	4.3 – 4.65
Titan HMXT /Teledyne	N/A	2.8 to 12 Nm^3/h	PEM	10 bar (g)	N/A	N/A
Titan EC /Teledyne	N/A	28 to 56 Nm^3/h	PEM	10 bar (g)	N/A	N/A

There are two ways to produce high pressure hydrogen gas with an electrolyser. The first way is to use a low pressure electrolyser with a large compression stage, and the second way is to use a high pressure electrolyser without compression or with a comparatively smaller compression stage [12]. By operating electrolysers directly at high pressure, the requirement for hydrogen compressors can be eliminated [2]. Making highly pressurised large-scale electrolysis units is difficult and more expensive due to an increase in the likelihood of gas leakage at higher pressures. Gas leakage losses in the system are directly influenced by the operating pressure.

The gas loss in alkaline electrolysers depends mostly on the operating current density of the stack, the operating pressure, membrane type and the design of the system. Due to higher leakage problems in pressurised electrolysers, their gas loss is higher than the loss in atmospheric systems.

Some research works have theoretically compared these two hydrogen production techniques, and have shown that high pressure electrolysis without using a compressor is around 5% more efficient than low pressure electrolysis followed by a compression system [39]. However, Roy [10] disagrees with this conclusion. He compared

atmospheric alkaline electrolysers with pressurised ones. He concluded that pressurised electrolysers are less energy efficient, less durable, more costly and not adequately compatible with renewable energy powered operation especially in standalone energy systems, compared to atmospheric electrolysers. However, this author would challenge Roy's conclusions as not correct, as explained in more detail in Chapter 2 with data from commercial electrolysers made by NEL Hydrogen. Roy concluded that for large-scale hydrogen production, atmospheric electrolysers with external compressors are a better option. It mentions that pressurised systems demand more maintenance and incur more hydrogen losses, but he does not express the nominal pressure of those systems that he used for comparison, and he does not report his experiments at different pressures to prove this. He concludes that pressurised electrolysers are less compatible with renewable energy powered operation because the pressurised electrolysers should spend a significant time in standby condition but states that the atmospheric electrolysers could be switched off in stand-alone systems. This is an obvious mistake because the atmospheric electrolysers also need some time to come to full operational mode due to the time they need to be purged with nitrogen gas, so in stand-alone systems they cannot simply be switched off and on quickly. Roy mentioned that the standby load of pressurised units is more than the standby loss of atmospheric ones, but this author knows that this difference is not significant especially in large scale units, and this is explained in more detail in Chapter 2.

Some other studies on high pressure (e.g. 400 bar) alkaline electrolysis systems show that it might be difficult to achieve high pressure electrolysis because high operating pressure can increase the cost of the system [40] due to increased material costs and also system engineering costs, as well as the extra costs for the safety and control systems [12].

Ulleberg et al. [12] concluded that operating the electrolysers at lower pressures of around 10 to 40 bar and using a hydrogen compressor to pressurise the hydrogen to higher levels for storage seems to be more efficient.

In the report by Ivy [25], a technical and economic overview of the hydrogen production by electrolysis systems commercially available in 2003 is provided. The work analyses the electrolysis units from five companies (Stuart IMET; Teledyne HM

and EC; Proton HOGEN; Norsk Hydro HPE and Atmospheric; and Avalence Hydrofiller). It also provides cost information of three systems with different size ranges and analyses their economics. An initial cost boundary analysis to find the impact of electricity price on hydrogen costs was also carried out.

The economic analyses in the report [25] used cost and economic data from three different systems, which were available at the time the report was published. Those three systems are listed below:

- A small neighbourhood system producing around 20 kg of hydrogen per day.
- A small forecourt system producing around 100 kg of hydrogen per day.
- A forecourt size system producing around 1,000 kg of hydrogen per day.

Its results, which are illustrated in Figure 1.6, show that in a forecourt plant, the cost of electricity makes up 58% of the total cost of the hydrogen produced, and the capital costs only contribute to 32% of the final cost. In the case of the small forecourt electrolysis plants, the electricity contribution drops to 35%, but the capital costs remain the main cost factor at around 55%. In the neighbourhood case, the capital costs of the plant contribute to 73% of the total cost of hydrogen produced, but electricity costs are at a lower level of only 17%. The analysis in this report shows that in spite of the electricity price being a contributor to the hydrogen price for all systems, in small scale electrolysers, the contribution of capital costs are more significant. In all of the above three cases, the electricity costs need to be considered as a major factor that can help in cost minimisation. It should be noted that the analysis in this report did not consider the case that the electrolyser demand follows the fluctuations in the renewable power generation. In that case, the capacity factor of electrolysers would be lower, and consequently the contribution of their capital cost will increase in the results.

In all electrolysis units, the capital and electricity costs are the main contributors to the cost of hydrogen production. The operation and maintenance costs are the third largest contributor to the total cost of hydrogen production by a plant. Alkaline electrolysers are not produced in large numbers nowadays, and it is expected that in the future when the demand for hydrogen and electrolysers increase, then the price of such units will

decrease as a result of their mass production. If capital costs of electrolysis plants reduce in future, then the electricity price will become the main factor affecting the cost of electrolysis. The smaller electrolysis systems benefit more from a reduction in capital costs because a large percentage of their hydrogen production cost is due to their capital costs. Large electrolysis units might be able to purchase cheaper electricity from electricity suppliers, especially when operating as dynamically controlled demand loads. By using the oxygen produced in the electrolysis process, the electrolytic hydrogen production will also become more economic [25].

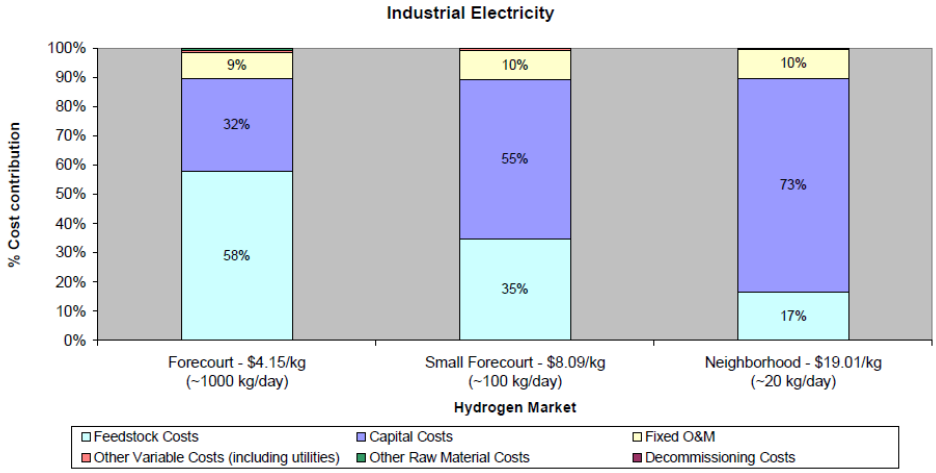

Figure 1.6 Cost contribution of different factors in the final price of hydrogen produced by electrolysers [25]

1.6 Electrolyser modelling in literature

Some previous work has been done by other researchers to develop practical models for electrolysers. For example, Ulleberg [21] has developed a mathematical model for an advanced alkaline electrolyser. His model is based on a combination of fundamental thermodynamics, heat transfer theory, and empirical electrochemical relationships, and it can be used to predict the cell voltage, hydrogen production, efficiencies, and operational temperature. Such models can be used for improvement of system design and also the optimisation of the control strategy to run the electrolyser. For example, the technical model can be coupled with economic models to find the best control strategy to maximise the profit from a plant. However, the thermal model in his work

is very simple and his model does not consider the dynamics of all of the components in an electrolyser.

In alkaline electrolysers, the gas produced in the cell stack cannot be measured directly, and it should be separated from KOH and purified before being measured by the hydrogen flow meter, so the measured mass flow rate does not represent the amount of instantaneous hydrogen production. Therefore, to verify the model of alkaline electrolysers, the aggregate amount of hydrogen over a time period should be used [10].

During the electrolysis process, heat is generated in the stack. An accurate electrolyser model should be able to predict the temperature of the lye during the electrolyser operation with very good precision, which will consequently help in assessing the overall efficiency of electrolyser. A proper thermal model needs very detailed information about the heat and mass transfer of the liquid and gases in the system. In addition, specific heat capacities of some system components such as electrodes, membranes, sealing materials and KOH solution, piping, fittings and solenoid valves are also needed [10].

Roy has also developed a mathematical model of a pressurised alkaline electrolyser in his thesis [10]. The model consists of various subsystems, such as current-voltage characteristics, Faraday efficiency, gas production, gas purity, differential pressure, temperature subsystem, parasitic losses, gas losses and efficiencies in different operating conditions. It predicts the current-voltage profile of a single cell while considering the reversible voltage, activation over-potential, Ohmic over-potential and also the bubble voltage loss. The power, energy and efficiency of the electrolyser can be found with his model. His model has some subsystems to calculate gas production, differential pressure, water consumption, thermal response, parasitic power, gas loss and overall energy efficiency. He has tested and verified his model with some measurements performed on a commercial alkaline electrolyser to predict the dynamic and transient behaviour of the system. Roy claims that his electrolyser model can be used to predict the amount of energy consumption by the electrolyser, impact of On-Off cycling on corrosion, the change in Faraday efficiency with respect to the stack current, amount of gas production, temperature, impurity, pressure, gas losses, and the

balance of plant losses. He also claims that the model can be used as a tool for system design and optimisation. The model can also predict an estimate of the cost of the hydrogen production by the electrolyser [10].

Artuso et al. also showed an analysis of the operational data collected from the 36 kW alkaline electrolyser installed as a part of the HARI project at West Bacon Farm, Loughborough, UK. It seems that the electrolyser modelled by them is the same unit modelled by Roy. In Artuso's work, a steady state model of the electrolyser is used to find its I/V curve and the amount of hydrogen production with respect to the current of the cell stack. The electrolyser operational data was used to verify the electrolyser model [41]. However, their model was not able to exactly predict the amount of hydrogen produced by the electrolyser on a second-by-second basis, because they did not consider many factors especially during transient periods. For example, their model did not consider the compressor operation cycles, but it was accurate enough to find the amount of hydrogen production during a certain period of time by taking the integral of hydrogen produced.

Lebbal and Lecoeuche [42] focused on the dynamic modelling and the monitoring of a PEM electrolyser. Their model consists of a steady-state electric model coupled with a dynamic thermal model. After creation of the dynamic model, the model was used to monitor the PEM electrolyser and to ensure that it was operating safely. An algorithm was also developed by them to detect and isolate faults on actuators, sensors or the electrolyser system [42].

Zhou and Bruno [43] implemented a control-oriented model of an electrolyser. Their model is capable of characterising the relations among the electrolyser's physical parameters and can be used to design a control system to ensure efficient and reliable operation of the electrolyser.

Electrolysers operating with fluctuating wind power input should be able to work efficiently and give an acceptable lifetime. Electrolysers have to be able to change their load dynamically when working directly with renewable input power profile. They should also be able to cope with many On/Off switching cycles and long periods of shut downs without significant degradation in their performance. There are some

previously published papers (e.g. in [8], [44], [45]), which explain the work of other researchers on investigation of the impact of variable load on the performance of electrolysers. However most of those research works focus on assessing electrolysers manufactured at least eight years ago. As recent as 2010, many electrolyser manufacturers such as NEL Hydrogen or Hydrogenics Corporation have started using new electrodes for their electrolysers, and they claim that those electrodes can now cope with variable input power, and that they do not degrade as a result of working with variable and intermittent input power, e.g. wind power input.

One of the common problems that used to exist in electrolysers was the degradation of their electrode performance as a result of time spent in standby condition or being maintained without power for a long time, so they needed a protection current passing through their electrodes to avoid such degradation in their performance due to reverse cathodic current, but as explained above this issue seems to have been solved in modern electrolysers, and they do not seem to show degradation as a result of having no current on their electrodes.

Gandía et al. [8] studied hydrogen production from renewable energy in the Public University of Navarra. They carried out experiments with a commercial 5 kW alkaline electrolyser working with wind power supplied to the system by a wind power emulator. They designed and built a new power supply, based on Insulated Gate Bipolar Transistors (IGBTs) driven by a microcontroller, to supply the electrolyser with a wind power profile. The electrolyser was able to produce hydrogen with the rate of 1 Nm^3/h at a pressure of up to 2.5 MPa and nominal temperature of 65 °C. They monitored the stack parameters such as voltage, efficiency, temperature and the gas purities [8]. However, their paper does not investigate the ramping rate of electrolyser.

1.7 Renewable Hydrogen systems

Over the past few years, a number of wind-hydrogen system concepts and designs have been studied, and also a few such systems have been installed. An overview of some of those systems could be found in [12]. Most of the wind-hydrogen installations are

small scale systems with only a few kilowatts of wind turbine capacity. One of the most important exceptions is the autonomous renewable hydrogen system at Utsira, Norway, because the system can provide power to ten households via a local AC micro-grid [12]. Another notable system is the renewable hydrogen system located at the West Beacon Farm in Loughborough, UK [46].

Norsk Hydro and Enercon launched an autonomous wind-hydrogen demonstration system at Utsira Island, Norway in July 2004. Figure 1.7 shows the schematic of the wind-hydrogen system installed there. The main components installed in the system are an alkaline electrolyser with nominal capacity of 10 Nm^3/h and rating of 50 kW, a 600 kW wind turbine, a 55 kW hydrogen engine, a 5.5 kW hydrogen compressor (11 Nm^3/h, 12–200 bar, 2-stage, diaphragm), a pressurised hydrogen storage system with a capacity of 12 m^3 at a pressure of 200 bar, a 5 kWh flywheel, a 50 kWh battery, a 100 kVA master synchronous machine, and a 10 kW PEM fuel cell. The components in the Utsira wind-hydrogen system are connected to a 400 V, AC mini-grid with nominal frequency of 50 Hz [12]. The hydrogen stored in Utsira system is enough to supply 10 households on the island for 2 to 3 days without any extra source of power. The system has some grid stabilising equipment available such as a flywheel and battery energy stores. The flywheel is utilised for frequency control, and the master synchronous machine assists in voltage control and short circuit power. The NiCd battery was installed for redundancy [12].

Ulleberg et al. [12] discussed the Utsira renewable-hydrogen system and analysed the data from the project. However, this paper does not explain the exact algorithm used to run the electrolyser or components in the system, and it does not mention the maximum rate acceptable for the load change of the electrolyser or whether it was considered in the control strategy to run the electrolyser or not.

The electrolyser in Utsira project needed to operate on grid electricity frequently in order to avoid low pressure in hydrogen storage tanks due to the lack of wind power generation. This proved a rather poor design of the system, which needed to produce hydrogen with the electrolyser and consume it with the fuel cell simultaneously in some occasions. In a well-designed system, even on some rare occasions when there is not enough wind power for a long period of time and the pressure in the hydrogen

tank decreases significantly, the demand loads have to be supplied from the grid directly, otherwise production and consumption of hydrogen simultaneously is not efficient due to the low overall round trip efficiency of the hydrogen system. In such systems, the wind turbine and hydrogen production and storage systems must be sized properly to avoid such rapid decrease in pressure of the hydrogen tanks. This sizing depends on the annual wind energy profile, the load profile and the efficiency of the device to convert hydrogen to power [12]. However, the trade-off between hydrogen availability and overall cost of the system should be considered in any system design.

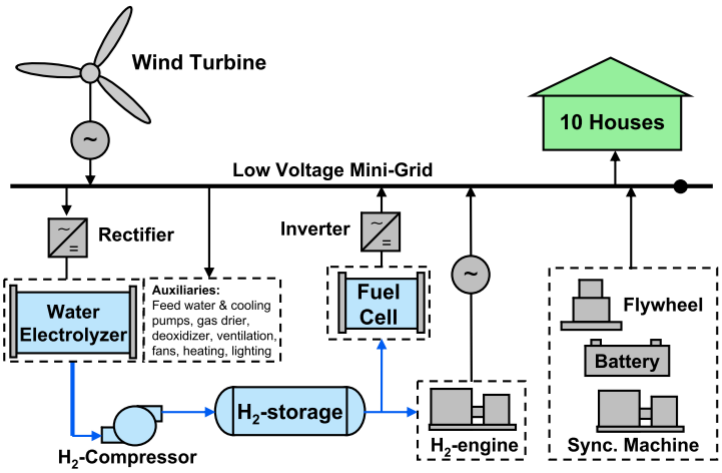

Figure 1.7 The schematic of the wind-hydrogen system installed at Utsira Island in Norway [12]

Unfortunately, it seems that the above factors were not considered in the design of the system for the Utsira project. For example, the electrolyser's nominal power demand (50 kW) was very small with respect to the installed wind turbine capacity of 600 kW, so the system was not able to capture all of the renewable power available during windy times [12].

The hydrogen and Renewable Integration (HARI) project, which became operational in 2004 near Loughborough, is also a project with operational experience [10]. The HARI project was the first demonstration project in the field of hydrogen production from renewable sources in the UK. The system had a 36 kW electrolyser to produce hydrogen from the excess renewable power in the system. The system had a compressed hydrogen storage facility and is large enough to accommodate inter-

seasonal storage. It had a hydrogen storage capacity of 2850 Nm^3 [12]. If the renewable power production in the system is not high enough to fulfil the demand, the hydrogen can be converted into electricity by fuel cells to compensate the power deficit in the system. The electrolyser in the HARI project has a nominal pressure of about 18bar, and the hydrogen is further pressurised using a mechanical compressor up to 137 bar before storage. The project is illustrated in Figure 1.8 and has been described in [46].

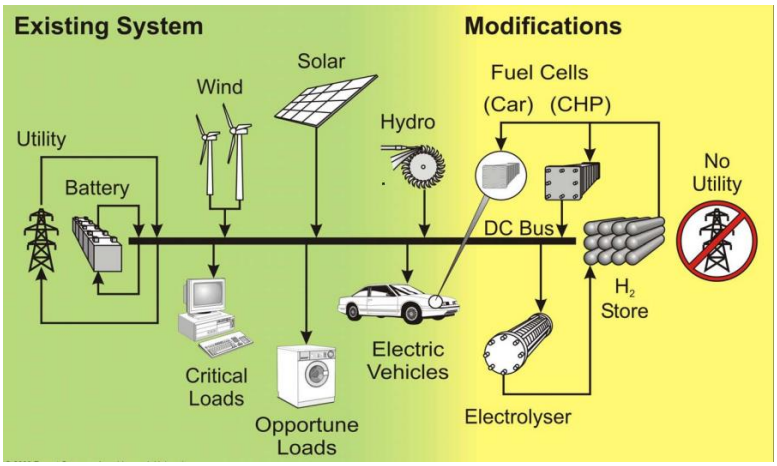

Figure 1.8 The installed system in HARI project at West Beacon Farm [47]

Deshmukh et al. [48] have simulated and assessed a solar-hydrogen system. This system consists of photovoltaic panels, electrolyser, fuel cell, compressor, and storage tank. The house in this system is able to receive electricity from grid, PV panels and also fuel cells. Their results show that there are no PV and electrolyser size configurations capable of providing both net-zero grid power and hydrogen balance for the system.

Kai et al. [49] have reported on a hydrogen filling station demonstration project located on Yakushima Island and included analysis of some operational data.

The PURE project is also another wind-hydrogen system in Shetland reported by Gazey et al. [50]. A detailed description of the project and the experience gained during the development and installation of the system is presented in [50].

The price of the components in a Wind/hydrogen system depend on their technology, their size, their manufacturer and some other factors such as the country that they were

manufactured in or purchased from. An estimation of the price of systems in a renewable hydrogen system in 2010 can be found in Table 1.2 [12].

Ulleberg et al. [12] concluded that further technical improvements and cost reductions need to be made before wind-hydrogen systems can compete with the existing commercial solutions, such as wind-diesel hybrid power systems, in remote areas. However, the introduction of 'green' incentives for hydrogen systems, an increase in oil and gas prices, and the security of supply advantage of hydrogen systems can eventually lead to the uptake of the hydrogen economy [12] and wind-hydrogen systems. It is also possible to utilise excess heat from electrolysers or fuel cells, or the oxygen produced, to achieve a higher overall efficiency in hydrogen systems.

Table 1.2 Typical price of main components in a wind-hydrogen system [12]

Component	Capital cost	Lifetime in years	Annual operation and maintenance costs (% of capital costs)
Wind turbine	800 €/kW (592 £/kW[1])	20	1.5
Alkaline electrolyser	2000 €/kW (1480 £/kW)	20	2.0
Hydrogen compressor	5000 €/kW (3700 £/kW)	12	1.5
Hydrogen Engine	1000 €/kW (740 £/kW)	10	2.0
Fuel cell	2500 €/kW (1850 £/kW)	10	2.0
Hydrogen storage	4500 €/m^3 (3330 £/m^3)	20	2.5

[1] The conversion factor of £1=€1.35 is used here

1.8 Demand Side Management (DSM)

Dynamic demand control is the method by which electrical devices can be operated to enable them to provide some important ancillary services to the power system without causing loss of service quality for consumers. These services include smoothing peaks in the daily electricity load profile and also helping to balance electrical demand and generation [51].

Many electrical devices, such as refrigerators, air conditioners, water heaters and pumps need energy to do their task, but they do not need to be operated continuously with an exact timing [51]. Dynamic demand appliances do not use less overall energy, but they simply do not consume electricity when there is not enough power generation, hence the aggregate impact of these appliances provides the potential for a significantly large dynamic demand response to reduce power system imbalances [51].

Demand Side Management (DSM) programs have been used for a long time to achieve different goals, such as increasing the efficiency of the power network [52]. There is a significant opportunity for DSM to increase the system investment efficiency due to the low utilisation of generation plants and the network, which is currently about 50% in the UK. The growth in renewable and other low-carbon generation technologies, the ageing of power system assets and advancements in information and communication technologies are major additional factors that could help the utilisation of DSM in the power system [53].

The power system, during times of high penetration of intermittent renewable power, is under stress due to the variations in the difference between generation output and demand and also the uncertainty in power market transactions. This can cause some problems such as network congestion, frequency fluctuations, voltage insecurity or even voltage instability [54]. Due to economic efficiency and technical constraints, some plants, such as nuclear or hydrothermal units, cannot be shut down immediately after start-up, or vice versa, but some other units, like gas turbine plant, can have quicker on/off cycles, but running gas units to supply load for a short time is very expensive [52]. It takes many hours for large thermal plants, such as coal and combined

cycle gas turbines, to increase their power output from a cold start due to the limitations on thermal stresses of turbines, pipes and boiler equipment [1].

Some general DSM benefits are listed below [53]:

- Utilisation of DSM devices on the power system can defer new network investment.
- It can increase the capability to install more distributed and stochastic (e.g. REs) generation.
- DSM devices can be connected to the currently available distribution network system.
- It can relieve voltage-constrained power transfer problems.
- It can relieve congestion in distribution substations.
- Outage management will be simplified and the quality and security of supply to critical load customers will be enhanced.
- It helps in the reduction of carbon emissions [53].
- It can improve the transmission capacity and also reduce the need for long-term network reinforcement [52].
- Responsive demands can reduce the problems with required spinning reserve resulting in a lower operational cost for the power system [52].

The utilisation of DSM technologies has not become widespread yet. Some of the reasons for such slow adoption of DSM technologies, particularly in the residential and commercial sectors, are listed below [53]:

- There is a need for a standard to be defined for dynamic demand appliances to determine which behaviours of an appliance qualify as dynamic demand response [51].
- To ensure system security, a legally defined and universally accepted and applicable standard is needed to be established through full public and technical consultation [51].
- There is not sufficient metering, information and communication infrastructure.

- The general understanding of the DSM advantages is not sufficient.
- Power system operation might become more complex with DSM systems.
- There are not enough market incentive strategies [53].
- If a large number of demand loads use off-peak electricity, then it will no longer be called off-peak, and also the price of electricity during those times will become higher. However, this will be self-regulating if the tariff systems works properly.

1.9 The rise of distributed generation and the need for Active Network Management

Transmission networks are already operating close to their capacity constraints, and adding renewable power generators at transmission level would require upgrading these networks with significant investment, so connecting generation to distribution networks has become more popular. As a result, there is a need to rethink about how to optimally arrange and operate the assets and devices on the distribution networks [55, 56]. The injection of power from Distributed Generators (DGs) can change the usual direction of power flows in radial distribution networks and can affect many factors such as power losses, voltage profiles and supply reliability [57]. Adding DGs can modify the costs of distribution network as outlined below [57].

- It can change operational and maintenance costs due to energy losses, the need for more sophisticated voltage control schemes, additional protection devices, and dealing with voltage quality problems.
- It can allow more local load to be added without reinforcement scince local generation could supply local demand.

Distribution companies (DISCOs) are responsible to make the decisions about feeder or transformer reinforcements if the system reaches one of the following technical or economic constraints [57].

- Unacceptable ohmic losses

- Network maximum power transfer capacity
- Maximum voltage deviation

Distributed Energy Resources (DER) are generation technologies (typically renewable generation), energy storage technologies and flexible demand located at distribution level [55]. Current distribution networks have been designed on a 'fit and forget' basis, so some technical issues could arise as a result of adding more distributed renewable generation within the network. Such issues include voltage rises due to the connection of generators or reverse power flows, which could result in the violation of network constraints. Therefore, there is a need to make distribution networks active by inclusion of responsive DER or controllable demands [58].

The voltage rise effect occurs due to the fact that the distribution networks are designed to be passive and pass power from the higher voltage transmission network down to consumers at the lower voltage, but DER can introduce power flows in two directions resulting in a change in the voltage profile on the distribution network. DGs need to operate at higher voltages to be able to export their power resulting in voltage rise problem on the distribution network. Without proper integration of DGs within the network, they can cause reverse power flows that exceed thermal limits in the distribution network and can put network assets at risk. Distribution networks are normally designed based on a 'fit and forget' approach which only considers the worst case scenario with maximum distributed generation and minimum demand, so the network will be able to operate in a passive way without a need for any control actions to limit the DG output. However, intermittent renewable resources such as wind farms only generate a fraction of their maximum output during most of their operational life, so the distribution networks are underutilised most of the time [58]. To reduce the electricity costs for consumers, the utilisation of the existing distribution assets should be maximised [58]. Active Network Management (ANM) techniques operate the network closer to its constraints by real time monitoring and controlling of the network parameters, such as currents, voltages, DG outputs and responsive or non-responsive load demands, and therefore their utilisation will allow more renewable power resources to be connected to the existing distribution networks while maximising the utilisation of network assets [59].

Some of the ANM techniques are listed below.

- Distributed generator dispatch control
- Renewable power curtailment [59]
- Load control
- Reactive power control [59]
- On-load tap changing (OLTC) transformer control [59]
- Energy storage
- Voltage regulators
- System reconfiguration

Some network operators can curtail wind energy to avoid violation of power system constraints. Energy storage systems are considered as a tool to avoid wind power curtailment [60].

1.10 Energy storage technologies and their role in power systems

The electrical energy can be stored in different forms such as mechanical, electro-chemical, chemical, electromagnetic and thermal energy [61]. Mathiesen and Lund [19] have presented different technologies to assist in the integration of fluctuating renewable energy sources into electricity supply systems, and electrolysis loads are considered as one of the options. The seven technologies identified in their paper to facilitate integration of more intermittent renewable power in the electricity network are listed below.

1) Heat pumps
2) Electric boilers
3) Electrolysers with local Combined Heat and Power (CHP)
4) Electrolysers with micro-CHP
5) HFCVs with electrolysers
6) Flexible electricity demand (around 5% of the electricity demand is flexible within one day and can be shifted according to the availability of wind power.)

7) BEVs

In addition, some of the other storage technologies are detailed in [61] and are listed below.

- Pumped Hydro Storage (PHS)
- Compressed Air Energy Storage (CAES)
- Flywheel Energy Storage (FES)
- Battery Energy Storage System (BESS). There are many different types of batteries available in the market, including Lithium Ion (Li-on), Lead Acid (LA), Nickel Metal Hybrid (NiMH), Nickel Cadmium (NiCd), Sodium Sulphur (NaS) and flow battery batteries. The typical flow batteries are Vanadium Redox Battery (VRB), Polysulphide Bromide (PSB) and Zinc Bromine (ZnBr).
- Superconducting Magnetic Energy Storage (SMES)
- Super-Capacitor (SC) [61]

Different storage devices have been explained and compared in details in [62], [61] and [63], and their applications, advantages and drawbacks are explained in details.

The main applications of energy storage devices are as following [61].

- Time-shift of generation and/or demand
- Load levelling
- Providing reserves
- Smoothing out the fluctuations of supply and improving supply continuity and power quality

Some of the applications of energy storage devices for power system operators to enable better integration of wind power are listed below [61].

- The storage devices can be controlled to use the limited transmission capacity effectively as the wind resources are usually located in rural areas that are far from existing transmission lines, which are already operating close to their constraints. Therefore, utilisation of energy storage can defer or avoid

transmission/distribution network upgrades (lines, cables and substations) and power system congestion.

- Storage can be used to time shift the supply to the time of high demand and avoid spillage of renewable electricity.
- The wind power variations can cause the frequency of the grid fluctuate. The energy storage devices can be used with a local droop control loop for the primary frequency control and smooth the variation of frequency. The droop control aims to produce an active power output change which is proportional to the frequency deviation. The energy storage devices can also be used as secondary reserves.
- They can be used to smooth fluctuations of the voltage on the power system as a result of variation in the wind power [61].

The energy storage technologies can have various benefits for different parties connected to a power system. The benefits of energy storage devices from the Distribution Network Operator (DNO) point of view are listed below [64].

- Voltage support
- Distribution losses reduction
- Capacity support and deferral of distribution investment

The benefits of energy storage devices from the Transmission System Operator (TSO) point of view are listed below [64].

- Reduction of transmission congestion
- Deferral of transmission investment

The benefits of energy storage devices from the Independent System Operators (ISO) point of view are listed below [64].

- Regulation
- Fast regulation
- Spinning reserve
- Non-spinning reserve

- They can enable the power system to be restarted after a black out [63]
- Price arbitrage

The benefits of energy storage devices from the end-users' point of view are listed below [64].

- Improvement of power quality
- Improvement of reliability by using local generation to supply local demands and reducing the occurrence of outages
- Reduction of time of use and demand charges

The UK network operator uses many different techniques to continuously match the supply with demand in the power system [65]. The electricity storage capacity of the UK has increased with much slower speed in comparison to the growth of the penetration of renewable power in the system, and so far other methods of matching supply and demand have been preferred [1]. The mere problem of low round trip efficiency in storage systems (e.g. less than 50% [11] in hydrogen systems with electrolysers and fuel cells) does not imply that there is no financial benefit from storing electricity. The strategy to store electricity could be based on market prices, hence when the electricity prices are low, the storage devices can store energy, and when the prices are high they can provide electricity back to the power system. Storage of renewable power offers benefits to both the supply and demand side of the power system, but the challenge lies in determining the best type, location and size of each storage technology. In the UK electricity market, the price differential between the input energy and output energy of storage facilities has to cover the round trip efficiency losses as well as other costs of the storage. The amount of investment in storage capacity in the UK also depends on the degree of integration of the UK power network with the EU and elsewhere in the future. For example, an adequate link to the Norway power system would provide access to more hydro power capacity [66]. A sufficient interconnection capacity between the UK and the EU power system can provide flexibility to both of the networks due to an increase in the effective network size by improving the import and export of electricity [1]. The government might also support storage in the future in the form of legally binding targets such as Renewable

Obligation Certificates (ROCs) or Feed-In-Tariffs (FITs). However, any government support should be based on proper life cycle and cost benefit analysis of storage technologies.

The different characteristics of energy storage devices need to be considered to find the best type and size of storage for each application. Such characteristics include capital, operational and maintenance costs, power and energy ratings, energy density, efficiency, ramp rate, response time, self-discharge losses, and life and cycle time [61]. Table 1.3 compares the main characteristics of some of the storage technologies.

Table 1.3 Details of energy storage technologies [61]

Storage name	Capital cost ($/kW)	Power rating (MW)	Discharge time	Response time	Efficiency (%)	Self-discharge per day (%)
PHS	600–2000	100–5000	1–24 h+	min	70–80	Very small
CAES	400–8000	5–300	1–24 h+	min	41–75	Small
FES	250–350	0–0.25	s–h	<s	80–90	100
LA	300–600	0–20	s–h	<s	75–90	0.1–0.3
NiCd	500–1500	0–40	s–h	<s	60–80	0.2–0.6
Li-on	1200–4000	0–0.1	min–h	<s	65–75	0.1–0.3
NaS	1000–3000	0.05–8	s–h	<s	70–85	20
VRB	600–1500	0.03–3	s–10 h	s	60–75	Small
ZnBr	700–2500	0.05–2	s–10 h	s	65–75	Small
FC	10,000+	0–50	s–24 h+	s–min	34–44	0
SC	100–300	0–0.3	ms–1 h	<s	85–98	20–40
SMES	200–300	0.1–10	ms–8 s	<s	75–80	10–15

As shown in Figure 1.9, Barton and Infield [62] have compared different feasible electricity storage technologies with respect to their economic suitability to balance the power system over different time scales. It shows that some storage devices like super-capacitors or flywheels are suitable for short term energy storage while hydrogen storage systems are more suitable for long term storage, i.e. storage for duration of more than a day. However, hydrogen storage in this figure refers to the case of producing hydrogen by electrolysers, storing it in tanks, and then using fuel cells to give electricity back to the grid when required. Such scenario is not considered in this thesis because a more efficient way of using hydrogen is to use them in HFCVs which will replace petrol or diesel ICE vehicles with lower efficiencies. In addition, the price of HFCVs will be paid by the owner of the car and not by the storage system operator, and thus the cost analysis for the work in this thesis is totally different from the one reported in [62].

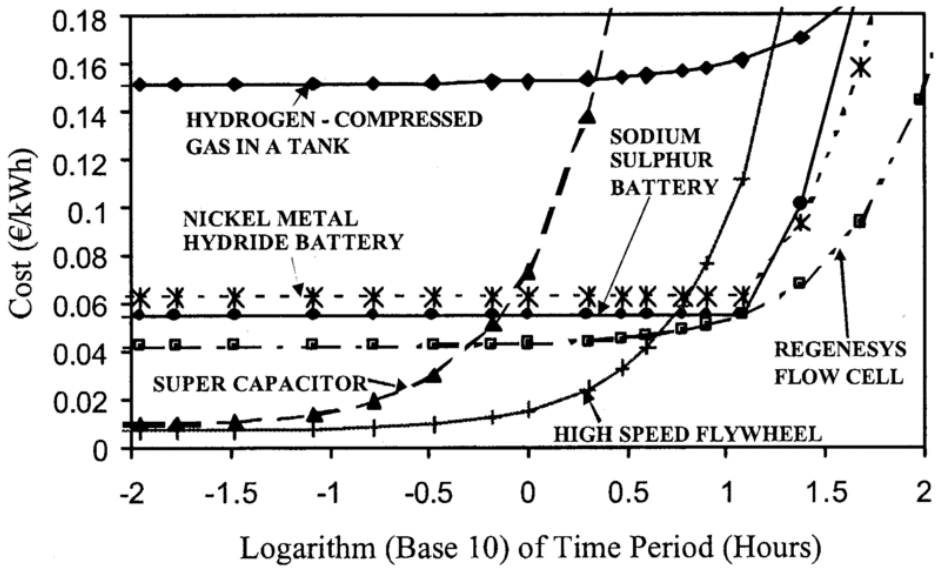

Figure 1.9 Costs of different energy storage technologies in different time scales [62]

Table 1.4 shows the suitability of various storage technologies to give different services to power systems with respect to the timescale of the service they can provide. However, again it should be noted that the electrolysis and fuel cell column in this table does not reflect the work in this thesis as the hydrogen is used in HFCVs in this PhD project.

Pumped-hydro storage schemes are the largest electrical energy storage facilities currently available within the UK with a round trip efficiency of around 70–80%. Pumped-hydro storage facilities mostly use their capacity for a daily cycle of buying and selling electricity. However, they are restricted to areas with specific geology and topography. Currently, the largest UK storage facility is the Dinorwig pumped hydro storage station in Snowdonia, North Wales which has a nominal capacity of 10 GWh. The total pumped-hydro storage capacity in the UK is 27.6 GWh, which is only 1.1% of the total electricity supplied to the UK grid in 2008 [1].

Table 1.4 Applications of various storage technologies [62]

Full Power Duration of Storage	Applications of Storage and Possible Replacement of Conventional Electricity System Controls.	Biomass.	Hydrogen. Electrolysis +Fuel Cell	Large Hydro	Compressed Air Energy Storage (CAES)	Heat Or Cold Store + Heat Pump.	Pumped Hydro	Redox Flow Cells.	New And Old Battery Technologies	Flywheel	Superconducting Magnetic Energy Storage (SMES)	Supercapacitor	Conventional Capacitor or Inductor
4 Months	Annual smoothing of loads, PV, wind and small hydro.	✓	✓	✓									
3 Weeks	Smoothing weather effects: load, PV, wind, small hydro.	✓	✓	✓									
3 Days	Weekly smoothing of loads and most weather variations.	✓	✓	✓	✓	✓	✓	✓					
8 Hours	Daily load cycle, PV, wind, Transmission line repair.	✓	✓	✓	✓	✓	✓	✓	✓				
2 Hours	Peak load lopping, standing reserve, wind power smoothing. Minimisation of NETA or similar trading penalties.	✓	✓	✓	✓	✓	✓	✓	✓				
20 Minutes	Spinning reserve, wind power smoothing, clouds on PV		✓	✓	✓	✓	✓	✓	✓	✓			
3 Minutes	Spinning reserve, wind power smoothing of gusts.		✓				✓	✓	✓	✓			
20 Seconds	Line or local faults. Voltage and frequency control. Governor controlled generation.							✓	✓	✓	✓	✓	✓

Another potential form of energy storage is adiabatic compressed air storage at a large scale; however, this still requires significant research. There is also significant potential for storing electricity in battery electric vehicles in the future if the number of these vehicles on roads increases significantly. This is a form of energy storage known as ‘Vehicle to Grid’ (V2G). However, due to the requirement of private transport vehicles to be charged and available most days, this type of storage is less able to provide acceptable benefits for the power system over weekly or longer timeframes [1].

Therefore, electrolysers should be considered as one of the options to improve the operational performance of the electrical grid, especially, in the case that the grid has a high penetration of variable intermittent renewable power [67]. Obviously, there are other options in the power system, such as batteries, fridges or pumped storage devices, which could be used for demand side management purposes, but they are limited, and they are not always available for participating in DSM. The other issue is that they might not be suitable for seasonal storage of electricity because in one season there might be significant amount of wind power, and in other seasons the amount of wind power might not be sufficient enough to satisfy the demand in the power system. However, but hydrogen could be stored for a long period of time and used whenever there is lack of generation in the system, or it also could be used in the transportation sector.

1.11 Optimal integration of storage devices within power systems

Non-optimal connection of DER could potentially affect the quality of energy supply and damage power system equipment. It can also result in violation of the power system constraints [56]. The optimal integration of storage devices in the network should be implemented to make sure that storage devices can improve the voltage profile and reduce line losses on the system, otherwise such storage devices can have an adverse impact on the network parameters, e.g. cause voltage drop. Therefore, the optimal integration of DER is essential to make sure they would have a positive impact on the network operation.

Some optimisation targets, from the DNO perspective, to integrate storage devices within the power system, are listed below.

- Finding the location and number of storage devices.
- Finding the size of storage to minimise capital costs.
- Finding the best load of storage during its operation to minimise the losses on the power system while respecting the power system constraints (thermal and voltage limits).

- Maximising renewable power integration.
- Minimising the costs of grid upgrade.

Solving such problem is usually addressed by using multi-objective optimisation methods [68].

Atwa and El-Saadany [60] have proposed a method to allocate energy storage in a distribution system with a significant penetration of wind power to maximise the benefits for the owner of DG and the utility operator. Their strategy tries to size the energy storage devices appropriately to avoid wind power curtailment and minimise the electricity bill. Their analysis compared the annual cost of different energy storage devices considering the total profit for both the utility and the DG owner.

Carpinelli et al. [64] have proposed a new cost-based optimisation strategy for the optimal placement, sizing and control of battery energy storage systems on the power system to provide different services such as loss reduction or reactive power provision. Their strategy minimises the whole system costs while considering the energy storage device profit from the price arbitrage.

Celli et al. [68] and Carpinelli et al. [69] have proposed methods to optimally allocate energy storage on the distribution network to reduce losses and defer network upgrades using Genetic Algorithms (GAs). Their method finds the optimal charge and discharge pattern of energy storage devices using inner algorithms based on Dynamic Programming (DP) [68] and Sequential Quadratic Programming (SQP) [69], respectively.

Nick et al. [70] addresses the problem of optimal siting and sizing of energy storage system using the multi-objective Alternative Direction Method of Multipliers process that considers the ancillary services, such as voltage support and loss reduction. Their proposed procedure also tries to manage congestion problems in addition to minimising the cost of electricity bills. They claim that their algorithm is capable of finding optimal solutions for large-scale networks.

Zheng et al. [71] have proposed a battery operation strategy to mitigate the operational risk from price volatility in a distribution network. In addition, they have addressed the problem of optimal sizing and siting for battery energy storage systems using a cost-benefit analysis method with the aim to maximise the profit of DNOs from energy transactions and operational cost savings.

Nick et al. [72] have worked on the problem of optimal siting and sizing storage systems within distribution networks to provide voltage support and reduce network losses using GA. Although their technique provides promising results, it is computationally expensive, and due to the non-convex and non-linear nature of the problem, finding the global optimal solution is not guaranteed.

An alternative approach to GA is Optimal Power Flow (OPF), which is a technique for optimal operation and planning of power systems [73]. Its aim is to optimise objective functions such as costs of fuel or the amount of losses on the power system by setting some control variables in an optimal way while satisfying the demand and grid operating constraints [73]. There are many possible control variables such as generator active or reactive powers, generator output voltages, and the demand from responsive loads or the ratio of tap changing transformers. The extended OPF formulation is a modified version of the standard OPF formulation, which includes additional variables, costs and/or equality and inequality constraints [74]. In this work, the utilisation of extended OPF will be investigated to size, place and control electrolysers in power systems using a heuristic approach to avoid the complications of control strategies that use GAs.

Different types of distribution network configurations are described in [75] and listed below.

- Meshed networks
- Interconnected meshed systems
- Ring systems
- Radial distribution networks

Radial distribution networks are normally used in rural areas for dispersed loads that typically cover large distances. The work presented in Chapter 3 of this thesis is mainly concerned with rural distribution networks.

1.12 Electrolysers in power systems

Currently most of the electricity generated for the UK power system is produced from fossil fuels. On average, there is 0.487 kg of CO_2 emission per kWh of electricity consumed in the UK [76], so if the electrolysers are run with such electricity, then it will result in 26 kg of CO_2 emission per kg of H_2 produced if the electrolysers consume 53.4 kWh/kgH_2. In hydrogen production by the methane reformation process, 7.33 kg of CO_2 is produced for each kg of hydrogen [77]. Therefore , if non-renewable power generation is used to produce electricity for water electrolysis, then hydrogen production can result in a significant amount of emissions [2], even more than the amount of carbon emissions from the SMR hydrogen production process, but this is highly depending on the mixture of power sources on the grid. However, in the case of high penetrations of renewable power, hydrogen production by electrolysers should cause less carbon dioxide emissions than direct hydrogen production from fossil fuels. It should also be noted that it is possible to control electrolysers to absorb the surplus carbon free power on the system to avoid causing any emission as a result of producing hydrogen. It is also important to note that for dynamically controlled electrolysers, the value of CO_2 emission for production of a kg of hydrogen will vary during the time depending on the variation of the amount of renewable power generation within the grid and also the carbon intensity of imported electric power.

As explained in the previous section, electrolysers could be used as dynamic demand in the power system to improve its performance. Unfortunately, there has not been any significant research work done by other researchers in the area of modelling electrolysers in the power system, or of quantifying their impact on the performance of the electricity network.

Most of the previous works in this area have made the assumption that electrolysers will be located next to wind farms and the extra renewable power from the wind farm will be injected to the electrolyser plant, but this cannot be a general assumption as future hydrogen filling stations might be tens or hundreds of miles away from the actual wind farms.

For example, Elbaset [78] worked on modelling and control analysis of a wind-hydrogen system that was supplying some local demands and had a connection to an electrical grid. He developed a program in *MATLAB* to simulate the operation and control of the wind-hydrogen system. However, the electrolyser and wind farms in his work were located close to each other, and this would certainly not be the case for all of the future UK hydrogen filling stations.

Barton and Gammon [79] have studied three UK energy supply pathways in which the greenhouse gas emissions would be reduced by 80% by 2050, and have investigated the role of electrolysers to address the problem of balancing the supply and demand within the UK energy system. However, they did not consider the impact of those electrolysers on the local network parameters or the need for upgrading the grid to accommodate those electrolysers. Their work considered different ways of hydrogen production and consumption. In contrast, the work presented in this thesis will only focus on the energy produced in electricity sector, and the hydrogen is assumed to be produced with electrolysers and consumed by HFCVs.

1.13 Utilisation of electrolysers for frequency stability of the power system

To keep the network frequency and voltage within its limits in real-time, the UK power network operator buys several different types of ancillary services such as frequency response and reserve services. It is more difficult and expensive to manage the power system with a high penetration of variable generation because the variability in supply would combine with the natural variability of the demand [51] and further complicate achieving supply/demand balance. If wind power penetration increases in a future power system, assuming there is only conventional supply side reserves available, the

amount of spinning reserve on the system needs to be increased due to increased uncertainty in the amount of this generation, and the conventional plants providing reserve would tend to work in part-loaded conditions with even lower efficiency and higher emissions [53].

In the UK balancing mechanism market, generators and suppliers of electricity provide bids and offers to adjust their generation. These bids and offers are complex and include the price of energy in the network and also various technical parameters such as the speed of change in the generation or demand. Different ways of providing balancing services should be viewed as complementary, rather than competitive, to promote low carbon energy resources in the power system [66].

Short et al. [80] have investigated the impact of dynamically controlled consumer demands (e.g. fridges and freezers) on the frequency stability of an electrical grid. Such devices would monitor system frequency, which is an indicator of supply-demand imbalance, and switch the appliances on or off, according to a compromise between the needs of the appliances and those of the grid. They made a simplified model of a power grid incorporating an aggregate generator inertia, governor action and load-frequency dependence, plus refrigerators with dynamic demand controllers, and modelled the frequency of the system during a sudden loss of generation and when the system had wind power generation. Their studies show that the frequency of the system will not fall immediately in the case of a decrease in the aggregate wind power generation in the system, and the dependence on rapid backup generation would be reduced if dynamically controlled fridges were to be used as dynamic demand to improve the frequency stability of the power system. They conclude that the use of dynamically controlled demand has the potential to provide a more cost effective solution for power delivery because it significantly delays the change of frequency at times of power imbalance. This delay would allow the power system operators to be able to utilise a wider range of backup generation and also use the generators that take more time to become available for serving the power system. Other demand loads, in the system, such as air conditioning devices or electric water heaters, can also provide frequency response services [80]. However, it is still not clear if the public will accept such demand side management schemes, or whether there are going to be any

significant financial benefits for the householders from participation. Such approaches are limited by the installed capacity of such appliances and the extent that they could be suitably modified. In addition, there are issues related to restoration of appliance temperatures following any significant use that reduces their availability as dynamic demand.

In June 2011, the Hydrogenics Corporation announced successful completion of a trial project with Ontario's Independent Electricity System Operator (IESO) demonstrating the grid frequency stabilisation capability of its electrolysers. During the trial period, the demand of a Hydrogenics HySTAT^{TM} electrolyser provided frequency regulation to the IESO system by responding to power regulation signals provided by the IESO on a second-by-second basis [81], but the project utilised only a single electrolyser to demonstrate such capability. It is expected that, in future, more electrolysers will participate in such schemes, and their aggregate impact should be further investigated from a grid stability point of view. The control strategy used by Hydrogenics in that project has not been published yet.

Vachirasricirikul et al. [82] have investigated the role of electrolysers in stabilising the frequency of a micro-grid in the presence of system parameter variations and different operating conditions, and a robust controller of the electrolyser and micro-turbine for frequency stabilisation was designed. A first-order transfer function is used as their electrolyser model. This is a rather inaccurate representation of the dynamics, because it does not consider the intrinsic ramping rate limitations of electrolysers. A sophisticated H-infinity loop-shaping method was used to design the controller. However, their system has a fuel cell, which is limited to constant power production, in the analysis. Simultaneous operation of electrolyser and fuel cell reduces the overall efficiency of their system significantly.

Li et al. [83] have also worked on the topic of stabilising the frequency of a micro-grid, and discusses the control techniques for combining a micro turbine with a fuel cell and electrolyser hybrid system to expand the micro-grid system’s ability to improve power quality issues resulting from frequency fluctuations. Their system comprised a micro-turbine, a housing load, a dynamically controlled HOGEN electrolyser, a hydrogen storage tank, 100 kW wind power source, 25 kW of

photovoltaic (PV), and a 5 kW proton exchange membrane fuel cell. The power consumption of the electrolyser in their system can be controlled over a period of milliseconds, which is sufficient to compensate for the power imbalances in the system. The paper proposes a fuzzy controller for controlling a micro-turbine with a fuel cell and electrolyser to deal with real-time frequency fluctuations. Their proposed control and monitoring system can also be used for the relaxation of tie-line power flow fluctuations [83]. However, the amount of hydrogen production and the amount of hydrogen stored in the system is not considered in their work. Many of the limitations of the approach of Vachirasricirikul and co-workers discussed above also exist in the work of Li.

A new generation of load controllers that can support stand-alone power systems and make use of standard grid-connected wind turbines was modelled by Miland et al. [84]. A hydrogen subsystem was included alongside a distributed intelligent load controller to control the frequency of the grid. The hydrogen subsystem was used as an energy store and also a dynamic demand at the same time. The stand-alone system in their research contained a 20 kW wind turbine, a 40 kVA synchronous compensator, a 6kW fuel cell, an 8 kW electrolyser, aggregate resistive load of 30 kW, base-load demand of 6 kW and a hydrogen storage facility. Their system also used the heat generated in the electrolyser and the fuel cell for local heating demands. The heat from their electrolyser and the fuel cell provided 33% of the annual heat demand. Their load controllers were based on fuzzy logic software algorithms, and they attempted to control the frequency of the power system by balancing the flow of active power in the system. The fuel cell in their system participates in the frequency control of the system, and it changes its output with respect to the frequency of the grid. In their work, the fuel cell is connected to the three-phase system through a DC machine and the mechanical shaft spinning the synchronous compensator. The efficiency of the system could be improved if power electronics were used instead of a DC machine and mechanical shaft spinning the synchronous compensator. The mechanical system used in their work also suffers from mechanical wear and maintenance problems in comparison to power electronics devices. A crude on/off control of the electrolyser was implemented, so no continuous dynamic control of the electrolyser loading was possible. In their control strategy, a minimum limit of two hours is considered for

on/off switching of the electrolyser. Due to the time period needed to purge the electrolyser with nitrogen gas before start-up and after shut-down, it is not recommended to frequently switch electrolysers on and off in stand-alone systems so such an approach has little value from a system frequency control perspective. In addition, as shown in Table 1.4, there are cheaper and more efficient ways of doing frequency control. The operation of the electrolyser with a constant load for a minimum period of two hours dropped the frequency below 48 Hz in some occasions during test because the electrolyser then consumed more power than the wind power available in the system. To have a better control strategy to run the electrolyser, they suggested adding average wind speeds for the last hour, a wind speed forecast, and the derivative of the system frequency as additional parameters to the control strategy. The amount of hydrogen production or the efficiency of the electrolyser were not considered in their work [84].

1.14 Objectives of this PhD work

If hydrogen becomes a widespread fuel in the future, then the total installed electrolysis plant may result in an aggregate capacity that equals or exceeds the other sources of dynamic demand, for example batteries, fridges or pumped storage devices. It is thus appropriate that the dynamic control potential of electrolysers is properly explored.

As explained in Section 1.6, some researchers have worked on electrolyser modelling, both in dynamic and steady state conditions, but the characteristics of electrolysers needed to model them in power systems have not been thoroughly investigated and explored in literature to date. In this thesis, for the first time, the characteristics of electrolysers required to adequately model them in the context of electrical power systems are explained and reported based on analysis of the results from experiments designed by the author. Such characteristics include minimum and nominal operational load, standby load, maximum time acceptable to stay in standby mode, impact of variable and intermittent load on the electrolyser lifetime, efficiency curve of the electrolyser with respect to its load, the maximum rate of power change acceptable by

the electrolyser, the number of times they could be switched on/off during a day, start up and shut down durations, and the nitrogen purging process.

Unfortunately, most of the power system models concerned with hydrogen production from electrolysers have been implemented in small stand-alone systems, rather than large integrated power systems. Most of the published papers in this area make the assumption that the wind turbines or photovoltaic cells are physically close to the electrolysers, behind the meter, and they only export electric power to the grid when there is more power available from the renewable sources than can be absorbed by the electrolyser because it exceeds the electrolyser maximum power demand. The point is that in real practical applications the electrolysers, as used in fuel stations for example, are unlikely to be located adjacent to wind farms or photovoltaic generation plants. The situation is very different if they are not on the same bus behind the same meter as the network operator has to deal with them separately, so there is a need to investigate other scenarios as well. Moreover, the published papers in this area do not address the problem of sizing or placement of electrolysers within power systems. This is an important problem as the benefits of energy storage devices are strictly dependent on their location, sizing and the control strategy to operate them as well as storage technology. Importantly, no one has considered the actual measured characteristics of alkaline electrolysers so as to realistically model them in the context of power system operation.

Lastly, nobody has considered electrolysers as tools to control the frequency of a large power system. However, as explained in Section 1.13, electrolysers have been modelled in small standalone micro-grids for the purpose of frequency control in a number of published papers, but even these works have many deficiencies.

Consequently, the aim of this thesis will be the identification and representation of alkaline electrolyser characteristics required to adequately model them as energy sinks within power systems and to explore their role in supplying hydrogen for FCVs in the context of power system operation. Such roles include:

- Utilisation of electrolysers to facilitate increases in the penetration of distributed wind power generation within the existing distribution networks while maintaining the power system within its constraints.
- Utilisation of electrolysers to stabilise the power system frequency during generation loss or in the case of high wind power penetration.
- Utilisation of electrolysers to absorb temporary excesses of clean carbon free power in various 2050 scenarios with different penetrations of wind, solar and nuclear generation, in addition to, various EV and HFCV demands within the UK power system.

The hydrogen produced by electrolysers is assumed to be consumed in future hydrogen filling stations which supply HFCVs. Figure 1.10 shows an overall view of the systems represented in this thesis.

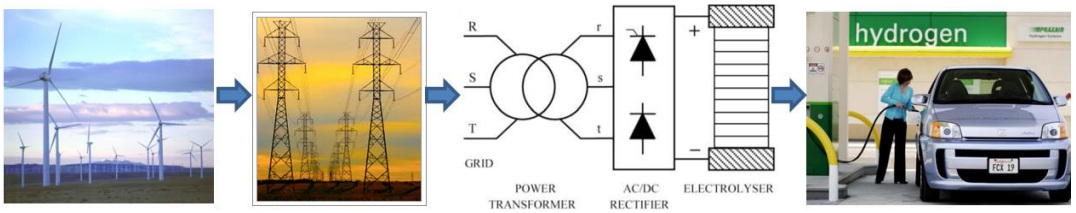

Figure 1.10 An overall view of the systems involved in this project

1.15 Thesis outline

To achieve the thesis objectives a research program was designed by the author which eventually led to the following outline for this PhD thesis:

In Chapter 1, a comprehensive literature review is carried out by the author and the areas that have not been investigated by other researchers in the field of modelling alkaline electrolysers in power systems have been identified and highlighted. It also includes a list of conference and journal publications by the author.

In Chapter 2, the characteristics of a 24 kW pressurised alkaline electrolyser from NEL Hydrogen Company are obtained using the experiments designed by the author. Some information about their large-scale (2 MW) atmospheric alkaline electrolysers is also

provided, which is useful in the modelling of such devices in electric power systems. In addition, a PEM electrolyser located at Strathclyde University has been tested and the results are included for comparison with the commercial alkaline units.

In Chapter 3, the use of alkaline electrolysers to increase the capacity of integrated wind power in the existing radial distribution networks is explored. A novel optimisation approach for sizing, placement and controlling electrolysers has been introduced, and its performance is assessed through modelling. The impact of increasing wind power capacity or the initial size of fuel stations has been investigated using a *UKGDS* model case study.

In Chapter 4, an investigation is carried out to find out the impact of alkaline electrolysers on the frequency stability of the power system in two cases: a 'generation loss event'; and also 'high wind power penetration'. The actual characteristics of alkaline electrolysers as reported in Chapter 2 are used for such modelling.

In Chapter 5, electrolysers are utilised to absorb surplus power within the UK electricity network and balance the system for different UK 2050 scenarios. Different penetrations of wind, solar and nuclear generation in addition to different penetrations of EVs and HFCVs will be considered for the different scenarios.

The conclusions and proposed future work are included in Chapter 6 of this thesis.

1.16 Thesis novel contributions

In this section, a summary of the thesis novel contributions to the research in the field of 'investigating the impact of alkaline electrolysers on the power systems' are listed.

- In Chapter 1 a comprehensive and crucial literature review on the hydrogen economy is presented including the role of alkaline electrolysers in a hydrogen economy, the modelling of alkaline electrolysers and their potential roles and benefits in the power systems.
- In Chapter 2, a report of the results of an experiment, which was designed by the author to identify the characteristics of a pressurised alkaline electrolyser,

is presented for the first time. Such characteristics, which are useful to model alkaline electrolysers in power systems, have not been previously reported in the literature. The novelty of this work is in the design and running of the experiment, and the interpretation and use of the results.

- In Chapter 3, a novel approach has been proposed to size, place and control electrolyser filling stations operating within power systems to increase the capacity of integrated wind power within radial distribution networks. The strategy uses an extended OPF approach to minimise network losses and maximise profit from operation of electrolysers while considering the network constraints and electrolyser characteristics. The actual characteristics of alkaline electrolysers are used for the first time to design a realistic control strategy to run them in the power system and find their impact on the electric network.
- In Chapter 4 electrolysers are utilised to stabilise the frequency of the power system in the case of a generation loss event and also in the presence of 25% wind power penetration. Again, the actual characteristics of alkaline electrolysers are used for the first time to design the control strategy. The amount of reduction in the power system frequency fluctuation and spinning reserve are quantified, and a new approach is proposed to find the aggregate nominal demand of electrolysers within the power system. The financial viability of using a droop control strategy to run the electrolysers is also assessed.
- The novel contribution of Chapter 5 is the determination of the size of electrolysers, their utilisation factor and the size of hydrogen storage capacity needed as well as the amount of hydrogen they can provide for fuel cell vehicles in different UK 2050 scenarios. Various capacities of wind, solar and nuclear power generation are considered in addition to different penetrations of EV and HFCVs. Moreover, the utilisation factor and size of conventional fossil fuel power plants needed to balance the system in each scenario is determined using simulation results.

1.17 List of published papers by the author

The journal and conference papers published or under preparation to be published by the author of this thesis as a result of this PhD work are listed below:

1.17.1 Journal papers

1.17.1.1 Published journal papers

1. Andrew Cruden, David Infield, Mahdi Kiaee, Tamunosaki G. Douglas, Amitava Roy, Development of new materials for alkaline electrolysers and investigation of the potential electrolysis impact on the electrical grid, Renewable Energy, Volume 49, January 2013, Pages 53-57, ISSN 0960-1481.
2. Mahdi Kiaee, Andrew Cruden, David Infield, Petr Chladek, Improvement of power system frequency stability using alkaline electrolysis plants, Proceedings of the Institution of Mechanical Engineers, Part A: Journal of Power and Energy, February 2013, 115-123, doi:10.1177/0957650912466642.
3. Mahdi Kiaee, Andrew Cruden, David Infield, Petr Chladek, Utilisation of alkaline electrolysers to improve power system frequency stability with a high penetration of wind power, IET Renewable Power Generation, 2014, 8, (5), p. 529-536, DOI: 10.1049/iet-rpg.2012.0190.
4. Mahdi Kiaee, Andrew Cruden, Petr Chladek, David Infield, Demonstration of the operation and performance of a pressurised alkaline electrolyser operating in the hydrogen fuelling station in Porsgrunn, Norway, Energy Conversion and Management, Volume 94, April 2015, Pages 40-50, ISSN 0196-8904, http://dx.doi.org/10.1016/j.enconman.2015.01.070.

1.17.1.2 Journal papers under preparation

5. Mahdi Kiaee, David Infield, Andrew Cruden, Utilisation of alkaline electrolysers in existing distribution networks to increase the amount of integrated wind capacity, Electric Power Systems Research, under preparation.
6. Mahdi Kiaee, David Infield, Andrew Cruden, Investigation of the prospect of hydrogen production with electrolysers in UK 2050 scenarios, International Journal of Hydrogen Energy, under preparation.

1.17.2 Published conference papers

1. Kiaee, M, Cruden, A, Infield, D, Ma, Y, Douglas, TG. The impact on the electrical grid of hydrogen production from Alkaline Electrolysers, 45th International Universities Power Engineering Conference, UPEC2010, Cardiff, 31st Aug – 3rd Sept 2010.
2. Andrew Cruden, David Infield, Mahdi Kiaee, Tamunosaki G. Douglas, Amitava Roy. Development of new materials for alkaline electrolysers and investigation of the potential electrolysis impact on the electrical grid, World Renewable Energy Congress XI and Exhibition 2010, Abu Dhabi, United Arab Emirates, 25-30 September 2010.
3. Kiaee, M, Cruden, A, Infield, D. The potential role of alkaline electrolysers on the frequency stability of the electrical grid, 2nd International Conference in Micro-generation and Related Technologies in Buildings: Microgen `II, Glasgow, United Kingdom, 4-6 April 2011.
4. Kiaee, M, Cruden, A, Infield, D. Demand Side Management Using Alkaline Electrolysers within the UKGDS simulation network, The 21st International Conference and Exhibition on Electricity Distribution, CIRED 2011, Frankfurt, Germany, 6-9 June 2011.
5. Mahdi Kiaee, Daniel Chade, Andrew Cruden, David Infield, Design of a system to investigate the performance of alkaline electrolysers during operation with intermittency of wind power, 4th World Hydrogen Technologies Convention Conference, WHTC 2011, Glasgow, United Kingdom, 14th to 16th of September 2011.

2 DETERMINATION OF ALKALINE ELECTROLYSER CHARACTERISTICS FOR POWER SYSTEM MODELLING

2.1 Introduction

To make a realistic model of alkaline electrolysers in the context of electrical power systems and, in particular, to identify appropriate control strategies for running them, a better understanding of their operational behaviour and their characteristics is needed.

In this chapter, two types of alkaline electrolysers, a pressurised and an atmospheric unit made by NEL Hydrogen Company, are detailed. In addition, a test on a PEM electrolyser located at Strathclyde University was carried out to compare its performance with the commercial alkaline units.

A technical visit to the Porsgrunn hydrogen filling station in Norway was undertaken in October 2011, during which a number of tests designed by the author were conducted and operational data was collected from the pressurised alkaline electrolyser installed at the site under different operational modes and then analysed. The author did not have the chance to obtain logged data from an operational atmospheric electrolyser; however the characteristics of an atmospheric alkaline electrolyser were obtained from the company and compared with the characteristics of pressurised units in this chapter.

This chapter presents a general overview of the Porsgrunn filling station and focuses on those characteristics of alkaline electrolysers relevant to their operational impact on electrical power systems. Performance of the electrolyser in different operational modes, especially when it is operating with time-varying renewable power sources, is discussed.

Understanding, in suitable detail, the characteristics of alkaline electrolysers will be important if such electrolysers become widely deployed. In particular, there is a need to develop appropriate control strategies such that the technology delivers the maximum economic and environmental benefits. To date, the relevant characteristics

of pressurised alkaline electrolysers have not been reported in open literature. This is regrettable since they are expected to become widely used for hydrogen production in the future, drawing energy from a power system anticipated to feature a significant proportion of its generation from time varying renewable sources. This chapter directly addresses these issues and provides detailed operational characteristics for this particular design of pressurised electrolyser.

At the end of this chapter a test, which was performed on a PEM electrolyser available at Strathclyde University, is reported to compare its characteristics with alkaline units. However, the PEM electrolyser has a constant rate of hydrogen production, so the operator is not able to change its demand to different levels while it is working in hydrogen production mode.

2.2 NEL Hydrogen

NEL Hydrogen is a company based in Norway with more than 80 years of experience in manufacturing alkaline electrolysers. The company mostly works on atmospheric electrolysers. The first pressurised electrolyser from NEL was introduced to the market in 2001.

The author contacted the NEL Hydrogen Company in March 2011 and received permission from the company to visit the Porsgrunn hydrogen filling station. The visit to the hydrogen fuelling station in Porsgrunn, Norway, was made in the last week of October 2011 to collect information and operational data from the pressurised electrolyser operating there and also to speak with the scientists and engineers working in the company about the characteristics of the electrolysers made by NEL Hydrogen.

2.3 NEL Hydrogen Electrolysers

A simplified flow diagram of the electrolysers designed by NEL Hydrogen is shown in Figure 2.1 [85].

This diagram shows the different parts of a commercial electrolyser. The functions of the individual parts are explained below.

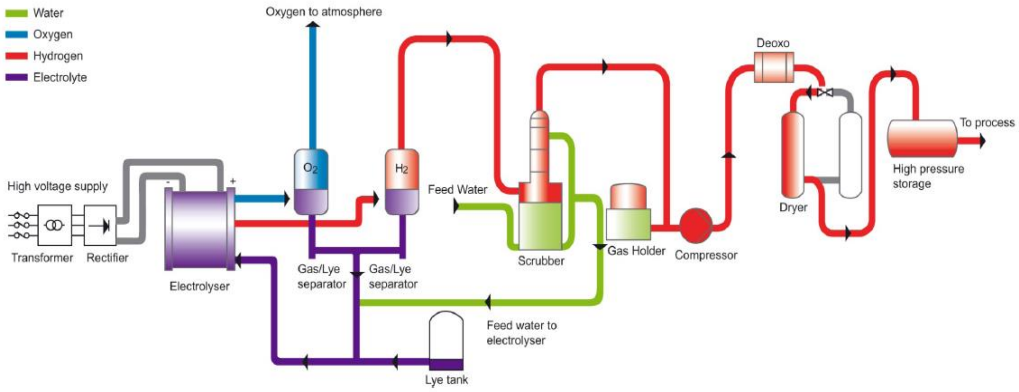

Figure 2.1 The simplified flow diagram of the electrolysers designed by NEL Hydrogen

Transformer: This changes the AC voltage level from the grid side to a level that is acceptable to the rectifier input. The input and output voltage of the transformer depends on the voltage of the grid connection point and also the required input voltage of the rectifier. For the 2 MW atmospheric electrolysers made by NEL Hydrogen operating at Rjukan-EKA Chemicals, the three phase voltage input of the transformer is 21 KV, and its three phase output voltage is 400 V.

Rectifier: This changes the AC voltage from the grid to a DC voltage that is acceptable for the cell stack. For the 2.1 MW atmospheric electrolysers made by NEL Hydrogen, the three phase voltage input of the rectifier is 400 V. The DC output voltage of the rectifier can change between 0 and 461 V, and its DC output current can change between 0 to 6,000 A. The rectifiers, which supply the cell stack, are of the current controlled type. There is always some loss in the system due to rectifier inefficiencies, which are variable, depending on the technology used to make the rectifier. The rectifier is normally included in the electrolyser package and should comply with consumer needs. The company that makes the rectifier must make sure that the rectifier complies with all of the appropriate electrical system standards, e.g. harmonic standards [86].

Electrolyser cell stack: Hydrogen and oxygen are produced through electrolysis of water in the cell stack. The bipolar electrodes of the filter press type electrolyser are

separated by diaphragms. Hydrogen gas is generated at the cathode and oxygen at the anode. The membrane is placed between the cathode and anode to separate the hydrogen and oxygen gases as they are produced, but it allows the transfer of ions between the two. The gas bubbles rise up through the electrolyte and are conveyed by internal ducts into separation tanks located at the front of the electrolyser.

Electrolyte System: This module consists of two gas separators and the electrolyte recirculation system. In the separators, the electrolyte is recovered and is then cooled and recycled into the cell stack. The electrolyte consists of a 25% (by weight) aqueous KOH solution. KOH acts as a catalyst to increase the speed of the reaction. The electrolyte also removes the heat generated inside the electrolyser. An increase in the rate of corrosion of the electrodes is a significant problem, which can happen in solutions with high KOH concentrations. Electrolyte is the main resistance component for the electrolysis process, and the 25% concentration value is selected to minimise the electrolyte resistance while considering its corrosion impacts.

Scrubber: The scrubber has three main functions, which are the removing of residual traces of electrolyte, the cooling down of the hydrogen and serving as a feed-water tank.

Separators: The hydrogen and oxygen produced in the stack are separated from the KOH solution in separation tanks.

Gas Holder: The gas holder acts as a buffer tank and is installed between the electrolyser and the compressor.

Compressor: There is an option of adding a compressor to the system to increase the output hydrogen pressure to higher levels, especially if the hydrogen is to be stored in pressurised tankers. The output pressure of atmospheric electrolysers is equal to 1 bar. At this stage, the output hydrogen gas from the gas holder is compressed to the required level (e.g. 400 bar) by one or more compressors.

Deoxidiser & Dryer: The hydrogen has a purity of 99.9% at the output of the gas scrubber. To achieve a higher purity level, the gas must be further purified. The impurities mainly consist of oxygen, water and nitrogen. The system removes oxygen

and water easily. The oxygen is removed by a catalytic recombination with hydrogen in a deoxidiser. The gas is dried by a twin absorption system consisting of two towers filled with a desiccant for water absorption. While one of towers is in operational mode, the other one is in regeneration mode. At the end of the process the purity of hydrogen will be very high, at close to 99.993%, depending on the plant configuration.

Gas Storage: A pressurised hydrogen storage system could be installed at the hydrogen production site. The size and pressure of the storage vessels will depend on the requirements of the customer and also the optimised technical and economical solutions.

The electrolyser has several auxiliary devices that together are called the balance of plant (BOP) and consume power, even in standby mode. The BOP load at each moment could be found by finding the difference between the input AC power of the system and the DC load of the stack. This extra load decreases the overall energy efficiency of system. The rectifier, compressor, instrumentation, Programmable Logic Controller (PLC), some of the valves and pumps, cooling fans, etc. are some of these parasitic loads.

There is the possibility of increasing the capacity of an installed electrolysis plant due to the modular design of the system. With an advanced PLC control system, the plant runs automatically and unattended, and only routine shift inspections are required. The electrolysis plant is continuously monitored by control and alarm devices, and a failure will always cause the plant to shut down automatically in a controlled manner.

A replacement of the cell stack would typically be required after approximately 10 years. The remaining electrolyser and plant can run for a long lifetime of 30-40 years provided a good maintenance schedule is followed.

2.4 Large-scale atmospheric electrolysers (2.1 MW)

Figure 2.2 shows a large-scale atmospheric electrolyser with its hydrogen and oxygen gas separation tanks. The nominal load of this electrolyser is rated at 2.1 MW and uses

a DC power supply rated at 5,150 A. It has 230 cells connected in series. The hydrogen production capacity of this unit is 485 Nm^3/h. These electrolysers have circular shaped cells with a diameter of two meters. Table 2.1 shows the technical specifications of these units. They operate at a nominal temperature of 80°C and pressure of 1.02 bar.

Figure 2.2 An atmospheric large-scale electrolyser with its separation tanks

The lifetime of these atmospheric electrolysers depends on the nature of the electrode activation layer. The activation layer of these units does not tolerate very high current densities, and working under such conditions can decrease their lifetime and efficiency.

Figure 2.3 shows the electrode of a large scale atmospheric electrolyser with a diameter of two meters. The electrodes are made from nickel based materials and have some coating materials that act as catalyst. NEL Hydrogen does not use expensive materials in the electrode coating. The two ducts on top of the electrodes are designed for hydrogen and oxygen gas flow. Hydrogen flows in the bigger duct while oxygen flows in the smaller one. The two smaller ducts at the bottom of electrodes are designed for circulation of lye in the system.

Table 2.1 Technical data of atmospheric electrolysers made by NEL Hydrogen

Hydrogen production capacity range	Up to 485 (Nm^3/h)
Maximum hydrogen production per cell	2.11 (Nm^3/h/cell)
Nominal load power	2.1 MW
Power consumption at DC current of 4000A	4.1±0.1 (kWh/Nm^3)
Power consumption at DC current of 5000A	4.3±0.1 (kWh/Nm^3)
Hydrogen purity before purification (%)	99.9±0.1
Oxygen purity before purification (%)	99.5±0.1
Hydrogen purity after purification (%)	99.9998%
Hydrogen outlet pressure after electrolysis	200-500 mm WG
Operating temperature	80° C
Operational range	20%-100% of maximum load
Electrolyte	25% of KOH solution
Feed water consumption	0.9 litre/Nm^3 of hydrogen
Weight	44 tons
The maximum acceptable current	5150 A
Nominal operating current density	250 mA/cm^2

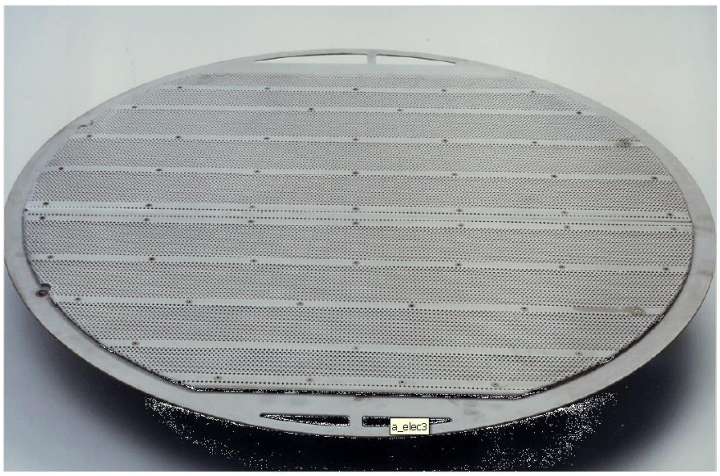

Figure 2.3 The electrode of a large-scale atmospheric electrolyser

Figure 2.4 shows the non-asbestos diaphragm of one of the cells in a 2.1 MW electrolyser.

Figure 2.4 The non-asbestos diaphragm of a large-scale atmospheric electrolyser

2.4.1 Characteristics of the large-scale atmospheric electrolysis units

There is a maximum rate of 135 kW/min (2.25 kW/s) for the acceptable power change by these atmospheric electrolysers. This limitation is to allow enough time for the system to remove the product gas from the cells, so that the volume of gas in the cells at any time will be fully controlled. The quantity of bubbles in the separators can also

limit the allowable power ramping rate, hence to have a fast response, the system needs large separators.

The system should allow enough time for the displacement of gas by lye or lye by gas. The flow rate of the electrolyte is sufficient to allow the required cooling and also the effective removal of the gas produced from the cells. It is not possible to increase the rate of this displacement by increasing the lye velocity because it can damage the stack and also the separator tanks due to the effect of water hammer. To increase this rate without increasing the pressure, the frame geometry would have to be re-designed. It is also worth mentioning that the ramp-down rate of the load of these units is the same as their ramp up rate.

The hydrogen and oxygen gases normally get mixed to some extent in the stack and separators, through the communicating KOH pipe or by diffusion of gases through membranes. It is more probable that the hydrogen diffuses into the oxygen compartments than vice versa as hydrogen has smaller molecules. Hydrogen and oxygen mixtures will become explosive if the amount of hydrogen in air exceeds the Lower Explosion Limit (LEL) of 4% [10], so the maximum limit for the amount of impurity of gases in any hydrogen system is 4%, but NEL Hydrogen normally sets this limit to 1.8% to have a better safety margin.

Alkaline electrolysers have a defined minimum operational load point because at lower current densities gas impurities build up, eventually to an unacceptable level. Gas quality decreases at low current densities due to secondary electrolysis[2], gas crossover through the diaphragm and gas mixing due to the mixing of anolyte and catholyte in the lye circuit. The anodic and cathodic chambers are completely gas isolated, and they are in communication only via lye exchange through the diaphragm and the common lye circuit. At low current densities, there is more leakage of gases from one chamber to the other [87].

[2] Secondary electrolysis is an undesired phenomenon caused by parasitic currents. Basically, it means that the gases are produced on other metallic surfaces rather than on electrodes and in other chambers rather than the intended ones, e.g. hydrogen on the anodic side and oxygen on the cathodic side.

The atmospheric electrolysers made by NEL Hydrogen have a 20% minimum load, and it takes 12 minutes to increase their load from the minimum amount to the nominal value of 100% with a ramping rate of 135 kW/min, and therefore the current atmospheric electrolysers made by NEL Hydrogen are not very suitable for operation with fast fluctuating wind power.

In standby condition, these electrolysers will consume approximately 1.5 kW/unit, mainly due to the electricity consumption of their control system and circulation pumps.

Electrolyser manufacturers often use the 'on-off cycle' term to represent the lifetime of their electrolysis units. Some electrolysers in the market, depending on the type of electrodes, have a maximum limitation for the number of times that they can be switched on/off or operated in standby mode during their lifetime. Their cell voltage could increase due to corrosion caused by such on/off switching without increasing the current, and this could increase the power consumption of the stack after a while. This corrosion happens due to the reversal of the cathodic current. An increase in the electrolysis voltage increases the energy consumption without increasing the hydrogen production [10]. In addition, the rectifier or transformer might not be able to cope with such excess power demand. The lifetime of electrolyser could be defined based on the maximum voltage acceptable for the electrolysis process considering technical and economic aspects. Some companies like Hydrogenics claim that they have solved this problem of degradation due to on/off switching. Appendix 7.1 explains their experiment on their alkaline electrolyser in more details.

Using the average electrode degradation during a long period of time, the number of times that the electrolyser can go into standby condition or be switched on/off during a day can be estimated. The atmospheric electrolysers made by NEL Hydrogen should not be switched on/off more than three times a day, due to the adverse impact of switching on the lifetime of their electrodes.

Generally, the lifetime of the electrolyser is determined by the needs of the customer, e.g. power consumption of the unit for production of a kilogram of hydrogen, or by the gas purity levels. Any time that the consumer feels that the energy consumption of

the electrolyser is more than they require, they can refurbish or change the electrolyser. It is possible to refurbish the electrolyser after its lifetime. The cost of such refurbishment is about 30% of the cost of the whole electrolysis system. As long as the atmospheric electrolyser works within its operational load limits, the variability of its load will not have an impact on its lifetime, but if the current of the stack becomes zero or negative then the electrodes might degrade.

It takes some time for electrolysers to begin working normally when they are started from the shut-down condition. For atmospheric electrolysers, it takes 25 minutes to purge the system with nitrogen gas before the start of their operation, and then it also takes approximately 12 to 15 minutes to get to the nominal hydrogen production state, so in total large-scale atmospheric electrolysers have an approximate start-up duration of 40 minutes to reach their nominal demand.

The electrolyser cell stack does not consume any power during the shut-down process. The controlled normal shutdown process takes about 30 minutes, which is mostly due to the nitrogen purging process that consists of 6 cycles of pressurisation and depressurisation of the electrolyser with nitrogen gas. Alkaline solution remains in the cells for a long time, even after the nitrogen purging process.

During the purging process, the nitrogen does not go into the cells, but rather into the separators and scrubbers. The main reason for purging the electrolyser is to ensure that all of the hydrogen is ejected safely from all parts of the electrolyser system. If the consumer wants to shut down the electrolyser and restart it again immediately, then one purging process would be enough.

Due to the existence of a minimum load in an electrolyser, the electrolysers in standalone systems should be sized properly; Otherwise, if the electrolyser is large with respect to the amount of installed renewable power generation capacity in the system, the system will have a significant decrease in the overall energy efficiency when there is not enough renewable power to run the electrolyser in hydrogen production mode. In addition, due to the duration of time needed to switch electrolysers on/off, an electrolyser in a standalone system cannot simply be switched off while there is not enough renewable power for a short period of time.

The electrolyser has a cooling system to maintain the temperature of the lye within the operational limit. This cooling system has a PID controller to cool down the lye with water. An atmospheric electrolyser does not have any heater to increase the temperature of the lye as it uses the heat from the electrolysis process to operate within its operational temperature limit, but a heater could also be incorporated in the system by the designer to increase the efficiency in cold-start situations when the lye is not warm enough. The extra dumped heat from the electrolyser could be used to heat houses or offices near the electrolysis plant.

These atmospheric electrolysers can stay in standby mode as long as their lye temperature is kept within acceptable limits, and if the system uses a heater to keep the lye warm, then the system can be kept in standby mode as long as the gas quality is within its acceptable limits. However, the gas quality will eventually deteriorate by diffusion, and then the electrolyser has to go into shut-down mode.

In alkaline electrolysers, there are always some bubbles generated within each cell, and they have an impact on the efficiency of the cell stack [24]. The atmospheric electrolysers made by NEL Hydrogen do not need to have a zero-gap configuration because they work at low current densities where the impact of bubbles is not significant, so there is a slight gap between the electrodes and the membrane, and the generated bubbles slightly degrade the performance of the electrolyser.

2.4.2 Costs of large-scale atmospheric electrolysers

This section provides some information about capital, operational and maintenance costs of large-scale electrolysis plants.

2.4.2.1 Capital costs

The contribution of each item to the total capital cost of the system is listed below in percentage terms.

1) Power supply equipment (e.g. transformer, rectifier): 15%
2) Hydrogen production equipment: 43%
    - Feed water (raw water and deioniser)
    - Cooling water
    - Electrolyte system
    - Hydrogen production system: 33%
3) Hydrogen processing equipment: 26%
    - Purification
    - Compression (30 bar): 16%
    - Export metering
4) Onsite infrastructure: 7%
5) Safety systems: 5%
    - Closed drain
    - Nitrogen system
    - Fire water
    - Vents
6) Instrument air[3]: 4%

2.4.2.2 Operational and maintenance costs

Most of the operation and maintenance costs of a large-scale alkaline electrolysis system is due to the electrical power consumption for hydrogen production. Less than 2% of the operation and maintenance costs is due to other factors. The percentage contribution of each item to the operation and maintenance costs is listed below.

1) Electricity: 98.3%

[3] Instrument air is used for plant pneumatic instruments such as pressure controllers and valve positioners. It supplies air to air-actuated automatic valves.

2) Remaining: 1.7%

    - Cooling water make-up[4]
    - Operation and maintenance
    - Electrolyte charge and make-up
    - Raw water
    - Purification cartridges
    - Emergency (Nitrogen, diesel back-up)

Labour costs are insignificant as the plant runs automatically and unattended, and only routine shift inspections are required. The annual maintenance costs are typically 1-2% of total investment, excluding major overhauls, which take place every 7-9 years.

2.5 Hydrogen filling station at Porsgrunn, Norway

The hydrogen station at Porsgrunn was opened in June 2007 by StatoilHydro (now NEL Hydrogen). Figure 2.5 shows the overall view of the Porsgrunn hydrogen fuelling station. It comprises the following sub-systems:

- A 12 bar(g) pressurised alkaline electrolyser system rated at 24 kW
- Compressors to pressurise the hydrogen gas
- Gas storage tanks with capacity of 6.3 m^3 in pressurised tanks at 450 bar(g)
- Two wind turbines (6 kW each)
- Two mono-crystalline PV panels (2.5 kW each)

One HFCV, and other cars with ICEs modified to burn hydrogen make use of the filling station. The electrolyser is directly coupled to the compressors and a gas storage sub-system. The hydrogen fuel dispenser has two nozzles with nominal pressures of 350 bar and 700 bar.

[4] Changing or replacing

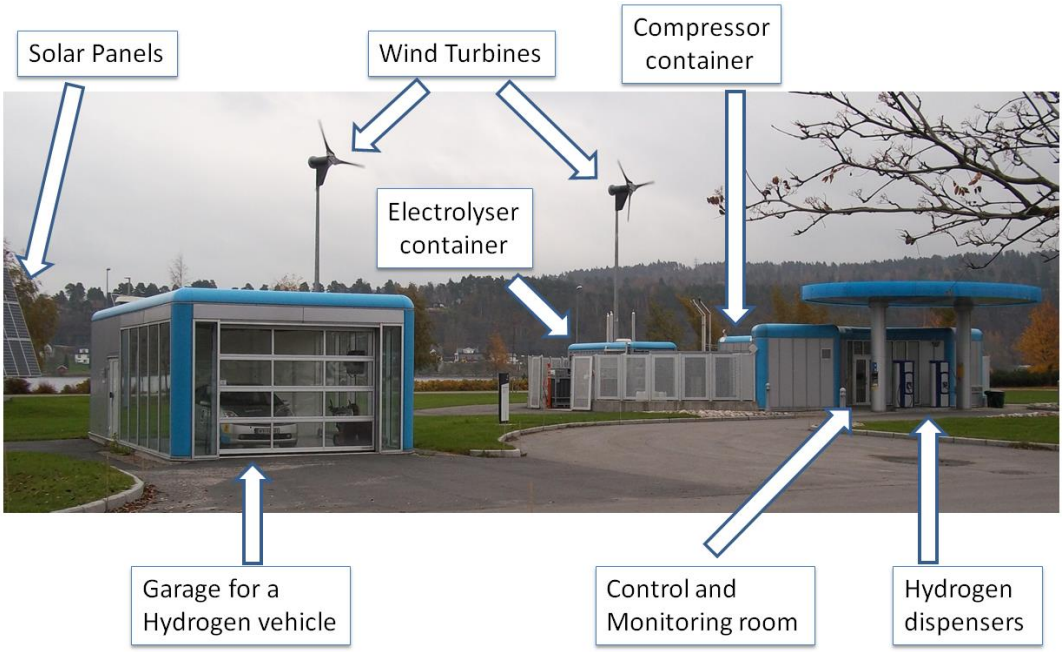

Figure 2.5 The overall view of the hydrogen fuelling station in Porsgrunn, Norway

The data acquisition system installed in the station has the ability to measure the voltage of the stack, DC current, pressure, temperature, purity of the gases, lye level in the separators, wind and solar power with a high time resolution of 10 ms. Figure 2.6 shows a schematic of the energy park and the way the sub-systems are connected together. The hydrogen needed for the cars can also be provided by the INEOS Company, which is located nearby and produces Chlorine, with hydrogen as a by-product, so the filling station has been designed to make use of the by-product hydrogen as well as the hydrogen specifically produced using the onsite electrolyser.

The pressurised alkaline electrolyser is designed to work with time-variable power from renewable resources, but the electrolysis system does not directly use the renewable power as the whole system is grid-connected. All of the renewable generation is exported to the grid via a DC to AC converter (grid-tied inverter), which is connected to a three phase 400V AC distribution line. However, the operators are able to adjust the power supplied to the electrolyser to reflect the time-varying output measured for the renewable sources at the site. In this way, the electrolyser is exposed to changes that would apply had it been an autonomous system, but without the requirement to maintain system stability, which can be a challenge with such systems.

The battery installed in the station is only used to support the control system during the loss of power from the grid or emergency conditions.

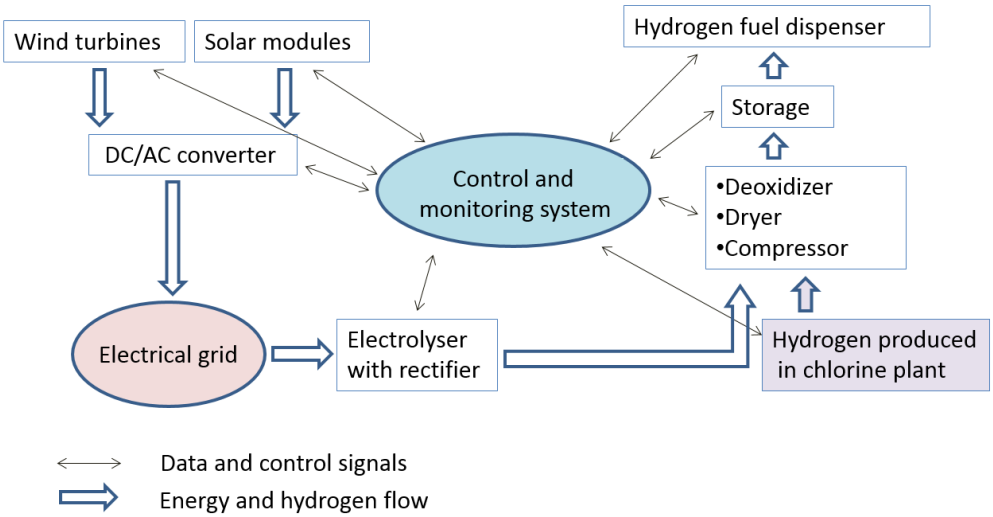

Figure 2.6 The connectivity between the different systems in the Porsgrunn energy park

2.6 Pressurised alkaline electrolyser in the station

The 24 kW pressurised alkaline electrolyser installed at the filling station is formed of a stack of 10 cells; Table 2.2 shows the technical specification of this unit.

The operating temperature and pressure of this electrolyser are 60°C and 9-15 bar(g). The consumer can select the exact operating pressure of the system using a set-point control signal, but the nominal pressure of the system is 12 bar(g). Operating the system at high temperatures can cause corrosion in the electrode material, and the rate of lye evaporation also increases, especially in atmospheric electrolysers. In pressurised electrolysers, there will be a problem with the stability of materials at high temperatures. Normally, the system experiences some limited oscillation (a few degrees) in the temperature while operating in the normal hydrogen production mode.

The operational range mentioned in Table 2.2 is based on the proposed minimum load for the electrolyser, but currently its minimum load is only 8.63% of nominal load. In the Porsgrunn hydrogen filling station, there is no sensor to directly measure the

amount of hydrogen produced, and this amount is therefore estimated based on the electrical current supplied to the cell stack. The electrolyser in the station has the ability to work with any power profile desired by the operator, e.g. solar power, wind power or solar and wind power combined.

Table 2.2 The specifications of the pressurised alkaline electrolyser

Electrolyte	30% weight KOH solution
Nominal pressure	12 bar(g)
Number of cells (N_C)	10
The active area of each electrode	1,900 cm^2
Operational load range	18%-100%
Operation temperature	60° C
Maximum acceptable current of the stack	1440 A
Maximum load ($P_{N.El}$)	24 kW
Ramp rate	18,480 kW/min (308 kW/s)

Due to the modular design of the system, there is a possibility that the capacity of the installed electrolysis plant could be expanded. Using an advanced PLC control system, the plant can run automatically and unattended with only occasional routine inspections required. The electrolysis plant is continuously monitored and alarms signalled in the event of problems, and any component or system failure will cause the plant to shut down automatically in a controlled manner.

There is a maximum acceptable rate of change for alkaline electrolyser loads. The maximum rate of power change that is acceptable for this particular 24 kW pressurised unit is 18,480 kW/min (308 kW/s), and in terms of current, this is approximately 924 kA/min. The nominal load of the electrolyser is 24 kW, so the maximum rate of

acceptable power change for this unit is 770 pu/min (12.8 pu/s). This means that the device can change its load from zero to nominal load in less than 1/12 of a second.

The lye (electrolyte) velocity should be enough to remove all gas from the cells in an acceptable time. Pressurised alkaline electrolysers have quicker response times than atmospheric designs because the total volume of gas within them during operation is less as a result of the high pressure working conditions. This is the main reason why, when the system is re-started following a shut down when the pressure has been reduced to atmospheric levels, it cannot immediately operate at full load. However, if the system is maintained in a pressurised standby condition, then it is possible to increase its load much more quickly. In addition, a system with larger separators offers a quicker response time.

The maximum rate of power change acceptable by NEL Hydrogen large scale 2.1 MW atmospheric alkaline electrolysers is 135 kW/min (2.25 kW/s), which is 135 times lower than the speed of the pressurised electrolyser at Porsgrunn, despite the fact that their nominal load is 87 times larger. This means that the maximum rate of power change of these atmospheric units is 0.064 pu/min (0.0011 pu/s). The pressurised electrolysers have quicker response time, so they are more suitable for operation with intermittency of wind power. If the 2.1 MW electrolysers were pressurised, then their maximum rate of power change could be increased significantly. It is difficult to make large-scale (2.1 MW) pressurised electrolysers due to leakage problems under pressurised conditions. The pressurised stack should be tight enough to avoid any leakage of gases.

A week before the experiment, the membranes of the cells were changed to new, more efficient, membranes having lower energy consumption. However, the impurity of gases as a result of using this membrane is higher. There is always a trade-off between the energy consumption of the membrane and the impurity of gases coming from the cells, which is dependent on the diaphragm. A more conductive diaphragm has lower energy consumption, but results in higher gas impurity. The first diaphragm, which was previously installed in the electrolyser, required about 10% more energy consumption.

There is not a visible gap between the electrodes and the membrane in the pressurised electrolyser (zero-gap configuration), and there is not any significant bubble impact on the performance of the electrolyser. There is a gap between the bipolar plate and electrode, which is filled with lye, and the bubbles are released there in the cell. In this gap (between bipolar plate and electrode), as shown in Figure 2.7, there is also a pressure element (current conductor), which performs the following functions.

1. It maintains the zero-gap between the electrodes and diaphragm by keeping the electrode in intimate contact with the diaphragm.
2. Conducts current between the bipolar plates and electrodes.
3. Provides space for gas bubbles.

Only one side of each electrode, which is the one closest to the other electrode, is activated and involved in the electrolysis reactions. It is true that the other side and also pressure elements and bipolar plates can be theoretically involved in electrolysis, but because they are further away from the zero gap, the ohmic resistance is higher, and thus the voltage required to produce the gas on them is also higher.

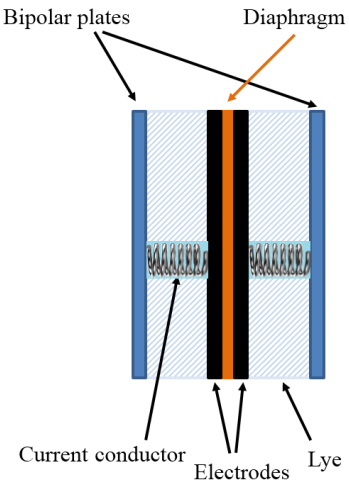

Figure 2.7 An electrolysis cell with zero-gap configuration

A limit of 80A is the minimum allowable set-point current for the cell stack to avoid an unacceptable increase in the impurity of gases in the system as a result of working under low current densities. However, the actual current is always slightly lower than this due to the fact that the rectifier output current is always lower than its set-point

because of the rectifier characteristics. If the set-point current for any reason falls below this value, the system goes into standby mode, maintaining the pressure of the system. To achieve this, the control system forces the current set-point to 0A as soon as the power supplied by the renewable energy resources falls below the required critical value. The standby load of this type of electrolyser is less than 1 kW/unit, regardless of its power rating.

The minimum power consumption of the electrolyser cell stack could be easily calculated from the following equation:

$$P_{Min.Stack} = I_{min} * V_{min} = 70 * 15.3 = 1071\ W \quad (2.1)$$

where

$P_{Min.Stack}$ is the minimum load of the electrolyser cell stack (W).

I_{min} is the actual minimum current acceptable by the cell stack (A). It is equal to 70A when the reference current is set at the minimum level of 80A.

V_{min} is the voltage of the stack when the cells have minimum current (V).

Therefore, the percentage of the minimum load of the electrolyser can be calculated from the following equation.

$$P_{Min.El}\% = \frac{P_{Min.El}}{P_{N.El}} * 100 = \frac{P_{Min.Stack} + P_{BOP}}{P_{N.El}} * 100 = \frac{1.07kW + 1kW}{24kW} * 100 =$$

$$\frac{2.07kW}{24kW} * 100 = 8.63\% \quad (2.2)$$

where

$P_{N.El}$ is the nominal load of the electrolyser (i.e. 24 kW).

$P_{Min.El}$ is the minimum operational load of the electrolyser plant to work properly in normal hydrogen production mode (kW).

P_{BOP} is the Balance Of Plant (i.e. 1 kW).

By separating the lye handling system for the anodic and cathodic parts, the gas quality could be improved, thus the electrolyser operational range could be broadened even further [87]. The electrolyser has been shown not to exhibit any additional degradation as a result of variable load operation within these limits.

The electrical rectifier supplying the cell stack is a three phase thyristor-based unit, and its output current is controlled, thus allowing regulation of the hydrogen production rate. Due to the specific I/V curve of the electrolyser, its voltage is not very sensitive to the small variations in its current, but the current and subsequently the load of the electrolyser are very sensitive to the voltage of the cells. Due to the aging of the electrodes, the IV curve of the electrolyser can shift upwards or downwards with time, depending on the design of the electrodes, so it is better to directly control the current of the cell stack, as done here, rather than its voltage. The rectifier can provide up to 42 kW (850A, 60V) to the electrolyser. In addition, the rectifier output current is controlled via a signal from the PLC device. It is possible to connect the pressurised units directly to the renewable power source without any rectifier.

The nominal operating current density of the electrolyser is 400 mA/cm^2, and the maximum acceptable current of this electrolyser is 1,440 A. This limit is imposed because of the current limit of the rectifier, but with a rectifier able to deliver higher current, this limit could be increased to 800 mA/cm^2.

A steady-state model of the electrolyser, in the form of an IV curve, is incorporated in the electrolyser control system, which calculates the current to be injected to the electrolyser to make it able to absorb the available renewable power. NEL Hydrogen claims that the total load of the electrolyser is approximately equal to the sum of BOP and load of the stack obtained from the IV curve. The temperature of the system in this model is assumed to be constant and equal to the operational value.

Table 2.3 summarises and compares the characteristics of the two types of NEL Hydrogen electrolyser mentioned in this chapter. NEL Hydrogen pressurised electrolysers with the nominal demand load of 24 kW offer a maximum load change of ±18,480 kW/min (770 pu/min), so if the load of each pressurised electrolyser in the

system was 2.1 MW, then by scaling up the above ramping value, the maximum load change of each 2.1 MW pressurised electrolysis load will be ±26.9 MW/s (12.8 pu/s).

Table 2.3 Comparison between two types of electrolysers made by NEL Hydrogen

Characteristic	Large scale Atmospheric (2.1 MW)	Pressurised (24 kW operating in Porsgrunn station)
Maximum rate of power change	135 kW/min (0.064 pu/min)	18,480 kW/min (770 pu/min)
Nominal load	2.1 MW	24 kW
Standby load	1.5 kW/unit	1 kW/unit
Operating temperature	80 °C	60 °C
Pressure	1.02 bar	9-15 bar(g)
Rectifier ratings	5150A/405V	850A/60V
Number of cells	230	10
Production capacity	485 Nm^3/h	3.4 Nm^3/h
Number of allowable times to switch the electrolyser On/Off per day	3 (times/day)	20 (times/day)
lifetime	7 years	7 years
Start-up time including nitrogen purge process	40 minutes	35 minutes
Normal shut down duration	30 minutes	30 minutes
Emergency shutdown duration	2 minutes	2 minutes
Nominal operating current density	250 mA/cm^2	400 mA/cm^2

Operational range	20%-100%	18%-100%
Duration allowed to stay in standby mode	As long as the temperature and gas impurities are kept within acceptable limits.	One day

Currently, NEL Hydrogen can deliver pressurised electrolysers up to a maximum rating of 300 kW. In the near future, they plan to increase the maximum demand of their pressurised electrolysers to 1.2 MW. The IHT Company in Switzerland [88] delivers large scale pressurised electrolyser units of (30 bar, 700 Nm^3/h) with nominal demand of 3.5 MW. It is expected that they have short response time. Figure 2.8 shows one of these large-scale pressurised units.

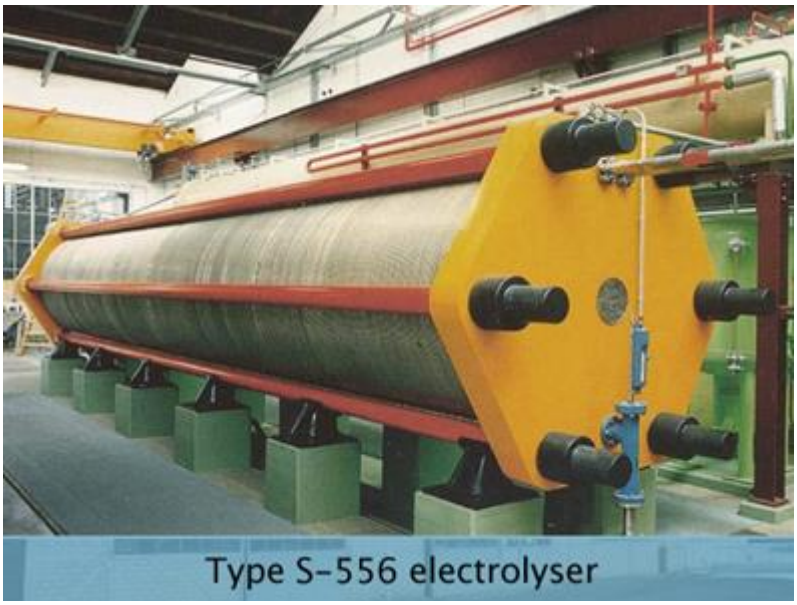

Figure 2.8 The pressurised large-scale electrolyser produced by IHT Company

2.7 Operation of the pressurised electrolyser under different operational conditions

2.7.1 Summary of the experiment

An experiment was carried out on the pressurised alkaline electrolyser operating at Porsgrunn station for a duration of 5 hours and 24 minutes from 9:49am to 15:13pm

on 25/10/2011. At the beginning and the end of the experiment the electrolyser was purged with nitrogen gas.

The data logging system, which belongs to NEL hydrogen and is located on site, acquires operational data with a sampling rate of 10 ms, and if the operator chooses a shorter sampling time, then the system will interpolate the data. At the start of the experiment, the operating pressure has to be set, so a value of 6 bar(g) was selected by the operator, which after 3 hours and 35 minutes, was increased to 12 bar(g).

Figure 2.9 shows the actual DC current of the stack during the whole experiment. This experiment consists of ten different operational phases. The reasons for recording the data at each stage and reporting it here are listed below the title of each operational phase.

1. Nitrogen purge before the start-up (‘A’ in Figure 2.9).

    a) To evidence how much time it takes to start the system and what happens during this process.
    b) To find how the temperature of the lye changes in this operational phase.
    c) To find out what major devices consume power during the start-up process and whether the system consumes any significant power and energy at this stage.

2. Cold start condition (‘B’ in Figure 2.9).

    a) To find out the ramp-up rate of the system immediately after the nitrogen purge process.
    b) To find out whether the system needs to be at the nominal temperature at this stage or the temperature can be lower during start-up.
    c) To find out how the pressure of the system changes during this process.

3. Normal operation at 6 bar(g) (‘C’ in Figure 2.9). The reason to carry out the experiment at this operational phase and report it here is to find out how the electrolyser parameters change when the system is at a stable operational mode with a constant current (or constant hydrogen production rate) set-point at the

pressure of 6 bar(g). In an ideal case the demand from the electrolyser cell stack should remain constant if the current set-point, temperature, pressure and KOH concentration remain constant. To verify that the demand of the stack does not change significantly, the data from this operational phase was recorded and analysed in this work.

4. Step increase in current ('D' in Figure 2.9).

    a) To verify the ramp rate of electrolyser when the stack current set-point is increased stepwise.
    b) To find out the steady-state relationship between the set-point and actual current of the stack at different step levels.
    c) To determine a more accurate IV curve of the electrolyser.

5. Normal operation at 12 bar(g) ('E' in Figure 2.9). The same reasons of conducting stage 3 (Normal operation at 6 bar(g)) also apply for this operational stage.
6. Standby mode operation ('F' in Figure 2.9).

    a) To find out how long it takes the system to go into standby mode from the normal operational mode.
    b) To find out how much the system is capable of keeping the temperature and pressure unchanged during standby mode.
    c) To investigate how long the system can stay in standby mode.
    d) To find out the actual demand of the electrolyser during standby condition.

7. Step change in current ('G' in Figure 2.9). The same reasons of conducting stage 4 (Step increase in current) also apply for this operational stage. The difference is that this experimental phase is carried out at the pressure of 12 bar(g) and the ramp-down rate is also investigated at different current levels in addition to the ramp-up rate.
8. Operation with renewable power ('H' in Figure 2.9).

    a) Finding out how the electrolyser parameters change when the system is operating with the available aggregate renewable power from solar and wind generators.

b) It is useful to know how much of the renewable power will be absorbed by electrolyser.
c) Finding out how the gas impurities in the system change in this operational phase, and how they will impact the performance of the system.

9. Shut down process ('I' in Figure 2.9). The reasons to carry out the experiment at this operational phase and report it here are listed below.

    a) To find out how long it takes for the system to go into shutdown mode.
    b) To find out how much power the system needs during the shutdown process.
    c) To find out how the temperature and pressure of the system change during the shutdown process.

10. Nitrogen purge at the end of experiment ('J' in Figure 2.9). The same reasons which were mentioned in operational phase 1 (Nitrogen purge before the start-up) are also applicable for this operational stage.

The small section between 'B' and 'C' and also the gap in the middle of section 'C' on Figure 2.9 indicate small tests that are not included in this thesis because other operational stages describe the behaviour of the electrolyser sufficiently.

During this experiment, the actual current supply to the stack was changed between 0A and 511A, corresponding to a current density range of 0 to 270 mA/cm^2. Unfortunately, at the time of the visit, the station was equipped with a small protective switch, which would trip at high loads, so the operator was not able to inject the nominal current of 850 A to the electrolyser cell stack. When the current of the stack in Figure 2.9 is zero, the electrolyser is in standby mode.

Figure 2.10 shows the IV curve of the cell stack obtained from the experimental data and also its cubic fit curve. This curve was obtained from all of the current and voltage data during the experiment, so the standard procedures to obtain an IV curve were not followed because of the limitations of the data acquisition system, but this curve roughly shows the IV curve of the cell stack, regardless of the 'noisy points' apparent in the figure. At about 500 A, the voltage of each cell is about 1.8V. It is obvious that

the electrolyser operates in the linear section of the IV curve where the Ohmic resistance is mainly responsible for the slope of the curve.

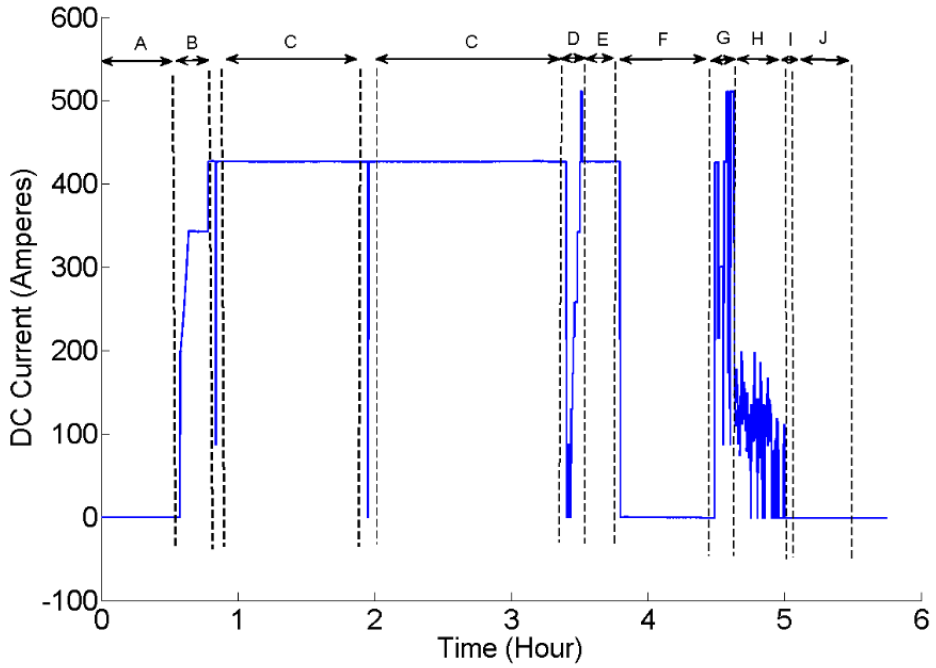

Figure 2.9 The actual DC current of the cell stack during the whole experiment

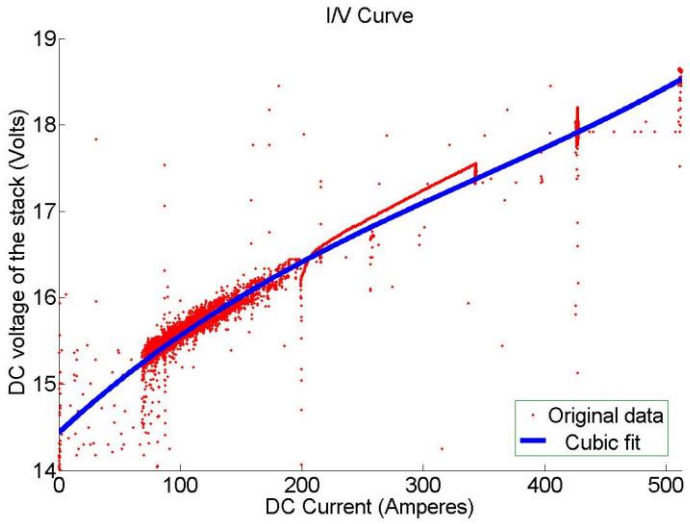

Figure 2.10 The IV curve of the cell stack and its cubic fit curve during the experiment

The best way of assessing the efficiency of the electrolyser is to use the amount of electrical energy consumed by the electrolyser to produce a specific amount of hydrogen, but the system in Porsgrunn did not have any sensor to measure the amount of hydrogen produced by the stack, so only the voltage efficiency is calculated in this

work based on the thermo-neutral voltage (V_{Thn}). The voltage efficiency is the ratio between the thermo-neutral voltage and a cell operating voltage. Equation 2.3 is used to estimate the voltage efficiency of the cell stack in the case that there are many cells in an electrolysis cell stack connected in series. It should be highlighted that this value is only the efficiency of the cell stack and not the efficiency of the whole electrolysis system.

$$\eta_{V.E.Stack}\% = N_C \times \frac{V_{Thn}}{V_{Stack}} \times 100 = N_C \times \frac{1.48}{V_{Stack}} \times 100 \quad (2.3)$$

where

$\eta_{V.E.Stack}$ is the efficiency of the cell stack based on the thermo-neutral voltage in percentage.

V_{Stack} is the DC voltage of the cell stack (Volts).

N_C is the number of cells connected in series in the cell stack (10).

Figure 2.11 shows the voltage efficiency of the stack versus its DC current based on actual logged data and also a cubic fit curve of the logged data. Like the I/V curve, this curve was not obtained from the standard procedure of finding the voltage efficiency curve, and that is why this graph has some noise, but it can approximate the relationship between the voltage efficiency of the stack and its DC current. When the current of the cell is almost zero, the voltage efficiency of the stack appears to exceed 100% due to small sensor calibration errors.

While the stack is working within its operational range, its efficiency decreases by increasing its load. This decrease is caused by the increase in the overall Ohmic over-potential of the cell in higher currents [10]. The stack has its highest efficiency at the lowest current density, but at this point, the electrolyser produces the minimum amount of hydrogen, and also the ratio of its BOP power to the total system load is higher and more significant, so the total efficiency might be very low in small-scale electrolysers operating at very low current densities. This issue has less importance in large-scale electrolysers because their BOP power is much lower than the minimum load of their cell stack.

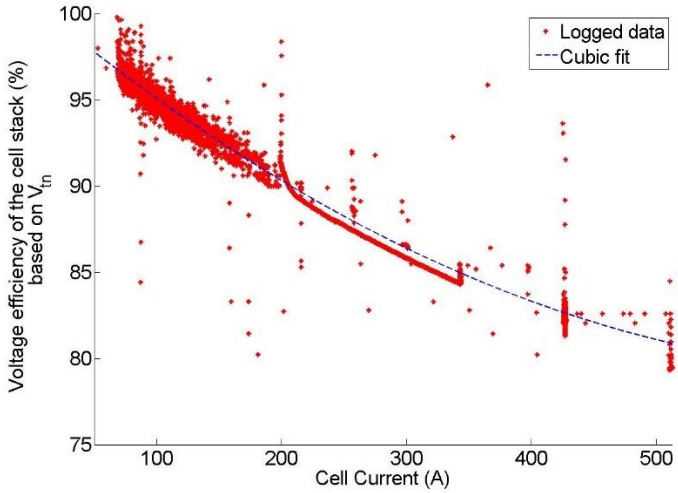

Figure 2.11 The voltage efficiency of the cell stack vs. its DC current during the experiment (actual logged data and also a cubic fit curve of the logged data)

To calculate the efficiency of the whole hydrogen production and storage system, some other parameters are needed, which are listed below, and they will be discussed in the following chapters.

- The efficiency of the rectifier
- The exact Balance of the Plant (BOP) of the system at each moment.
- Faraday efficiency of electrolyser
- The efficiency of the deoxidizer and dryer
- The amount of gas losses in the system
- The efficiency of the compressors.

At very low current densities, i.e. below the minimum acceptable load, if the current density of the stack decreases, then its efficiency decreases as well due to an increase in the impurity of gases. This case is not examined in this experiment because it happens while the electrolyser load is below its minimum operational limit.

The amount of hydrogen produced in electrolysis cells is directly related to the current density supplied to the electrodes, and the hydrogen production rate is not affected by the cell voltage in a certain current density, but the energy needed by the stack to produce a certain amount of hydrogen is affected by the operational voltage of cells.

The cell voltage increases due to increasing the current density supplied to the electrodes, and this causes an increase in the energy consumption of the cell.

The designers of electrolysers have the choice to improve the efficiency of electrolysers by increasing the size of their electrodes. This effectively decreases the current density of electrodes while the electrolyser generates a certain amount of hydrogen, and therefore the efficiency will be increased in the electrolyser, but an increase in the size of electrodes will increase the capital cost of the plant.

To minimise the cost of hydrogen production from an electrolyser located at a specific site, the electrolyser should be designed by considering the trade-offs between the capital cost of installation, hydrogen production rate needed for the electrolyser and the electricity cost at that location [10]. In large scale electrolysers, it is better to invest more on the capital cost of the plant in the first place instead of spending more on the electricity consumption or early refurbishment costs. The activation layer of pressurized electrolyser electrodes can safely tolerate up to 1 A/cm^2, but deteriorates quickly at 2 A/cm^2, so increasing the current density in a pressurised electrolyser up to 1 A/cm^2 does not degrade its lifetime. NEL Hydrogen claims that they have an electrode available that can tolerate up to 2 A/cm^2 without any degradation, but it is not economically viable. Ultimately, it depends on the customer decision to have a more expensive electrolyser with a better efficiency and lifetime or a cheaper electrolyser with lower nominal efficiency. Moreover, in electrolysers working as dynamic demands, the variation of the electrolyser demand and efficiency during its lifetime should also be considered to make an appropriate decision about the design of the electrolyser.

2.7.2 Nitrogen purge before start-up

At the beginning and end of the electrolyser operational cycle, the system must be purged with nitrogen gas to ensure that all of the hydrogen is removed safely from all parts of the electrolysis system. During this purging process, the nitrogen does not go

into the cells, but it just goes into the separators and scrubbers. The voltage and current of the stack are almost zero during this process.

Figure 2.12 shows the pressure of the electrolyser during the start up nitrogen purging process. The pressure of the system is increased with nitrogen to 2.03 bar(g) and decreased to 0.59 bar(g) in 6 cycles during 25 minutes to make sure that all of the electrolyser parts are safe for the start-up.

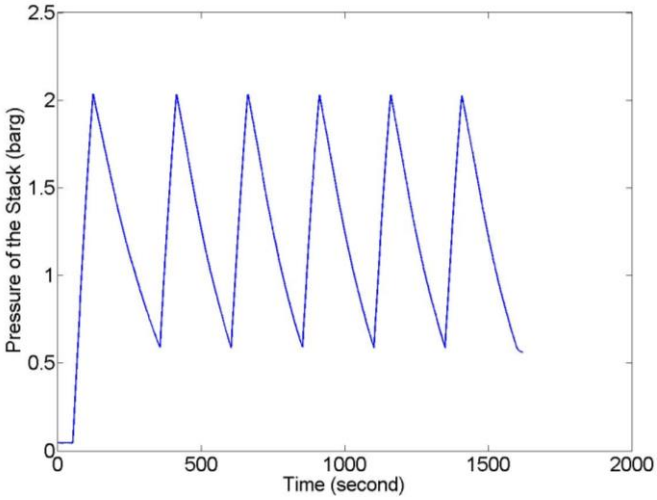

Figure 2.12 The pressure of the system during the start-up nitrogen purging process

Figure 2.13 shows the temperature of the lye in the hydrogen compartment, which is used as the temperature of the cell, during the start-up purging operation.

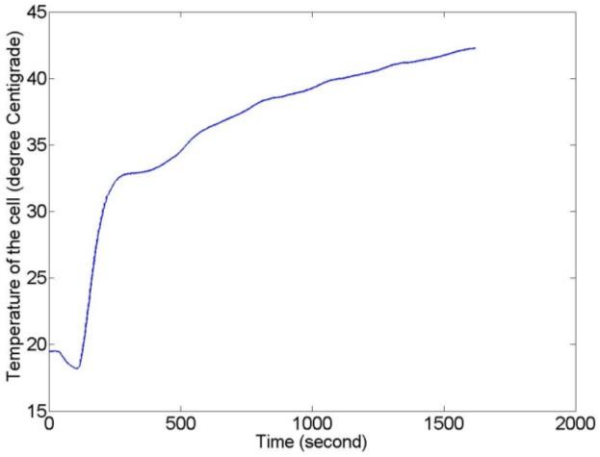

Figure 2.13 The temperature of the lye during the start-up nitrogen purging process

The separator tanks are heat-traced, and as the lye pump starts circulating the electrolyte, warmer fluid is transferred to the vicinity of thermocouples, and thus the measured temperature of the lye increases during the purge time. It takes about 30 minutes to purge the system with nitrogen, and there is about 200 litres of lye in the electrolyser, so there is sufficient time to increase the electrolyte temperature from ambient to the nominal operational value without consuming significant power.

2.7.3 Cold start condition

After the nitrogen purging process, the electrolyser became ready to start its normal operation. At this stage, the value of 6 bar(g) was selected as the operating pressure set-point. At the beginning of the operation, the system pressure has to build up, so the operator cannot increase the electrolyser load very quickly.

Figure 2.14 shows the voltage and current of the stack during the cold-start phase. At the beginning of the operation, the current sensor was showing -0.29 A, which is believed to be due to a slight problem with its calibration. Despite the fact that the current set-point of the system was set to 400A, it did not immediately increase towards this target value.

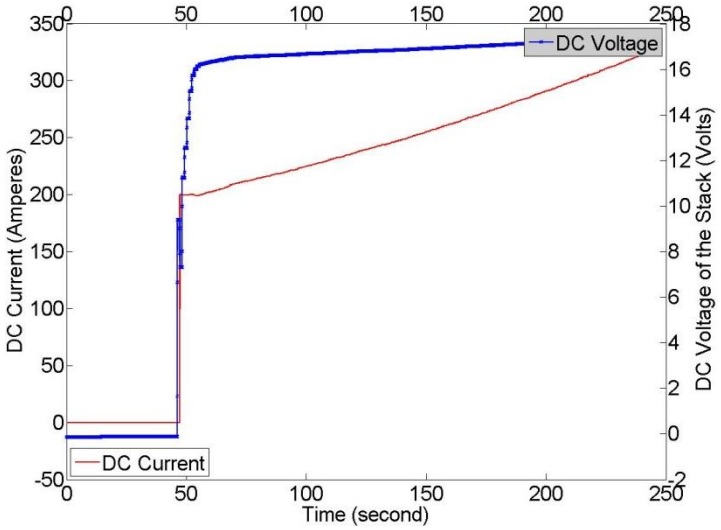

Figure 2.14 The voltage and current of the stack during the cold start process

It took about 34 seconds for the actual current of the stack to start increasing after the set-point was increased. It then increased up to 200 A very quickly in about 300 ms and then subsequently increased with a much slower slope of 0.508 A/s. This change in the ramp rate of the electrolyser happens because the system is not at a high pressure in the beginning of its operation, and it takes some time for the pressure to build up to 6 bar(g). As a consequence, the system is not able to remove all gas produced in the stack fast enough and therefore inhibits a quick jump to higher currents. Once the pressure gets to higher values, the electrolyser responds much quicker.

Figure 2.15 shows the temperature of the electrolyser, which was still increasing towards its operational range during the start-up phase. Despite the fact that the temperature set-point is 60°C, the actual temperature did not go above 54°C during the whole experiment. Most of the heat within the system during the operation is generated from the electrolysis process itself, and the current of the electrolyser was much lower than the nominal current during most of the experiments, so the temperature did not reach the nominal value of 60ºC in the experiments reported in this work.

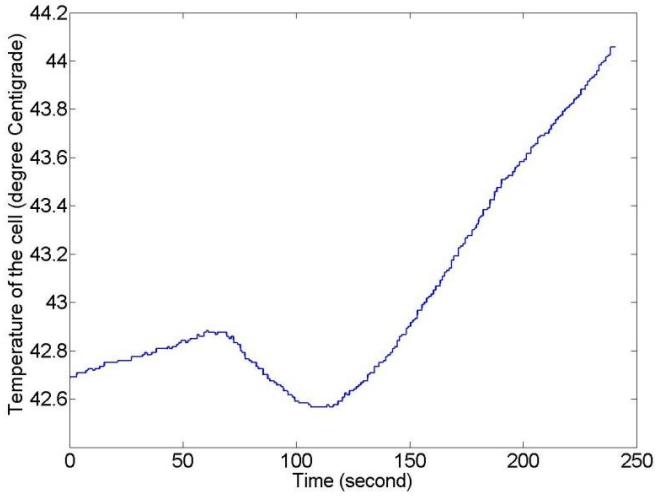

Figure 2.15 The temperature of the lye during the cold start process

Figure 2.16 shows the pressure of the electrolyser, which was increasing linearly towards the set-point value of 6 bar(g) during the start-up operation.

Figure 2.17 shows the DC set-point and actual current of the stack during the cold start phase. It is clear that there is always some difference between the set-point and actual

current of the cell stack, which is due to the design of the electrolyser rectifier, and the set-point current therefore has a higher value than the actual current. However, this has not been independently verified as the author did not have further access to the electrical and electronic equipment of the electrolyser to measure them due to safety and Intellectual Property (IP) issues. It is also worth mentioning that, in the beginning of the start-up operation, there is a significant delay of 34s between the set-point current and the actual current. This could be due to the time that the rectifier needs to start its operation.

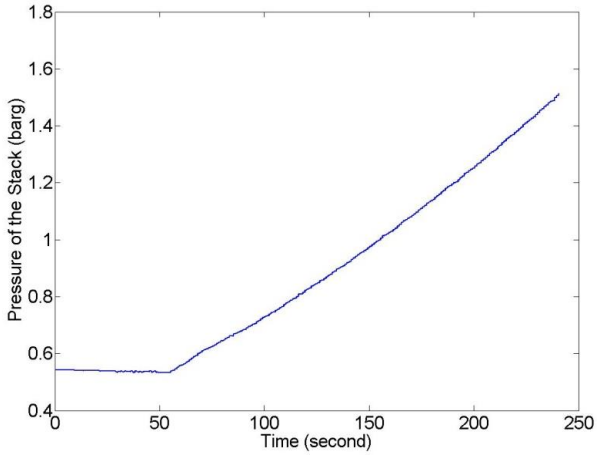

Figure 2.16 The pressure of the system during the cold start process

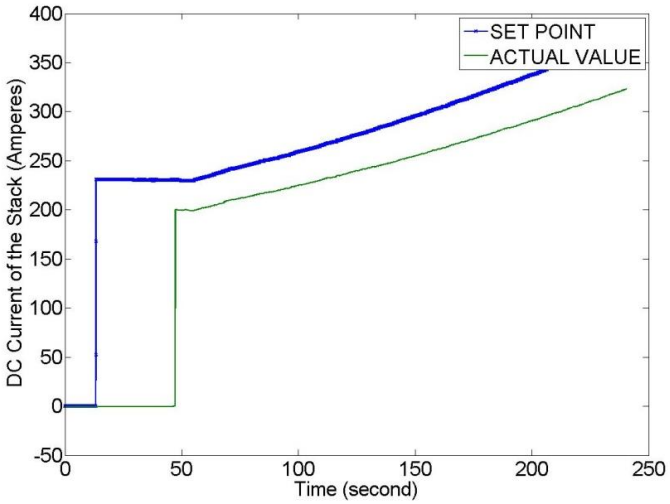

Figure 2.17 The DC set-point and actual current of the stack during the cold start phase

The DC load of the cell stack is shown in Figure 2.18. Up to 3.15 kW, the electrolyser had a quick rate of load change of 470.3 7 W/s, and after that its power ramp-up rate

is reduced to 12.32 W/s because at the beginning of the operation, the pressure has to build up, so the system cannot increase its load quickly.

The electrolyser needs some time to start working normally from a cold-start. In pressurised electrolysers, it takes about 25 minutes to purge the system with nitrogen and about 10 minutes to get to the nominal hydrogen production rate, so in total they have a typical start-up time of 35 minutes. Electrolysers with large stacks have a reduced hydrogen production ramp up time of about 3-5 minutes, so their total start-up time is only about 30 minutes.

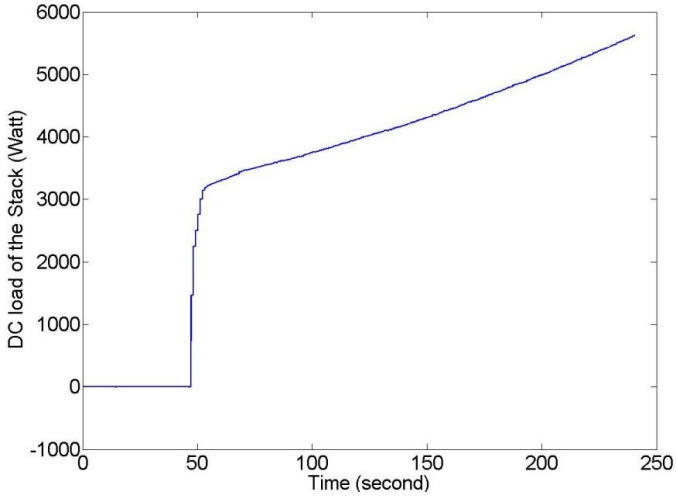

Figure 2.18 The DC load of the stack during the cold start phase

2.7.4 Normal operation 6 bar(g)

At the beginning, the operating pressure was set to 6 bar(g). During this time, the current set-point of the electrolyser was set to 500 A. Figure 2.19 shows the voltage and current of the stack during normal operation at 6 bar(g). The actual current of the electrolyser was not exactly constant during this period, changing between values of 426.55 A and 426.95 A, despite the fact that the set-point current was constant.

The standard deviation of the actual stack current during this time was equal to 0.073A, which was about 0.017% of the average current of the stack, so the amount of ripple on the current of the electrolyser was very insignificant. It should be noted that these

ripples could be as a result of the Analogue-to-Digital Converter (ADC) errors in the DAQ system. The voltage also decreases slightly during this period due to an increase in the temperature of the electrolyser.

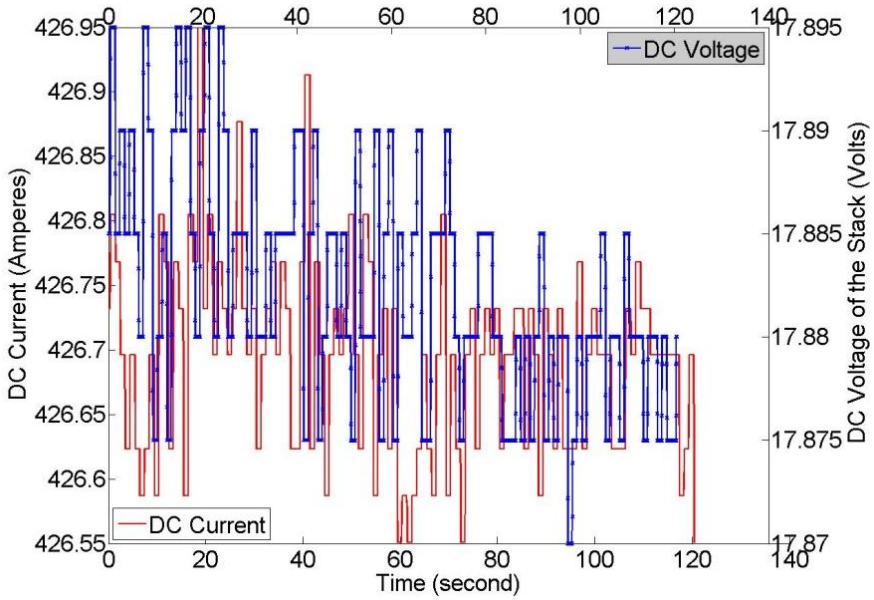

Figure 2.19 The voltage and current of the stack during the normal operation at 6 bar(g)

Figure 2.20 shows that the temperature of the cell was still increasing during this period because the electrolyser was started from shut-down condition, and it took some time for the temperature of the lye to reach its nominal value. The impact of temperature on the voltage of the electrolyser is significant. Normally, the system temperature has some slight oscillation around its nominal operational value when the system is operating in normal operational mode.

Figure 2.21 shows the pressure of the system during normal operation at 6 bar(g). The pressure showed small fluctuations between 5.975 bar(g) and 6.05 bar(g). This fluctuation was occurring as a result of the opening and closing of valves in the system.

Figure 2.22 shows the DC load of the stack during normal operation at 6 bar(g). Despite the fact that the current set-point was constant during this operational phase, the DC load was slightly decreasing because the voltage was slightly decreasing as a result of an increase in the lye temperature.

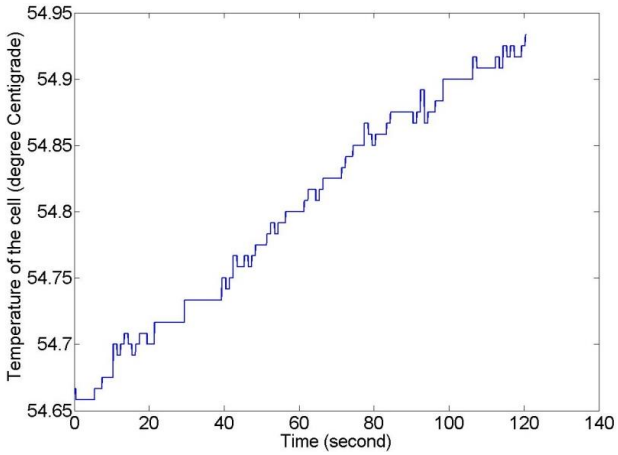

Figure 2.20 The temperature of the lye during normal operation at 6 bar(g)

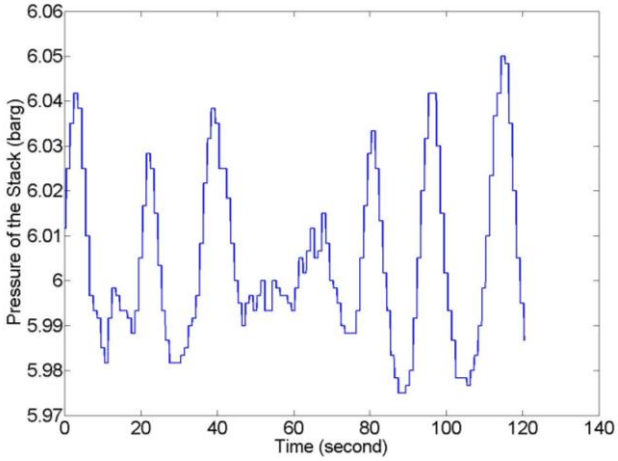

Figure 2.21 The pressure of the system during normal operation at 6 bar(g)

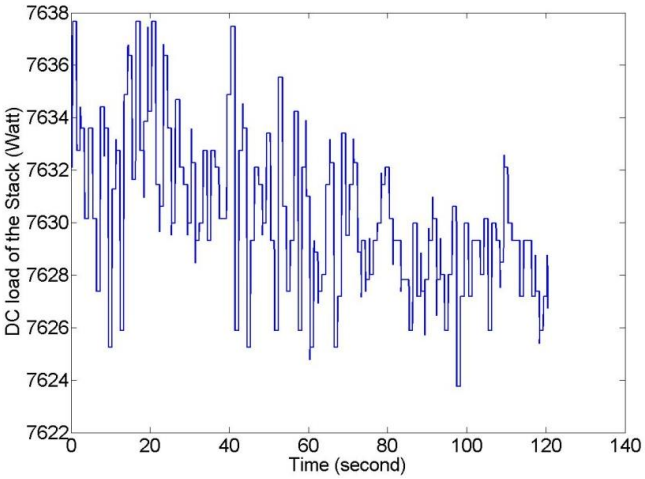

Figure 2.22 The DC load of the stack during normal operation at 6 bar(g)

The voltage efficiency of the electrolyser was almost constant and equal to 81.95% during this operational phase. The amount of oxygen in hydrogen was almost zero, but the amount of hydrogen in oxygen was almost constant and equal to 0.5% during this phase.

2.7.5 Step increase in current

At this operational phase, the current of the electrolyser was increased step by step from 0A to 400A to observe the response of electrolyser and the IV curve with a better accuracy. The operational pressure was set to 6 bar(g) throughout this stage.

Figure 2.23 shows the DC set-point and actual current of the stack during the step increase experiment. The current set-point of the electrolyser is always higher than the actual current of the stack due to the specific design of the electrical parts of the electrolyser and the rectifier. It is also clear that at lower currents the difference between the actual current and the current set-point is lower, and as the set-point current is increased, this gap also increases. In other words, the difference between the set-point and actual current of the electrolyser is proportional to the set-point current selected by the operator, and the actual current of the cell stack is normally about 14% lower than the set-point current.

There is a slight delay between the set-point and the actual current of the stack. Figure 2.24 shows the DC set-point and actual current of the stack while the current increased from 250 A to 300 A. It took about 10 ms for the actual current to start rising after the set-point current (shown with ‘A’ in Figure 2.24). This 10 ms delay is due to the time resolution of data acquisition system. However, in cases that ‘A’ is more than 10ms, it could indicate a delay in the rectifier response. The current set-point also did not increase step wise, having a slope instead. In addition, the actual current increased with a lower slope than the slope of the set-point current. The total delay between the time that the set-point current started increasing and the time that the actual current reached its final value was about 30 ms (shown with ‘B’ in Figure 2.24). Table 2.4 shows the values for ‘A’ and ‘B’ durations for the current step increase experiment.

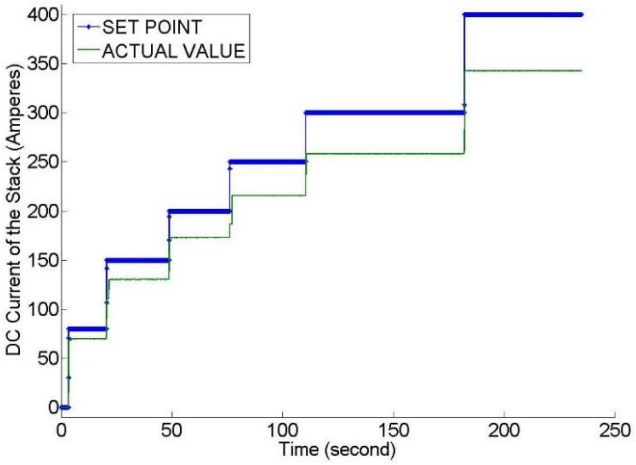

Figure 2.23 The DC set-point and actual current of the stack during the step increase experiment

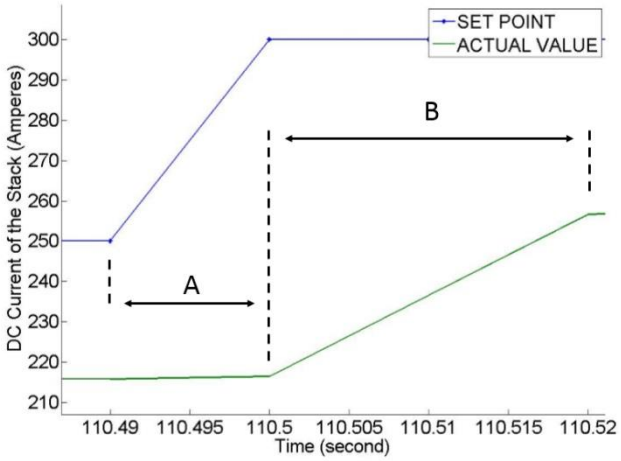

Figure 2.24 The DC set-point and actual current of the stack while the set-point current increased from 250A to 300A

As shown in Figure 2.25 and apparent in Table 2.4, it seems that there exists another extra delay in the transition duration (B) that appears in the response occasionally, and it could be as long as 1.02 s. Figure 2.25 shows that this occasional delay is not due to the delay in the current set-point or due to a planned action of the electrolyser controller, but it is rather a problem of the rectifier, which occasionally does not increase its output current in one single transition to match the set-point value. In

addition, in the last four rows of Table 2.4 the current set-point is increased by 50A in each transition, but the rectifier exhibits this extra delay only once, which is during the transition from 200 to 250 A. This proves that the delay is not really related to the amount of load change in the rectifier, so it cannot be an intentional action by the rectifier due to a deliberate design plan, but it is rather a fault in the design of the rectifier. This extra occasional delay was not expected or explained by NEL hydrogen, and the author did not have access to the electrical parts of the electrolyser or the rectifier to investigate this further.

Table 2.4 Time delays of the actual current in the current step increase experiment

Set-point current increase	Delay before change (A)	Transition duration (B)
0 to 80A	20 ms	20 ms
80A to 150A	20 ms	1050 ms
150A to 200A	20 ms	30 ms
200A to 250A	10 ms	1040 ms
250A to 300A	10 ms	20 ms
300A to 400A	10 ms	30 ms

Figure 2.26 shows the IV (Current density/Voltage) curve of a cell during the step increase experiment based on actual logged data and also a quadratic fit curve of the logged data. The temperature of the lye remained in the vicinity of 53 ºC during this operational stage and was almost stable during this phase, so this I/V curve is more reliable than the one showed in Section 2.7.1. The system pressure was kept almost constant around 6 bar(g) during this operational phase.

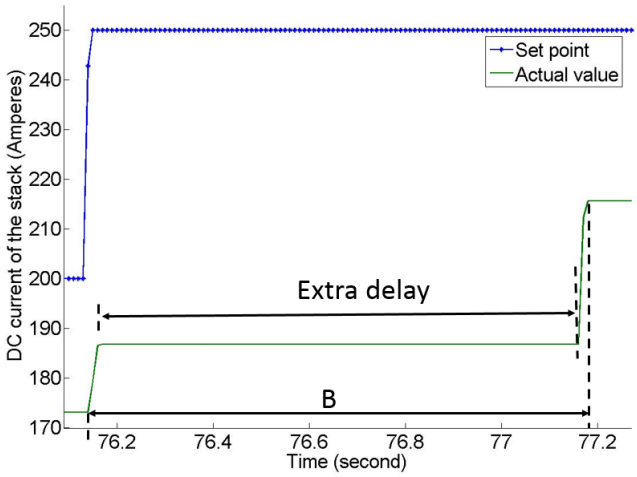

Figure 2.25 The DC set-point and actual current of the stack while the set-point current increased from 200A to 250A

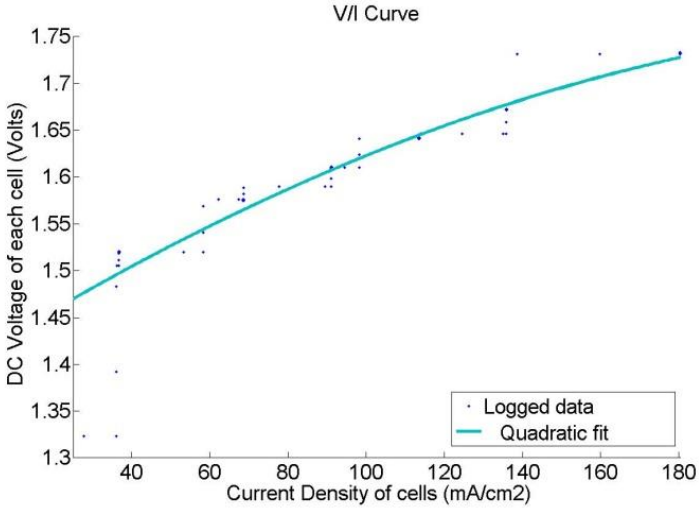

Figure 2.26 The I/V (current density) curve of a cell during the step increase experiment (actual logged data and also a quadratic fit curve of the logged data)

Table 2.5 shows the ramp rate of the stack excluding the extra occasional delay during different current transitions in this operational phase. Apparently, the ramp rate is lower than nominal ramp rate stated by NEL hydrogen and varies depending on the transition steps. In addition, it seems that the ramp rate is lower at smaller step

changes. This variation in the ramp rate is due to the response of the rectifier; otherwise, the control system designed by NEL hydrogen only imposes the ramp rate of 12.8 pu/s.

The impurity sensors are at the top of the gas/lye inlet from the electrolyser to the separators. They are not exactly in the separators but in the nitrogen purge line to the separators and are as close as possible to the separators to minimise the delay between the change in operational parameters and the actual gas quality. Figure 2.27 shows the impurity of the gases during the step increase experiment. The impurity of hydrogen gas in oxygen slightly increased due to operation of electrolyser at low current densities for a while. However, as it takes some time for the sensors to measure this increase in the impurities, this increase in Figure 2.27 is a bit delayed with respect to the time of the decrease in the load of the electrolyser.

Table 2.5 Ramp rates in the current step increase experiment

Transition	kW/s	pu/s
0 to 80A	45.25	1.88
80A to 150A	31	1.29
150A to 200A	11.61	0.48
200A to 250A	13.31	0.55
250A to 300A	17.64	0.73
300A to 400A	40.45	1.68

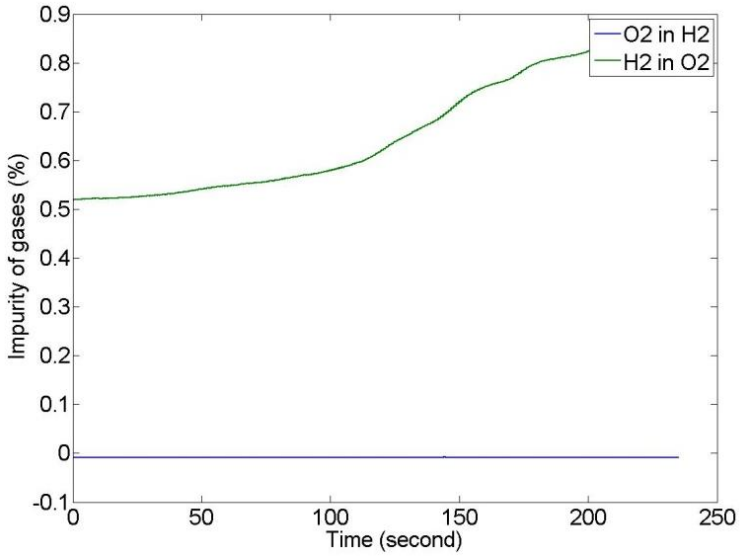

Figure 2.27 The impurity of the gases during the step increase experiment

2.7.6 Normal operation at 12 bar(g)

After operating the system at 6 bar(g) for some time, the pressure set-point was increased to 12 bar(g). The set-point current was again set to 500A, and the actual current of the cell was 426.9A. When a constant current is applied to the cell stack, the voltage will not be constant, mainly due to the variation in the temperature of the lye. Figure 2.28 shows the voltage and current of the stack during normal operation at 12bar(g). The voltage was increasing slightly due to the decrease in the temperature of the lye during this operational stage.

Figure 2.29 shows that the temperature of the lye was decreasing due to the fact that the controller does not keep the temperature constant during all of the operational period, and the temperature fluctuates within a range at all times.

The pressure of the system varied between 11.86 bar(g) and 12.03 bar(g) during this operational period. At a constant current of 427A and pressure of 6 bar(g), the temperature was oscillating between 54.65°C and 54.95°C, and the voltage efficiency was between 82.7% and 82.82%. In contrast, while the system was operating with the same constant current at 12 bar(g), the temperature changed between 52.8°C and 54.2°C, and the voltage efficiency was between 81.67% and 81.99%. Therefore it

seems that the change of pressure from 6 bar(g) to 12 bar(g) does not have any significant impact on the voltage efficiency of the electrolyser, mainly because of the logarithmic nature of the impact of pressure on the efficiency [10]. Most of the efficiency change in this case seems to be due to the change in the temperature rather than pressure.

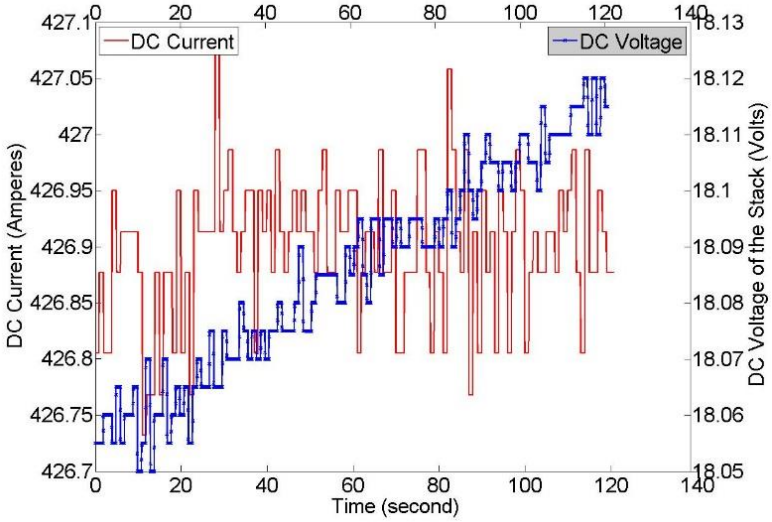

Figure 2.28 The voltage and current of the stack during the normal operation at 12bar(g)

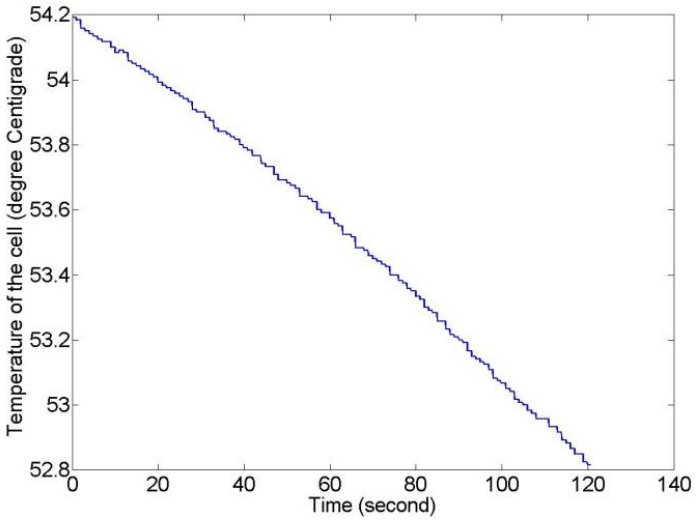

Figure 2.29 The temperature of the lye during normal operation at 12 bar(g)

The gas impurities were almost constant and well below the hazardous limits during this operational phase. Figure 2.30 shows the DC load power of the stack during

normal operation at 12 bar(g). The DC power consumption of the cell was increasing due to an increase in the voltage of the cell, which itself happened due to a decrease in the temperature. The temperature decreased about 1.4°C during this test, and as a result, the DC load of the stack increased by a negligible amount of 0.41%.

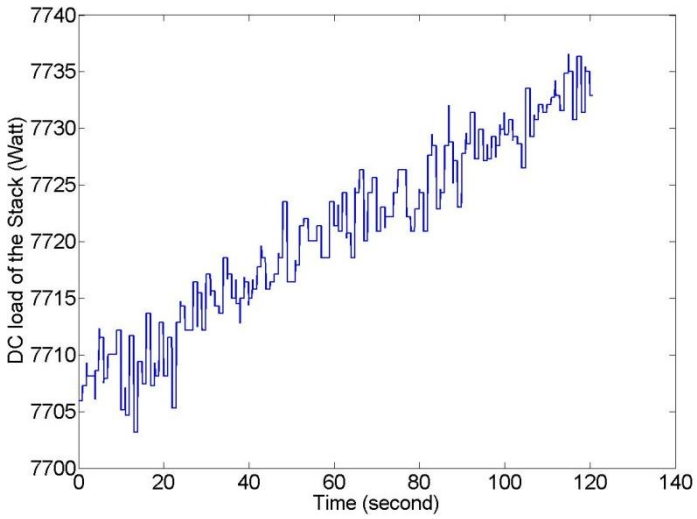

Figure 2.30 The DC load of the stack during normal operation at 12 bar(g)

2.7.7 Standby mode operation

After steady state operation of the system at 12 bar(g) with the current of 427A, the electrolyser was forced to go into standby mode by changing its current set-point to zero. The electrolyser was left in standby mode for about 42 minutes to observe its behaviour.

It is only possible to keep the system in standby mode whilst the pressure is kept above the minimum operational limit of 2 bar(g). Pressurised electrolysers could be designed in a way that they could remain in standby mode for a week, but the typical commercial ones made by NEL Hydrogen can only stay in the standby condition for about 24 hours before being shut down automatically. In standby mode, this electrolyser will still consume approximately 1 kW power, mainly due to the electricity consumption of the control system and lye circulation pumps.

Figure 2.31 shows the voltage and current of the stack during the standby condition. Due to the discharging of the stack double layer capacitance shown in Figure 1.4, the

voltage of the cell did not go to zero immediately after the set-point current was set to zero. Instead, it decreased exponentially until it reached 2V after about 42 minutes.

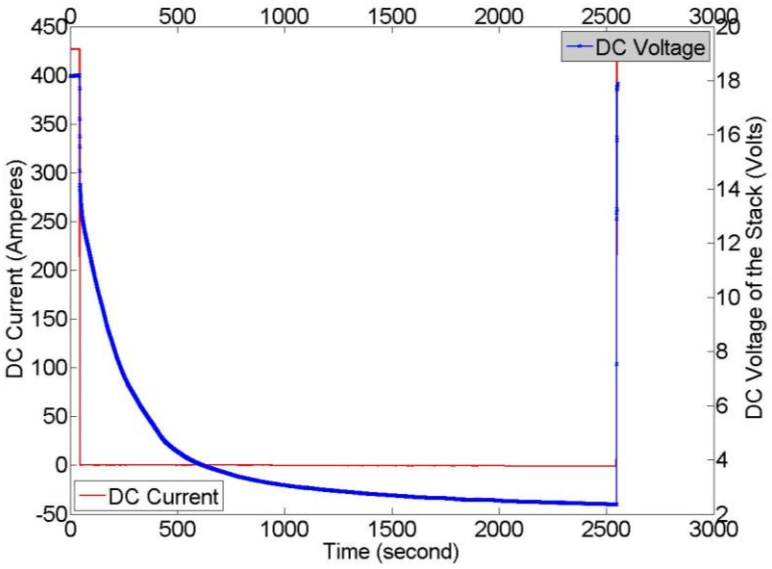

Figure 2.31 The voltage and current of the stack during the standby condition

Figure 2.32 shows the actual and set-point current of the electrolyser when the system goes into standby mode instigated by a signal from the operator. There was a 20 ms delay between the set-point and the actual current of the cell stack, and it also took about 30 ms for the actual current to become zero, so in total it took about 50 ms to take the system into standby mode from the initial stack current of 427A. Due to the small size of this electrolyser, when it is warm and pressurised, there is no ramping rate limit for the load of cell stack, so this 50 ms delay in the system response could be the aggregate delay of the rectifier and the PLC system. The ramp rate of the electrolyser in this stepwise power change was -8.1 pu/s.

Figure 2.33 shows the temperature of the lye during the standby condition. Due to the thermal isolation of the stack, even after 42 minutes of the system being in standby mode, the lye temperature did not drop significantly and was still kept around 45.5°C without any heating being available to the cells. There is a possibility to add a heater to the system to maintain the temperature during standby condition.

Figure 2.34 shows that the pressure of the system dropped slightly from 11.89 bar(g) to 11.75 bar(g) from 150s to 1112s. There is some leakage from the valves during

operation in standby mode, so the pressure decreases slowly during this phase, and eventually the system will go into shut-down mode should the pressure drop below 2 bar(g). From extrapolating the pressure drop curve, it is found that it takes about 24 hours for the pressure of the system to drop to 2 bar(g) if the initial pressure is set to 15 bar(g). The electrolyser has therefore the ability to stay in the standby mode for approximately one day without experiencing any problem.

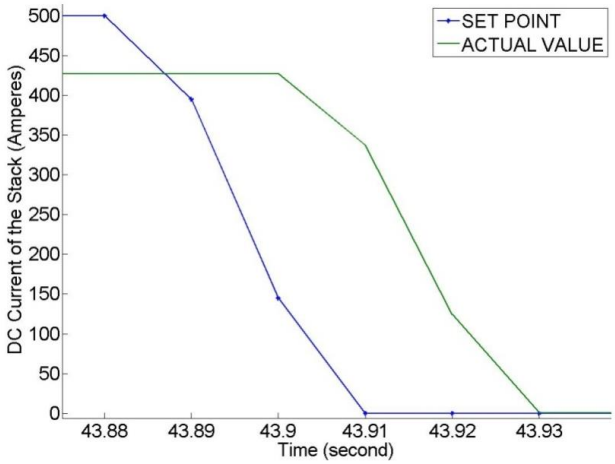

Figure 2.32 The set-point and actual current of the stack when the electrolyser is signalled to go into standby mode

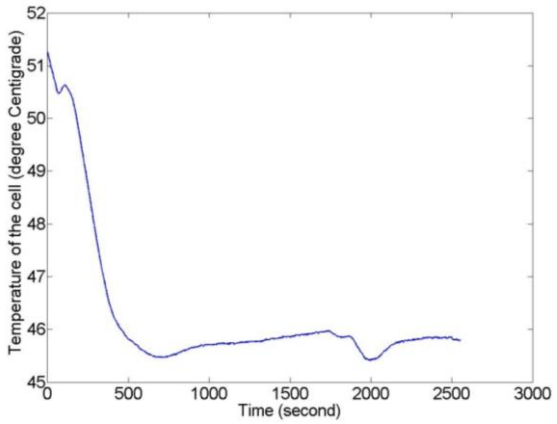

Figure 2.33 The temperature of the lye during the standby condition

The amount of hydrogen impurity in oxygen was kept almost constant at 0.5%, and also the impurity of oxygen in hydrogen was very close to zero during this operational phase.

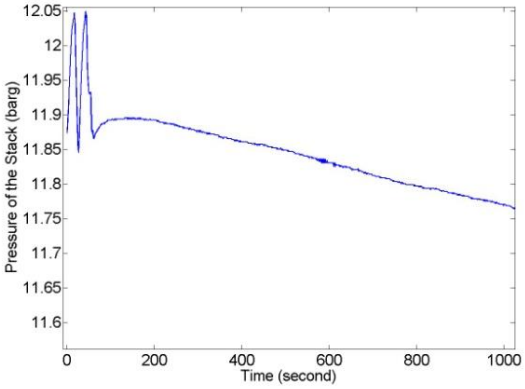

Figure 2.34 The pressure of the system during the standby condition

2.7.8 Step change in current

After operating the electrolyser in standby mode, the current demand to the cell was changed to different load levels for about 9 minutes to record the response of the electrolyser to a dynamic command signal. Figure 2.35 shows the voltage and current of the stack during the step-change experiment. The low voltage (2V) of the cell stack at the start of this stage of the experiment is due to the operation of the electrolyser in standby mode for a while. The pressure of the system during this operational phase was kept to 12 bar(g), and the impurity of the gases was also within the acceptable limits, e.g. lower than 1.8%.

At the beginning of this operational phase, the current of the electrolyser was increased suddenly from 0A to 425A, but there was one second delay between the set-point and the actual current, which is shown in Figure 2.36. This is very different from the normal electrolyser operational results because it takes a much longer time for the actual current to increase towards the set-point value. It is worth mentioning that the slope of the actual current increase is pretty fast (17,000 A/s), but there is a significant delay between the increase in the set-point and the actual current. As explained before, this delay might be a result of the specific rectifier characteristics. The ‘A’ and ‘B’ delays between the set-point and the actual current of the stack, which were defined in Figure 2.24, are also detailed in Table 2.6 for the step change experiment.

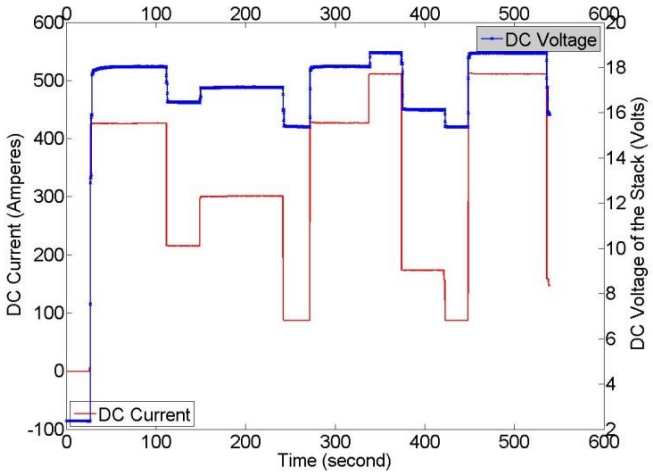

Figure 2.35 The voltage and current of the stack during the step change experiment

It is obvious that the extra delay illustrated in Figure 2.25, also exists in some occasions in this stage of the experiment, and it could occur both during ramp up or ramp down of the electrolyser, and its occurrence is independent of the amount of load change in each transition. Considering the results in the third column of both Table 2.4 and Table 2.6, it can be concluded that 40% of the time there exists an extra delay in the response of the rectifier with an average of 1015 ms during ramp up or ramp down of the system.

Table 2.7 shows the ramp rate of the stack during different current transitions excluding the extra occasional delay. Again, it is evident that the ramp rate is lower than the nominal rate of 12.8 pu/s stated by NEL hydrogen and varies depending on the transition steps. The biggest ramp rate observed here was 6.75 pu/s. Therefore, the response of rectifier is the most important factor in determining the ramp rate of electrolyser in this small scale electrolysis unit. However, NEL hydrogen claims that in larger units with more powerful rectifiers, the response of the rectifier becomes less important in comparison to the response of the mechanical parts of the unit, especially during larger transition steps.

Table 2.6 Time delays in the response in the current step change experiment

Set-point current increase	Delay before change (A)	Transition duration (B)
0 to 500A	30 ms	1010 ms
500A to 250A	20 ms	20 ms
250A to 350A	20 ms	1050 ms
350A to 100A	10 ms	1040 ms
100A to 500A	20 ms	30 ms
500A to 600A	20 ms	30 ms
600A to 200A	20 ms	20 ms
200A to 100A	10 ms	1050 ms
100A to 600A	20 ms	30 ms

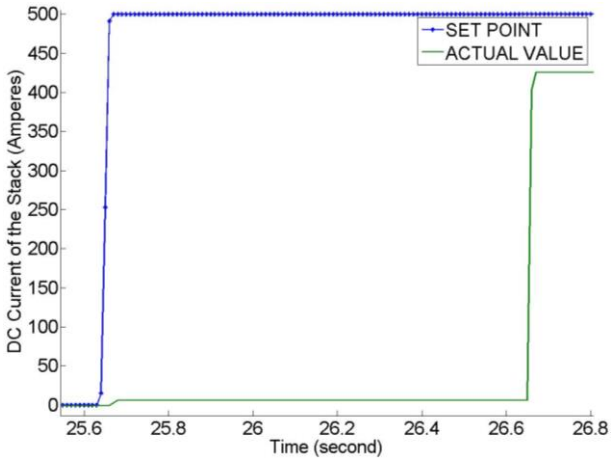

Figure 2.36 The set-point and actual current of the cells during the current increase from zero

Table 2.7 Ramp rates during the step change experiment

Transition	kW/s	pu/s
0 to 500A	139.03	5.79
500A to 250A	-98.8	-4.11
250A to 350A	27.62	1.15
350A to 100A	-92.8	-3.86
100A to 500A	157.68	6.57
500A to 600A	50.01	2.08
600A to 200A	-159.3	-6.63
200A to 100A	-23.65	-0.98
100A to 600A	162.12	6.75

The main reason that the electrolyser has limits on the speed of its load change is the problem of the imbalance between the amount of circulating lye and generated gas. This imbalance problem was not apparent in this experiment because the electrolyser was a small scale unit.

NEL Hydrogen claims that the variability of the electrolyser load does not degrade the lifetime or performance of the electrolyser due to the specific characteristics of the materials used in its electrodes.

2.7.9 Operation with renewable power

For the final experiment, the system was powered only from available local wind and solar power, which were operating at very low outputs at the time of this testing, hence

the cell stack had considerably low current densities and very high efficiencies, but eventually the impurity of hydrogen in oxygen gas became higher than the accepted threshold, and the system went into shut-down mode. This implies that the minimum current limit of the electrolyser should be increased to a higher value to make sure that the impurities do not reach the unacceptable limit as a result of sustained operation at very low current densities.

Figure 2.37 shows the voltage and current of the stack during operation of the electrolyser with renewable power. The system uses a simple IV curve to find the current that should be injected to the electrolyser to make it able to absorb the available renewable power. The minimum set-point current limit of the electrolyser is set to 80A, and if the renewable power available is below this, then the electrolyser changes to standby mode (i.e. with no current). As the wind and solar power were not consistently high enough, the electrolyser went into standby mode many times during this period. It is clear that, when the current of the stack becomes zero, the voltage of the cell stack decreases exponentially because of the impact of the double layer capacitance.

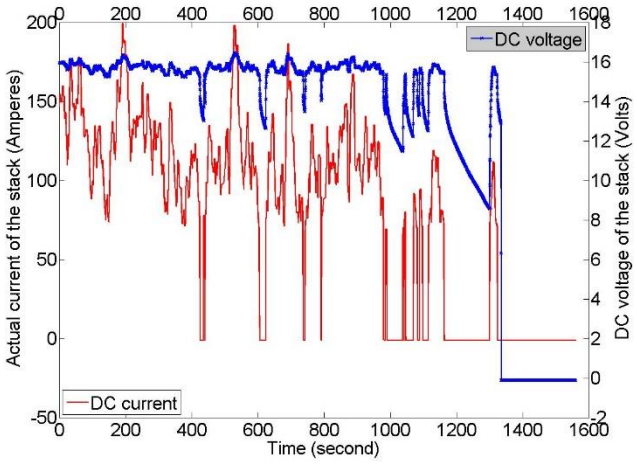

Figure 2.37 The voltage and current of the stack during the operation with renewable power

After about 900 seconds, the gas impurity became high due to repeated stack operation at very low current densities, and as a result, the electrolyser went into full shut-down mode at 1,160 seconds. By resetting the alarms, the operator was able to bring the

system back into operation, but after a short while, the electrolyser again went into shut-down mode due to a high gas impurity level.

Figure 2.38 shows the renewable power and stack load during this operational phase. There is clearly always some difference between the generated renewable power and the power consumed by the stack. A number of factors that could be causing this are listed below.

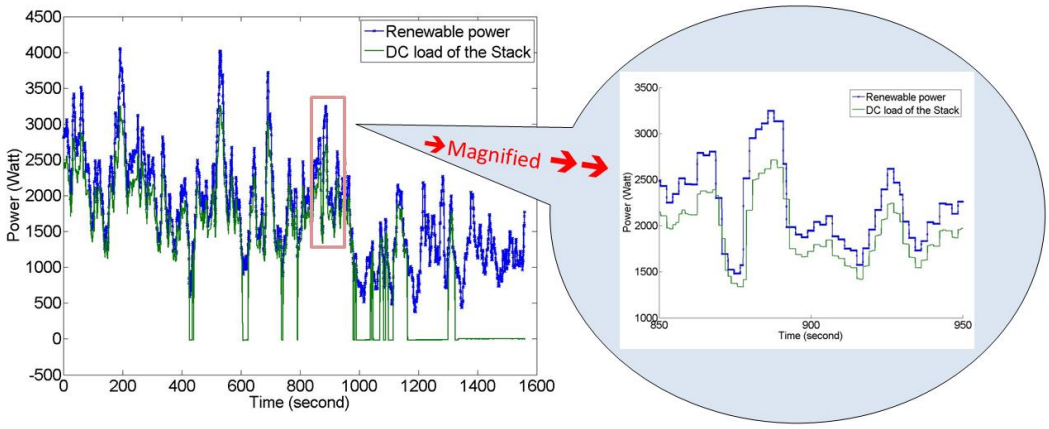

Figure 2.38 The renewable power and stack load during the operation

1. The power consumed by the electrolyser Balance of Plant.
2. An error from the PLC controller in the calculated stack current that should be injected to the electrolyser to make it capable of consuming all the available renewable power. As mentioned before, a week before the experiment, the membranes of the cells were changed to more efficient membranes with lower energy consumption. Consequently, the IV curve of the stack was changed, but the IV curve stored in the system, which was used to calculate current required by the electrolyser to absorb a specific power, was not changed. This could be one of the reasons for the difference that was observed between the available renewable power and the power used by electrolyser. NEL Hydrogen staff just used a simple IV curve to calculate the current set-point. They did not consider the impact of temperature on IV curve of the system because they assumed that the temperature fluctuations would be very small, and this added to aggregate errors.
3. There appears to be a permanent offset error between the reference current and the actual current of the electrolyser, as shown in Figure 2.23.

4. When the electrolyser goes into standby mode, the stack does not consume any power, so depending on the renewable power available this difference will be higher.

Figure 2.39 shows the difference between the renewable power and stack demand during the operation with renewable power. This difference is at its maximum when the system goes into standby mode; otherwise it is always less than 1.5 kW. This difference should be minimised in large-scale electrolysers working in stand-alone systems; otherwise it can cause instability in the system.

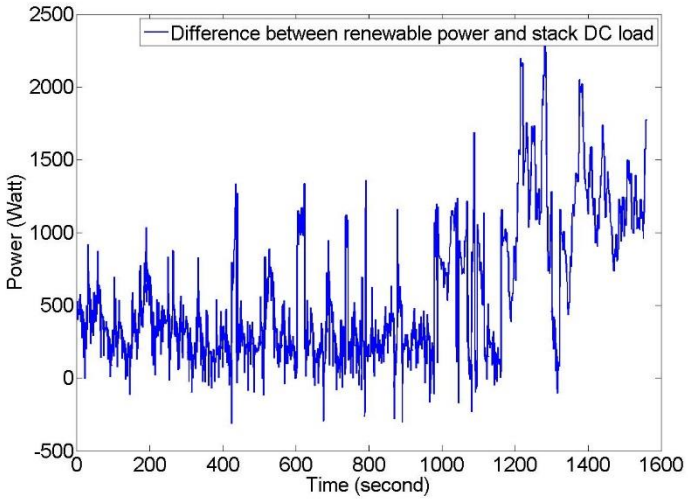

Figure 2.39 The difference between the renewable power and stack load during the operation with renewable power

Figure 2.40 shows the temperature of the lye during operation with renewable power. It was kept almost constant at 47°C, but when the electrolyser went into shut-down mode, it decreased with a sharp slope. The original heat is produced by the electrolysis process itself, and the temperature is controlled by removing the extra heat from the system.

Figure 2.41 shows the pressure of the stack during operation with renewable power. The pressure was kept at around 12 bar(g) during this period, and at the end of operation it decreased sharply as the electrolyser went into shut down mode.

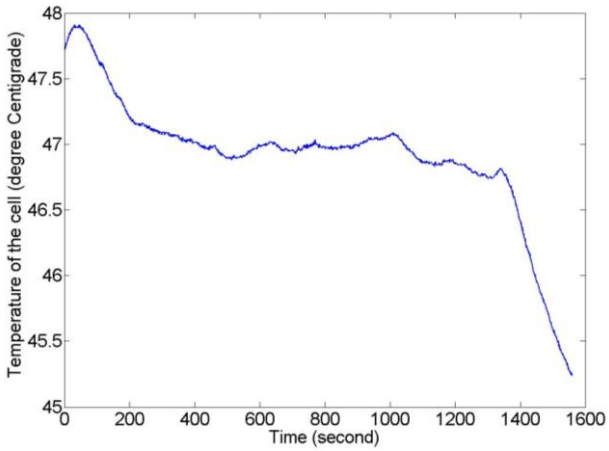

Figure 2.40 The temperature of the lye during the operation with renewable power

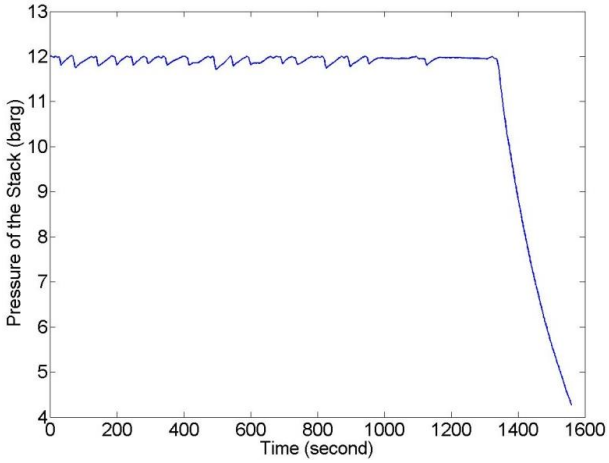

Figure 2.41 The pressure of the stack during the operation with renewable power

Due to the low amount of renewable power available during this period of operation, the current density of the cell stack was very low (between 36 to 104 mA/cm^2), resulting in a very high voltage efficiency, which was almost always above 90% during this operational period.

Figure 2.42 shows the gas impurity during operation using renewable power. The impurity of oxygen in hydrogen was lower than the impurity of hydrogen in oxygen, which increased significantly during this period due to very low cell current densities. The maximum allowable limit of the impurity of gas in any hydrogen system is 4%,

but the alarm system for this electrolyser has a safety margin such that if the impurities go above 1.8%, then the electrolyser goes into shut-down mode automatically.

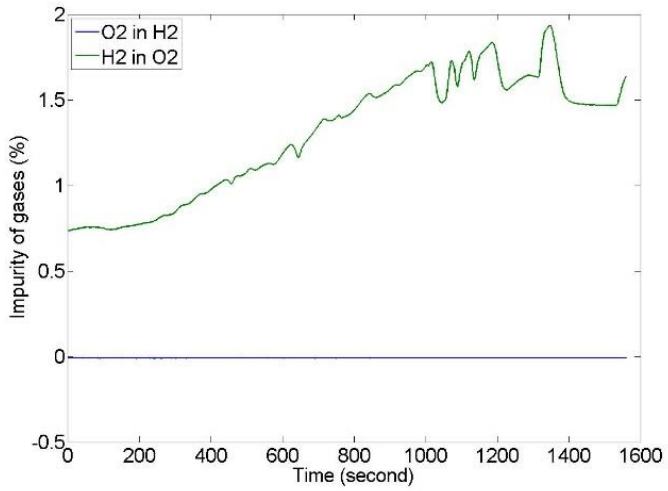

Figure 2.42 The impurity of gases during operation with renewable power

The electrolyser went into shut-down mode once, at 1162.5 s when the impurity reached the maximum threshold of 1.8%, and then the alarms were manually reset by the operator at 1,300 s, so the electrolyser was forced to come back to the operational mode again. During a short period of time, the impurity of gas was decreased because the stack current was zero. Then, as soon as the electrolyser went back into the hydrogen production mode, the impurity of gas increased again. This time, the alarms were not reset, and the system was left to follow its automatic shutdown procedure. From this experiment it is concluded that the minimum current limit of 80 A for the set-point of the cell stack is very low, so this limit should be increased to a higher value.

It is proposed by NEL Hydrogen engineers that the minimum stack current limit should be increased to 200A to avoid the shutdown of the system as a result of an unacceptable amount of gas impurities. In that new case, the minimum load of the stack will be equal to:

$$P_{Min.Stack} = I_{min} * V_{min} = 200 * 16.4 = 3.28\ kW \quad (2.4)$$

Therefore, the percentage of the minimum demand load of the electrolyser can be calculated from the following equation.

$$P_{Min.El}\% = \frac{P_{Min.Stack}+P_{BOP}}{P_{N.El}} * 100 = \frac{3.28kW+1kW}{24kW} * 100 = 17.8\% \quad (2.5)$$

This higher value for the minimum load of the electrolyser reduces the hydrogen yield if the electrolyser is directly connected to renewable resources (e.g. in standalone renewable hydrogen systems), but if many electrolysers work on a grid and are powered from the aggregate power from renewable resources, then this increase in the minimum load of each electrolyser will not be very important for the whole system because their aggregate minimum load will be the same as the minimum load of only one electrolyser, but their aggregate nominal load will be equal to the sum of their nominal loads. Therefore, if the electrolysers on a grid are similarly rated, then the percentage of their aggregate minimum load depends on the minimum load of each electrolyser and also the number of electrolysers available on the system. As the number of electrolysers controlled centrally on a grid increases, their aggregate minimum load percentage becomes smaller.

2.7.10 Shut down process

Before going into shut-down mode, the electrolyser was powered with renewable sources, but the amount of the renewable power was not very high during the electrolyser operation, so the impurity of gases increased significantly. The electrolyser therefore went into shut-down mode, and as a result, the current and the voltage of the cell stack became zero immediately.

Figure 2.43 and Figure 2.44 show the temperature and pressure of the electrolyser during the shutdown process. The temperature of the lye started decreasing as the system went into shutdown mode, and the pressure of the system decreased sharply, reaching 0 bar(g) in a period of only 10 minutes.

The cell stack does not consume any power during the shutdown process, which takes about 30 minutes in normal conditions, mainly due to the nitrogen purging process. It

takes about two minutes to completely shut down the electrolyser in an emergency condition.

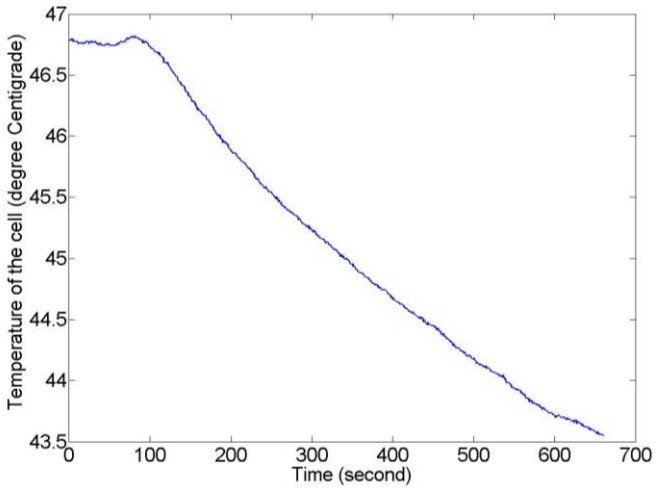

Figure 2.43 The temperature of the lye during the shutdown process

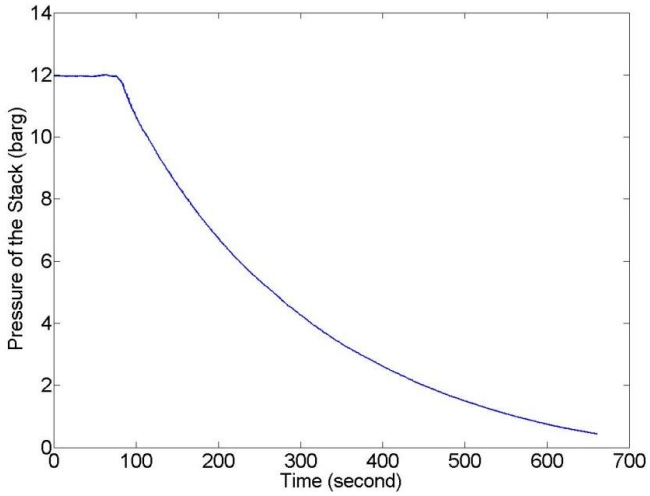

Figure 2.44 The pressure of the stack during the shutdown process

2.7.11 Nitrogen purge at the end of experiment

At the end of the electrolyser operation and after its shut down process, the system must be purged with nitrogen to remove all of the hazardous gases from the system.

Figure 2.45 shows the temperature of the lye during the shutdown nitrogen purging process. The temperature was decreasing as a result of zero current and voltage of the

cells. The reason for the slight increase in the lye temperature in five local small peaks in this figure might be the slight grounding effect of other signals in the system on the measured signal or due to the influx of nitrogen gas at ambient temperature.

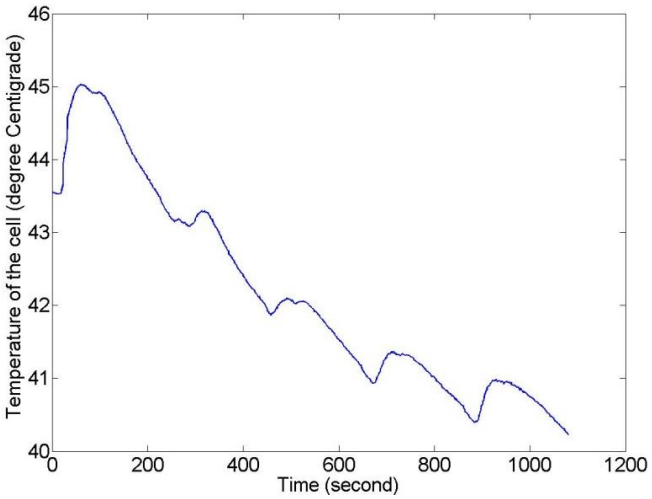

Figure 2.45 The temperature of the lye during the shutdown nitrogen purge

During the shutdown nitrogen purge process, the system was pressurised and depressurised several times with nitrogen gas to make sure that all of the parts of the system were clear of any traces of hydrogen. During this period, the pressure of the system oscillates between 0.6 bar(g) and 2 bar(g).

Due to the time required to perform a start-up and shut-down process, of about 35 minutes each, there is a limit of about 20 start/stop (On/Off) cycles per day. In the case that the operator starts the electrolyser immediately after a shut-down, it is possible to omit one purging sequence, thus increasing the maximum number of On\Off cycles to approximately 40 times per day. NEL Hydrogen claims that there is no degradation in the electrode performance as a result of start/stop switching cycles.

2.7.12 Harmonics of the AC grid

The manufacturer of the electrolyser rectifier is required to make sure that it complies with all relevant electric power system standards, including for harmonics. To record the amount of harmonics injected to the grid from the rectifier input, an oscilloscope

and a current sensor were used to monitor the AC voltage and current of the electrolyser while the stack DC current was 428A. The sampling frequency of the oscilloscope was 5 kHz.

Figure 2.46 shows the AC voltage of one of the phases of the electrolyser grid connection while the electrolyser was producing hydrogen. It had a sine wave shape with a frequency of 50Hz and RMS value of 247.05V.

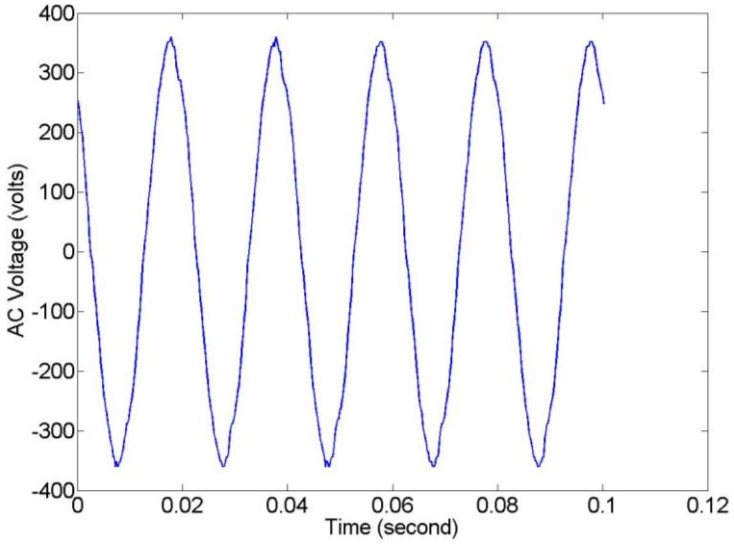

Figure 2.46 The AC input voltage of rectifier while the electrolyser was producing hydrogen

Figure 2.47 shows the single-sided amplitude spectrum of the voltage signal while the electrolyser was producing hydrogen. It is obvious that the main frequency component was 50Hz, and there were no significant harmonics on the voltage of the AC supply.

The calibration coefficient of the current sensor used in this experiment was not known exactly, and the value of the AC current should be multiplied by that coefficient; however, this does not affect the Total Harmonic Distortion (THD) reading. Figure 2.48 shows the current waveform of one of the AC phases supplying the electrolysis system, and Figure 2.49 shows the associated single-sided amplitude spectrum of that current wave. It is clear that there are some harmonic components on the AC current that are occurring at 250 Hz and 350 Hz (i.e. 5^{th} and 7^{th} harmonics).

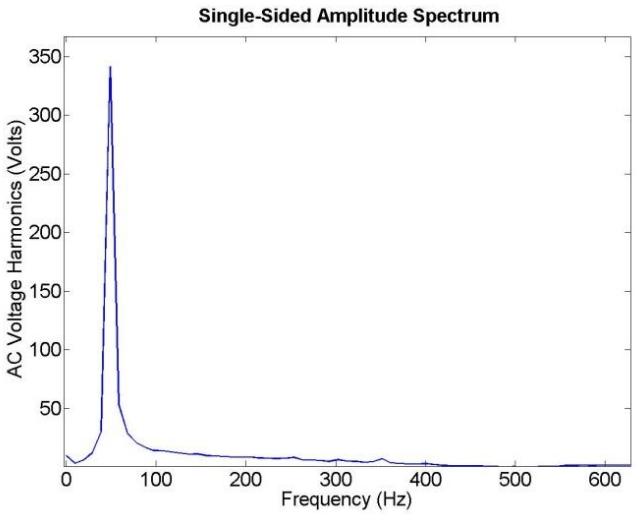

Figure 2.47 The single-sided amplitude spectrum of the AC voltage signal while the electrolyser was producing hydrogen

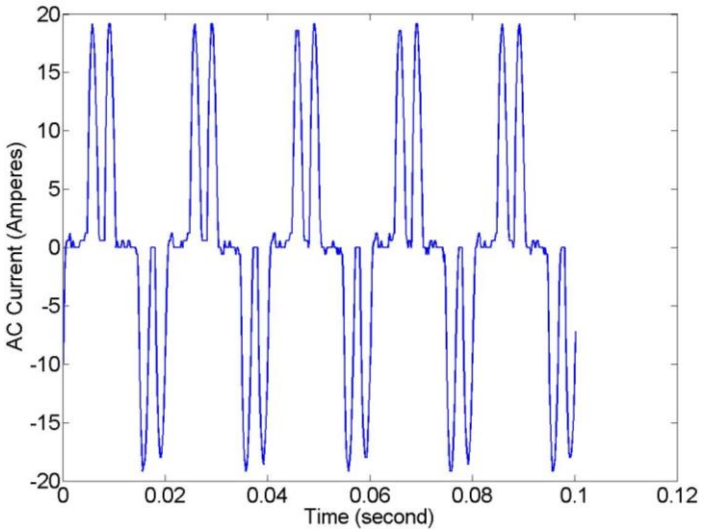

Figure 2.48 The AC current of one phase while the electrolyser is producing hydrogen

The Total Harmonic Distortion (THD) of an AC current signal $i(t)$ is a measure of its distortion [89] and is defined by the following equation which is expressed as a percentage:

$$THD\% = \frac{\sqrt{I_2^2 + I_3^2 + \cdots + I_\infty^2}}{I_1} * 100 \quad (2.6)$$

where I_j, $j \neq 1$, is the amplitude of the j[th] harmonic of the signal, and I_1 is the amplitude of the fundamental.

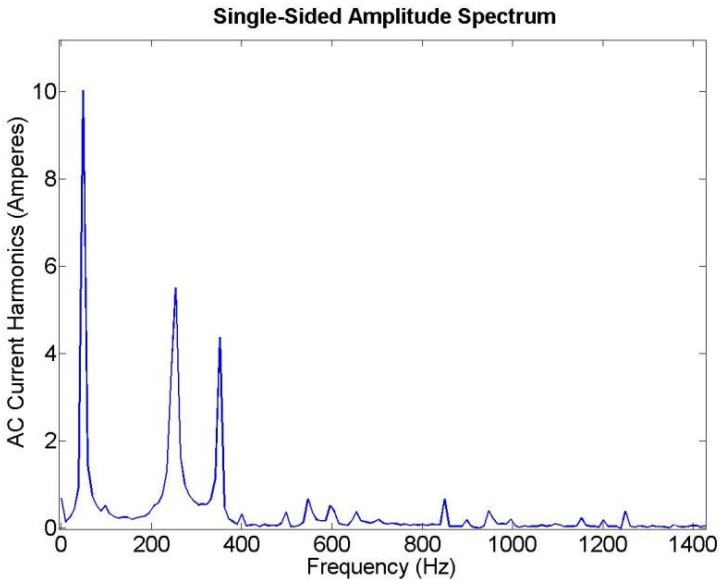

Figure 2.49 The single-sided amplitude spectrum of the AC current waveform while the electrolyser is producing hydrogen

The Total Harmonic Distortion of the AC current signal can be found from Equation 2.6 and Figure 2.49:

$$THD\% = \frac{\sqrt{(5.51)^2+(4.38)^2}}{10.02} * 100 = 70.2\% \quad (2.7)$$

The THD of the AC current signal is very significant, and if there were many of these electrolysers connected to the power system, their aggregate impact on the voltage waveform might well be unacceptable. The rectifier is rated at 42 kW for this small unit, and its THD figure is expected to be high. Nevertheless, the 70.2% THD reflects a rather poor rectifier design [90]. Engineering Recommendation G5/4 [86] sets the planning levels for harmonic voltage distortion to be used in the process of connection of non-linear equipment. It also describes a process of establishing individual customer emission limits based on these planning levels. Rectifiers used in larger electrolysers must be designed to comply with grid codes, so their design will be different from the one connected to the electrolyser in Porsgrunn.

2.8 Experiment on a PEM electrolyser at Strathclyde University

To compare the performance of alkaline electrolysers with PEM units, an experiment was carried out on an 8 KVA PEM electrolyser available at Strathclyde University. However, the PEM electrolyser was working on an On/Off basis, and the operator was not able to vary its demand, so it had a constant rate of hydrogen production.

The name of this commercial PEM electrolyser shown in Figure 2.50 is Hogen 40 Hydrogen generator from Proton Energy Systems Company. The nominal rate of hydrogen production by this electrolyser is about 1 Nm^3/h. The electrolyser is powered from a 230V, 50Hz, 63A single phase AC supply.

The voltage and current of the AC supply of the electrolyser and the DC supply of the cell stack are measured with four Hall effect sensors in this experiment from the point when the electrolyser is started towards the steady-state operating condition, when the electrolyser is producing hydrogen, and eventually until the point where the electrolyser is shut down by the operator.

An overview of the data acquisition system is shown in Figure 2.51. A data acquisition system (*NI USB-6218*) from National Instrument is used to connect the output of sensors to a laptop that records the data using a *LabVIEW* program.

Table 2.8 contains the timeline of the experiment which lasted for only 339 seconds. Figure 2.52 shows the AC current during the experiment. There is some inrush current at the beginning of the electrolyser start-up. The auxiliary equipment in the electrolyser start consuming power immediately after electrolyser start-up, and after some initial preparation process the electrolyser becomes able to produce hydrogen. The electrolyser went into hydrogen production mode after 67s from the start of the electrolyser. This shows how quick these PEM electrolysers can be started in comparison to the alkaline units, which need more than half an hour for start-up process. The electrolyser AC current RMS value reached 2.4A and 30.4A during electrolyser start-up and hydrogen production mode, respectively, while the voltage of the grid was 228V. This means the AC demand of the electrolyser during electrolyser

start-up (or standby) and hydrogen production mode are equal to 0.54 kW and 6.9 kW, respectively.

Figure 2.50 The side view of the PEM electrolyser

Figure 2.53 shows the DC demand of the cell stack during the experiment. The demand reaches 5.6 kW in 80 ms from zero, meaning that the ramp rate of the device is 70 kW/s (8.75 pu/s). It is interesting to note that this value is even slightly lower than the nominal ramp rate of pressurised alkaline units, which is 12.8 pu/s.

The electrolyser also has an input power line filter, which is responsible to filter the harmonics created by the rectifier. It is located after the input of AC supply of the unit, and as a result, there were almost no harmonics observed on the AC current of the electrolyser.

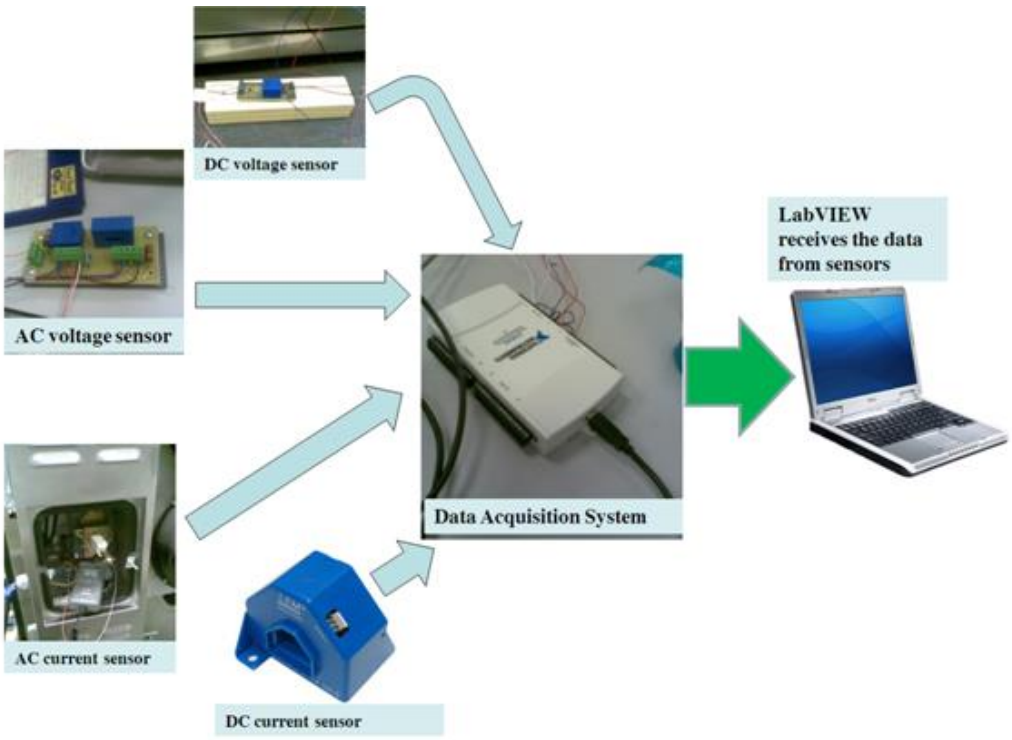

Figure 2.51 An overview of the data acquisition system designed to test the PEM electrolyser

Table 2.8 PEM electrolyser experiment timeline

Event	Time (s)
Starting electrolyser	34
Start of hydrogen production	101
Stop hydrogen production	220
Electrolyser shutdown	309
End of experiment	339

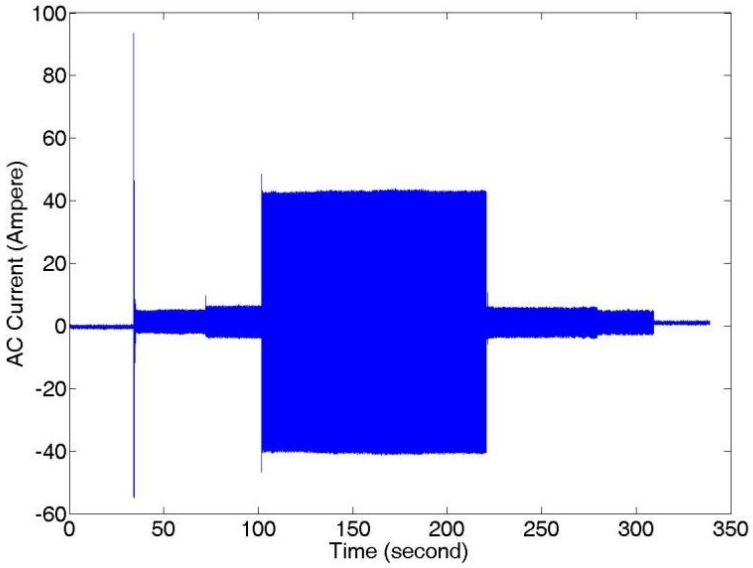

Figure 2.52 The AC current of the PEM electrolyser during the experiment

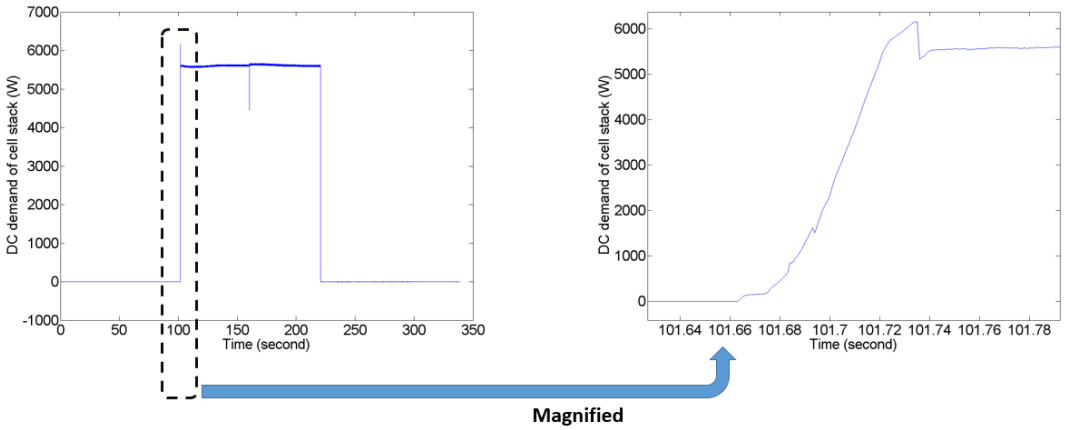

Figure 2.53 DC demand of the PEM electrolyser cell stack

2.9 Chapter summary

The characteristics of a 24 kW pressurised and a 2.1 MW atmospheric electrolyser made by the NEL Hydrogen Company were detailed in this chapter. A comprehensive experiment has been designed to obtain the characteristics of the pressurised alkaline

electrolyser which are useful to make a realistic model of alkaline electrolysers in the context of electrical power systems and, in particular, to identify appropriate control strategies for power system operation. The operational data from experiments on the pressurised electrolyser installed at the Porsgrunn Hydrogen filling station were obtained and then analysed. The experiment had ten different operational phases including cold start, load step change, standby mode, operation with renewable power and shutdown stage. The specifications of the atmospheric and the pressurised units were given in Table 2.1 and Table 2.2 respectively, and then the specifications of both of the units were compared in Table 2.3. In addition, an 8 KVA PEM electrolyser located at Strathclyde University has been tested and its start-up time, ramp rate and standby loss are identified by analysing the experimental results. The characteristics of the alkaline electrolyser mentioned in this chapter will be used in the following chapters to identify appropriate control strategies to run such electrolysers to improve the performance of the electric power system in the presence of renewable power generation.

3 UTILISATION OF ALKALINE ELECTROLYSERS IN EXISTING DISTRIBUTION NETWORKS TO INCREASE THE AMOUNT OF INTEGRATED WIND CAPACITY

3.1 Introduction

In this chapter, the role of alkaline electrolysers located at hydrogen filling stations will be investigated to assess their potential to increase wind generation capacity in an existing distribution system while satisfying mandatory grid constraints. The novelty in this chapter is in the strategy and algorithm used to size, place and control hydrogen production stations within a feeder of a radial distribution network so as to increase wind power capacity and network asset utilisation. The characteristics obtained in Chapter 2 will be used in the simulations to determine the aggregate impact of such units on the performance of the network. The effectiveness of the proposed strategy is investigated through modelling using *MATLAB* software.

3.2 Methodology

In this section a number of hydrogen filling stations with electrolysers and wind farms will be added to a feeder of a radial distribution network. The possibility of consuming some of the surplus power from these wind farms using the electrolysers will be investigated. The electrolysers in this system are assumed to be able to change their demands dynamically within their maximum and minimum demand limits. It is assumed that the Distribution Network Operator (*DNO*) owns and operates the electrolysers, and there is a communication system between the (*DNO*) and each hydrogen filling station that allows adjustment of their electricity demand. The following optimisation steps are proposed to size, place and control these hydrogen filling stations within a feeder of a radial distribution network so as to maximise the utilisation of grid assets while respecting the power system constraints. The aim is to increase the local wind penetration whilst producing green hydrogen for transport using alkaline electrolysers.

1. A number of wind farms will be added to a feeder of a radial distribution network without any storage until they breach the power system constraints during the simulation period or require curtailment to meet the constraints.
2. A number of filling stations with electrolysers will be added to the same feeder of the network. The stations will have a reasonable distance from each other and they will not be placed on the same buses as wind farms in order to reflect locational constraints. Each filling station will comprise a number of equally sized electrolyser units. The initial aggregate rating of filling stations will be chosen to be close to the aggregate rating of the wind farms. However, after the simulation the minimum size of stations needed to satisfy the algorithm objectives and constraints will be identified.
3. An extended Optimal Power Flow (OPF) controller with a primary cost function will be used to minimise the electricity demand of the filling stations and distribution losses at each time step while satisfying the power system constraints. The reason to minimise the demand of each station is to maximise efficiency of hydrogen production and minimise the final size (hence the capital costs) of each station. The electrolyser characteristics identified in Chapter 2 will be used in the optimisation process. The difference between the surplus wind power and electrolyser demand should be positive all the time. This decision is made to ensure that hydrogen production is not occurring using power from conventional plants, which would introduce unwanted carbon dioxide emissions into the energy supply chain of the hydrogen. The electricity demand of each station will be determined by the optimisation algorithm, and then the demand of each individual electrolyser making up a station will be determined by a local controller at each filling station considering the characteristics of electrolysers. The minimum electricity demand at a station is equal to the minimum demand of an electrolyser unit at that site.
4. After running the simulation for a duration of a year, the maximum electricity demand of each station during the simulation will be used to determine its optimal rating.
5. The location of the hydrogen stations on the feeder will be varied and then the above steps (3 and 4) will be repeated to find the best solution to minimise the

size of stations and network losses while maximising the profit from selling hydrogen according to an income function.

Figure 3.1 summarises the heuristic optimisation algorithm proposed in this work to size, place and control electrolysis hydrogen filling stations within a radial distribution network.

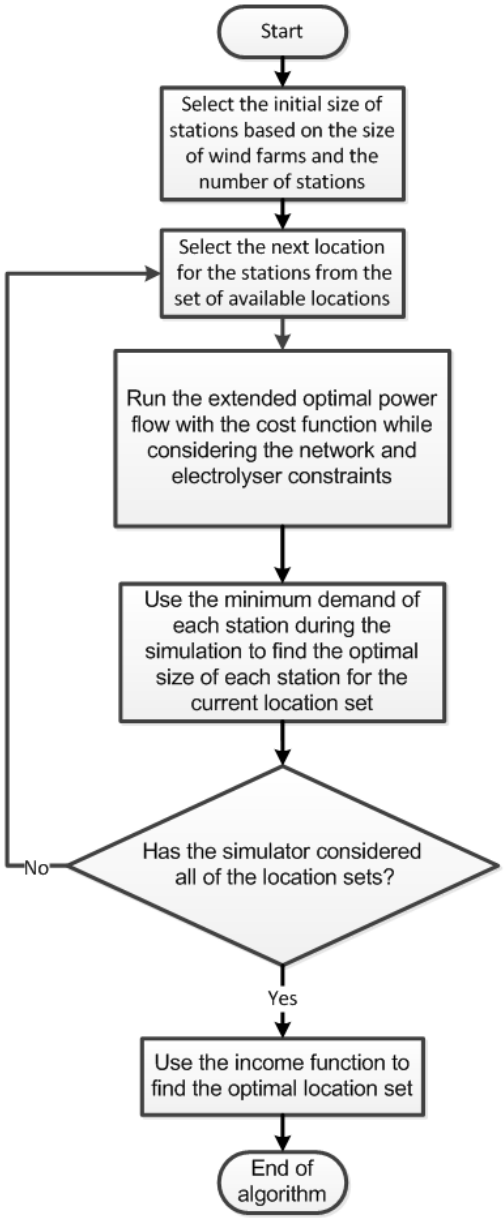

Figure 3.1 The algorithm used to size, place and control the hydrogen stations

It is also assumed that each electrolyser behaves like a linear load consuming only active power within its acceptable operational range. The minimum demand of each electrolyser is assumed to be equal to 20% of its nominal demand.

After the simulation, the results of currents and voltages and distribution losses before and after adding hydrogen filling stations will be compared to assess the role of electrolysers in improving power system operation. In the cases that the voltage of busses or flow of the branches are out of limits, the probability of voltage violations or overload in different scenarios will be compared.

3.3 Network case study: *UKGDS* High Voltage (HV) Underground (UG) Network

The United Kingdom Generic Distribution System (*UKGDS*) is a resource for simulation and analysis of the impact of distributed generation on the UK power network. These models were developed by a group of researchers in the UK to provide test platforms to facilitate research on the subject of power system modelling for the purpose of meeting the government's objectives for distributed generation in the UK. The models represent the most common architectures used by the UK Distribution Network Operators (*DNOs*), but they are slightly altered to facilitate testing and evaluation of new concepts. The source data for the *UKGDS* models were taken either from the relevant Long Term Development Statement or from simulation software data files, but the models were modified to disguise the original source and make the models suitable as generic test network models. Load characteristic profiles and typical generation patterns were added in the *UKGDS* models to support temporal analysis by the model developers. The *UKGDS* network models are realistic, so the test results from the models are credible [91].

A radial distribution network is used as a case study in this chapter to evaluate the effectiveness of the proposed strategy. This type of network is used as it is much easier to consider the distance of stations from each other while placing them on the network. In real life, it is not very useful to put the filling stations on every node of the power

system and then run the optimisation process, which might lead to cases of having some filling stations very close to each other, and on the other hand, having some areas not covered by any nearby hydrogen filling station. Therefore, a radial distribution network will best suit the aim of the work in this chapter to show the effectiveness of the control strategy.

The *UKGDS* phase one library of network models consists of two types of networks:

- Extra High Voltage (*EHV*) networks, which extend from a grid supply point at 275kV or 400kV (or 132kV in Scotland) down to the primary substations feeding 11kV or 6.6kV networks.
- High Voltage (*HV*) networks, which consist of 11kV and 6.6kV networks fed from primary substations.

There are six EHV models and seven HV models [91]. A *UKGDS* phase one High Voltage (*HV*) Underground (*UG*) network is used in this study.

3.4 Modelling details

Software was developed by the author using *MATLAB* and *MATPOWER* [74] to simulate the proposed scenarios applied to the *UKGDS* model. Figure 3.2 shows a *UKGDS* phase one High Voltage (*HV*) Underground (*UG*) network, [91], with added hydrogen filling stations and wind farms. The parameters for the simulation of the *UKGDS* power system are taken from [91]. The other distributed generators that are not needed in this modelling work are removed from the network.

The aggregate total demand on the *UKGDS* HV UG network is 24.2 MW [91], so the electricity demand profile for the United Kingdom [92] is scaled down to match to the load profile of this *UKGDS* system, and then it is used in the simulation process.

It is assumed that the loads on each node of the power system are constant during each simulation time interval. The amount of demand at different system nodes is equal to the proportion of loads defined in the *UKGDS* load profile.

In this work, the hydrogen stations and wind farms are modelled on only one feeder of the system (feeder number 8, which is the last one) to assess the performance of the proposed control strategy. The filling stations are added on three buses, and the wind farms are also added at bus 58 and 63 of the *UKGDS* model. Table 3.1 contains the location of each hydrogen filling station proposed for each simulation scenario. The location of each station in each of the five sets is selected in a way that the stations have a reasonable distance from each other, and they are not placed on the same bus as the wind farms. In addition, it can be assumed that the locational constraints, e.g. being close to the main roads/motorways where HFCVs can refuel, have played a role in determining these specific locations for hydrogen filling stations.

To scale the wind farms to the *UKGDS* model and cause a violation of power system constraints without utilisation of electrolysers, their nominal generation capacity was selected to be 10 MW. Table 3.2 also shows the location and size of wind farms used in this work.

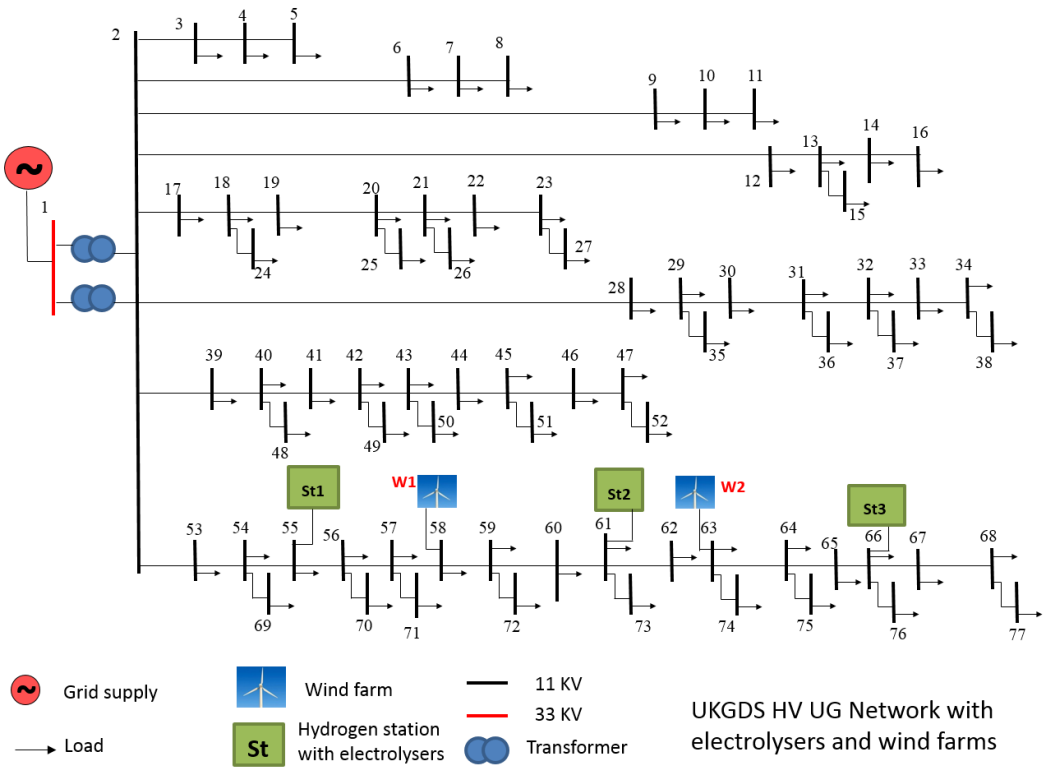

Figure 3.2 UKGDS HV UG network with wind farms and hydrogen filling stations

Table 3.1 The location of hydrogen filling stations in each set

Set number/station location	Station bus number		
	Station 1	Station 2	Station 3
Set 1	53	59	64
Set 2	54	60	65
Set 3	55	61	66
Set 4	56	62	67
Set 5	57	64	68

Table 3.2 Wind farm location and size

	Location (bus number)	Capacity (MW)
Wind farm 1	58	10
Wind farm 2	63	10

Wind speed data with resolution of one hour from two UK regions (Tain Range and Peterhead [93]), which was obtained from the UK meteorological office for the duration of one year, was used in the analysis. For simplicity, it is assumed that the wind turbines used in the wind farms are of the same type and with the same rating, and they have a power curve as shown in Figure 3.3. This power curve was taken from a 2 MW wind turbine made by Repower, [94]. It is assumed that the efficiency of electrical generation and power conversion is included in this curve in conformity with power curve measurement standards. Using the wind speed data, the turbine power curve in Figure 3.3 and the rated size of wind farms in Table 3.2, a simple *MATLAB* program was developed to calculate the output of each wind farm during a year with one hour resolution.

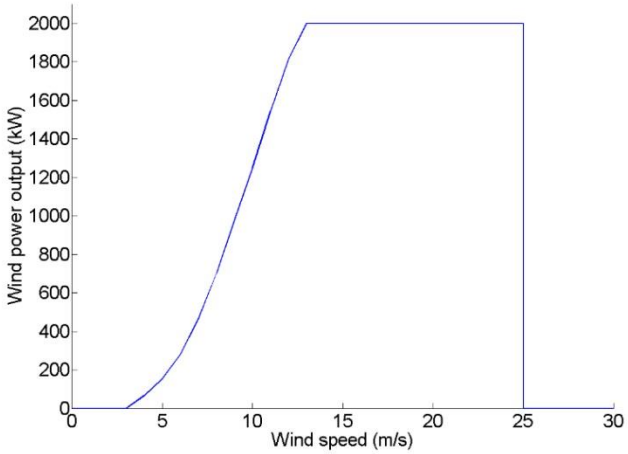

Figure 3.3 The power curve of a 2 MW wind turbine from 'REpower systems' company, [94]

To select the initial size of stations, the following assumptions were made.

- The initial size of each station is an integer multiple of 2 MW which is the assumed size of each electrolyser.
- The initial size of all the stations are equal (i.e. they have the same number of electrolyser units).
- The aggregate nominal demand of stations is chosen to be as close as possible to the aggregate capacity of wind farms.

Based on these assumptions, the following equation is used to find the initial size of each station (S_{St}) in MW. The 'Round' operator is used to make sure the initial proposed size of each station is an integer multiple of the size of each electrolyser.

$$S_{St} = Round\left(\frac{1}{NS*P_{N.El}} * \sum_{i=1}^{NW} S_W^i\right) * P_{N.El} \quad (3.1)$$

where

NS is the total number of filling stations.

$P_{N.El}$ is the size (nominal demand) of each electrolysis unit located at each filling station in MW (assumed to be 2 MW here).

S_W^i is the size of i[th] wind farm in MW.

NW is the total number of wind farms placed within the network.

By inserting the corresponding values in Equation 3.1 the initial size of each station was found to be 6 MW.

The number of electrolysers at each station (N_{El}^{EST}) can be calculated from the following equation.

$$N_{El}^{EST} = \frac{S_{St}}{P_{N.El}} \tag{3.2}$$

This means that 3 electrolysers with a rating of 2 MW are located at each station at the start of the simulation in this first case study.

Two scenarios are considered in the simulations. In the first scenario, the system only has two wind farms without any electrolysers, and the fluctuation in the difference between the local generation and demand must as far as possible be compensated by import/export of power from the distribution substation. In the second scenario, electrolysers are also operating in the system to capture some of the surplus wind power generated within the feeder to alleviate the problems caused by the distributed wind generation within the network. The assumptions and strategy used in the second scenario to operate the electrolysers is explained below.

It is assumed that the demand of each station is controllable from the distribution network control centre.

A cost function ($Cost(t)$) is defined to minimise the electricity demand from stations and also the losses within the distribution system. The objective of the optimisation is to find the optimal demand of each station to minimise $Cost$ (£) at each simulation time step.

$$Cost(t) = C_1 * T * \sum_{i=1}^{NS} SD_i^t + C_2 * T * \sum_{i=1}^{NB} P_{Loss_i}^t \tag{3.3}$$

where

‘t’ is the current time interval number in the simulation.

‘T’ is the simulation time interval in hours. (T=1 hour).

C_i are the cost function coefficients.

SD_i^t is the demand from station ‘i’ during the current time interval of ‘t’ in MW.

NB is the number of branches on the power system.

$P_{Loss_i}^t$ is the amount of power loss on branch ‘i’ of the power system at the time interval ‘t’ in MW.

The capital, operational and maintenance costs of alkaline electrolyser from Table 1.2 are used to find C_1 in £/MW/h.

$$C_1 = \frac{Capital}{Life*365*24} + \frac{OM}{365*24} = \frac{1480{,}000}{20*365*24} + \frac{1480{,}000*0.02}{365*24} = 11.82\ (£/MW/h) \quad (3.4)$$

where

$Capital$ is the capital cost of an electrolyser in £/MW.

OM is the annual operational and maintenance cost of an electrolyser in £/MW/year.

$Life$ is the lifetime of an electrolyser in years.

C_2 is the cost of electricity loss and selected to be £35/MWh [95].

There are some limits on the demand of stations and also power system constraints that should be respected during the optimisation process. Before detailing those limits, some additional variables are defined here.

The surplus wind power on the last feeder of the network can be calculated from the following equation. The controller needs to know the amount of wind generation and non-electrolysis demand on each bus of the feeder at each time step in order to calculate the surplus wind generation.

$$Surplus(t) = \sum_{i=1}^{NW} W_i^t - \sum_{i=53}^{77} D_i^t \quad (3.5)$$

Where

W_i^t is the output of wind farm 'i' in MW at the current time step t.

NW is the number of wind farms on the considered feeder.

D_i^t is the amount of demand (excluding the demand of electrolysers) in MW on bus 'i' of the last feeder (from bus 53 to bus 77) at the current time step t.

If, at a given time step, the surplus power is not sufficient to supply the minimum demand for all of the stations (i.e. to keep at least one of their electrolysers in hydrogen production mode), then the stations with least energy delivered to them up to the current time step will be selected to be removed from list of active stations and their demand will be assumed to be zero. This decision is taken to make sure that the stations which have received more energy during the simulation will be more likely to stay active (produce hydrogen) and continue providing service to improve the performance of the power system, and the stations which have had lower demand in the previous time steps and are more likely to have less impact on the improvement of the results become deactivated when there is not enough surplus power within the system. Figure 3.4 shows the algorithm used at each time interval to choose which station is active and which stations do not have any active electrolysers if the surplus wind power is not sufficient enough to provide the minimum demand for all of the stations.

The '$Surplus$' value could become negative at some points when the aggregate wind power generation is below the aggregate local non-electrolysis demand. Therefore another variable called 'Aggregate Station Demand Limit' ($ASDL$) is defined to be used as the limit in the simulations to make sure the aggregate demand from the local hydrogen stations does not exceed the surplus wind (in the case that the surplus wind is positive), and therefore avoid conditions that the electrolysers consume power from thermal generation plant and thus produce hydrogen from non-renewable sources. In addition, when the '$Surplus$' value is negative, the hydrogen stations should not consume any power.

$$ASDL(t) = \max(Surplus(t), 0) \tag{3.6}$$

$ASDL$ will always have a non-negative value. This means that if '$Surplus(t)$' is positive then $ASDL(t)$ will be equal to $Surplus(t)$, but if $Surplus(t)$ is negative, then $ASDL(t)$ will be equal to zero.

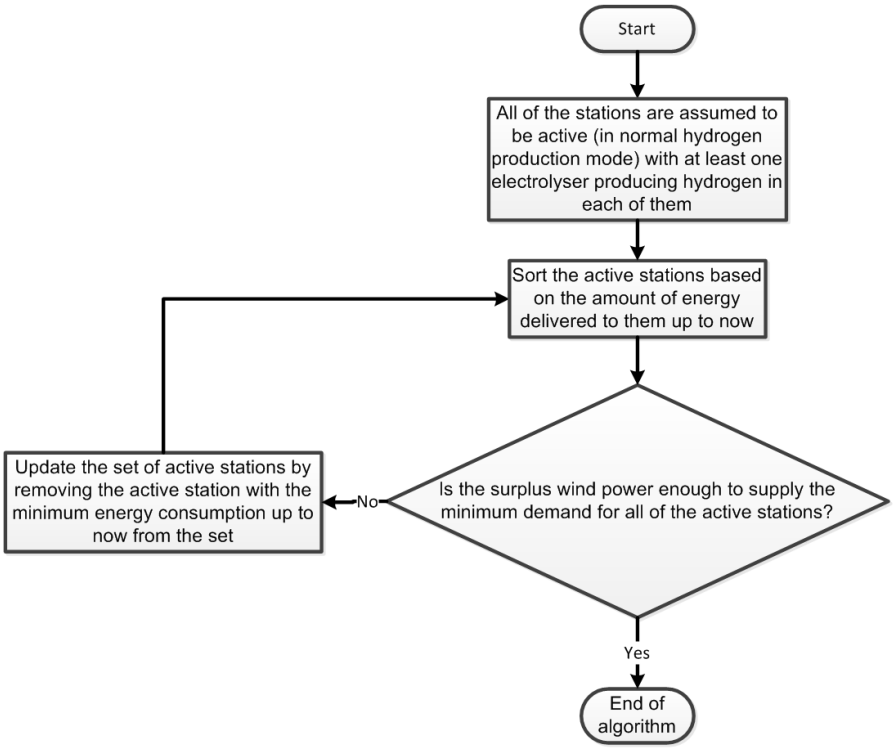

Figure 3.4 The algorithm used at each time interval to update the supplied stations (active stations) when there is lack of surplus power for all of the stations

The limits for the aggregate demand of the active stations are defined by the following equation.

$$NAS^t * P_{Min.El} \leq \sum_{i=1}^{NS} SD_i^t \leq ASDL(t) \qquad (3.7)$$

where

NAS^t is the number of active stations at the current time interval of 't'.

$P_{Min.El}$ is the minimum demand from an electrolyser to stay in active hydrogen production mode, and it is equal to the minimum demand of a station in MW.

The following limit will also be applied to the electricity demand of each active station as the minimum demand of one station will be equal to the minimum demand of one electrolyser.

$$P_{Min.El} \leq SD_i^t \leq S_{St} \quad (3.8)$$

The constraints of the power system should be respected during the optimisation process.

Apparent power constraints:

$$\left|S_{ij}^t\right| \leq \left|S_{ij}^{Lim}\right| \quad \forall\, i,j \in B \quad (3.9)$$

where

S_{ij}^t is the complex power flow between bus 'i' and 'j' of the network in MVA in the current time interval of 't'.

$\left|S_{ij}^t\right|$ is the apparent power between bus 'i' and 'j' of the power system in MVA in the current time interval of 't'.

$\left|S_{ij}^{Lim}\right|$ is the apparent power limit between bus 'i' and 'j' of the power system in MVA.

B is the set of bus numbers within the network.

Voltage constraints:

$$\left|V_i^{Min}\right| \leq |V_i^t| \leq \left|V_i^{Max}\right| \quad \forall\, i \in B \quad (3.10)$$

where

$|V_i^t|$ is the magnitude of voltage on bus 'i' of the power system in pu in the current time interval of 't'.

$\left|V_i^{Min}\right|$ and $\left|V_i^{Max}\right|$ are respectively the minimum and maximum limits for the voltage magnitude on bus 'i' of the power system in pu. The voltage variation limits in the

UKGDS network are ±3% of the nominal nodal voltage, [91]. In this study, the power system limits are assumed to be constant during the whole year.

After running the simulation and finding the optimal demand of each station at each time step, the distribution network control centre can send the demand set-point of each station to the local station controllers, which are responsible to operate individual electrolysers according to their operational status and constraints. Figure 3.5 shows the algorithm used at each time interval to select the number of active electrolysers (electrolysers in hydrogen production mode) and their demand at each active station.

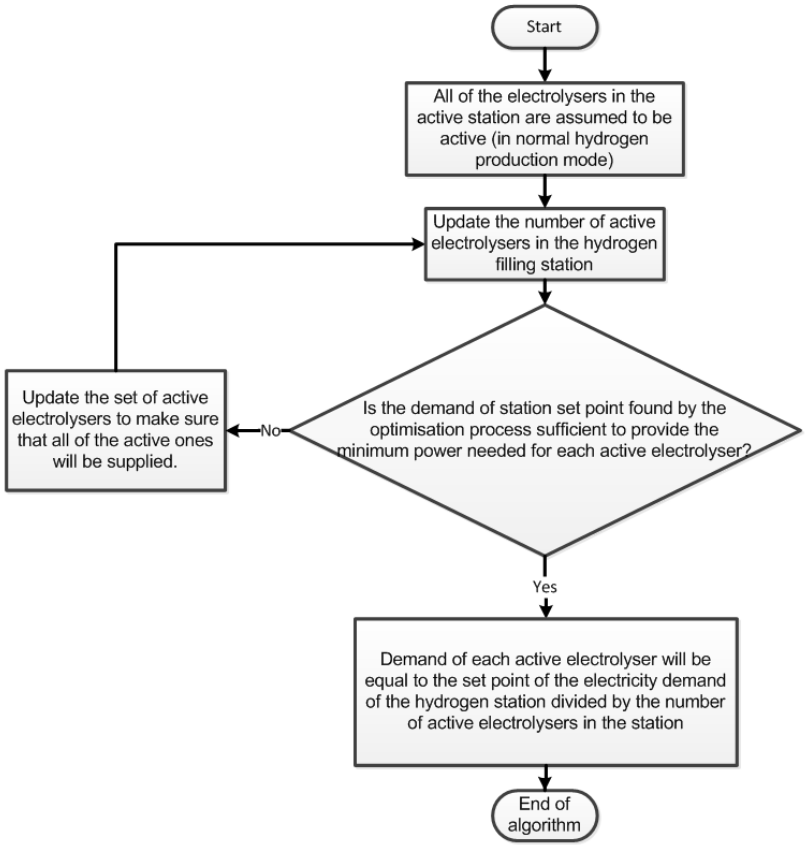

Figure 3.5 The algorithm used to select the number of active electrolysers and their demand at each active station

The objective of this algorithm is to keep as many electrolysers as possible in hydrogen production mode to maximise the efficiency of hydrogen production in each filling

station. The controller selects the number of active electrolysers ($NAEL_j^t$) at active filling station 'j' at each time interval 't' using the following equation.

$$NAEL_j^t = \min\left(\left\lfloor \frac{SD_j^t}{P_{Min.El}} \right\rfloor, N_{El}^{EST}\right) \quad \forall \ \ (1 \leq j \leq NAS^t \ , \ j \in \mathbb{N}) \qquad (3.11)$$

The 'min' operator is used to make sure that the number of active electrolysers in each active station at each time interval is not bigger than the total number of electrolysers at each station (N_{El}^{EST}). The 'floor' operator ($\lfloor \ \rfloor$) is used to make sure that demand set-point of each active station is sufficient to provide the minimum demand of each active electrolyser located in the station all the time ($NAEL_j^t * P_{Min.El} \leq SD_j^t$).

To calculate the amount of hydrogen production in each station, an efficiency curve must be used for the electrolysers operating at each station. As explained in Chapter 2 the efficiency curve of electrolysers depend on their design, but the efficiency curve of alkaline electrolysers have a general shape typical of Figure 3.6. To calculate the amount of hydrogen production in this thesis, it is assumed that all of the electrolysers operating in the filling stations have the efficiency curve presented in Figure 3.6. These electrolysers have an energy efficiency of 80% when they operate at their minimum demand (20% of nominal demand), and a minimum efficiency of 65% when they are operating at their maximum demand. It is assumed that the efficiency of the rectifier, Faraday efficiency and Balance of the Plant (BOP) of the electrolyser were considered while obtaining this efficiency curve. The author has studied a number of rectifiers available for use in electrolysis plant made by Beijing Chunshu Rectifier Company Ltd., and most of their rectifiers have a quoted efficiency of between 89%-96% [96]. The efficiency of the rectifiers change with respect to the load they supply, but in this work it was assumed that the efficiency of the rectifiers supplying electrolysis cell stacks are constant and equal to 94% during the electrolyser operation. In addition, according to NEL Hydrogen, the current efficiency (Faraday efficiency) of their electrolysers is about 99.7% mainly due to the loss of hydrogen going into the oxygen gas part (gas impurity problem). The lowest current efficiency of their electrolysers is 99.3%, and it happens when the stack current is at its minimum level. In this work, the Faraday efficiency of the electrolyser is assumed to be constant and equal to 99.5% during the operation of electrolyser, and it is also assumed that this efficiency was

considered when obtaining the efficiency curve in Figure 3.6. In this curve, it was assumed that the operating temperature and pressure of the electrolyser will remain constant during the simulation.

The controller gives the same amount of power to each active electrolyser in each station. This means that the hydrogen production system will operate with the maximum efficiency because the electrolysers will consume the minimum possible power at all times. Therefore, the demand of 'i'th active electrolyser (ELD_{ij}^{t} in MW) located at 'j'th active filling station can be calculated using the following equation.

$$ELD_{ij}^{t} = \frac{SD_{j}^{t}}{NAEL_{j}^{t}} \qquad \forall\, (1 \leq i \leq NAEL_{j}^{t}\ ,\ 1 \leq j \leq NAS^{t}\ ,\ \ i,j \in \mathbb{N}) \qquad (3.12)$$

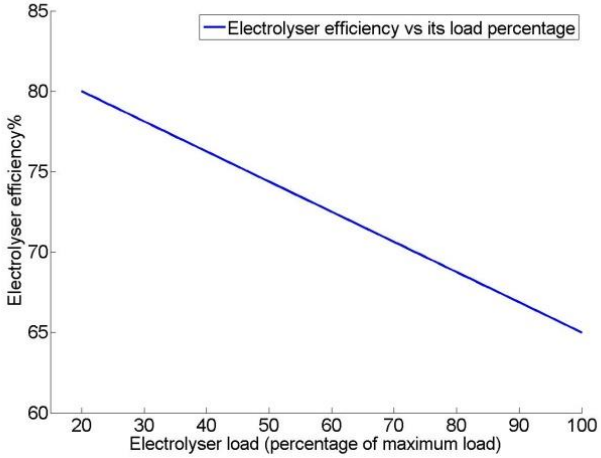

Figure 3.6 Energy efficiency curve of the electrolysers used in the models in this chapter

Using the efficiency curve in Figure 3.6 and the above equation, the amount of hydrogen produced ($H2P_{ij}^{t}$ in kg) by 'i'th active electrolyser at 'j'th active hydrogen filling station can be found using the following equation.

$$H2P_{ij}^{t} = \eta_{ij}^{t} * \frac{ELD_{ij}^{t} * 1000}{E_{HHV}} \qquad \forall\, (1 \leq i \leq NAEL_{j}^{t}\ ,\ 1 \leq j \leq NAS^{t},\ i,j \in \mathbb{N}) \quad (3.13)$$

where

η_{ij}^{t}% is the efficiency of the 'i'th active electrolyser in the 'j'th active station in percentage.

E_{HHV} is the Higher Heating Value (HHV) of hydrogen (39 kWh/kg, [25]).

3.5 Simulation results and discussions

This section contains the results of running the simulation for a duration of 24 hours and a year using an extended OPF feature in *MATPOWER* implemented in *MATLAB*. For the 24 hour period simulation, the location Set1 is used to show the effectiveness of the control strategy. However, at the end of this section, the results from all location sets, while running the simulation for a year, is presented so as to identify the best location for the stations.

The UK electricity demand profile on the 6th of January 2014 is scaled down to *UKGDS* demand scale and used the simulation. Figure 3.7 shows the total demand profile which was applied to the *UKGDS* model.

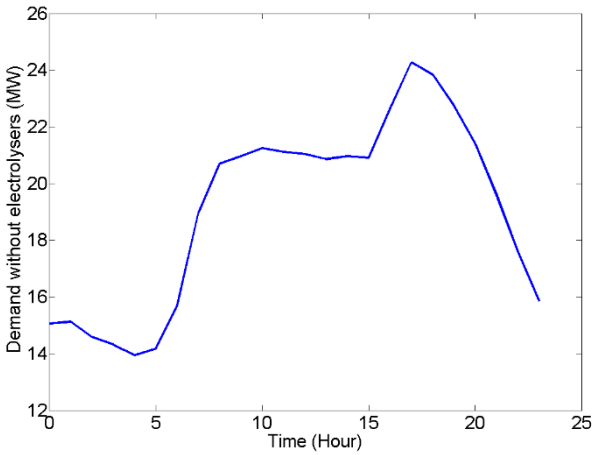

Figure 3.7 The demand profile used for the 24 hour simulation

To achieve the optimisation goal, the algorithm illustrated in Figure 3.1 is applied to the system for a 24 hour period with a time resolution of one hour to match the available wind speed data. The other loads in the systems were assumed to be constant during each simulation time interval. A further assumption is that the outputs of the

wind turbines are constant during each time interval. Such requirement of constant voltage and power, over a fixed time interval is necessary to run the power system load flow analysis. The active output powers from the wind farms used in the simulation are plotted in Figure 3.8.

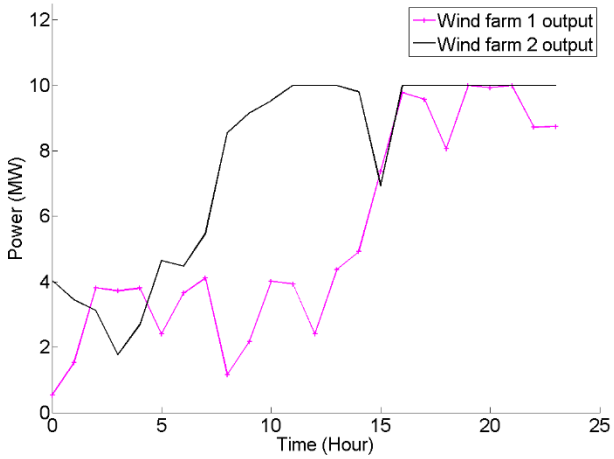

Figure 3.8 The output power from two wind farms during the simulation

Figure 3.9 shows the demand from the three filling stations within the network during the simulation. The result show that the demand of station 1 which is located at bus 53 (in location set 1) is much lower than the demand of other stations. This means that just two filling stations were able deal with most of the problems created as the result of adding intermittent renewable power from wind farms, and there was no need to increase the demand of the first station to any significant level to improve the performance of the grid. Therefore, station 1 will have the lowest hydrogen production, and according to the algorithm in Figure 3.4 it is more likely to go into standby condition during the simulation if there is lack of wind power generation.

Figure 3.10 shows the aggregate surplus wind power on feeder 8 and also the aggregate demand from all stations. As specified in the control strategy, the aggregate demand of electrolysers is always below or equal to the surplus wind power within the system if this surplus power is a positive value. The difference of power between two curves in Figure 3.10 is the power that is exported to other feeders of the power system. In cases where the aggregate surplus power becomes negative or zero, the demand of the filling stations will be zero to avoid the electrolysers working with non-renewable

power. In such cases, some limited power will also be imported from the substation to supply some of the local non-electrolysis demands which were not fully supplied due to lack of local wind power generation.

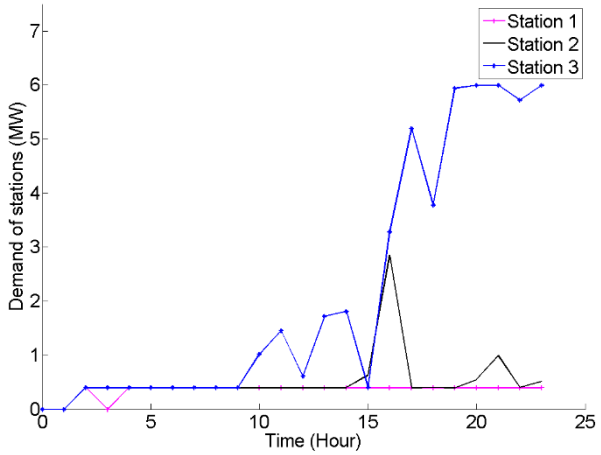

Figure 3.9 Demand of stations within the network during a 24 hour simulation

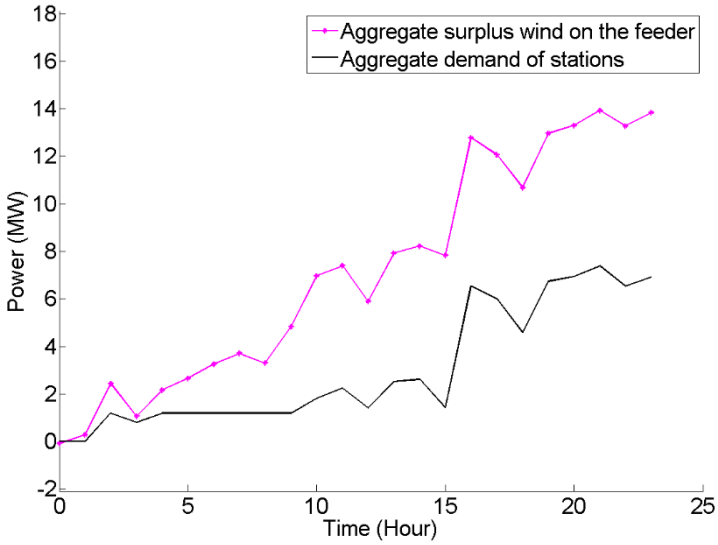

Figure 3.10 Aggregate surplus wind power and aggregate demand of hydrogen stations

The total amount of wind energy absorbed by the network during the one day was equal to 300.6 MWh, and about 69.4 MWh of energy was used by electrolysers in the filling stations. The rest of the wind energy was consumed by the local demand on the same feeder or the demand on other feeders.

Figure 3.11 shows the total amount of wind power absorbed by the electrical system, and also its difference from the total demand (including electrolysers) on feeder 8. Obviously, this difference is smoothed as a result of utilisation of electrolysers resulting in less fluctuation in the amount of power output of thermal power plants, which will lead to an increase in their efficiency and reduce the amount of their carbon dioxide emission.

With the introduction of the electrolysers to the system, the voltages on different system nodes change. For example, the voltage on bus 63, which has a nominal voltage of 11KV, is shown in Figure 3.12. This bus was selected because it had the maximum voltage rise as a result of adding wind farms without the utilisation of electrolysers. As was expected, the maximum voltage rise occurred on one of the buses where wind farms were added to the system. After utilisation of electrolysers, the voltage of the bus remained within the acceptable limits. In addition, the electrolysers smooth the voltage fluctuation on this bus in comparison to the first scenario. The standard deviation of the voltage on this bus without utilisation of electrolysers was 0.0229 pu, which reduced to 0.0056 pu after utilisation of electrolysers during a 24 hour simulation.

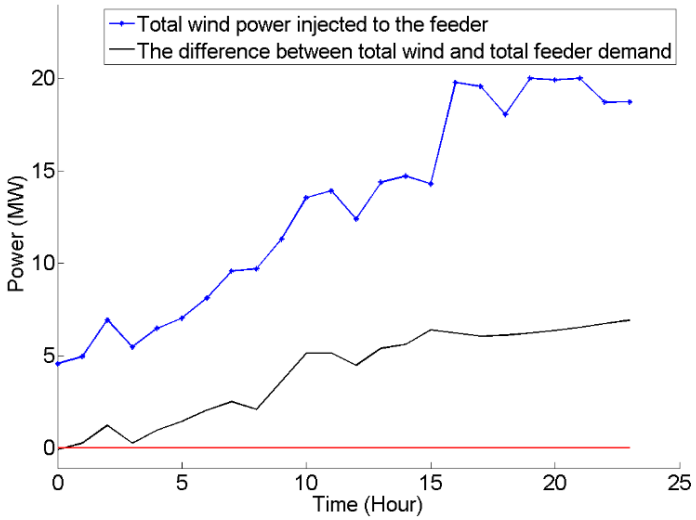

Figure 3.11 The total amount of wind power injected to the grid and its difference with the aggregate demand on the feeder

The simulation results show that the voltage limit on many buses were breached at least once during the simulation in the system without electrolysers, and that all of them are driven back within the limits as the result of utilisation of the control strategy with electrolysers.

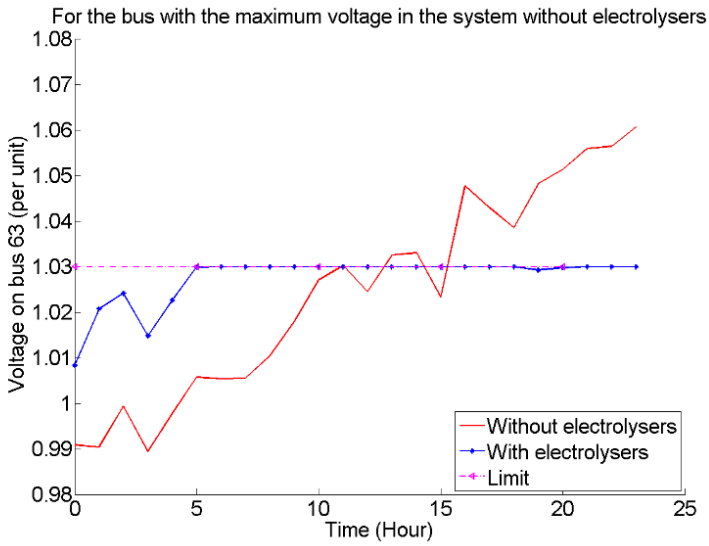

Figure 3.12 The voltage on bus 63 before and after adding electrolysers to the system

Figure 3.13 shows the amount of apparent power on the branch of power system which has the maximum peak value, in percentage terms, without using electrolysers during the simulation. It is obvious that the after using the electrolysers within the system the apparent power of this branch was controlled to remain within the acceptable limits. The simulation results show that the apparent power limit on branches 53, 54, 55, 56, 57 and 58 were breached at least once during the 24 hour simulation in the system without electrolysers, and all of them were driven back within the limits as the result of utilisation of the control strategy with electrolysers.

On the other hand, there were some branches of the power system which were underutilised in the system without electrolysers and their apparent power peak was only a fraction of the nominal capacity limit of the branch. Figure 3.14 shows the apparent power of branch 64 of the power system with and without utilisation of electrolysers. It has reached a much higher average apparent power while operating with electrolysers. This shows the effectiveness of the control strategy to increase the utilisation of network assets and to remove the need for grid upgrades and associated

costs while respecting the power system constraints and producing green hydrogen for the transport sector.

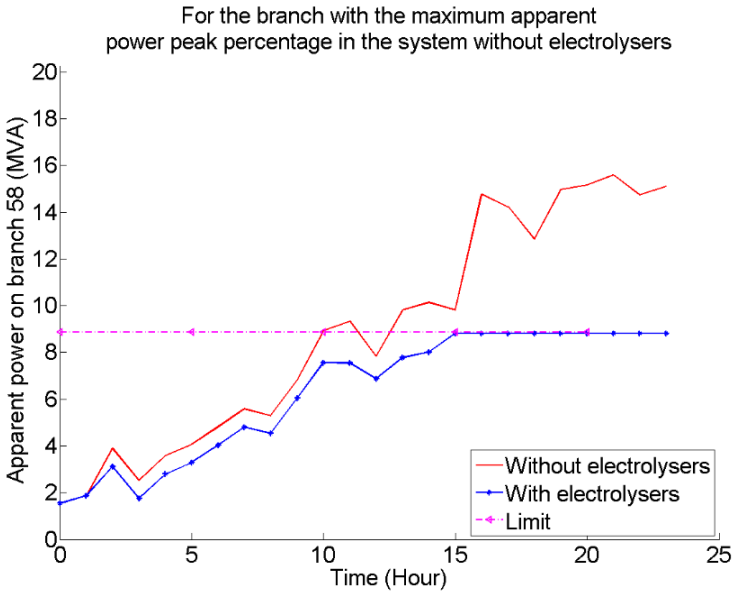

Figure 3.13 Apparent power on a branch of power system with the biggest peak percentage during the simulation

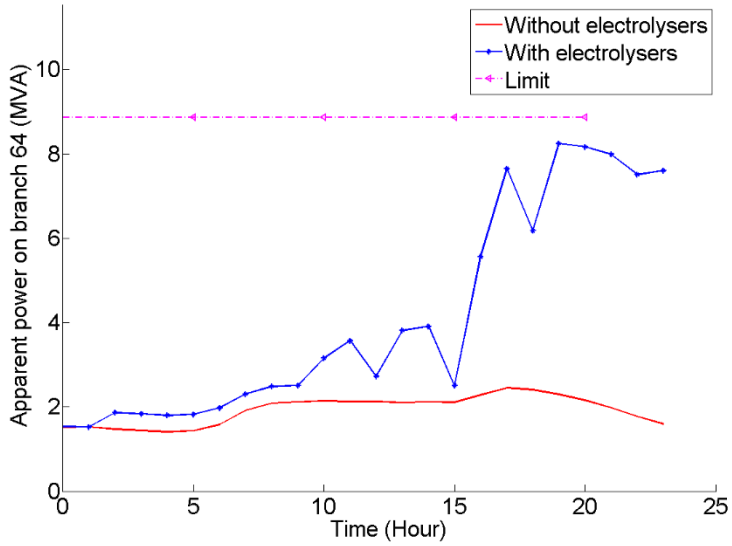

Figure 3.14 The apparent power of branch 64 of the power system with and without utilisation of electrolysers

To quantify the probability of constraint violations the following attributes, which were proposed in [97], are used in this work.

The probability of voltage constraint violation ($VB_{Prob}\%$) is calculated as the ratio of the total number of time steps that at least one node within the network had a voltage constraint violation divided by the total number of simulation time steps.

$$VB_{Prob}\% = \frac{\sum_{t=1}^{NDP} VB_t}{NDP} * 100 \tag{3.14}$$

where

NDP is the number of data points during the simulation (e.g. if the simulation is carried out for a duration of 24 hours with time interval of 1 hour, then NDP=24).

VB_t is the function that indicates whether there has been any voltage violation within the grid at time interval 't'.

$$VB_t = \begin{cases} 0 & if\ (\left|V_i^{Min}\right| \leq |V_i^t| \leq \left|V_i^{Max}\right| \quad \forall\ i \in B) \\ 1 & otherwise \end{cases} \tag{3.15}$$

Similarly, the probability of thermal limit violations ($TLB_{Prob}\%$) is calculated as the ratio of the total number of time steps that at least one branch within the network was overloaded divided by the total number of simulation time steps.

$$TLB_{Prob}\% = \frac{\sum_{t=1}^{NDP} TLB_t}{NDP} * 100 \tag{3.16}$$

where TLB_t is the function indicating whether there has been any thermal limit violation within the grid at time interval 't'.

$$TLB_t = \begin{cases} 0 & if\ (\left|I_{ij}^t\right| \leq \left|I_{ij}^{Lim}\right| \quad \forall\ i,j \in B) \\ 1 & otherwise \end{cases} \tag{3.17}$$

where

$\left|I_{ij}^{t}\right|$ is the magnitude of current (A) flowing between bus 'i' and 'j' of the power system in the current time interval of 't'.

$\left|I_{ij}^{Lim}\right|$ is the limit for the current magnitude (A) flowing between bus 'i' and 'j' of the power system.

These attributes measure the probability of any bus or branch in the system being out of acceptable limits. The probability of a particular bus or branch being out of bounds is equal to or lower than the probability of the system being out of bounds, so such attributes provide a measure of the worst case performance of the system [97].

The one day simulation results show that the voltage violation and overload probability were 70.83% and 50%, respectively, before adding electrolysers to the power system. However, after utilisation of electrolysers, those values were found to be zero due to successful enforcement of the constraint limits by the system central controller.

Total energy loss (MWh) during the simulation on the distribution network is calculated using the following equation:

$$E_{Loss} = T * \sum_{t=1}^{NDP} \sum_{i=1}^{NB} P_{Loss_i}^{t} \tag{3.18}$$

The amount of reduction in the total energy loss on the distribution network during the simulation (ΔE_{Loss}) in MWh can be calculated from the following equation:

$$\Delta E_{Loss} = E_{Loss}^{Without} - E_{Loss}^{With} \tag{3.19}$$

where

$E_{Loss}^{Without}$ and E_{Loss}^{With} are respectively the total energy loss on the distribution network in the system without and with electrolysers, in MWh.

The percentage reduction in the total energy loss on the distribution network during the simulation ($\Delta E_{Loss}\%$) can be calculated from the following equation:

$$\Delta E_{Loss}\% = \frac{\Delta E_{Loss}}{E_{Loss}^{Without}} * 100 \tag{3.20}$$

The total distribution loss through the system during one day is also shown in Figure 3.15. The energy flow from the network to the electrolysers caused a reduction of 5.2 MWh in the total energy loss of the distribution network. This is around 41.5% less than the distribution loss on the system without electrolysers. Despite the fact that the electrolysers act as additional demand on the electrical network, they reduced the distribution losses significantly in this study. The reduction in distribution losses is due to consumption of power generated by wind farms with local electrolysers rather than exporting all of the surplus power to the other feeders.

After proving the effectiveness of the control strategy during the one day simulation using set1 for the location of hydrogen stations, the simulation was run for a duration of one year with time interval of one hour for all of the location sets and the results are included in Table 3.3. The demand profile of the UK during 2014 [92] was scaled down to match the *UKGDS* demand level and was used for this simulation.

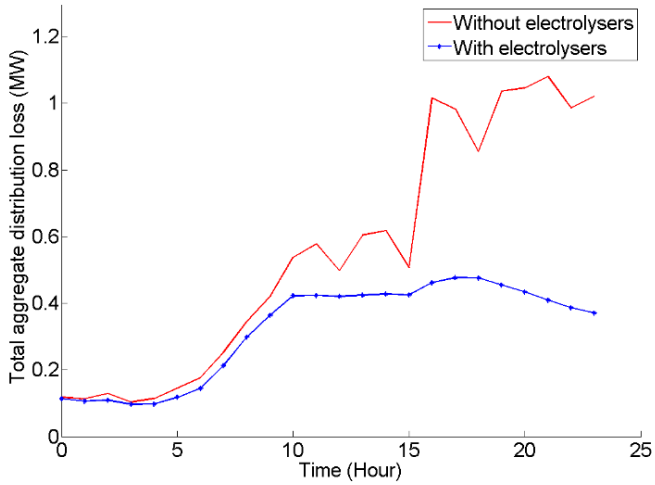

Figure 3.15 The total distribution loss in the grid before and after adding electrolysers

The total hydrogen produced ($TH2P$ in metric tonne (**t**)) during the simulation at all of the electrolysis hydrogen filling stations is calculated from the following equation.

$$TH2P = \sum_{t=1}^{NDP} \sum_{J=1}^{NAS^t} \sum_{i=1}^{NAEL_j^t} H2P_{ij}^t /1000 \qquad (3.21)$$

The total energy (MWh) delivered to all of the stations is calculated from the following equation.

$$E_{St} = T * \sum_{t=1}^{NDP} \sum_{i=1}^{NS} SD_i^t \quad (3.22)$$

An income function ($Income$) is defined to find the best location set to minimise the aggregate size of the stations, the total energy loss on the network and energy cost of stations during the simulation while maximising the amount of hydrogen production and consequently the profit from selling hydrogen. The objective is to maximise this income function.

$$\text{Income} = C_3 * TH2P - C_4 * E_{St} - C_5 * \text{NDP} * \text{T} * \sum_{i=1}^{NS} OSZ_i - C_6 * E_{Loss}^{With} \quad (3.23)$$

where, OSZ_i is the optimal size of station 'i' in MW, and it is determined by the maximum demand of each station during a year simulation.

The first term in Income, which is $C_3 * TH2P$, is included to increase the chance of selecting the best answer with the highest hydrogen production. This also increases the chance of selecting the answer with a higher utilisation factor for stations which will result in more hydrogen production and more profit. C_3 is the selling price of hydrogen (£8/kg or £8000/**t** [98]).

The second term in Income, which is $C_4 * E_{St}$, is included to reduce the cost of electrical energy form the function value, and it is also assumed that $C_4 = C_2$. Usually filling station operators who have electrolysers to produce hydrogen can accept electricity from the grid at any time during a day. If an operator agrees to take some of the surplus electricity produced by a wind generator at any time and accepts the peaks and troughs of the received power, then the electricity price for that consumer would fall to a lower price, and it will result in a price reduction of the hydrogen produced by the electrolysers. However, such price reduction is not included in the simulation here.

In this work, it is assumed that $C_5 = C_1$ and $C_6 = C_2$ as both C_1 and C_5 are the coefficients to size stations and C_2 and C_6 are the coefficients for the cost of energy loss on the system.

Results of Table 3.3 show that selection of location set 3 will lead to minimum aggregate size for hydrogen stations, and the best result that has the maximum 'Income' value belongs to this location set as well. Interestingly, the percentage of

distribution loss reduction for all of the location sets are close to 27%. The final size of some of the stations is found to be lower than 2 MW, inferring that only one electrolyser with a lower nominal demand will be sufficient for those stations. In such cases, the minimum demand of the station will be lower than the initial minimum demand assumed in the control strategy. In addition, for the cases where the final size of a station is not an integer multiple of 2 MW, smaller electrolysers can be used to fill the fraction, although, in practice, the commercial availability of electrolysers would be constrained to limited sizes.

Table 3.3 Results of a year simulation for different location sets in case study 1

Location set	Set 1	Set 2	Set 3	Set 4	Set 5
$TH2P$ (**t**)	210.3	208.6	207.4	206.5	211.9
E_{St} (MWh)	10,912	10,848	10,789	10,738	11,034
ΔE_{Loss} (MWh)	765	757.2	750	747.5	769.8
$\Delta E_{Loss}\%$	27.3%	27%	26.7%	26.7%	27.5%
OSZ_1 (MW)	0.4	0.4	0.4	0.4	6
OSZ_2 (MW)	3.86	3.1	2.76	5.9	6
OSZ_3 (MW)	6	6.0	6.0	6	6
Income (£k)	165.8	234	260.7	-69.3	-634.2
$VB_{Prob}^{With}\%$	0%	0%	0%	0%	0%
$TLB_{Prob}^{With}\%$	0%	0%	0%	0%	1.4%

The final results show that after applying the control strategy, the voltage and apparent power limits were fully within the limits for all of the location sets except set 5. For this last location set, the voltage violation probability was reduced from 72.9% to 0,

but the overload probability was reduced from 19% to 1.4% and did not reach zero. This means that location set 5 is not suitable for electrolysis stations if the power system operator wants to operate electrolysers with the existing network without any grid upgrade or wind power curtailment. The value of 'Income' was also minimum for this location set, emphasising its lack of suitability for the system.

One of the advantages of the presented control strategy used in this chapter is that there is no need to forecast the wind power availability within the system, and it is assumed that the grid control centre can just use the real-time data from the wind power generation units and local demand to calculate the set-point for the demand of each hydrogen station.

To investigate the impact of initial power rating of filling stations and size of wind farms on the results two more case studies are simulated for a duration of a year, and their results are included in Table 3.5 and Table 3.7, respectively.

Case study 2: The rating of wind farms is unchanged, but the initial size of stations has increased by 50%. Details of this case study are included in Table 3.4.

Case study 3: The rating of wind farms is increased by 50%, and as a result the initial size of stations has increased using Equation 3.1. Details of this case study are included in Table 3.6.

Table 3.4 Details of case study 2

Parameter	Value
S_W^i (MW)	10
S_{St} (MW)	10
$VB_{Prob}^{Without}$%	72.9%
$TLB_{Prob}^{Without}$%	19%

As shown in Table 3.4, the size of wind farms remained unchanged at 10 MW while the initial size of stations is increased from 6 MW in case study 1 to 10 MW in case study 2. The voltage break and overload probabilities have also remained unchanged in the system without electrolysers in comparison to case study 1.

As shown in Table 3.5, despite the fact that the maximum final size that the stations were allowed to reach was 10 MW in this case study, the maximum optimal size found is only 7.8 MW. This shows that there is no need to increase the initial size of stations to a very high limit as the optimisation process will try to find the minimum size able to satisfy optimisation objectives.

Table 3.5 Results of case study 2 for a year simulation

Location set	Set 1	Set 2	Set 3	Set 4	Set 5
$TH2P$ (**t**)	216.3	214.7	213.5	212.5	221.7
E_{St} (MWh)	10,911	10,845	10,783	10,730	11,203
ΔE_{Loss} (MWh)	765	753.6	744	739.2	781.8
$\Delta E_{Loss}\%$	27.3%	26.9%	26.5%	26.3%	27.9%
OSZ_1 (MW)	0.4	0.4	0.4	0.4	7.8
OSZ_2 (MW)	3.1	3	1.1	7	7.8
OSZ_3 (MW)	7.8	7.8	7.8	7.7	7
Income (£k)	94.2	102.8	298.3	-318.3	-1054.3
$VB_{Prob}^{With}\%$	0%	0%	0%	0%	0%
$TLB_{Prob}^{With}\%$	0%	0%	0%	0%	1.47%

Interestingly, the percentage of distribution loss reduction for all of the location sets has remained close to 27% without significant change in comparison to the first case study. In addition, increasing the initial size of stations did not improve the voltage

and thermal limit violation probabilities in location set 5 which had the worst income. The value of income function for all location sets except set 3 are worse in comparison to the first case study. However, the value of income function is bigger for set 3, which is also the optimal solution. This means that case study 2 has a slightly better optimal solution in comparison to the first case study. Therefore, it can be recommended that the initial size of stations proposed in the beginning of this chapter can be increased by 30% to achieve a better optimal solution. However, adopting this new sizing approach can lead to accepting large gaps between the optimum size of one station and the other ones, i.e. in the results from set 3, the optimal size of station 3 is 7.8 MW while the optimum sizes of other two stations are only 1.1 and 0.4 MW.

In case study 3, the size of wind farms has increased to 15 MW and the initial size of stations has also increased to 10 MW according to Equation 3.1. As a result, the voltage break and overload probabilities in the system without electrolysers have also increased to 78.9% and 41.4%, respectively.

Table 3.6 Details of case study 3

Parameter	Value
S_W^i (MW)	15
S_{St} (MW)	10
$VB_{Prob}^{Without}$%	78.9%
$TLB_{Prob}^{Without}$%	41.4%

As shown in Table 3.7, the percentage of loss reduction has increased significantly to around 54% in case study 3, due to injection of a significant amount of wind power to the system during the simulation. In addition, the amount of hydrogen production, energy absorbed by stations, and income have also increased significantly. However,

the controller has not been able to satisfy the overload problem completely and just managed to reduce it to 1% during the simulation for most of the location sets. The highest amount of income in this case study belongs to location set 5. However, the overvoltage and overload probabilities were rather higher and equal to 2.42% and 16.7%, respectively, for this location set. Obviously, the system operator cannot add unlimited capacity of wind farms and electrolysers to the system expecting that the controller should achieve the power system constraint limits. If more wind farms were added to the system, then they would generate more power, and more electrolysers could be added to the network to absorb this extra energy. However, the power system operator should make sure that the network limits will not be violated as a result of adding extra wind power capacity or electrolysis demand.

Table 3.7 Results of case study 3 for a year simulation

Location set	Set 1	Set 2	Set 3	Set 4	Set 5
$TH2P$ (**t**)	601.7	597.4	593.9	589.7	674.7
E_{St} (MWh)	32,130	31,906	31,711	31,450	36,885
ΔE_{Loss} (MWh)	3145.8	3,078	3,013	2,964	3210.4
$\Delta E_{Loss}\%$	55.2%	54%	52.9%	52%	56.4%
OSZ_1 (MW)	8.4	8.4	8.5	8.6	10.2
OSZ_2 (MW)	10	10	10	10	10.5
OSZ_3 (MW)	8.5	8.1	8.1	8.6	7
Income (£k)	802.7	805.9	782.2	699.5	1137.3
$VB_{Prob}^{With}\%$	0%	0%	0%	0%	2.42%
$TLB_{Prob}^{With}\%$	1%	1%	1%	1%	16.7%

3.6 Chapter summary

In this chapter a novel approach that uses an extended OPF was proposed to size, place and control pressurised alkaline electrolysers located at hydrogen filling stations to increase the amount of wind power generation capacity within an example radial distribution network while satisfying the power system constraints and electrolyser characteristics. A *UKGDS* power systems was used as a case study to assess the effectiveness of the proposed strategy. Software was developed using *MATLAB* and *MATPOWER* [74] to be used for the simulations.

The optimal ratings of the hydrogen filling stations were selected for each proposed location by minimising a primary cost function at each time step, and then the best location for the stations were selected to maximise an income function that considered the amount of hydrogen production, cost of energy to produce hydrogen, costs of stations and the amount of energy loss within the distribution system. Simulation results show the effectiveness of the proposed control strategy to maintain the power system parameters within acceptable limits, while directing some of the surplus power to the electrolysers to produce 'green' hydrogen. The proposed strategy increases the network asset utilisation while deferring the need for network upgrade investment for the integration of more intermittent wind power. The impact of increasing the initial size of stations or the size of wind farms on the simulation results has also been investigated.

Despite the fact that the electrolysers act as additional load on the electrical network, they significantly reduced the distribution losses in this study. Such reduction in distribution losses happens as the result of the close location of electrolysers to the wind farms and the proper control strategy to dispatch electrolysers.

It was shown that, despite having the same initial size, the hydrogen stations at different locations had different demand set-points selected by the control strategy, and therefore they had a different final size in the optimised system. It is also not practical to balance the amount of hydrogen produced in the stations with this control strategy, resulting in different amounts of hydrogen production at different stations.

4 STABILISING THE FREQUENCY OF THE GRID BY DYNAMIC CONTROL OF ELECTROLYSERS

4.1 Introduction

Large scale alkaline electrolysers used in future hydrogen filling stations could be utilised to improve the frequency stability of the electric power system, as these electrolyser loads can be controlled to respond to power system frequency variations and rapidly change their load to maintain the power balance within the network.

In this chapter, the potential of alkaline electrolysers to dynamically stabilise the frequency of the power system is assessed. A model of a lumped steam turbine generation unit has been presented using *MATLAB* Simulink to assess the dynamic response of the system, and two cases in which there is a sudden loss of generation or when the power system has a high penetration of wind power are examined. The characteristics of electrolysers previously explained in Chapter 2 are utilised here for modelling purposes.

The novelty in this chapter will be in determining the size of electrolyser and the amount of reduction in the spinning reserve and frequency fluctuations as a result of utilisation of electrolysers for frequency stability. In addition, it will be demonstrated that electrolysers have sufficient ramp rate (even when considering the occasional delays detailed in Chapter 2) to stabilise the frequency of the power system while acting together.

4.1.1 Frequency stability in power systems

Frequency stability and control is an important issue for electricity power systems, and the system frequency should remain within a specified range at all times. In the UK, National Grid is responsible for the management of the transmission network in a secure way, and it is also responsible for balancing generation with the load demand in real time.

The frequency of the grid should remain constant to ensure the satisfactory performance of the power system. Proper control of frequency is needed to ensure that the speed of induction and synchronous motors are constant. If the frequency drops significantly in an electrical grid, then the magnetizing current in induction motors and transformers could increase beyond their limit [99]. There are also some hazards that are related to under-frequency operation of a steam turbine, and they are mentioned below.

- Operation of steam turbines below a certain limit is restricted, as it could increase vibratory stress on long, low-pressure turbine blades. The effects of vibratory stress are cumulative with time, so, following a transient event, the frequency of the system must return to the nominal value as quickly as possible. The duration of vibration must be kept at minimum to reduce the maintenance and inspection needed for the plant and to insure the system operates safely [100].
- The performance of plant auxiliaries, driven by induction motors, degrade at lower frequencies. In particular, a decrease in the speed of blowers would reduce the amount of combustion air injected into the turbine, and therefore the plant capabilities could decrease.

In the case of a significant generation loss in the power system, the frequency could drop significantly, which eventually leads to the triggering of automatic low-frequency relays to restore the stability of the power system [101].

The National Grid has the following steady-state operational and statutory limits for the frequency of the electrical network [102]:

- Statutory steady state limits of ±0.5 Hz (i.e. 49.5 Hz to 50.5 Hz)
- Operational limits of ±0.2 Hz (i.e. 49.8 Hz to 50.2 Hz).

The Great Britain Security and Quality of Supply Standard (*GB SQSS*) determines the limits of frequency deviations as a result of secured faults, which include loss of output from a single generating unit [101]. The limits are listed below.

- The maximum frequency deviation from nominal should not exceed 0.5 Hz in the case of a Normal Infeed Loss Risk of 1,000 MW.
- The frequency of the UK grid should not remain above 50.5 Hz or below 49.5Hz for more than 60 seconds in the case of an Infrequent Infeed Loss Risk of 1,320 MW [101].

The largest infrequent infeed loss of 1,320 MW is derived from the largest possible generation infeed loss on the Great Britain Transmission System that can happen due to a single loss event. If an Infrequent Infeed Loss Risk occurs, then National Grid tries to limit the maximum frequency deviation to 0.8 Hz and return the frequency to the nominal operational range in less than 10 minutes. To prevent a total or partial shutdown of the electric power system due to instability during a generation loss of larger than the Infrequent Infeed Loss Risk, the National Low Frequency Demand Disconnection (LFDD) scheme automatically disconnects some loads from the power system. Figure 4.1 shows the frequency and time limits that the frequency control system in the Great Britain uses to stabilise the power system.

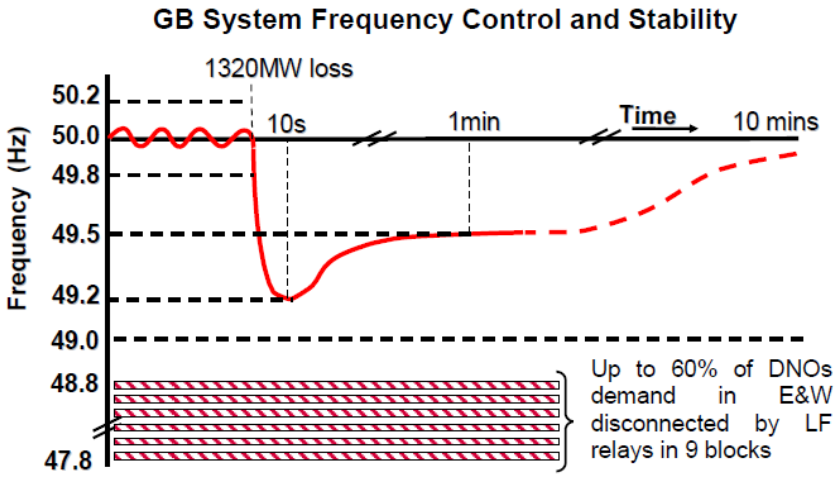

Figure 4.1 The limits used for the frequency stability of Great Britain [101]

It is expected that the following factors will increase the risk from system frequency incidents in the future UK power system.

- The size of the biggest single loss will increase to 1,800 MW.

- The number of generation plants equal to the largest loss on the system will increase in the future.
- It is more likely that the new generation units might trip due to commissioning and new technology used in them.
- Many of the renewable generation technologies utilise power electronic converters to connect to the power system. This is the case for variable speed wind turbines, which are thus mechanically decoupled from the power system frequency and do not automatically contribute to power system inertia [103]. Therefore, system inertia is going to decrease in the future as a result of an increase in the wind power contribution to the power system.
- The reliability and availability of the frequency response in the power system will decrease in the future. It is expected that future generation plants will have less capability to provide frequency response services in comparison to the current generation mix [100].

Therefore, it is expected that future power plants will have larger size with smaller inertia, so a larger frequency drops could occur following a sudden generation loss [104].

In December 2015, the cumulative installed capacity of onshore and offshore wind power generation in the UK was 8.5 GW and 5 GW, respectively [105]. The amount of embedded generation and wind power in the UK grid are increasing. The Electricity Market Reform (EMR) Delivery Plan shows a potential deployment of up to 13 and 41 GW of onshore and offshore installed wind capacity by 2030 in its high offshore wind deployment scenario [106]. This increase in wind power generation can delay restoration of frequency in the power system when a frequency incident occurs. However, it is also worth mentioning that the output from a wind farm could be predictable, to some extent, a couple of hours ahead [100].

Due to variability and uncertainty of the electricity demand and the probability of breakdown of some generation units, National Grid maintains a ‘safety cushion’ or ‘operating margin’ at all times. This means that the system has the ability to increase its generation or reduce its demand by a command in varying timescales, from minutes

to hours ahead, to ensure that the total generation meets the aggregate demand on the system. This safety cushion consists of four main factors listed below.

i. **Contingency Reserve**: This consists of the generation plant available with 4 to 12 hour notice to start their power generation. The size of the 'contingency reserve' changes with respect to the time of day or year and also with the demand forecast.
ii. **Short Term Operating Reserve (STOR)**: This consists of those generators or demand loads typically available to respond to a command within 5 to 20 minutes.
iii. **Regulating Reserve**: This consists of those generation units synchronised with capacity and ready to be instructed to increase or decrease their output to assist the system while there are short term demand forecast errors or generation losses on the power system.
iv. **Frequency Response**: Some automatically-controlled generators help in frequency deviation corrections. As generation losses often happen suddenly without being predicted, National Grid has some contracts with generator operators and demand side participants that automatically provide commercial frequency response services to keep the frequency within the operational limits [101].

Due to the difficulty of forecasting the exact demand from consumers, there must be enough spinning reserve[5] available in the system to supply additional power when required. In addition, when there is a sudden loss of generation, it takes some seconds for the spinning reserve to become fully available, and slower backup generation might take up to 30 minutes to become available [101].

[5] Spinning reserve is the extra generation capacity which can be added to the system at very short notice, and it is provided by some generators that continuously monitor system frequency and change their output to compensate for any imbalances in the power system [51].

If, in an electric system, the amount of generation is not able to maintain the frequency because there is excess demand on the system, then the frequency will drop. The frequency drop in the system could cause tripping of steam turbine generators, which have under-frequency protection relays, and this can exacerbate the system condition causing further reductions in frequency and so on. If there are severe disturbances in the electrical system, then many outages could occur one after another. In those critical situations, when the frequency is under a certain limit, load-shedding schemes are employed. Such schemes reduce the connected load to a certain level that can be safely supplied by the available generation.

The ability of the power system to restore the frequency to its nominal values has some limitations, which are listed below:

- The amount of spinning reserve is limited in each electrical grid due to the available capacity limits, emission issues and also the high cost of maintaining spinning reserve within a power system. This limits the maximum generation power that could be added in a short time.
- The amount of load that could be picked up by a turbine is limited because of thermal stress. The amount of rated turbine output that could be picked up initially, without causing any rapid heating in the system, is 10%. Then the output of a turbine could be increased by only 2% per minute [99].
- A conventional steam cycle boiler has a limited ability to pick up load. If the turbine valves open, then the steam flow will increase, and this will cause a pressure drop in the turbine valves, and therefore the fuel input of the boiler should be increased to maintain the pressure in the system. This process takes several minutes, and it is not very useful to control the frequency in a short time [99].

The costs of operating generators in frequency sensitive mode are high because the generator operators must be paid for lost generating opportunity and also for wear and tear to their generators. It is also less efficient to operate generators at partial load because generators are designed to have the best efficiency when operating at full

power [51]. The current costs of providing balancing services in the UK are significant, and some of these costs in March 2012 are listed below [107]:

- Short Term Operating Reserve (STOR): £11.07m
- Mandatory Frequency Response: £4.97m
- Commercial Frequency Response: £6.97m
- Fast Reserve: £6.52m

Currently, the annual cost of providing spinning reserve and demand response for frequency regulation in the UK is around £260m, and it is predicted that in 2020, this amount will increase to £550m because of the problem of uncertainty in wind forecasting [108]. This highlights the potential financial benefits of the utilisation of electrolysers as dynamic loads to stabilise the frequency of the UK power system in future.

Active power control is closely related to frequency control. Any imbalance between generation and demand will result in a deviation from the nominal frequency. With excess generation in the system, the frequency will rise, and if there is a lack of generation, then the frequency will fall, reflecting the amount of mismatch between generation and demand. The rate of change of frequency will also be determined by the effective inertia of the power system. It is impractical for generators to perfectly match their output to the amount of demand at every moment, so there is always some minor deviation from the nominal frequency in the system [80].

4.1.2 Controlling the frequency with dynamic demand

To reduce the amount and, consequently, the cost of spinning reserve on the system, control strategies can be used to vary key demand loads; this is known as demand side management (DSM). Suitable control of loads can be used in place of part of the spinning reserve to control the frequency of the system.

Currently, the National Grid controls the frequency of the system using different strategies like Frequency Control by Demand Management (FCDM) [109]. In FCDM,

the under-frequency relays connected to some demands cut off, i.e. power will be disconnected, from certain demand loads to help in balancing the power system. An FCDM provider must be able to satisfy the following conditions [109].

- Provide the service within 2 seconds of instruction.
- Deliver for a minimum duration of 30 minutes.
- Deliver minimum 3 MW, which may be achieved by aggregating a number of small loads at same site.
- Have suitable operational metering
- Provide output signal into National Grid's monitoring equipment [109].

DSM is able to help maintain the system frequency to a useful extent. In particular, alkaline electrolysers have characteristics that allow them to be used as DSM tools. This will be of increasing importance with high penetrations of time-variable and intermittent renewable generation. In addition, when there is a loss of generation, such electrolysers can rapidly reduce their load on the power system, thus providing immediate reserve to support the restoration of frequency.

4.2 Modelling of a power system with electrolysers for frequency stability analysis

The balance of active power in an electrical system could increase the stability of the frequency in the system. A change in the active power demand or generation in the power system could change the frequency of the entire electrical system. There might be many generators operating in an electrical system, so the change in load must be allocated properly to generators. A speed governor provides primary speed control ability to each generator. In addition, a central controller allocates generation as a supplementary control. The control of generation and frequency is commonly named load-frequency control (LFC).

A steam turbine is able to convert the energy from high pressure and high temperature steam into rotating energy. A generator converts this mechanical energy into electrical energy. The basic concept of speed control and hence frequency control in a steam

turbine that is used for electrical power production is shown in Figure 4.2. The load change in the system can change the speed of the turbine rotor, and as a result of that the governor will act as a controller to change the steam valve set-point and consequently maintain the speed of the turbine [99].

There are a variety of electrical devices that act as demand loads in an electrical power system. Some of the loads, such as lighting and heating loads, do not depend on the frequency of the system. On the other hand, the electrical power consumption of motor loads changes with respect to the frequency of the grid. The relationship between the frequency change in the grid and the overall load change in the system is as follows:

$$\Delta P_e = \Delta P_L + D\Delta\omega_r \tag{4.1}$$

where

ΔP_e is the total load change in the system in per unit values.
ΔP_L is the change in load as a result of the change in non-frequency sensitive load in per unit.
D is the load damping constant.
$\Delta\omega_r$ is the change in the rotor speed per unit.

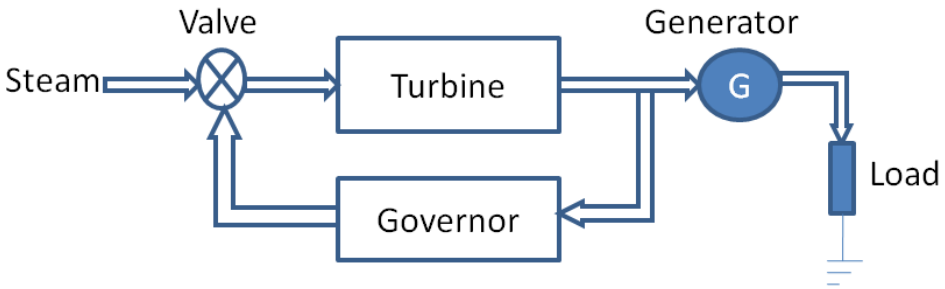

Figure 4.2 The basic concept of speed control in a steam turbine

The damping constant (D), which represents the impact of frequency-sensitive loads, is expressed as the percentage change in load for a one percent change in the frequency, and it has typical values of 1 or 2 percent. If D=1.5, then it means that the load will change 1.5 percent when the frequency changes one percent. In the system without a speed governor, the system will respond to the load change with respect to the inertia constant of the generator and the damping constant of the loads [99].

If there is a load change in an electrical system, then all of the generators with speed governing connected to the system will change their output generation to recover the frequency of the system. The governor is responsible for maintaining the frequency at or near its nominal value by changing the position of the valve of the turbine. When there is a sudden increase in the load of system, then the speed of the generator drops with a rate that is determined by the inertia of the rotor. The governor in this case opens the input valve further to increase the mechanical power from the turbine. If there is enough spinning reserve, then the speed of the rotor and the frequency of the system will return to their nominal values, and the increase in the steady-state turbine power will be equal to the increase in the demand on the system. When a generator is working separately, and it supplies an isolated load, then an isochronous governor will be able to service the system properly, but if a load is powered by multiple generators, then speed regulation or droop control must be used on each generator to control the frequency of the grid; otherwise, all of the generators in the system would try to control the frequency with respect to their own settings. Such droop control ensures that the change in demand will be shared properly among the generators. Droop (R) in a turbine controller determines the steady-state speed versus load characteristic of the generating unit [99]. It is expressed by the following equation:

$$R\% = \frac{\Delta f\%}{\Delta P_G\%} * 100 = \frac{f_{NL} - f_{FL}}{f_0} * 100 \tag{4.2}$$

where

$\Delta f\%$ is the percentage of the frequency change in the system.
$\Delta P_G\%$ is the percentage of the power output change of the generator.

f_{NL} is the steady state frequency of the generating unit at no load (Hz).

f_{FL} is the steady state frequency of the generating unit at full load (Hz).

f_0 is the nominal or rated frequency of the power system (Hz).

Therefore, if R=4%, then it means that the output of the generator will increase by 100% if the frequency drop is 4% [99].

When there is a loss of generation in the system, or when there is a sudden increase in the demand, the rotational inertia of all of the generators and all of the rotational loads in the system lose energy to provide the power deficit, so their speed will decrease, and therefore the frequency of the system will decrease. Under steady-state conditions, the frequency of the system will fall to a level that the power deficit is met by the released demand of the frequency sensitive loads (represented by the D constant in Equation 4.1) and the increased generation, which is a result of the governor response. In actual power systems, a secondary response will start to return the frequency to its nominal value within around ten minutes.

In the case where there is more than one generator operating and all of them have droop governor characteristics, then the system will have a common frequency, and all of the generators in the system share the load change. When there is a load increase in the system, the droop characteristic causes a steady-state deviation from the nominal frequency. The relationship between the load and the frequency could be changed by adjusting the load reference set-point, which in effect moves the speed droop characteristic up or down. The output of each generating unit at each frequency can only be changed by a change to its load reference set-point.

The collective performance of all of the generators in an electrical system will determine the frequency of the grid. It is shown by Kundur [99] that, if there are many generators in a system, then for the analysis of the system frequency, these generators may be represented by one single generator that has an inertia constant equal to the sum of the inertia constants of the individual generators. The frequency characteristic of the electrical grid also depends on the combined effect of the droops of all generator speed governors. An equivalent droop (R) can be found for the combined effect of all the individual generators.

Fossil fuelled steam turbines may be of either the reheat type or non-reheat type. In a reheat type turbine, steam is recycled in the system to increase the efficiency of the turbine. A block diagram of a generator, based on a steam turbine with reheat, which is taken from [99], is shown in Figure 4.3. This can be used for the analysis of frequency deviation following a sudden mismatch between the generation and the demand. This block diagram comprises a speed governor, turbine, model of rotor

inertia, and demand load. For simplicity, as is conventional, it has been assumed that the boiler pressure is constant during power generation transients. The values for the parameters of the steam turbine used in this study are typical of present plant and are taken from [99].

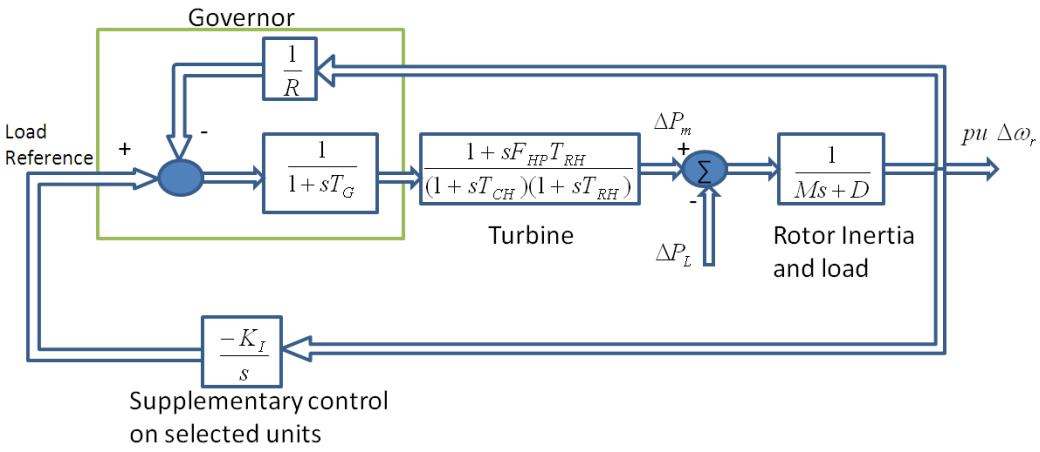

Figure 4.3 The block diagram of a typical reheat steam turbine, governor, rotor inertia and load [99]

$R = 0.05;\ T_G = 0.2\ s;\ F_{HP} = 0.3;\ T_{RH} = 7.0\ s;\ T_{CH} = 0.3\ s;\ M = 10\ s;\ D = 1;$

$K_I = 0.2$

where

R is the speed droop characteristic.

T_G is the governor time constant (s).

F_{HP} is the fraction of total turbine power generated by the high pressure stage.

T_{RH} is the time constant of re-heater (s).

T_{CH} is the time constant of main inlet volumes and steam chest (s).

M is the inertia constant (s).

D is the load damping constant.

K_I is the integral control gain.

ΔP_m is the total mechanical power change in the system in per unit.

A sudden drop in the amount of generation in the system will have the same impact on the frequency of the system as a sudden increase in the aggregate load on the system.

The load reference set-point determines the output of each generating unit as a function of system frequency. Due to the governor droop characteristic, if a system has only primary speed control action, then a change in the system load would cause a steady-state deviation from the nominal frequency. If the frequency of the system is to be restored to its nominal value, supplementary control action must be used to adjust the load reference set-point. An automatic generation control system can restore the frequency by using an integral controller to change the load reference set-point. This integral controller, which is shown in Figure 4.3 as supplementary control, ensures zero frequency error under steady state conditions. The primary speed control acts much faster than the supplementary generation control. The K_I gain (0.2) in Figure 4.3 is determined so that the controller returns the frequency of the system to its nominal value within 10 minutes after a step change in load, provided that there is sufficient reserve available on the system. The ability of the system to restore the frequency to its nominal value has some limitations. The amount of spinning reserve is limited in each electrical grid, and this limits the maximum generation power that can be achieved quickly.

In actual electrical power systems, the generators have complex dynamics, and their models differ from each other. To construct an accurate model of a grid for frequency analysis purposes, many different generator models may need to be considered [80]. In this study, all of the generators are considered to be of the same steam turbine type and are considered to have governor control action for speed control.

In this chapter, two cases were considered to find the impact of alkaline electrolysers on the frequency stability of power systems:

1. There is a sudden loss of generation in the system, and electrolysers are utilised to reduce their loads to avoid any sudden decrease in the frequency of the system.

2. The system has around 25% penetration of wind power, and electrolysers are utilised as dynamic loads to reduce the frequency fluctuations in the power system.

A *MATLAB* Simulink model was developed, based on the system in Figure 4.3 (the model is taken from [99]), to represent the frequency of the electrical system using electrolysers as dynamic demand. A single generator, which has the aggregated characteristics of all the governor controlled generators, is modelled. This generator is responsible for delivery of all power to the system and maintaining the frequency within operational limits. The spinning reserve that is provided with the governor controlled generator is assumed to be equal to the aggregated amount of spinning reserve available from all of the steam turbine generators on the system. The input of ΔP_L in Figure 4.3 is effectively the only input of this model, and it can be changed by the simulation program to represent the amount of mismatch between power generation and load demand. If there is sufficient spinning reserve, then this unit must increase its output power when a frequency drop occurs.

A number of assumptions have been made in this work, and they are listed below:

- It has been assumed that, during the simulation period, the loads from non-electrolysis plant in the electrical power system do not change, due to constant demand from consumers. However, if they are frequency sensitive loads, then they could change as a result of frequency variation as shown in Equation 4.1.
- It is assumed that the electrolysers operating in the future electrical power system will produce hydrogen for FCVs refilled at hydrogen filling stations, and hydrogen will be stored at the filling stations. The storage of hydrogen would be required to accommodate the expected time variations of hydrogen demand for vehicle filling, but it can also be used to allow the electrolysers to act as controllable loads. The electrolysers will then not be constrained to operate at a fixed constant load at all times.
- It is assumed that the variable load operation of the electrolyser does not result in any significant degradation of its performance or the lifetime of electrodes and other key components. However, depending on the design and type of the

electrolysers, this assumption might not be applicable for every alkaline electrolyser in operation today.

- It is assumed that every electrolysis plant on the grid has a controlled rectifier that is able to supply up to the acceptable load limit of the electrolyser.
- It is assumed that the generators comply with UK grid connection standards, [102].
- If the electrolysers are providing DSM, then their operating points must, of course, be constrained between agreed maximum and minimum values. The minimum load of the alkaline electrolysers is assumed to be 20% of their nominal demand, so the electrolysers used for this work can accept power variations of up to 80% of rated demand.
- The frequency detection system installed on the control system is assumed to have a time constant (T_d) equal to 0.2 s [110], therefore it will have the following transfer function.

$$D(s) = \frac{1}{1+sT_d} \tag{4.3}$$

- According to the UK National Grid code, all Balancing Mechanism participants must ensure that appropriate electronic data communication facilities are in place to permit the submission of data to National Grid Electricity Transmission plc [102]. However, to provide a communication system between the dynamic load and the network control centre, a substantial investment would be needed [52].
- The load of the electrolysers can be changed with a signal from a local controller associated with each electrolyser. The electrolysers should have a proper system to detect the power system frequency because the local controller has to make the decision about how to change the electrolyser load with respect to the frequency of the power system. The frequency of the UK power system is effectively the same at any particular point across the country, so all of the dynamically controlled electrolysers connected to the grid will receive an identical input signal [51].
- It is assumed that electrolysers stay in hydrogen production mode all the time.

- The rectifier occasional delay, which is detailed in Chapter 2 and has an average value of 1015 ms, is assumed to be real and is included in the simulations. The probability of this delay's occurrence, which is found to be 40%, is included in the simulations.

4.3 Frequency stability during a loss of generation event

In this section, the potential aggregated impact of alkaline electrolyser on the frequency stability of the power system after a generation loss event is investigated. Table 4.1 shows the ratings of different power system elements modelled in this section.

Table 4.1 Ratings of different power system elements modelled in this section

Item	Rating
The aggregate nominal power of all the thermal generators	75.6 GW
Amount of generation loss	11.35 GW
Aggregated nominal demand of electrolysers	21 GW
Aggregated non-electrolysis demand	54.6 GW

The maximum electricity demand in the UK is around 55 GW [92], so the aggregate size of non-electrolysis load used here almost matches that value. The way that the aggregate demand of electrolysers is determined will be explained later in this section. Considering the current commercial technology and the average efficiency of electrolysers to be 73% [25], the aggregate nominal demand of electrolysers assumed here will produce 9,438 tons of hydrogen every day, which can provide more than 44.7% of the UK road transport energy requirement, assuming the hydrogen will be used in HFCVs (More details are included in Chapter 5).

The penetration of different energy resources in the future energy network is not exactly known, but the UK Department of Energy and Climate Change has published the '2050 Pathways Analysis' report [111], which describes six different scenarios for the UK electricity network in 2050. Its Alpha Pathway considers the total decarbonisation of the UK electricity generation system by utilising nuclear power plants, non-thermal renewable generators and combustion generators with carbon capture and storage systems. In that case, there would be no carbon dioxide emissions resulting from hydrogen production by electrolysers.

In this study, the response of the generators to a sudden loss of generation of 0.15 per unit is investigated. This means that the input of ΔP_L in Figure 4.3 has a step change of 0.15 at the beginning of the simulation. This amount of nominal loss is selected in this work to create a situation in which the frequency of the system violates its constraints without utilisation of DDC. Two scenarios are considered:

i. The generators are provided with enough spinning reserve, and the electrolysers are not used as dynamically-controlled loads to control the frequency of the grid.
ii. There is no spinning reserve provided on the system, and electrolysers are utilised to control the frequency of the grid following a loss of generation.

Before the generation loss event, the total amount of load in the system, which is made up of electrolyser loads and conventional system loads, is equal to the amount of generation, and the frequency of the system is assumed to be 50 Hz. The strategy that is used in the second scenario to control the electrolyser is explained below.

The electrolyser demand must be changed with respect to the frequency deviation in the system to provide frequency response. For system frequencies between 49.9 Hz and 50 Hz the electrolysers are controlled to load the system by the following equation which is equivalent to a droop characteristic of 0.25%.

$$P_{El} = P_{N.El} - \frac{(P_{N.El} - P_{Min.El}) * (50 - f)}{0.1} \tag{4.4}$$

where

P_{El} is the load of each electrolyser (MW).

$P_{N.El}$ is the nominal load of each electrolysis plant (MW).

$P_{Min.El}$ is the minimum operational load of the electrolyser plant to work properly in normal hydrogen production mode (MW).

f is the power system frequency (Hz)

Figure 4.4 shows the resulting relationship between the electrolyser demand and the frequency. The frequency of 49.9 Hz is chosen because the operational frequency limit in the UK is 49.8 Hz, and under these conditions, the electrolysers should consume the minimum allowable power. However, we know that it takes some time for the system to sense this frequency drop and react to the situation, so the value of 49.9 Hz is selected to provide some safety margin, and if the frequency drops below this value, the electrolysers will consume their minimum demand. If the frequency goes above 50Hz, then the electrolysers will run at rated load.

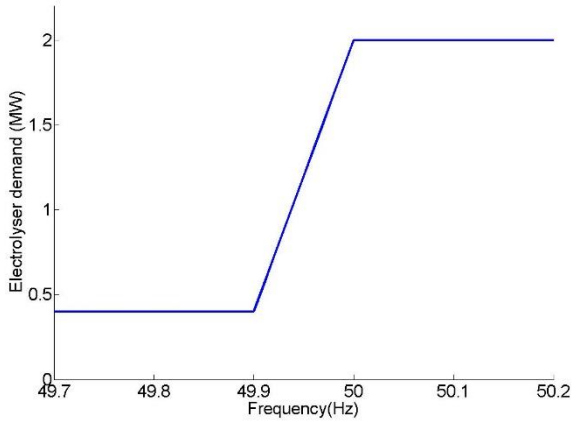

Figure 4.4 The relationship between the demand of each electrolyser and the frequency of the grid used in the control strategy

If electrolysers reduce their loads, then ΔP_L in the turbine model will decrease, and this means that the amount of mismatch between generation and demand will decrease.

4.3.1 Results of the simulation of power system frequency during a generation loss event

Immediately following the loss of generation event, which occurs 2s after the start of the simulation, the frequency decreases as energy is extracted from the aggregate rotor inertia and other frequency-sensitive loads in the system. Figure 4.5 compares the primary system responses for the two scenarios when there is 0.15 (per unit) step-change power generation loss in the system. The time resolution of the Simulink file for this short time analysis is one millisecond.

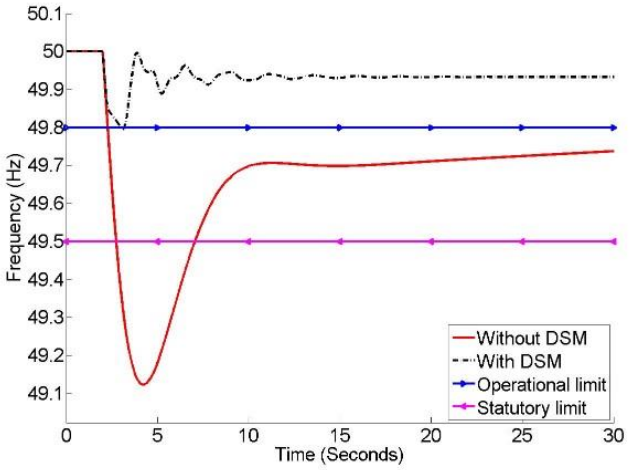

Figure 4.5 The frequency of the grid with or without dynamic demand control in the first 30 seconds of the simulation

The frequency of the system without dynamic demand control drops very sharply below the statutory limit, and it takes more than 50 seconds for the system frequency to recover. On the other hand, in the system using electrolysers as dynamic demand, the frequency drop is much reduced, and it remains above the operational limit at all times. It is worth mentioning that the aggregate size of electrolysers in this section was selected to be just large enough to avoid the frequency of the power system going below the operational limit after the generation loss event.

Figure 4.6 shows the aggregate set-point and actual load of electrolysers in the first 30 seconds of the simulation in with the DSM scenario. To assist the system in frequency stabilisation, the electrolysers must be able to change their load with a very fast rate.

This capability is confirmed by experiments undertaken on the pressurised electrolyser in collaboration with the NEL Hydrogen Company at the Porsgrunn Research Park in Norway which were detailed in Chapter 2 of this thesis.

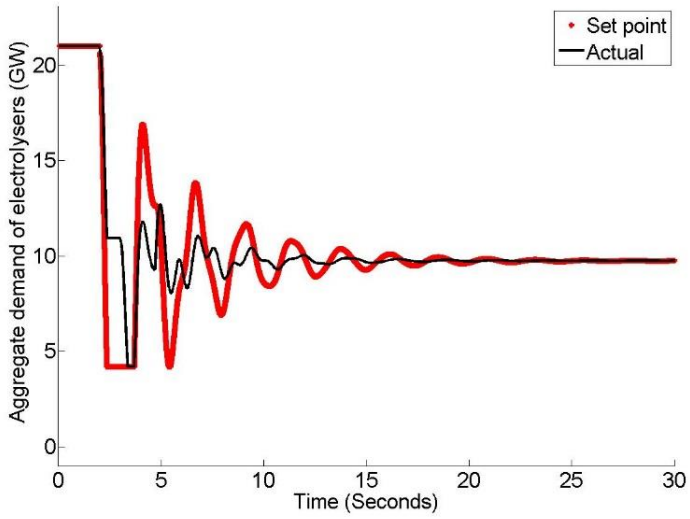

Figure 4.6 The load of electrolysers during the first 30 seconds of the simulation

Figure 4.7 shows that the change in the aggregate set-point demand of electrolysers in each time step in the system with DSM in the first 30 seconds of the simulation stays within the limits acceptable by electrolysers. Such alkaline electrolyser systems can thus offer the required degree of flexible control to allow them to be used to compensate for sudden imbalances in a power system. It should be noted again that the 2 MW electrolysers used in this analysis are assumed to be pressurised units, which are not produced by NEL hydrogen, and that atmospheric units do not respond as quickly as the pressurised ones. However, there are some other companies, like IHT [88], that produce large-scale pressurised units.

The contribution of spinning reserve in the system without dynamically controlled electrolysers, in the first 30 seconds from the start of simulation, is shown in Figure 4.8. When the system experiences the generation loss, the power from spinning reserve is released to stabilise the frequency. The spinning reserve contribution overshoots to 12.9 GW, and then after around 10 minutes it settles to around 11.35 GW, which is equal to the amount of generation loss. In the system with DSM, this

contribution from spinning reserve is zero because the system did not have any support from spinning reserve.

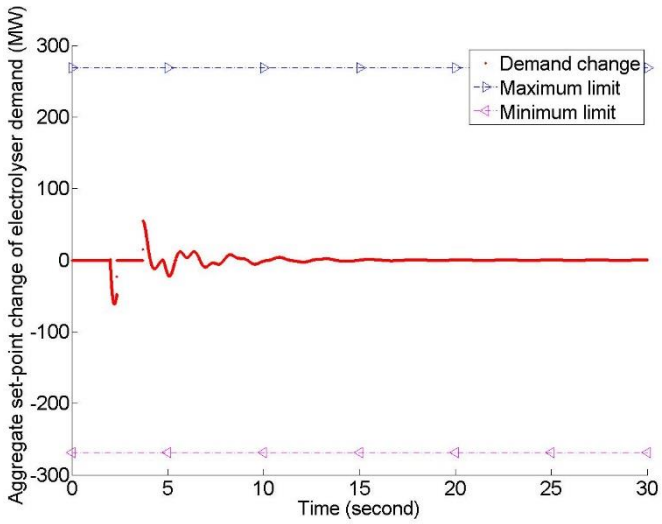

Figure 4.7 The change in the aggregate set-point demand of electrolysers in the system with DSM in each time step in the first 30 seconds of the simulation

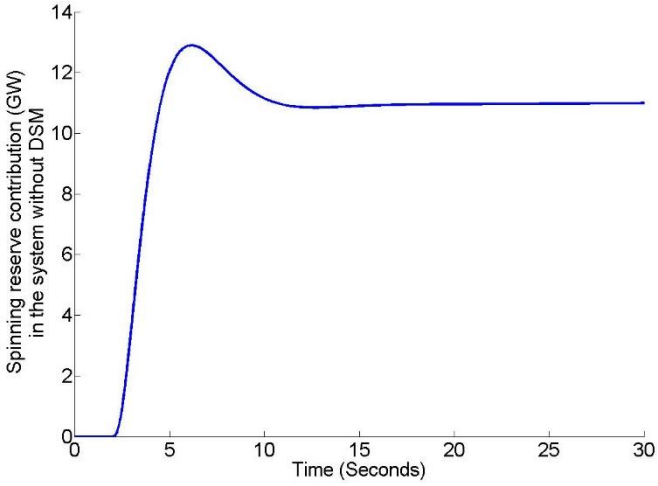

Figure 4.8 The contribution of spinning reserve in the system without dynamically controlled electrolysers in the first 30 seconds of the simulation

Figure 4.9 shows the frequency of the grid with or without dynamic demand control in the first 600 seconds of the simulation. In the system without dynamically controlled

electrolysers, the frequency of the grid returns to 50 Hz after 600 seconds from the start of the simulation. In actual power systems, secondary response will start to return the frequency to its nominal value within around ten minutes. However, after 10 minutes, the frequency of the system with dynamically controlled electrolysers does not return exactly to the nominal frequency of 50 Hz because the electrolysers are controlled using a droop control strategy and do not compensate generation loss completely, but this deviation is very small (0.067 Hz).

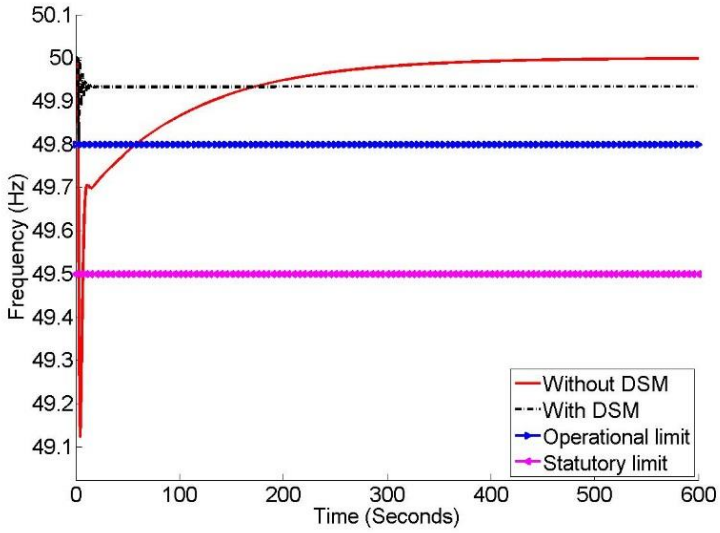

Figure 4.9 The frequency of the grid with or without dynamic demand control in the first 600 seconds of the simulation

Thirty minutes after the loss of generation, backup generation is connected to the system resulting in a linear increase from zero within 10 minutes until it compensates for the power deficit caused by the generation loss. Figure 4.10 shows the response of system in the first 3000 seconds (50 minutes) of the simulation. The resolution of the Simulink file for this longer analysis is 100 ms. When backup generation is added to the system, the frequency of the system without DSM overshoots, exceeding 50 Hz, but the frequency of the system that has dynamically controlled electrolysers does not do this. Instead, it increases linearly until the frequency reaches its nominal value.

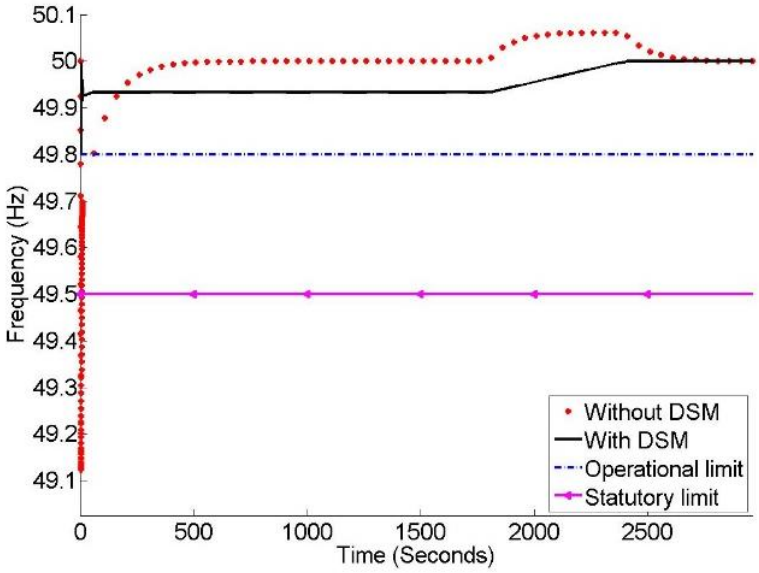

Figure 4.10 The frequency of the grid with or without dynamic demand control within 50 minutes from the generation loss

Figure 4.11 shows the electrolyser load during the first 3,000 seconds of the simulation. After 30 minutes from the start of simulation the electrolysers start to increase their demand because the backup generation is able to compensate the system for the loss of generation.

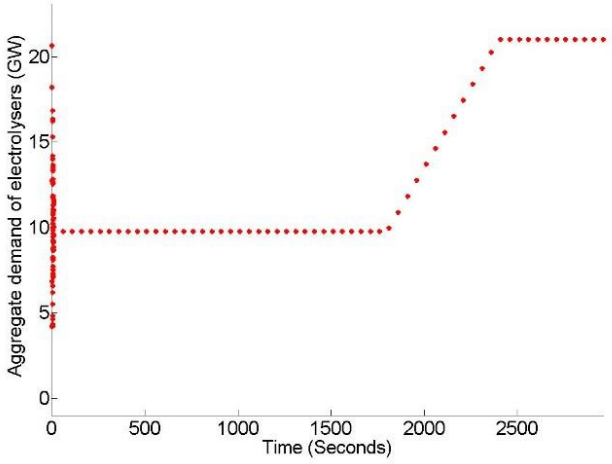

Figure 4.11 The aggregate demand of electrolysers during the first 3000 seconds of the simulation

4.4 Utilisation of alkaline electrolysers to improve power system frequency stability with a high penetration of wind power

Many countries around the world have ambitious targets to increase the penetration of wind power in their electrical power systems, but the variability of this renewable source remains a challenge to power system operators who are responsible for balancing generation with demand in real time [112]. As wind power penetration increases, controlling the frequency of the grid will become increasingly difficult because of high variations in the wind generated power, and also because wind turbines do not contribute naturally to system inertia but displace conventional generation, thereby effectively reducing the total inertia of the power system. Due to the difficulty of forecasting the exact demand and renewable power generation, there must be enough spinning reserve available in a system to automatically supply additional power when required, but spinning reserve does not become fully available immediately, and it is also very costly [80].

One potential solution to this problem is the utilisation of control strategies that vary loads supplied by the power system in response to power imbalances. As electrolyser controllers can react much faster than thermal plant governors, it is expected that the use of electrolysers as dynamic loads would help to smooth the frequency variation of systems with high wind penetration. The usage of these dynamic demand control tools could smooth the output power from generators, so the spinning reserve generators change their output much more gradually, and this could provide considerable benefit when considering the wear and tear on the generator [80]. Therefore, alkaline electrolysers have great potential to help in stabilisation and control of power system, particularly as the penetration of the integrated renewable energy resources increases.

4.4.1 Modelling method

In this part of the work, the model of a steam turbine generator detailed in Figure 4.3 is used within *MATLAB* Simulink environment to investigate a scenario in which there

is a 25% penetration of wind power in the system. The assumptions mentioned in Section 4.2 are also valid in this section, unless otherwise stated.

It is assumed that this electrical system also includes electrolysers, wind farms and non-electrolysis loads. Table 4.2 shows the ratings of different power system elements modelled in this section. The aggregate conventional load on this power system is assumed to be constant at 53.1 GW. However, as mentioned before, some of the demand loads are sensitive to frequency variations on the system, and their loads could change, as shown in Equation 4.1. The approach used to find the aggregate demand of electrolysers will be explained later in this section.

Table 4.2 Ratings of different power system elements modelled in this section

Item	Rating
The aggregate nominal capacity of the thermal power plants	66.9 GW
Aggregate installed wind power capacity	29.5 GW
Aggregate nominal demand of electrolysers	23 GW
Aggregate non-electrolysis demand	53.1 GW
Spinning reserve on the system without DSM	29.5 GW
Spinning reserve on the system with DSM	5.9 GW

It is assumed that the electrolysers are located at future hydrogen filling stations, and the size of storage at each station is sufficient to accept the excess hydrogen produced, so the hydrogen demand and supply will be decoupled through storage. In this manner the electrolysers can vary their electrical load to provide service to the electrical power system. For example, their loads can be adjusted explicitly to stabilise the frequency of the system.

To select an initial value for the amount of power generation from thermal generators, it is assumed that the system operators can predict the average amount of wind power generation during the next hour, so the operators can allocate the amount of thermal generation and spinning reserve on the system for the next hour. The aggregate size of wind power capacity is selected in a way that the wind power penetration in the system would be equal to 25% during the simulation. In other words, in order to provide sufficient wind input, it is assumed that, when the generated wind power is equal to its average value during the one hour time slot, the wind power provides 25% of the total generation in the system, so if the wind power becomes zero, then it will affect the system in the same way as a generation loss of 0.25 pu.

In this study, the fluctuations in frequency of the system that result from variations in wind power are investigated by considering two scenarios:

i. The electrolysers are not used as dynamically controlled loads to control the frequency of the grid, and the generators provide a significant amount of spinning reserve (Equal to wind power capacity).
ii. There is a very limited spinning reserve (5 times less than in the above case) provided on the system, and electrolysers are utilised to stabilise the frequency of the grid during the simulation.

It is assumed that, in both of the scenarios, the spinning reserve was half-loaded when the wind power was equal to its average value during the simulation period. The value of spinning reserve on the system without DSM is chosen to be equal to wind power capacity to ensure that there is enough spinning reserve to stabilise the system with high wind power fluctuation during the simulation period. It was also found that, in the system with DSM, only a fifth of that reserve is needed to keep the frequency within operational limits during the simulation period.

To be able to fairly compare the two scenarios, it is assumed that the electrolysers in the system without DSM operate at 60% of their nominal power all the time. It is further assumed that, at steady state conditions in the system with DSM when the wind power is equal to its predicted hourly average, the frequency of the system is 50 Hz, and the electrolysers operate at 60% of their nominal load. This 60% value was

selected to give electrolysers an equal chance to stabilise the frequency during the times that the aggregate wind power is below or above its hourly average value.

The electrolysers in the system with DSM must change their loads with respect to the frequency deviation in the system. The following three step algorithm is used to run the electrolysers in the context of dynamic demands on the power system.

1. If the system frequency is between 49.9 Hz and 50.1 Hz, then the electrolysers will consume power as follows, which is equivalent to a droop characteristic of 0.5%.

$$P_{El} = P_{N.El} - \frac{(P_{N.El} - P_{Min.El}) * (50.1 - f)}{(50.1 - 49.9)} \quad (4.5)$$

where

P_{El} is the load of each electrolyser (MW).
$P_{N.El}$ is the nominal load of each electrolyser (MW).
$P_{Min.El}$ is the minimum load of each electrolyser to work properly in normal hydrogen production mode (MW).
f is the frequency of the power system (Hz).

2. If the frequency drops below 49.9 Hz, then the electrolysers will operate at their minimum demand.

3. If the frequency goes above 50.1 Hz, then the electrolysers will run at rated demand.

Figure 4.12 illustrates the relationship between the electrolyser load and the frequency of the system. The frequency of 49.9 Hz and 50.1 are chosen for the control strategy limits because the operational frequency limits in the UK are 50±0.2 Hz, and when the frequency reaches these limits, the electrolysers should consume the minimum or maximum allowable power; however, it is known that it takes some time for the system to sense the frequency change and react to the situation, so the above values (50±0.1 Hz) were selected to provide a slightly improved and safer response.

If wind power increases in the system and exceeds its average hourly value, then this will result in a decrease in ΔP_L in Figure 4.3, and if the electrolysers reduce their loads,

then ΔP_L will similarly decrease. The resolution of the simulation is 100 ms to capture the dynamics of the power system with an acceptable precision.

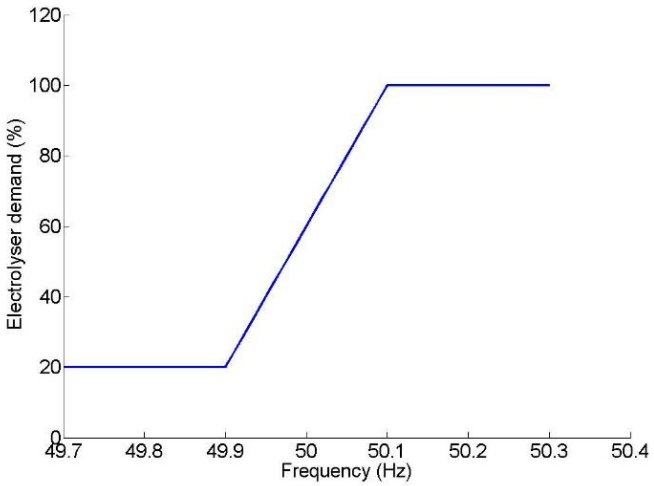

Figure 4.12 The control strategy to change the demand of each electrolyser with respect to the frequency of the grid

In the system with DSM, if the wind power exceeds its average hourly value, then in the steady state condition the electrolyser will consume more than 60% of its rated load so as to consume the surplus power available in the power system.

4.4.2 Simulation of the system in *MATLAB Simulink*

The wind data used in the system study has been taken from an actual wind farm located in the north of China. The wind turbine parameters are detailed below.

- Rating of the turbine: 1.5 MW
- Cut-in speed: 3 metres/sec
- Cut-out speed: 25 metres /sec
- Rated speed: 12 metres /sec

Interpolation is used to generate a wind power time series with a resolution 100 ms from available data that had a resolution of 10s. This value is scaled up to represent the aggregate value of the wind output into the power system. Figure 4.13 shows the

aggregate power time series for the assumed installed wind capacity used in the analysis over a duration of one hour.

For better illustration of the impact of wind power fluctuations on the frequency of the system, the wind time series was selected for a period when the wind power exhibited significant variation. The wind power during this simulation period has an average value of 16.7 GW. It should be noted that, because the output of one wind turbine is scaled up to represent the wind power generation in the UK, the variation of wind power on the system is very high because the smoothing effect of numerous geographically-dispersed wind turbines is not accounted for, so a large amount of spinning reserve was needed to stabilise the system. As the results for the first few seconds of the simulation are affected by the initialisation of the system, the graphs only show results from 300 s after the simulation start-up.

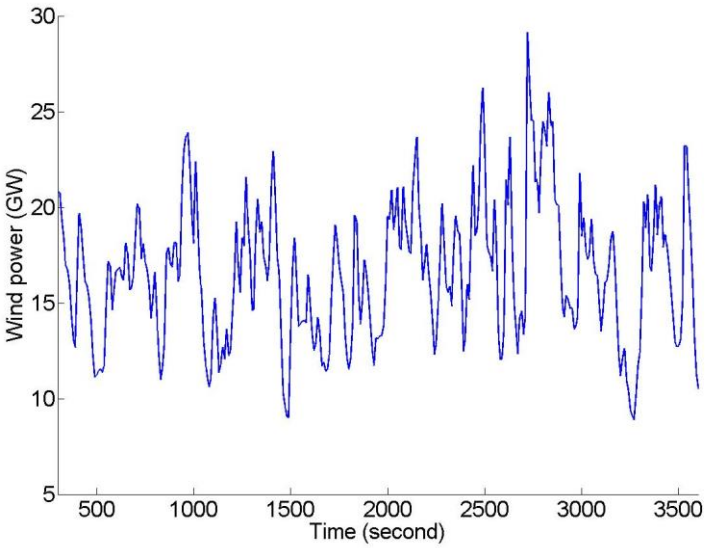

Figure 4.13 Wind power profile used in the simulation

To find out a reasonable aggregate nominal value for the demand of electrolysers, an initial value had to be selected. This Initial Nominal Aggregate Electrolysis Demand (*INAED*) value was set to 42 GW because, with respect to the control strategy, 40% of this value should be bigger than, or equal to, the average wind power during the simulation to be able to fully balance the system in the case of zero wind power production. In addition, 40% of *INAED* should be bigger than or equal to the difference

between the nominal and average wind power during the simulation to be able to fully balance the system in the case of maximum wind power production.

$$\begin{cases} \bar{W} \leq (INAED * 0.4) \\ (W_N - \bar{W}) \leq (INAED * 0.4) \end{cases} \Rightarrow 16.7 \leq INAED * 0.4 \Rightarrow 42 \leq INAED \qquad (4.6)$$

where

$\bar{W}$ is the average wind power during the simulation in GW.

W_N is the wind power capacity within the system in GW.

Then this initial value was reduced by a decrease factor of 0.55 to make the frequency of the system with DSM remain within the operational frequency limits during the simulation period with a lower aggregate nominal electrolysis demand size; therefore, eventually the value of 23 GW was selected for the aggregate nominal load of electrolysers. This reduction in the aggregate size of electrolysers was performed to minimise the size and, consequently, costs of electrolysers. However, it is worth mentioning that, in the real world, the penetration of electrolysers in future power systems will depend on many factors such as the number of HFCV users, the need to produce hydrogen from the electrolysis process, and the amount of interest and investment in the hydrogen economy.

The aggregate non-electrolysis demand (*ANonED*) on the system is assumed to be constant and equal to 53.1 GW in both of the considered scenarios. This value is derived from the fact that, when the wind power is equal to its average hourly value, the electrolysers consume 60% of their rated demand, so the aggregate electrolysis demand in such situation will be 13.8 GW. In such a case, the wind farms will provide 25% of the total power generation, so the total power generation will be 66.9 GW. Therefore, the aggregate non-electrolysis load will be 53.1 GW.

$$AED + ANonED = \frac{\bar{W}}{WPen} \Rightarrow ANonED = \frac{\bar{W}}{0.25} - ANED * 0.6 \Rightarrow$$

$$ANonED = \ 66.9 - 23 * 0.6 = 53.1\ GW \qquad (4.7)$$

where

AED is the aggregate electrolysis demand in GW.

$ANED$ is the aggregate nominal electrolysis demand in GW.

$WPen$ is the wind power penetration.

The electrolysis loads are constant in the non-DSM system and their aggregate load is equal to 13.8 GW because electrolysers are using 60% of their rated demand.

Figure 4.14 shows the frequency of the electrical systems with and without DSM. It is evident that the high penetration of wind power can cause significant fluctuations in the frequency of the system without DSM, and the frequency can go beyond the operational limit in some occasions. On one occasion, the frequency of the system exceeds the statutory limit for about 6 seconds. If the demand fluctuations were added to the system, then these frequency fluctuations could become more severe. On the other hand, in the system with electrolysers used as dynamic demand, the frequency fluctuation was reduced significantly, and the frequency remained within the operational limits during the simulation period.

The mean value of the frequency in the system without DSM was 49.9967 Hz, and that system had the standard frequency deviation of 0.1215 Hz. The mean value of the frequency in the system with DSM was 49.9983 Hz, and that system had the standard frequency deviation of 0.0297 Hz. This means that the standard frequency deviation of the system without DSM was about 4.1 times higher than that of the system with DSM.

It should be noted that, in the actual electrical power systems with 25% penetration of wind power, the fluctuation of frequency might not be as harsh as the case in this work, because different wind farms in different locations connected to a grid might compensate each other's output power to some extent, and the aggregate power from wind farms might not fluctuate as harshly as the case in this simulation. However, these simulation results show that by controlling some key demand loads (e.g.

electrolyser loads) in the system, the operators can significantly stabilise its frequency fluctuation with very limited resources of spinning reserve.

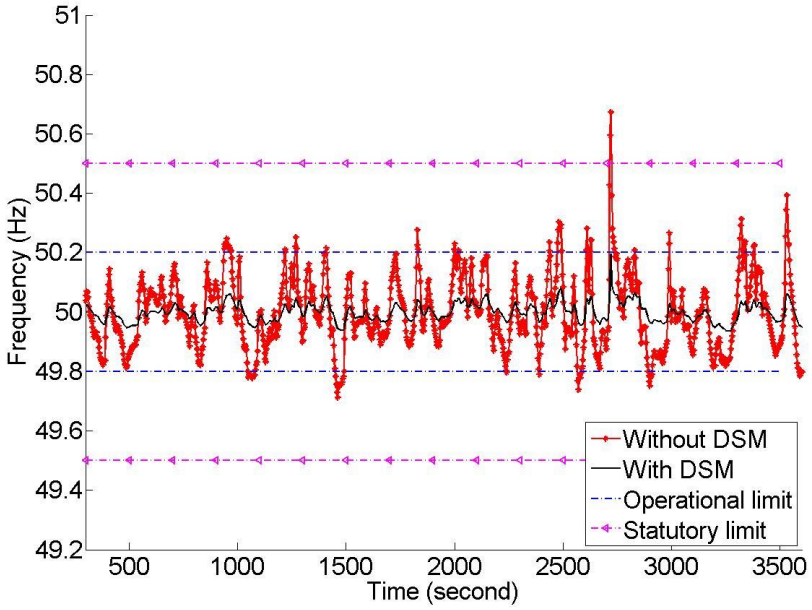

Figure 4.14 The frequency of the grid with or without dynamically controlled electrolysers

Figure 4.15 shows the aggregate load of the electrolysers in the system with DSM during the simulation period. To help with the stability of the system, these electrolysers must be able to change their demand dynamically similar to that shown in Figure 4.15. This implies that the electrolysers must have sufficient dynamic response to change their power consumption, otherwise they will not be able to provide appropriate frequency response.

In the simulations, the electrolysers were considered as ideal loads, but after running the simulations, the aggregate load changes experienced were analysed to check compliance with ramp rate limitations. The maximum and minimum limits for the load change speed of the electrolysers are taken from the pressurised alkaline electrolysers made by NEL Hydrogen. As explained in Chapter 2, the NEL Hydrogen electrolysers with nominal load of 24 kW offer a maximum load change of ±12.8 pu/s, so if the aggregate load of electrolysers in the system is 23 GW, then by scaling up the value

given by NEL Hydrogen, the maximum load change of the aggregate electrolysis load in the system simulated in this work at each simulation time step will be ±29.5 GW.

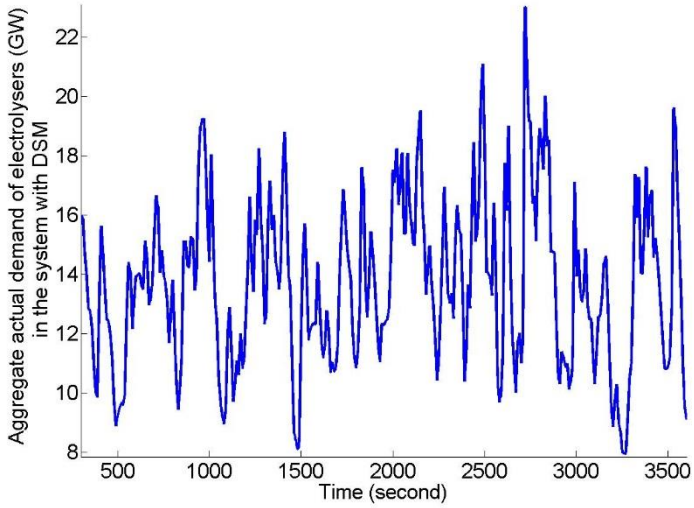

Figure 4.15 The aggregate load of electrolysers in the system with DSM

Figure 4.16 shows the change in the aggregate electrolyser load in each time step during the simulation. It was much lower than the limits found earlier from commercial electrolysers, so the ramping rates of the electrolysers available on the market today are fast enough to work with such control strategies and reduce frequency fluctuations in the power system as indicated by the results shown in this section.

Figure 4.17 shows the aggregate wind power injected into the grid and also the difference between the wind power and the aggregate load of electrolysers in the system with DSM. It is evident that the electrolysers can absorb a significant amount of wind power fluctuation and the difference between the aggregate wind power injected into the system and the aggregate electrolysis load does not fluctuate significantly. Actually, the system experiences this condition as an indirect result of the control strategy, i.e. the control system changes the load of the electrolysers to stabilise the frequency of the system, but due to the relationship between the frequency and the power imbalance, this difference value is smoothed significantly.

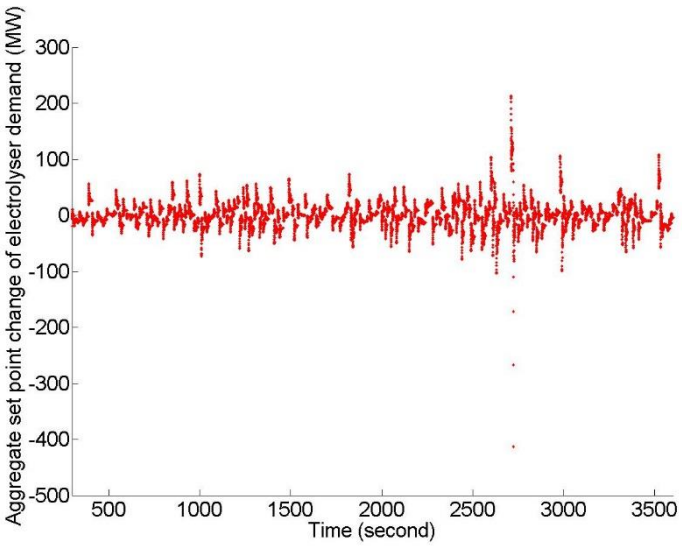

Figure 4.16 The change in the aggregate demand of electrolysers in the system with DSM

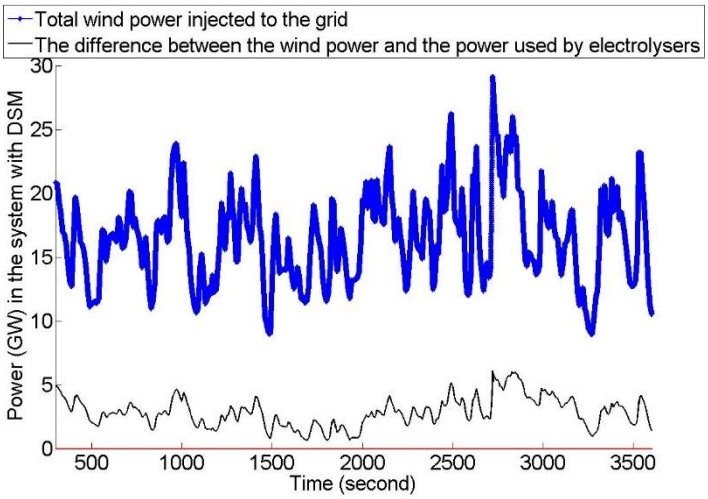

Figure 4.17 The wind power and the difference between the wind power and the aggregate demand of electrolysers in the system with DSM

Figure 4.18 shows the wind power and the difference between the wind power and the aggregate load of electrolysers in the system without DSM in which the difference value fluctuates exactly in line with the rate of wind power fluctuations because the electrolysers have a constant demand (60% of $P_{N.EL}$) at all times. The steam turbine generation units in the non-DSM system have to compensate for these fluctuations. This difference value becomes negative in some occasions in the non-DSM system,

and it means that the thermal generation units are providing the power for the operation of the alkaline electrolysers at those times. This is not desirable because it means that during such periods, the hydrogen is produced with non-renewable resources that emit significant amounts of carbon dioxide.

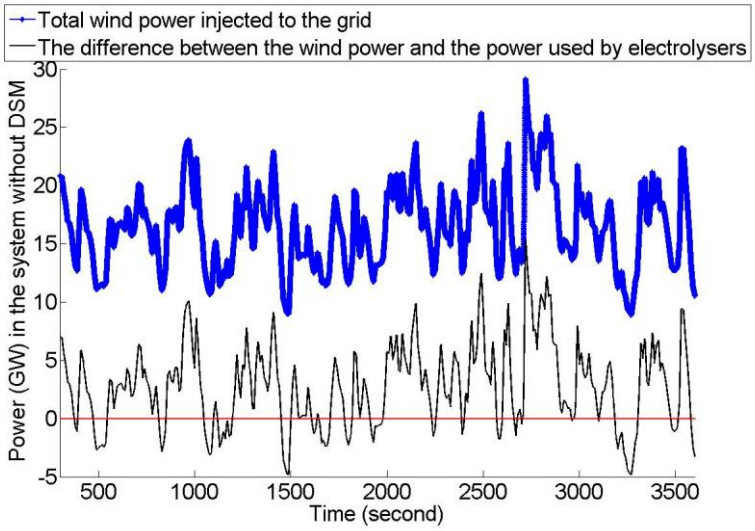

Figure 4.18 The wind power and the difference between the wind power and the aggregate demand of electrolysers in the system without DSM

Figure 4.19 shows the aggregate power generated from the steam turbine generation units. The aggregate output power from the thermal generators in the system with DSM is less time variable than without DSM. The mean value of aggregate output power from the thermal generators in the system without DSM was 50.4 GW, and the system had a standard power deviation of 3.4 GW. The mean value of aggregate output power from the thermal generators in the system with DSM was 50.2 GW, and that system had a standard power deviation of 1.1 GW. This means that the standard power deviation of the system without DSM was about 3.1 times higher than that of the system with DSM. The utilisation of alkaline electrolysers as DSM can thus decrease the degree of power fluctuations of thermal generators, and consequently, minimise the wear and tear and maintenance on those generators. The system with DSM will also result in reduced carbon dioxide emissions from thermal electric power plants as a consequence of the reduced need for spinning reserve on these generation units.

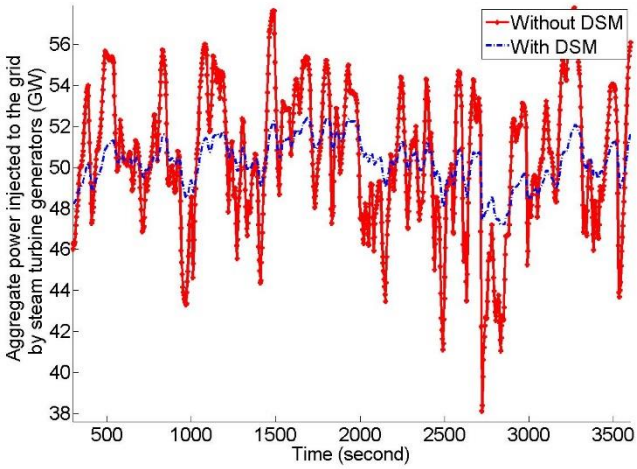

Figure 4.19 The aggregate power generated from steam turbine generation units

4.4.3 Financial viability of the proposed scenario

It is believed that, if the electrolysers are already installed to produce fuel for HFCVs, then they can also be used to provide frequency support for the power system. In the work in this chapter, it is assumed that electrolysers consume 60% of their nominal load when the frequency is 50 Hz. This means that the electrolysers are overrated by 66% (40/60×100) to provide frequency stability. Therefore, the amount of extra capital, operational and maintenance cost ($ECOM$ in £/h) for each hydrogen filling station can be calculated using the following equation.

$$ECOM = C_1 * 0.4 * S_{St} \tag{4.8}$$

where

S_{St} is the aggregate size of electrolysers in each station in MW.

C_1 is the capital, operational and maintenance costs of alkaline electrolyser taken from Equation 3.4 in Chapter 3 and is equal to 11.82 (£/MW/h).

Based on the data in Post Assessment Tender Reports [113] published by National Grid, it is assumed that the hydrogen filling station operators can receive $Payment$=8.7 (£/MW/h) for providing frequency response with electrolysers.

To prove the financial viability of the proposed scenario, we need to show that the capital and operational costs of the extra installed electrolysis capacity at each filling station ($ECOM$) is lower than the amount of extra income gained ($Payment * 0.8 * S_{St}$ in £/h) due to participation in frequency regulation schemes. To include the factor that, in the control strategy, only 80% of the electrolyser capacity is used for frequency stability purpose, the coefficient of 0.8 is included in the following equation.

$$Profit\ \left(\frac{£}{h}\right) = Payment * 0.8 * S_{St} - ECOM = \tag{4.9}$$

$$Payment * 0.8 * S_{St} - C_1 * 0.4 * S_{St} = (8.7 * 0.8 - 11.82 * 0.4) * S_{St} = 2.23 * S_{St}$$

It is obvious that the above profit value is positive all the time, and there will be about 20 (£k/MW/year) financial profit for the electrolyser operators if they provide frequency support. This equation assumes that the average frequency of the power system remains at 50 Hz during the lifetime of electrolysers, and therefore on average the electrolysers consume 60% of their nominal demand using the proposed control strategy. It should be noted that this profit value is the additional profit gained by electrolyser operators due to participation of electrolysers in frequency stability schemes, and the electrolyser operators were already making profit by selling hydrogen, which is the main purpose of installing them. This means that the amount of hydrogen sale in both of the scenarios, with or without electrolysers, are assumed to be the same. It is worth mentioning that the financial value of reduction in the carbon dioxide reduction in transport and electricity sectors, which would surely improve the results, are not included here.

4.5 Chapter summary

In this chapter, the impact of dynamically controlled electrolysers on the frequency stability of the power system was investigated in two cases of generation loss and also in the case of a high penetration of wind power in the system. A *MATLAB* Simulink model was presented to simulate the scenarios. The delay in frequency measurement,

occasional delay and the ramp rate of electrolysers detailed in Chapter 2 were considered in the simulations.

Such electrolysers can help maintain the network frequency within operational limits, even in the case where there is no spinning reserve on the system, by reducing their demand in response to frequency deviation after a sudden loss of generation. On the other hand, the system without dynamically controlled electrolysers could not keep its frequency within operational or statutory limits after a significant generation loss of 0.15 pu.

In addition, the simulation results show that alkaline electrolysers can help maintain network frequency within operational limits by changing their demand as a function of the power system frequency deviation from nominal in the case of 25% penetrations of wind power. The amount of deviation in the frequency of the power system is quantified in different scenarios in the chapter. The simplicity of the control strategy used here to achieve frequency support is one of the attractive features of this work. In addition a new way to size electrolysers have been used to minimise the capital cost of electrolysers utilised for frequency stability.

Unlike the FCDM scheme, in the scenario explained in this work, the power is never disconnected from the electrolysers, and only the load levels of the electrolysers are modulated with respect to the frequency deviation in the system.

As long as there is enough hydrogen stored to meet the demand at each filling station, there would not be any risk for the electrolyser operators to participate in this sort of dynamic demand scheme, and there are even be some long-term financial benefits for electrolyser operators providing frequency response services.

5 HYDROGEN PRODUCTION WITH ELECTROLYSERS IN THE UK 2050 SCENARIOS

5.1 Introduction

In the first part of this chapter, a scenario involving the widespread availability of hydrogen at UK fuel stations for the purpose of supplying fuel to HFCVs is investigated. Calculations have been carried out to find out how much hydrogen is needed for all road transportation in the UK to be met in this way, and then the power and energy needed to operate alkaline electrolysers in the UK power system to supply all these vehicles with hydrogen is calculated.

In the second part of this chapter, a number of different scenarios are simulated to investigate the role of electrolysers to absorb the surplus power produced by clean power sources in the UK in 2050. The results of nine different 2050 scenarios with three different capacity ratings for wind, solar and nuclear power and three different penetrations of EVs and HFCVs are included at the end of the chapter. Furthermore, the size and utilisation factor of electrolysers and fossil fuel power plants (FFPPs) needed to balance the system for such scenarios, as well as the aggregate size and cost of hydrogen storage, are identified.

5.2 Calculation of the additional demand of electrolysers on the UK electrical grid

In this section, the amount of hydrogen needed to allow a change of all of the vehicles on UK roads from fossil fuelled to hydrogen powered vehicles and the extra aggregate electrolyser capacity needed to provide that amount of hydrogen from the power supplied by UK electrical grid are calculated. This is an extreme case, and if the penetration of HFCVs is less than 100%, then the results can be easily multiplied by a fractional coefficient to reflect such cases.

Currently, fuel demand for road transport in the UK is equal to 46 million litres of petrol and 74 million litres of diesel per day [114]. The energy efficiency of HFCVs is better than petrol or diesel ICE vehicles [115], implying that they use less energy to move the same distance. Furthermore, hydrogen-powered fuel cells and electric motors do not have Carnot cycle losses, and they consume minimal energy when they are in standby condition or while they are stationary in traffic. Many common automobile engines today are only around 21% efficient, and modern diesel engines are about 30% more fuel-efficient than similar-sized petrol engines, meaning that their average efficiency is about 27% [116].

The efficiency of HFCVs ($\eta_{FCVs}\%$) can be calculated using the following equation. Losses due to mass, drag, friction, different driving patterns and electricity consumption of services other than those related to the electric engine, e.g. lights and cooling system are ignored in the calculation.

$$\eta_{FCVs}\% = \eta_{FC} * \eta_{IM} * \eta_{gb} * 100 \quad (5.1)$$

where

$\eta_{FC}\%$ is the efficiency of fuel cells. It is assumed that the average efficiency of fuel cells is 51% [13].

$\eta_{IM}\%$ is the efficiency of the inverter and electric motor together in an EV or a FCV and is assumed to be 86.7% [13].

$\eta_{gb}\%$ is the efficiency of the gear box in an EV or FCV and assumed to be 91.5% [13].

By substituting the corresponding values in the above equation, the efficiency of a HFCV is found to be 40.5%.

In this thesis, it is assumed that the average efficiency of petrol engines is about 21%, and the average efficiency of diesel cars is about 27%. We also know that one kilogram of hydrogen contains approximately the same energy as a US gallon (3.785 litre) of petrol [117]. In addition, each litre of diesel contains 13.7% more energy than a litre of petrol [118]. Using this data, the daily amount of hydrogen (DH_2 in kg) needed for

all the HFCVs if they replace all of the vehicles on roads in the UK is calculated by the following equation.

$$DH_2 = \frac{L_{Petrol} * \eta_{Petrol} + L_{Diesel} * \eta_{Diesel} * C_{DP}}{C_{Gal} * \eta_{FCV}} \quad (5.2)$$

where

L_{Petrol} is the daily amount of petrol consumption for the vehicles on road in the UK in litres.

L_{Diesel} is the daily amount of diesel consumption for the vehicles on road in the UK in litres.

η_{Petrol} is the average efficiency (%) of petrol cars.

η_{Diesel} is the average efficiency (%) of diesel cars.

η_{FCV} is the efficiency of HFCVs (%).

C_{DP} is the conversion factor (1.137) used to change the amount of energy in a litre of diesel into the amount of energy in a litre of petrol.

C_{Gal} is the coefficient used to change a US gallon to litre.

By substituting the corresponding values in the above equation, it is found that, on average, 21.1 million kg of hydrogen is needed daily to support all the UK road transport. There are about 8,591 petrol stations operating in the UK [114]. Therefore, if all of the current petrol stations in the UK become replaced by hydrogen stations, the average amount of hydrogen needed per fuel station in the UK per day will be equal to 2,461 kg.

It is assumed that type 5040 electrolysers from NEL Hydrogen that consume 53.4 kWh of electricity to produce one kilogram of hydrogen [85] were used for this purpose. The efficiency of electrolyser rectifier is assumed to be included in this efficiency. The efficiency of hydrogen production by electrolysers (η_{El}%) can be calculated from the following equation.

$$\eta_{El}\% = \frac{E_{HHV}}{E_{El}^{kg}} * 100 \quad (5.3)$$

where

E_{HHV} is the Higher Heating Value (HHV) of hydrogen (39 kWh/kg, [25]).

E_{El}^{kg} is the energy needed to produce a kg of hydrogen with the electrolyser (kWh/kg).

By inserting the corresponding values in the above equation, the efficiency of electrolysers used in this chapter are found to be 73%. The energy (E_{St}^{Day} in MWh) needed to be supplied to each station for hydrogen production and compression every day can be calculated from the following equation.

$$E_{St}^{Day} = \frac{DH_2 * E_{El}^{kg}}{NS*(1-\eta_{El}(1-\eta_{Comp}))*1000} \quad (5.4)$$

where

NS is the total number of hydrogen filling stations in the UK.

η_{Comp} is the efficiency of the hydrogen compressors and assumed to be constant and equal to 93% [119].

Using this equation, the amount of energy that each station needs to produce and compress the required amount of hydrogen each day will be equal to 138.5 MWh. If each electrolyser works 24 hours a day, the electrical supply needed per filling station for electrolysers and compressors will be 138.5 MWh/24=5.77 MW.

The total power (P_{FCVs}^{Total} in GW) needed to supply all of the stations can be calculated using the following equation.

$$P_{FCVs}^{Total} = \frac{E_{St}^{Day} * NS}{24*\eta_{grid}*1000} \quad (5.5)$$

Where $\eta_{grid}\%$ is the average efficiency of the electrical power system to transfer electricity from the point of generation to the point of consumption and is assumed to be 92% [13].

Therefore, the total amount of electrical power (including all of the losses) needed to be generated to supply all of the hydrogen fuel stations in the UK will be 53.9 GW, and the amount of electrical energy needed per year to produce hydrogen for all of the vehicles on road in the UK would be 53.9 GW×24×365= 472 TWh. The total amount of electrical energy consumed in the UK in 2011 was about 374 TWh [120], so a 126.2% increase in the total electrical energy demand in the UK is estimated if such a change occurs. This amount of power is required all the time, and if hydrogen production only occurs during night-time or the electrolysers are used to absorb the surplus variable renewable power, then the amount of required power generating capacity would be much larger than this amount, and of course, higher rated electrolysers would be needed in each filling station to provide sufficient hydrogen. For context, it should also be considered that the UK has the aggregate nominal electricity generation capacity of about 88 GW (2010 Data) [121].

Using hydrogen vehicles requires installation of the proper refuelling infrastructure. Economic designs require a reasonable demand of hydrogen to justify their capital cost. However, due to the limited deployment of hydrogen vehicles, hydrogen fuelling stations have not become widespread yet [4].

5.3 Hydrogen production with clean surplus power in the UK 2050 scenarios

In this section, a number of scenarios for hydrogen production using electrolysers in the UK 2050 electric system are investigated. The 2050 Pathways Analysis Report [111] contains some suggested scenarios for the amount of wind, solar and nuclear power capacity in the UK. Such data is used in this work to introduce some plausible scenarios.

In addition, for each generation capacity scenario, three options for UK road transport will be explored.

- EVs dominate: 90% of the fleet are EVs and the rest of them are HFCVs.
- HFCVs dominate: 90% of the fleet are HFCVs and the rest of them are EVs.

- There is an equal mix of both: 50% of the fleet are EVs and the rest of them are HFCVs.

Table 5.1 introduces different scenarios used in this work. Scenarios 1.1, 1.2 and 1.3 illustrate a pathway with largely balanced effort across all electricity generation sectors. Scenarios 2.1, 2.2 and 2.3 look at the case where there is more wind power capacity, and scenarios 3.1, 3.2 and 3.3 present a case with more renewable power generation capacity, meaning an increase in both wind and solar capacity in comparison to the first scenario but with no nuclear power generation.

Table 5.1 Details of different 2050 scenarios simulated in this thesis

Scenario	Wind (GW)	Solar (GW)	Nuclear (GW)	EV penetration	HFCV penetration
1.1	80	70	39	90%	10%
1.2				10%	90%
1.3				50%	50%
2.1	120	70	39	90%	10%
2.2				10%	90%
2.3				50%	50%
3.1	132	90	0	90%	10%
3.2				10%	90%
3.3				50%	50%

The figures in this section will illustrate the results of simulation of scenario 1.3, but at the end of the section, the results from all of the scenarios will be included in a table and will be compared and discussed.

We know that there should be a balance between supply and demand in the power system all the time, so the following equation is used during the simulation to balance the electricity grid.

$$P_{Wind}^{t} + P_{Solar}^{t} + P_{Nuclear}^{t} + P_{FPP}^{t} = D_{N}^{t} + D_{EVs}^{t} + D_{ElComp}^{t} \quad (5.6)$$

where

P_{Wind}^{t} is the total aggregate wind power generation (GW) within the system at time interval 't'.

P_{Solar}^{t} is the total aggregate solar power generation (GW).

$P_{Nuclear}^{t}$ is the total aggregate nuclear power generation (GW).

P_{FPP}^{t} is the total aggregate power generation (GW) from conventional FFPPs.

D_{N}^{t} is the aggregate electricity demand (GW) excluding the demand from EVs and electrolysis hydrogen filling stations.

D_{EVs}^{t} is the aggregate EV demand (GW) including all of the additional losses that they cause on the system.

D_{ElComp}^{t} is the aggregate demand of electrolyser and compressors including all of the additional losses that they cause on the system (GW).

It is assumed that total demand profile (without electrolysers or EVs) in 2050 is the same as the current UK demand profile because the efficiency gains of electric devices is assumed to be cancelled out by their increased uptake. Figure 5.1 shows the demand profile of the UK during 2014 [92] which is used for the simulation.

To find out the aggregate amount of wind power generation in the UK in each 2050 scenario, a scenario using the estimated amount of wind power generation in different regions in GB in year 2020 is modelled and then scaled up to match the aggregate wind capacity in each 2050 scenario.

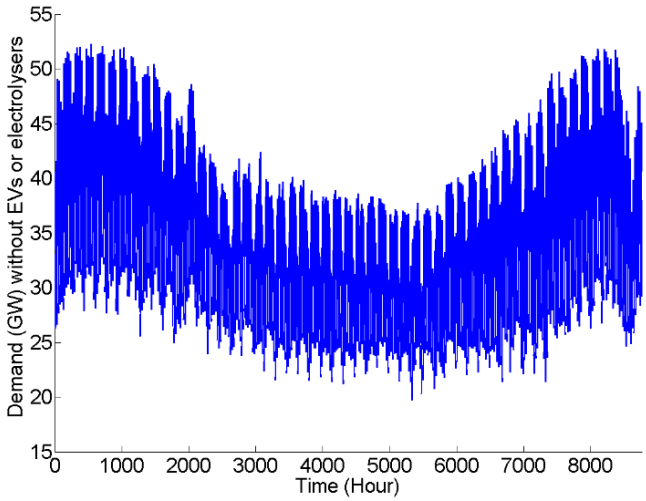

Figure 5.1 UK electric demand (without electrolysers or EVs) in all 2050 scenarios

In this analysis the GB power system is divided into 17 study regions which are consistent with the 17 boundaries presented within the National Grid Seven Year Statement [122]. Wu and Infield [123] approximated the wind power capacity for 17 different regions in GB for year 2020, considering both onshore and offshore wind farm capacities that were based on the data from Renewable UK's website [124]. Figure 5.2 shows the 17 regions used in their work. Their estimation [123] for the aggregate wind power capacity for those regions is provided in Table 5.2 and will be equal to 27.3GW. In addition, Table 5.3 shows more details about the way they estimated the amount of onshore and offshore wind power capacity for those regions [123].

In this work, most regions are represented by a meteorological station at which average hourly wind speed data was measured. Wind speed data with resolution of one hour from 14 regions was obtained from the UK meteorological office for the duration of one year. This was used in the analysis to find the aggregate wind power generation during the year 2020. However, for three regions (4, 14 and 16), the wind speed was estimated using the data from their neighbouring regions due to lack of reliable wind data from local meteorological stations. Wind speed data from regions '1', '12' and '17' are used instead of data from regions '4', '14' and '16', respectively. As is shown in Table 5.2, those three zones have limited wind power capacity, and this simplification will have no significant impact on the overall results. The names of

those meteorological stations where the data was collected from are listed in Table 5.4 [93].

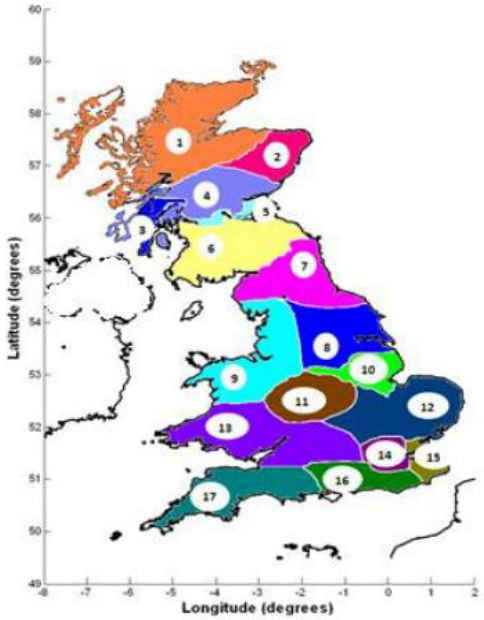

Figure 5.2 The GB map divided into 17 different regions [123]

For simplicity, it is assumed that the wind turbines used in all of the wind farms are from the same type and with the same rating, and they have a power curve shown in Figure 3.3. Using the wind speed data from different regions in the UK, the wind power generation capacity mentioned in Table 5.2 and the power curve in Figure 3.3, a *MATLAB* program was developed to find how much wind power will be generated for each scenario during 2020 with a one hour resolution. Then the aggregate wind power result was scaled up to match each 2050 scenario detailed in Table 5.1. Figure 5.3 shows the aggregate wind power generation from all of the wind farms in the UK in scenario 1.1, 1.2 and 1.3 with total generation of 231.2 TWh during 2050.

To simulate the solar power generation in 2050 scenarios, the power output data from 50 solar sites across different areas in the UK during 2014 was obtained from Microgen Database provided by Sheffield Solar group located at the University of Sheffield [125]. The output power from each site was normalised using the installed solar capacity at each site, and then the average of the normalised output power of all of the sites was used to represent the aggregate normalised solar power generation in the UK.

This implies that we assume that the solar capacity of all of the 50 sites will be equal in each scenario. In other words, the nominal solar capacity of each site will be equal to the total solar capacity in each scenario (mentioned in Table 5.1) divided by 50.

Table 5.2 Estimation of the aggregate wind power capacity for 17 different regions in GB in 2020 [123]

Region	Capacity (MW)	Name	TSO
1	2047	North West (SHETL)	SHETL
2	247	North (SHETL)	SHETL
3	369	Sloy (SHETL)	SHETL
4	439	South (SHETL)	SHETL
5	1296	North (SPT)	SPT
6	4245	South (SPT)	SPT
7	4127	North & NE England	NGET
8	2246	Yorkshire	NGET
9	3498	NW England & N Wales	NGET
10	2284	Trent	NGET
11	163	Midlands	NGET
12	3044	Anglia & Bucks	NGET
13	876	S Wales & Central England	NGET
14	6	London	NGET
15	1825	Thames Estuary	NGET
16	187	Central S Coast	NGET
17	493	South West England	NGET

The solar power generation (P_{Solar}^{t} in GW) in the UK at each time interval 't' in 2050 is then calculated using the following equation.

$$P_{Solar}^{t} = \frac{S_S}{N_{SS}} * \sum_{i=1}^{N_{SS}} \frac{PS_i^t}{TIC_i} \quad (5.7)$$

where

S_S is the total aggregate installed solar power capacity (GW) in each UK 2050 scenario.

N_{SS} is the total number of solar sites.

PS_i^t is the power output (kW) from solar site 'i' at time interval 't'.

TIC_i is the total installed solar capacity (kW peak) at site 'i'.

Table 5.3 More details about the estimation of installed wind power capacity in 17 regions in GB in 2020 [123]

Region	Onshore (MW)			Offshore (MW)				Total
	Operational	Under construction	Consented	Operational	Under construction	Consented	In planning	
01	785	284	393	10	0	0	575	2047
02	132	29	61	0	0	0	25	247
03	137	54	5	0	0	0	173	369
04	389	32	18	0	0	0	0	439
05	2	25	58	0	0	6	1205	1296
06	2152	740	903	0	0	0	450	4245
07	262	188	206	184	62	0	3225	4127
08	131	175	400	0	0	540	1000	2246
09	310	25	59	847	576	389	1292	3498
10	123	9	62	194	270	1200	426	2284
11	31	29	103	0	0	0	0	163
12	141	61	161	60	821	0	1800	3044
13	206	83	212	0	0	0	375	876
14	6	0	0	0	0	0	0	6
15	60	31	146	563	1000	12	13	1825
16	1	0	20	0	0	0	166	187
17	128	29	36	0	0	0	300	493
Total	4996	1794	2843	1858	2729	2147	11025	27392

Table 5.4 The names of meteorological stations where the wind speed data was collected

Number	Name	Number	Name	Number	Name
1	Tain Range	7	Boulmer	13	Rhoose
2	Peterhead	8	Spurn Point	14	No data
3	Machrihanish	9	Hawarden Airport	15	Langdon Bay
4	No data	10	Coningsby	16	No data
5	Leuchars	11	Shawbury	17	Chivenor
6	West Freugh	12	Gorleston		

.

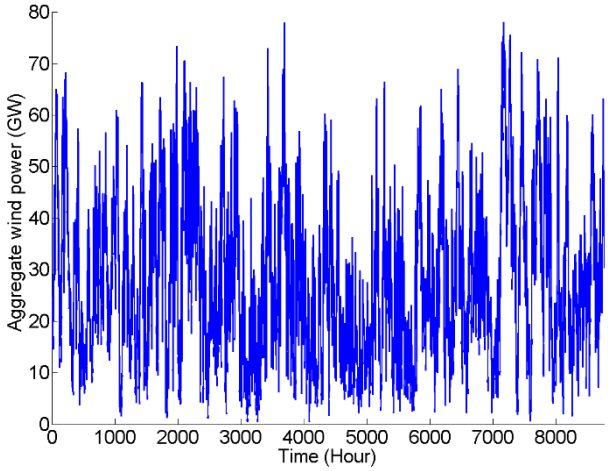

Figure 5.3 The amount of aggregate wind power generation in scenario 1.3

Figure 5.4 shows the aggregate solar power generation on the system in scenarios 1.1, 1.2, 1.3, 2.1, 2.2 and 2.3 with total generation of 69.8 TWh during 2050.

The output from nuclear generators was assumed to be constant during the simulated year and equal to their nominal aggregate capacity mentioned in Table 5.1.

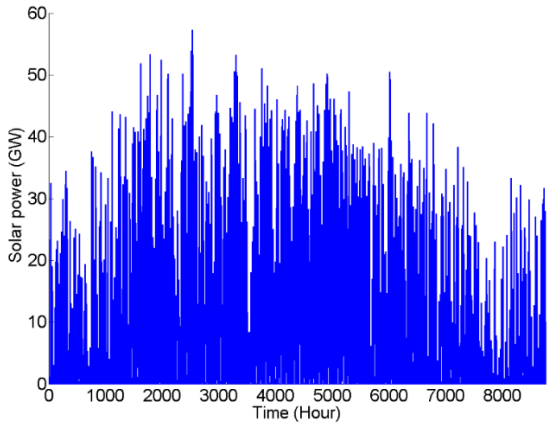

Figure 5.4 Aggregate solar power generation on the system in scenario 1.3

To present the way that the simulator calculates the amount of power and energy needed by HFCVs and EVs in each scenario a number of equations are introduced here.

The efficiency of the system with HFCVs ($\eta_{FCV}^{System}\%$) from after the grid electricity generation point to wheels can be calculated from the following equation:

$$\eta_{FCV}^{System}\% = \eta_{grid} * \eta_{El} * \eta_{Comp} * \eta_{FCV} * 100 \quad (5.8)$$

By substituting the corresponding values in the above equation $\eta_{FCV}^{System}\%$ is found to be 25.3%.

The efficiency of the system with EVs ($\eta_{EV}^{System}\%$) from after the grid electricity generation point to wheels can be calculated from the following equation:

$$\eta_{EV}^{System}\% = \eta_{grid} * \eta_{Rec} * \eta_{Bch} * \eta_{Bdis} * \eta_{IM} * \eta_{gb} * 100 \quad (5.9)$$

where

η_{Rec} is the efficiency of the rectifier to charge the batteries of an EV, and it is assumed to be 96% [13].

η_{Bch} is the efficiency of the batteries during charge in an EV and assumed to be 94% [13].

η_{Bdis} is the efficiency of batteries during discharge in an EV and is assumed to be 90% [13].

By substituting the corresponding values in the above equation $\eta_{EV}^{System}\%$ is found to be 59.2%.

The ratio showing how much the system with EVs is more efficient than the system with HFCVs can be found using the following equation.

$$R_{EVFCVs} = \frac{\eta_{EV}^{System}\%}{\eta_{FCV}^{System}\%} \tag{5.10}$$

Therefore, the efficiency of the system with EVs will be 2.34 times higher than the efficiency of the system with HFCVs.

The total energy needed per year for HFCVs ($E_{\kappa FCVs}^{Total}$ in TWh) if only $\kappa\%$ of vehicles on road become replaced by HFCVs can be calculated from the following equation.

$$E_{\kappa FCVs}^{Total} = \kappa * \frac{P_{FCVs}^{Total} * 24 * 365}{1000} \tag{5.11}$$

The value of P_{FCVs}^{Total} found in Section 5.2 is also used for all 2050 scenarios in this section. On the other hand, the total energy needed per year to supply all EVs ($E_{\kappa EVs}^{Total}$ TWh) if only $(100 - \kappa\%)$ of the vehicles on road get replaced by them can be calculated from the following equation.

$$E_{\kappa EVs}^{Total} = (1 - \kappa) * \frac{P_{FCVs}^{Total} * 24 * 365}{1000 * R_{EVFCVs}} \tag{5.12}$$

It is assumed that EVs will only be charged during off-peak times. Generally, Economy 7's cheap hours start at around 11pm–1am and will last until 6–8am [126]. In this work it is assumed that aggregate charge profile of all the EVs looks like an isosceles trapezium, starting at 11pm and finishing at 8am with their aggregate peak demand lasting from 1am to 6am. Figure 5.5 shows the aggregate EV demand during 48 hours applied in scenarios 1.3, 2.3, and 3.3. It is worth mentioning that if the penetration of electric vehicles is high, then the demand from electric vehicles will create another peak in the total demand of the power system. However, investigation

of more sophisticated control strategies to charge EV batteries is out of the scope of this project.

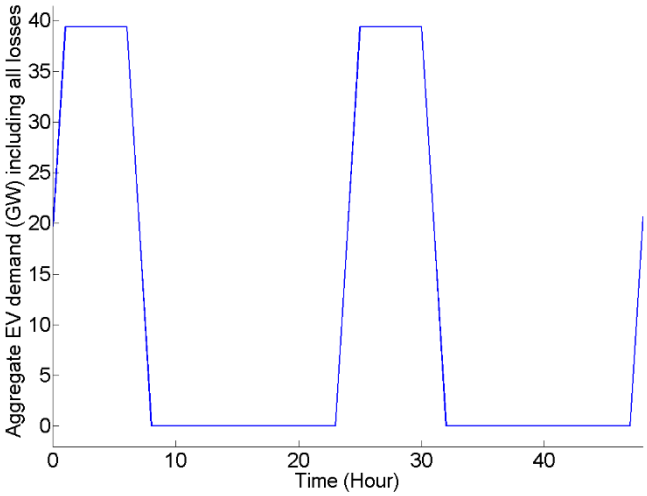

Figure 5.5 Aggregate EV charging demand during 48 hours in scenario 1.3

The surplus power ($Surplus(t)$ in GW) on the network before adding electrolysers to the system can be calculated from the following equation. The controller needs the amount of wind, solar and nuclear generation and non-electrolysis demand to calculate this surplus power.

$$Surplus(t) = P^t_{Wind} + P^t_{Solar} + P^t_{Nuclear} - D^t_N - D^t_{EVs} \quad (5.13)$$

Figure 5.6 shows this surplus power on the system in scenario 1.3. The '$Surplus$' value could become negative at some points, so the aggregate demand from electrolysers and compressors (D^t_{ElComp}), including the losses they add on the system, can be calculated using the following equation to make sure it has a non-negative value.

$$D^t_{ElComp} = \max(Surplus(t), 0) \quad (5.14)$$

This means that if '$Surplus(t)$' is positive then D^t_{ElComp} will be equal to '$Surplus(t)$', but if '$Surplus(t)$' is negative, then D^t_{ElComp} will be zero. In conditions when the surplus value is negative, the power from FFPPs should compensate the lack of power generation and supply some of the non-electrolysis demand on the system.

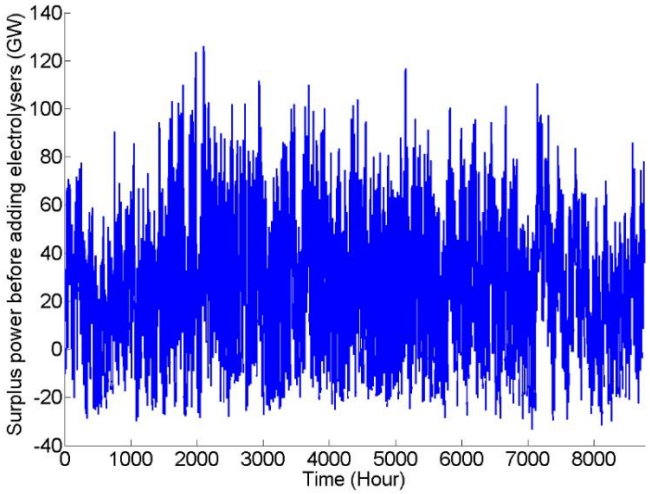

Figure 5.6 The surplus power before adding electrolysers in scenario 1.3

The aggregate electrolyser demand (D_{El}^{t} in GW) excluding the grid and compressor losses at each time interval can be found using the following equation.

$$D_{El}^{t} = D_{ElComp}^{t} * \eta_{grid} * (1 - \eta_{El}(1 - \eta_{Comp})) \quad (5.15)$$

Figure 5.7 shows the aggregate demand from electrolysers in Scenario 1.3. The maximum aggregate demand of the electrolysers during the simulation, which is equal to 110 GW in this scenario, can be used as the aggregate size of electrolysers ($S_{A.El}$ in GW).

$$S_{A.El} = Max(D_{El}^{t}) \quad (5.16)$$

The utilisation factor of electrolysers ($UF_{El}\%$) is defined as the amount of energy used divided by the maximum possible to be used by electrolysers and can be calculated using the following equation.

$$UF_{El}\% = \frac{100}{NDP * S_{A.El}} * \sum_{t=1}^{NDP} D_{El}^{t} \quad (5.17)$$

Where NDP is the number of data points in the simulation (24×365=8760).

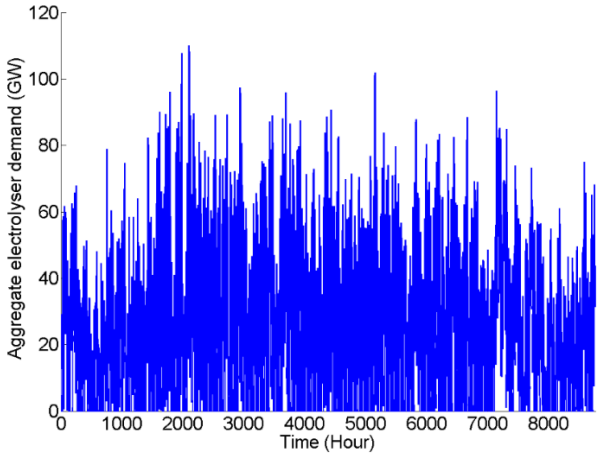

Figure 5.7 Aggregate demand from electrolysers in scenario 1.3

Figure 5.8 shows the remaining surplus power on the system after adding electrolysers in Scenario 1.3. This power is negative all the time, meaning that the FFPPs should provide it. It is worth repeating that, during the time that the surplus power is negative, all of the electrolysers are deactivated to avoid hydrogen production with the power generated by fossil fuels. The minimum value of the remaining surplus power (33.3 GW in Scenario 1.3), after subtracting the aggregate demand of electrolysers during the simulation, can represent the aggregate FFPP capacity needed to balance the system in each scenario.

Apparently, after applying the control strategy all of the positive surplus power has been absorbed by electrolysers, but when the surplus power goes negative, the FFPPs should compensate for its fluctuations. As explained in Chapter 4, such fluctuations are very costly for power system operators, and therefore this is considered as a deficiency in the control strategy used in this chapter in comparison to the control strategies proposed in Chapters 3 and 4. It is worth mentioning that some of these fluctuations can be compensated by importing electricity to the UK power system via international interconnectors.

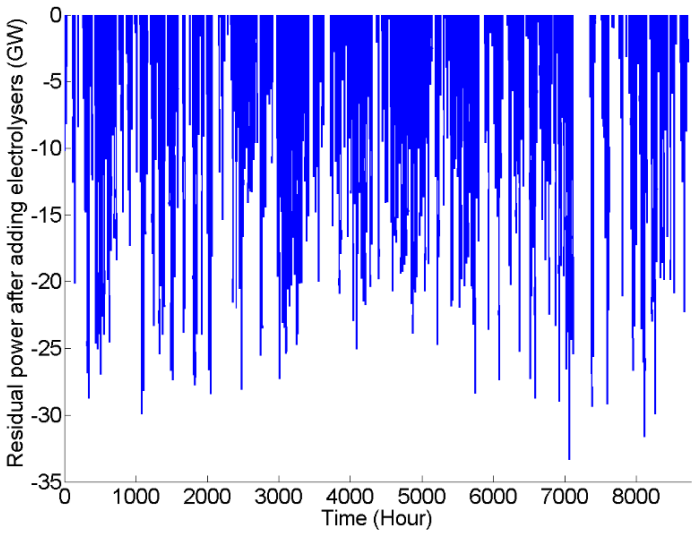

Figure 5.8 The remaining surplus power after adding electrolysers in scenario 1.3

The amount of hydrogen produced by electrolysers during the simulated year (YP_{H_2} in kg) in each scenario can be calculated from the following equation and might mismatch the total required hydrogen for all of the HFCVs.

$$YP_{H_2} = \frac{10^6 * \sum_{t=1}^{NDP} D_{El}^t}{E_{El}^{kg}} \quad (5.18)$$

The demand of individual electrolysers located at hydrogen filling stations are not calculated in the work reported in this section because different stations can have different sizes and different demand for hydrogen. It is assumed that the demand of individual stations can be found by another secondary algorithm that considers both the set-point for the aggregate demand of electrolysers on the power system, and also the amount of hydrogen needed for each station. Such secondary control strategy is not modelled here, in order to avoid unnecessary complication of the problem or using unreliable assumptions. That is why the variation of the efficiency that is due to changing the demand of each station is not considered here, and only a constant value for the efficiency of electrolysers is used in the simulations.

The amount of hydrogen consumption by HFCVs during the simulated year (YC_{H_2} in kg) can be calculated using the following equation.

$$YC_{H_2} = \kappa * DH_2 * 365 \quad (5.19)$$

It is assumed that the amount of hydrogen demand is constant all the time and is distributed evenly during the day. Each filling station should have enough storage capacity to store the excess hydrogen produced and they should hold enough initial hydrogen stored in the beginning of the simulated year to be able to satisfy hydrogen demand despite variable rate of hydrogen production. However, in this work, only the aggregate hydrogen storage capacity, the aggregate hydrogen stored in stations and the aggregate amount of initial hydrogen in storage are explored, because looking at individual stations needs more information about the hydrogen demand of each station.

To make sure that there is enough hydrogen stored within the system during the year to satisfy the hydrogen demand of HFCVs, a limit of 10% is used for the minimum amount of aggregate stored hydrogen. This means that the amount of hydrogen stored across the system will not become less than 10% of the maximum capacity of storage during the simulated year. To satisfy this goal and satisfy hydrogen demand at the same time, there should be enough hydrogen storage capacity and enough hydrogen in storage at the beginning of simulation. To make sure that there is always enough capacity to store all the hydrogen produced in the system, it is further assumed that the maximum aggregate amount of hydrogen in the storage during the simulated year never exceeds 90% of the maximum aggregate capacity of the storage across the UK.

Figure 5.9 shows the aggregate amount of hydrogen stored in all filling stations in Scenario 1.3 during the simulated year. During the first two months of the year the amount of surplus power on the system is not high enough to produce hydrogen for all HFCVs, so the aggregate amount of stored hydrogen in each filling station is decreased, and later on in the year the amount of hydrogen stored in the system increases. However, in the last month of the year, the average surplus power decreases again leading to a reduction in the amount of hydrogen in storage.

The simulation results show that the aggregate nominal hydrogen storage capacity needed for all filling stations is equal to 753 million kg. This is equal to an aggregate capacity of 20.1 million cubic meter, if the storage is going to take place in pressurised tanks of 400 bar. Using the data provided in Table 1.2 and considering the conversion rate of £1 = €1.35, the total capital cost of storage within the network will be 69.8 billion pounds in Scenario 1.3.

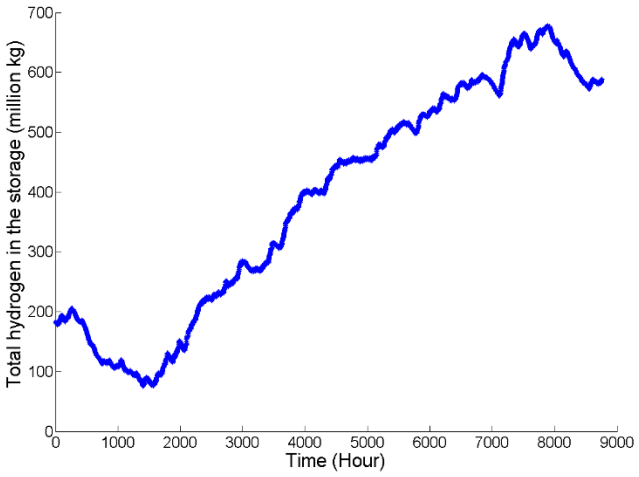

Figure 5.9 The aggregate amount of hydrogen stored in all filling stations in scenario 1.3 during the simulated year

The total excess amount of hydrogen produced during the year might be negative if there is not enough positive surplus power on the system. The percentage of the excess hydrogen produced during a year can be calculated from the following equation.

$$Excess_{H_2}\% = \frac{YP_{H_2} - YC_{H_2}}{YC_{H_2}} * 100 \qquad (5.20)$$

In Scenario 1.3, the amount of hydrogen production during the year is 10.5% more than the total amount of hydrogen consumption, so the level of hydrogen in the storage has increased in comparison to the initial aggregate value of stored hydrogen in the beginning of the year. This excess hydrogen could be used for different purposes other than transport or it could be exported to other countries. It could also be injected into the natural gas distribution system, so domestic consumers would be supplied with gas containing up to 12% hydrogen [127]. If there is lack of hydrogen production by electrolysers due to lack of surplus power, then the deficit can be provided by other methods of hydrogen production as explained in Chapter 1.

The simulation is run for the duration of a year with time resolution of an hour for different 2050 scenarios and the results are included in Table 5.5. Some of the variables used in this table, which have not been defined yet, are introduced below.

E_{Wind} is the total wind energy (TWh) delivered to the grid during the simulated year.

E_{Solar} is the total solar energy (TWh) delivered to the grid during the simulated year.

S_{FFPP} is the aggregate size of FFPPs (GW) needed to balance the system.

$UF_{FFPP}\%$ is the utilisation factor of aggregate FFPP capacity.

$S_{Storage}$ is the total size of hydrogen storage (million kg) needed in the UK.

$Cost_{Storage}$ is the cost of hydrogen storage in billion pounds. It is assumed that hydrogen is stored in pressurised tanks of 400 bar.

Table 5.5 Results of different scenarios for the whole year in 2050

Scenario	1.1	1.2	1.3	2.1	2.2	2.3	3.1	3.2	3.3
E_{Wind} (TWh)	231.2			346.8			381.4		
E_{Solar} (TWh)	69.8			69.8			89.8		
$S_{A.El}$ (GW)	110	110	110	140.7	140.7	140.7	128.4	128.4	128.4
$UF_{El}\%$	22.3%	29%	23.6%	24%	30.9%	26%	13%	15.1%	13.4%
S_{FFPP} (GW)	64.8	7.4	33.3	62.2	5.3	30.7	100.7	43.9	69.2
$UF_{FFPP}\%$	15.4%	0.3%	7.2%	11.9%	0.17%	4.6%	20.3%	12%	17.3%
$Excess_{H_2}$ (million kg)	3260	-1705	405	4781	182	2154	1964	-3758	-1023
$Excess_{H_2}\%$	422%	-24%	10.5%	619%	2.6%	55.8%	254.5%	-54%	-26%
$S_{Storage}$ (million kg)	4075	2133	753	5976	561	2695	2457	4698	1284
$Cost_{Storage}$ (billion £)	377	197	69.8	553.8	52	249.8	227.7	435.3	119

The aggregate size of electrolysers vary between 110 GW in the first scenarios to 140 GW in Scenario 2.1. Such massive increase in the nominal aggregate demand within the power system would need significant investment for the upgrade of the grid infrastructure.

The utilisation factor of electrolysers remained below 31% in all of the scenarios. The lowest utilisation factor, 13%, belongs the scenario with the biggest renewable power capacity, i.e. Scenario 3.1.

The aggregate size of FFPPs needed to balance the system in different scenarios vary significantly from 5.3 GW in Scenario 2.2 to 100.7 GW in Scenario 3.1. Therefore, the adoption of Scenario 3.1 will not only lead to the minimum utilisation factor of electrolysers, but it will also requires the biggest aggregate installation of FFPP capacity to balance the UK grid.

In most of the simulated scenarios, the hydrogen produced by electrolysers is more than enough to supply all of the HFCVs. Adoption of Scenario 2.1 will lead to the maximum excess hydrogen production of 619%, due to lower number of HFCVs and high volume of surplus power in this scenario. On the other hand, in Scenarios 1.2, 3.2 and 3.3, there is lack of hydrogen production for HFCVs. In such cases, some hydrogen could be imported from other countries or produced by other methods of hydrogen production to satisfy the deficit. In the worst case, which happens in Scenario 3.2, about 3758 million kg of hydrogen must be imported or produced from other resources to satisfy the yearly hydrogen demand for HFCVs.

The cost of storage also varies significantly from £52 billion in Scenario 2.2 to £553.8 billion in scenario 2.1. The cost and size of storage calculated in this work will be different if we also consider the import and export of hydrogen from/to stations due to the mismatch between the total hydrogen generated and consumed during a year at each station. Such scenarios are not simulated here as this requires much more information and assumptions about the timing and amount of hydrogen import/export from stations.

The results from Scenario 2.2 show that, despite the requirement for the biggest aggregate electrolyser size, the adoption of this scenario will lead to maximum utilisation factor for electrolysers, minimum aggregate size and utilisation factor of FFPPs, minimum size and cost of storage and the minimum positive amount and percentage for the excess produced hydrogen.

Figure 5.10 shows the remaining surplus power on the system after adding electrolysers in scenario 2.2. The 5.3 GW installed capacity of FFPPs in this scenario will be only used during a very limited number of time intervals just to balance the grid, resulting in very little of CO_2 emission within the UK electricity sector. The fact that all of the energy for the UK road transport was provided by clean energy in this scenario also leads to the conclusion that adoption of this scenario will lead to a full decarbonisation of the UK road transport sector.

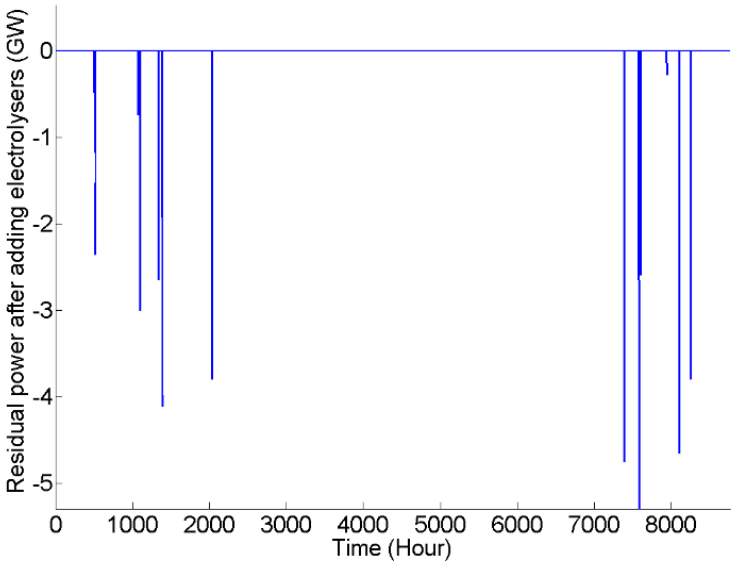

Figure 5.10 The remaining surplus power after adding electrolysers in scenario 2.2

5.4 Chapter summary

In the first part of this chapter, an extreme scenario is considered in which all of the vehicles on the road in the UK will be changed to HFCVs. The hydrogen needed to run those vehicles is assumed to be generated solely by electrolysers. In that case, all of the filling stations in the UK are assumed to be changed to hydrogen filling stations.

Many factors, such as daily hydrogen and total electrical power requirement, are identified through modelling. It was also found that 472 TWh of electrical energy is needed to satisfy that goal.

In the second part of the chapter, several scenarios with different penetrations of wind, solar, nuclear, EV and HFCVs have been modelled to determine the aggregate size of electrolysers, their utilisation factor and the size of hydrogen storage capacity needed as well as the amount of hydrogen they can provide for HFCVs in the UK in year 2050. The possible wind and solar power generation from different parts of the UK are used in the simulation to generate more realistic results. In addition, the size and utilisation factor of FFPPs needed in each scenario to balance the system are identified. It is found that about 110 to 140 GW of aggregate electrolysis capacity is needed to absorb the surplus power in the UK 2050 scenarios.

6 CONCLUSION AND PROPOSED FUTURE WORK

6.1 Conclusion

This chapter contains the conclusions that can be drawn from this research work. To satisfy the objectives of this PhD project, a comprehensive literature review was carried out and reported in Chapter 1 on the various topics related to the integration of alkaline electrolysers into power systems, and three main areas were identified and selected for investigation:

- Sizing, placing and controlling alkaline electrolysers within the radial distribution networks to increase the penetration of integrated wind power
- Utilisation of alkaline electrolysers to stabilize the frequency of the power system especially in existence of high volume of variable renewable power
- Investigation of the potential role of alkaline electrolysers to produce hydrogen for transport sector from the surplus carbon free power in the future UK power system scenarios

However, before moving towards the above objectives, it was necessary to obtain the characteristics of alkaline electrolysers needed in order to propose or tune appropriate control strategies for running them in power systems so as to improve the performance of both electrolyser and power systems, especially with a high penetration of renewable power generation.

Thus, a series of experiments over a range of different operational modes were designed by the author on a 24 kW pressurised alkaline electrolyser installed at the Porsgrunn Hydrogen filling station, and the results were analysed and reported in Chapter 2. In addition, the characteristics of a 2.1 MW atmospheric electrolyser made by NEL Hydrogen Company were detailed in the same chapter. A list of findings from the work in Chapter 2 is mentioned below:

- Alkaline electrolysers have a minimum operational load level to avoid an increase in their gas impurities at lower current densities. This minimum limit in atmospheric

units is 20% of their nominal power demand, and for the pressurised unit operating at Porsgrunn, the minimum load is proposed to be 18% of its nominal demand.

- The variability of the power demand of both types of alkaline electrolysers made by NEL Hydrogen does not degrade the lifetime or performance of the electrolyser due to the specific characteristics of the materials used in their electrodes.
- Large-scale 2 MW atmospheric units have a maximum acceptable rate of power change of 135 kW/min (2.25 kW/s) or 0.064 pu/min (0.0011 pu/s). The maximum rate of power change acceptable for the pressurised 24 kW unit is 18,480 kW/min (308 kW/s) or 770 pu/min (12.8 pu/s). Pressurised electrolysers have a far quicker load change rate, so they are more suitable for operation with variable sources of power, e.g. wind, and also for assisting with power system stability. Large-scale atmospheric alkaline electrolysers can service the grids, but they either have to be pressurised to get a good response time or have to be combined with smaller pressurised or PEM units, which are already available. Large-scale atmospheric plants could be controlled to follow general renewable power generation trends whilst the pressurised ones could be controlled to pick up the fast variations in renewable power and stabilise the frequency of the power system.
- Despite the fact that NEL hydrogen specifies the ramp rate of the pressurised electrolyser to be 12.8 pu/s, the experimental results on the 24 kW electrolyser only achieved a maximum ramp rate of 8.1 pu/s. In addition, the ramp rate was not constant all the time, varying with respect to the amount of change in the set point of the current. This variation in the ramp rate is due to the response of the rectifier in this rather small electrolyser; otherwise, the control system designed by NEL hydrogen only imposes the ramp rate of 12.8 pu/s on the pressurised units.
- The standby load of the pressurised unit is less than 1 kW/unit, regardless of the power rating. This loss in atmospheric units is 1.5 kW/unit, mainly due to the electricity consumption of their control system and circulation pumps.
- Atmospheric electrolysers can stay in standby mode as long as their lye temperature and gas quality are kept within acceptable limits, but pressurised units can stay in standby mode only up to 24 hours due to the decrease in pressure below their operational limit.

- While the stack is working within its operational range, its energy efficiency decreases with increasing its load. In other words, the electrolyser cell stack has higher energy efficiency at lower current densities. However, at very low current densities, the impurity of the output gases increases, and also depending on the size of electrolyser, the overall energy efficiency of the system might decrease as a result of the increase in the proportion of the BOP losses compared to the load of the cell stack.
- The atmospheric electrolysers made by NEL Hydrogen cannot be switched on/off more than three times a day due to the adverse impact of this switching on the lifetime of their electrodes. However, in the pressurised unit, the electrolyser could be switched on/off as much as needed without any degradation in its performance due to the novel material used in their electrodes.
- It takes 25 minutes to purge the system with nitrogen gas before the start-up and after the shut-down operation.
- Due to the time required to perform start-up and shut-down processes (about 35 minutes each), there is a limit of about 20 on/off cycles per day for pressurised units.
- The cell stack does not consume any power during the shutdown process, but the BOP does.
- It is also found that the rectifier in the pressurised electrolyser has an occasional extra response delay of 1015 ms in about 40% of the load change transitions which is most likely due to a flaw in its design, but cannot be investigated further in this study.
- Electrical harmonics at the grid connection point of the electrolyser were also measured and analysed in this study. The THD of the AC current signal is 70.2% which is very significant, and if there were many of these electrolysers connected to the power system, their aggregate impact on the voltage waveform might well be unacceptable.

Very highly pressurised alkaline electrolyser units have higher leakage, so they are not very efficient and suffer from safety issues. Therefore, it appears better if electrolysers are moderately pressurised, e.g. up to 18 bar, to have a better response rate. In addition, the load of a compressor, which is used after the electrolyser, will be reduced for such

pressurised systems because the compressor load depends on the ratio between its output and input pressures.

In addition, in a separate experiment, an 8 KVA PEM electrolyser located at Strathclyde University has been tested and it was found that it can start up within a minute and can ramp up with the speed of 8.75 pu/s. It is interesting to note that the ramp rate of the PEM electrolyser was about 30% slower than the nominal ramp rate of the pressurised alkaline unit. The standby loss of the PEM unit is found to be 0.54kW.

In Chapter 3, a simulation was carried out whereby alkaline electrolysers were used to increase wind generation capacity in an existing radial distribution network and maintain the system parameters within acceptable limits. A novel control strategy, based on an extended OPF, has been proposed to size, place and control these filling stations. The objective of optimisation process is to minimise the aggregate size of the stations, the total distribution energy loss on the grid and energy cost of stations, while maximising the profit gained from selling hydrogen. The performance of the strategy has been proved through simulation in *MATLAB* using a *UKGDS* case study. The control strategy was able to increase the network asset utilisation while considering the electrolyser characteristics.

Despite the fact that the initial size of stations were selected to be equal, the demand of different stations, which were determined by the optimisation process, were different and this resulted in different final sizes for each station. In the simulation, a fuel station might have a significantly lower demand in comparison to other stations due to its location during the simulation, meaning that its impact on the improvement of power system operation is very small.

Three cases were investigated in Chapter 3. In the first case study, which represented the main strategy used in Chapter 3, the initial size of filling stations were selected based on the strategy proposed in the chapter. The simulator was easily able to find the optimal solution, which resulted in completely satisfying the voltage and thermal limit constraints during one year simulation. The results did not show zero overload probability for only one of the location sets. However, the optimal location set was

able to fully satisfy grid constraint during the simulated year. Even for the location Set 5, which was not able to fully satisfy the overload constraints during a year, the overload probability was reduced significantly from 19% to 1.4%. However, the reduction of overload probability means that, if there is the possibility to curtail wind power, then it will still less often happen while using the proposed control strategy with location Set 5.

The energy flow from the network to the electrolysers caused a reduction of around 27% in the total energy loss of the distribution network for all of the location sets in the first case study during the one year simulation. Despite the fact that the electrolysers act as additional demand on the electrical network, they reduced the distribution losses significantly in this study. The reduction in distribution losses is due to the consumption of some of the surplus power generated by wind farms by electrolysers on the local feeder, instead of exporting all of the surplus power to other feeders.

In the second case study in Chapter 3, the size of wind farms was unchanged, but the initial size of fuel stations were increased by 50%. The optimal location set was found to be the same as the first case study but with a slightly better income of £298.3k instead of £260.7k during the one year simulation. However, the income for other location sets were lower than the income of their corresponding location set in the first case study. This means that, if the optimal location set is not available for construction of filling stations using this strategy, then the strategy used in the first case study would be preferred to find the best size of stations.

In addition, it is found that adopting the new initial sizing approach in the second case study can lead to large gaps between the optimum sizes of one hydrogen filling station compared with the other ones. This is not really preferable from practical point of view as it will cause placing one big station and another very small station on the network, and therefore they will have big differences in the amount of hydrogen they produce.

In the third case study, the size of wind farms was increased by 50%, and as a result, the initial size of fuel stations was increased according to Equation 3.1. Due to this change, as was expected, the amount of hydrogen production and the income also

increased significantly. However, the extended OPF strategy was not able to fully solve the overload and overvoltage problems during all of the time steps. In other words, the optimal location set with the best income did not have zero voltage and overload probability. However, for other non-optimal location sets, which have lower income, the voltage constraints were satisfied, but the overload probability reduced to 1%. This proves that, if we combine this control strategy with wind power curtailment schemes, then we would be able to increase the integrated wind power capacity within the system significantly by only curtailing the wind power during 1% of the time.

In Chapter 4, the impact of dynamically controlled electrolysers on the frequency stability of the power system was investigated in two cases of generation loss in the system and also in a case of high penetration of wind power in the system. A *MATLAB Simulink* model was developed to simulate the scenarios. Due to the faster response rate of pressurised alkaline units in comparison to the governor controllers of the thermal power plants, it was already expected to find improvement in the frequency fluctuation of the power system while using such units with a simple droop control strategy. However, the work presented here aimed to quantify the amount of reduction in the power system frequency fluctuation and spinning reserve due to utilisation of pressurised alkaline electrolysers while considering the actual characteristics of such units obtained in Chapter 2. In addition, a new approach is proposed to find the aggregate nominal demand of electrolysers within the power system to maintain the frequency of the power system within operational limits.

It is shown through simulation results that pressurised alkaline electrolysers can help maintain the network frequency within operational limits by reducing their load as a function of the frequency deviation after the generation loss event even in the case that there is no spinning reserve on the system. On the other hand, the system without dynamically controlled electrolysers could not keep its frequency within operational or statutory limits after a significant generation loss of 0.15 pu, despite the fact that it had enough spinning reserve to deal with the generation loss.

In the second case, a *MATLAB* Simulink model of an electrical power system, comprising steam turbine generation units, electrolysers, conventional loads and wind farms was developed to investigate the impact of alkaline electrolysers as dynamically

controlled loads for stabilisation of system frequency in the case of 25% penetrations of wind power. Unlike the FCDM scheme, in the scenario suggested in this work the power is never disconnected from the electrolysers, and only the loads of electrolysers change with respect to the frequency deviation in the system. The simulation results show that alkaline electrolysers can help maintain network frequency within operational limits by changing their load as a function of deviation of the power system frequency from its nominal level. The standard deviation of the frequency and the aggregate output power from the thermal generators of the system without DSM was about 4.1 and 3.1 times higher than that of the system with DSM, respectively. This means that the utilisation of these electrolysers as dynamic loads can smooth the output power fluctuations from the thermal generators and will result in a reduced need for maintenance of the generation units that are involved in this service provision.

Used in this way as dynamic demand, electrolysers can also help in the reduction of spinning reserve levels required in the electrical power system. For the case examined, five times less spinning reserve is required in order to maintain the power system frequency within operational limits when electrolysers are utilised as a form of demand side management (DSM), compared to the base case where no electrolyser DSM plant is available.

As long as there is enough hydrogen stored to meet the demand at each filling station, there would not be any additional cost or risk for the electrolyser operators to participate in this sort of dynamic demand scheme. The financial viability of using the droop control strategy to run electrolysers is also assessed, and it was shown that, by oversizing the electrolysers installed at filling stations, it would be possible to involve the electrolysers in frequency stability schemes with a droop control strategy and increase the profit gained by the electrolyser operators.

The aggregate size of electrolysers in Chapter 4 was selected to make sure that the frequency of the system remains within operational limits during the whole simulation period. The selected aggregate nominal demand of stations were selected to be 23 GW to maintain the frequency of system within operational limits with an aggregate wind power capacity of 29.5 GW in the context of the UK power system. This shows that if electrolysers were the only dynamic demands to help in frequency stability of power

system, then a significant aggregate electrolysis capacity would have been needed to achieve such goal. However, it is expected that if the smoothing effect of wind farms located at different locations were considered, then the aggregate electrolysis capacity needed would have been lower than the value identified in this work.

In all of the simulation results in Chapter 4, the aggregate load change of the electrolysers in each station remained well below the acceptable limit, meaning that the electrolysers currently available on the market can easily operate with such control strategies.

In this way the electrolysers can reduce carbon dioxide emissions as follows:

- More intermittent renewable power can be added to the electrical power system, facilitating further decarbonisation.
- The hydrogen produced by electrolysers can be used in HFCVs helping in the decarbonisation of the transportation sector.
- Reduction of spinning reserve will directly reduce carbon dioxide emissions caused by the part loading of the fossil fuelled conventional plant involved.

Associated with these changes, there will of course be economic benefits for the power system operator because of the reduced need to purchase conventional frequency response services and also due to the reduction in the amount of spinning reserve on the system.

In Chapter 5, the amount of hydrogen needed to support all of the energy needed for the whole UK road transport is calculated, and then several scenarios were investigated to find the potential role and impact of electrolysers while absorbing the surplus clean power in the UK power system in 2050.

It is found that, on average, a daily amount of 21.1 million kg of hydrogen is needed to provide all the vehicles on road with hydrogen if all were to be converted to HFCVs. In such an extreme scenario, there would be a requirement for 53.9 GW continuous power generation in the UK power system to produce the hydrogen needed for HFCVs using electrolysers in the UK. This will amount to 472 TWh of electrical energy, which is 126% more than the UK energy consumption in 2011.

In nine different 2050 scenarios, hydrogen was assumed to be produced from surplus power on the system using alkaline electrolysers after supplying normal demand and charging electric vehicles.

It was found that the aggregate size of electrolysers to absorb all of the surplus power in UK 2050 scenarios is in the range of 110 GW to 140 GW, so a significant grid upgrade would be needed to accommodate such demand in the UK power system.

In most of the simulated scenarios, there was an excess amount of hydrogen production. Especially, in EV dominated scenarios, the amount of excess hydrogen production was much higher than other scenarios, e.g. it reached 619% in scenario 2.1. The excess hydrogen produced within the system could be used for other purposes rather than as fuel for HFCVs or it could be exported to other countries. On the other hand, in Scenarios 1.2, 3.2 and 3.3 there was lack of hydrogen production. The worst hydrogen deficit case belongs to Scenario 3.2, which is a HFCV dominated scenario, with a 54% hydrogen deficit. In such cases, the rest of the hydrogen needed for HFCVs can be provided by other methods of hydrogen production or by importing hydrogen from other countries.

One of the problems associated with the control strategy used in Chapter 5 is the low utilisation factor of electrolysers, which was below 31% in all of the scenarios. In Scenarios 3.1, 3.2 and 3.3, which have significantly more integrated variable renewable power, the electrolyser utilisation factors were much lower, in the vicinity of 13-15%. One might think that these low utilisation factors might not justify the use of electrolysers with such control strategies, due to the high capital costs of these units. However, these units use the surplus power within the system, which would otherwise be curtailed due to lack of electric demand on the system. Therefore, there is a high chance that the electrolysers working with such control strategies could work with very cheap electricity compensating for their high capital costs.

Despite utilising electrolysers for absorbing the surplus generation, there is a need in all of the scenarios to use fossil fuel power plants to address the power deficit when the carbon-free power generators are not even capable of supplying non-electrolysis demand. The aggregate capacity of FFPPs that is needed to supply the system in the

case of lower renewable power generation varies significantly in different scenarios. Adoption of Scenario 3.1 would lead to the biggest aggregate size of 100.7 GW in the UK power system for FFPPs with a utilisation factor of only 20.3%. This means that high penetration of EVs that are being charged during off-peak times without any sophisticated control strategy while the system has a high penetration of variable renewable power, can lead to a requirement for high capacity of FFPPs with relatively low utilisation factor, even when electrolysers absorb the surplus power within the system.

In addition, the utilisation factor of FFPPs is below 21% in all of the scenarios in Chapter 5, which demonstrates a drawback of the proposed control strategy in comparison to the control strategies proposed in Chapter 3 and 4, where the smoothness of the residual surplus renewable power injected to the grid can help in increasing the utilisation factor of the FFPPs.

The maximum cost of storage in pressurised tanks of 400 bar was found in Scenario 2.1, where the lack of hydrogen consumption pushed its cost up to £553.8 billion. However, if the UK exports its excess electricity or hydrogen, then such a requirement for hydrogen storage and costs would reduce accordingly. The high capital cost of hydrogen storage in pressurised tanks in most of the scenarios means that significant research and development should be carried out on novel hydrogen storage technologies (some of them are summarised in Section 1.3 and [20]) to make such scenarios more realistic for a low-carbon future.

The most interesting results in Chapter 5 come from Scenario 2.2, which is a HFCV dominated case with the following outcomes:

- The largest requirement for aggregate size of electrolyser (140.7 GW), which would lead to maximum investment for electrolyser capital, operational and maintenance costs.
- The maximum utilisation factor for electrolysers, 30.9%, which would lead to the maximum profit percentage from hydrogen production by electrolysers.
- The minimum aggregate size for FFPPs (5.3 GW).

- The minimum utilisation factor of FFPPs (0.17%), leading to minimum of CO2 emissions in the electricity generation sector.
- The minimum size and cost of storage, which are 561 million kg and £52 billion, respectively.
- The minimum percentage for the excess hydrogen produced within the network (2.6%).

Therefore, adoption of Scenario 2.2 would almost lead to total decarbonisation of transport and electricity sectors with minimum effort to invest on FFPPs or hydrogen storage capacity.

As demonstrated in this work, there are different ways to use alkaline electrolysers within the future UK power system, and each of them has its own advantages. At this stage, it is not still clear which control strategies will be adopted in future; however, it is expected that the future power system will use a mixture of different control strategies to dispatch dynamic demands and storage devices to ensure the quality and security of the supply for consumers while attempting to meet carbon emission targets.

As the number of time varying renewable power generators in the electrical power system increases, utilisation of demand side management tools becomes more important. Electrolysers are more attractive than other sorts of demand side management, e.g. heat pumps or refrigerators, which have very limited availability and cannot help in the decarbonisation of the transportation sector in the way electrolysers and HFCVs can. Electrolysers can produce clean fuel for future transportation needs and, at the same time, be used as dynamic load to improve the performance of power system while absorbing the additional power generated by variable renewable resources. Such electrolysers can provide long-term energy storage and provide load control on a short-term basis. Should hydrogen be accepted as a widespread fuel, then a significant production, storage and distribution infrastructure needs to be created.

6.2 Proposed future work

There are some areas of interest related to this work that could be investigated in future work by other researchers. In this section, some recommendations are provided for such future work.

It is recommended that a multi-objective optimisation analysis should be carried out to find the best way to run the electrolysers in the power system to maximise the economic and environmental benefits from operation of electrolysers in power systems, and the following factors should be considered from both the electrolysers' and grid's point of view to achieve such targets.

1. Dynamic pricing of electricity should be considered.
2. The location of electrolysers on the power system should be determined based on the potential location of future hydrogen filling stations while considering the other optimisation targets to minimise whole system costs.
3. The size of electrolysers should be minimised to avoid additional capital cost.
4. The cost of infrastructure for the power system to accommodate electrolyser and renewable power generators should be considered in any analysis.
5. The future hydrogen demand from fuel cells or fuel cell vehicles should be determined. It should be noted that the adoption of fuel cell vehicles depends on many factors, such as the price and availability of these cars and hydrogen filling stations, government policies, social acceptability, etc.
6. Storage capacity should be minimised while satisfying the hydrogen demand. In any scenario, the hydrogen stored in the system should stay within the acceptable limits of the storage capacity.
7. Capital, operation and maintenance costs of electrolysers, storage systems, filling stations and fuel cell vehicles should be considered in any economic analysis.
8. The profit from selling oxygen produced by electrolysers can be considered. However, this could turn out to be too marginal while considering the cost of its storage and transport.
9. The economic and environmental benefits from reduction of carbon dioxide emissions in both electricity and transport sectors should be considered.

10. Reduction in maintenance costs of thermal generators as a result of smoothness of their output power due to utilisation of electrolysers could be considered in the analysis.
11. The characteristics of electrolysers explained in Chapter 2 should be considered in the design of any control strategy.
12. The control strategy should be designed in a way that the efficiency of electrolysers would be maximised.
13. Renewable and nuclear power generation data for the future UK power system, e.g. 2050, with a realistic penetrations, should be considered.
14. Any feasibility study of such systems should ideally be based on more than a single year of wind speed or solar power data because a single year analysis might give too optimistic or pessimistic results when compared with long-term data.
15. Curtailment of variable renewable power should be minimised.
16. Cost of generation from controllable power plants could be considered in the optimisation process to find the best control strategy.
17. The control strategy can include measures to stabilise the frequency of the grid and keep it within operational limits. However, other types of storage devices that can provide such services should also be included in any optimisation analysis.
18. Voltages and currents in different nodes and branches of the power system should stay within acceptable limits.
19. Transmission and distribution losses of the power system should be optimised.
20. Costs of import and profits from export of power to/from neighbouring networks could be considered in the simulations.
21. The variation of other controllable or non-controllable demands, the impact of other storage devices, the variation of power from other generation units due to their start/stop process and also the variation in the import and export of power can also be considered.
22. Different mixtures of renewable and nuclear power generation, including wind, solar, nuclear, wave and tidal generators, can be considered.
23. The amount of hydrogen production from other methods should be considered.

A number of cost or profit functions could be defined by considering the above factors to determine the best size and location for electrolysers and storage or the best control strategy to run the system. Such multi-objective optimisation analysis has not been carried out in this work because it is beyond the scope of this PhD project.

It is proposed that other types of storage devices, detailed in Chapter 1, could be considered in a techno-economic analysis that considers the characteristics and costs of all of storage types to find their size location, and demand or generation in a 2050 scenario.

In addition, in an ideal case a full techno economic analysis should be carried out to find the best mixture of different storage technologies to address the problems on the power system created to adding variable renewable power.

As was found in Chapter 2, the ramp rate of the electrolyser varies dynamically depending on the response of the rectifier. A detailed modelling of the electrolyser's rectifier is required to represent an accurate model of the system.

In Chapter 3, the main strategy to operate electrolysis filling stations is purely designed by considering network optimisation results, while looking at the system from DNO perspective. Otherwise, if the owner of the system is not the DNO, then one station might have low hydrogen production and the other ones can have higher hydrogen production. In such case, where the owners of the hydrogen filling stations and the DNO are different parties, the requirement of different players should be considered while designing the control strategy to run electrolyser. Such scenarios might lead to defining different tariffs for different filling stations on the network.

In addition, the work in Chapter 3 can also include the cases that due to a significant demand for hydrogen or integration of large wind farms, avoiding the grid reinforcement would be impractical. In such cases, a part of the problem could be solved by reinforcing the grid.

Due to the limitation of the computational capability of the personal computer used by the author, the analyses in Chapter 4 were carried out only for the duration of one hour. Ideally, it is recommended that such power system analysis should be carried out for

duration of one year to find out the best sizing for the electrolyser and the best control strategy to run them and to be able to generalise the simulation results with more reliability. If the average amount of wind power is very low during some time periods, then some of the electrolysers could be switched off to avoid the operation of electrolysers with non-renewable power. In such analysis, the impact of seasonal storage on the control strategy could also be investigated. In addition, it is recommended that the variability of average wind power over a number of years should be considered to validate the conclusions.

The power system model used in Chapter 4 is based on a simple model of one generation unit, and it has not been verified by real data from a real system yet. The real dynamic response of the UK electricity network is much more complicated than the case considered in this work. To have a better understanding of the power system dynamics, it is recommended to use more detailed data from the UK power system generation units to simulate more representative future scenarios. It is recommended to choose the size of the system based on the size of UK power network and future penetration of variable renewable power and fuel cell vehicles in the UK at the same future date. In addition, it was assumed that all of the non-renewable generation units are from the same steam turbine units. This assumption could be changed by considering other sorts of generation units.

The cost of connection of electrolysers to the power network has not been explored in this work. Such cost analysis, in future work, should include location, local connection possibilities and the amount of investment needed for such infrastructure [19].

Adding wind power forecasts in control strategies to run electrolysers or fuel cells, if used in the system, can improve the performance of the power system. A day-ahead weather forecast can also help in optimisation of the control strategy to run electrolysers or to export power in grid-connected renewable hydrogen systems [11].

To calculate the size and cost of storage in each hydrogen refuelling station, a number of factors need to be determined or analysed for a long duration of time, e.g. one year, and those factors are listed below.

- The average number of vehicles using each specific refuelling station and their average fuel consumption.
- The type of hydrogen storage technology utilised at each refuelling station.
- The size and the efficiency of the electrolyser used at each site.
- The amount of hydrogen production at each refuelling station, based on the aggregate intermittent renewable power and total demand profile and the control strategy used to run electrolysers at each time step.
- The pressure of storage tanks if gaseous hydrogen is stored in pressurised tanks.

In this work, the electrolysers are assumed to operate in future hydrogen filling stations. 2050 has been adopted as the reference year to allow time for the creation of the new infrastructure and to allow all vehicles to be replaced by HFCVs. The energy mix of the UK's electrical network in that time is hard to predict, so it is not possible to give a precise value for the amount of carbon dioxide emissions for the production of one kilogram of hydrogen by electrolysers using the electricity from the UK power system at that time in the future. However, to have a reasonable estimation of the economic and environmental benefits of hydrogen production by electrolysers, this factor should be considered. It is worth mentioning that if the hydrogen is produced from surplus carbon-free power, as assumed in Chapter 5, then the carbon intensity of hydrogen produced would be equal to zero.

A detailed model of compression units, which shows the variability in the compressor load, could be used in the future work. Some of the factors that can affect the power consumption of a compression unit are listed below.

- Initial pressure from output of the electrolyser and the target output pressure of the compression unit.
- Size of gas holder (buffer tank).
- Demand of electrolyser and its hydrogen production rate.

In a power system in which many electrolysers of different types (pressurised or atmospheric, alkaline units or PEM) are operating together, the PEM or pressurised alkaline units can respond to fast variation in wind power and the atmospheric ones

can respond to the general trend of wind power. Some of the electrolysers could also be switched off during low wind periods. Such scenarios could also be investigated in the future power system, but at the beginning of such analysis, the aggregate nominal demand from each type of electrolyser should be determined.

In the work in Chapter 4 and 5, it is assumed that the network has the appropriate infrastructure to accept the power from wind farms and to supply electrolysers. Power systems need to be designed specifically to deal with high wind penetrations, both to minimise curtailment of wind and to maintain overall reliability of the power system. In the longer term, European policy leaders have expressed a desire for greater sharing of the renewable energy potential across the continent to contribute to the collective meeting of carbon reduction targets. This would require investment in new interconnectors, many of which would be highly capital intensive undersea links [93]. The network infrastructure capacity should be sufficient for the export of power in areas where wind generation is dominant at times of high wind speeds and the import of power when wind speeds are low. To gain regulatory support for reinforcement investment and any associated planning permissions, a robust technical case must be made by the system developers.

The author has tried to address all of the aims of this PhD project during his studies; however, there are many other areas of interest that are related to this work. Some of them are listed in this section, but they are not limited to the topics mentioned here.

7 APPENDICES

7.1 Hydrogenics experiment on the performance of their alkaline electrolyser

Hydrogenics Company carried out an experiment on the performance of one of their alkaline electrolysers by switching it on/off continuously for a long period of time. Figure 7.1 shows the average voltage of half of their electrolyser cell stack during experiment.

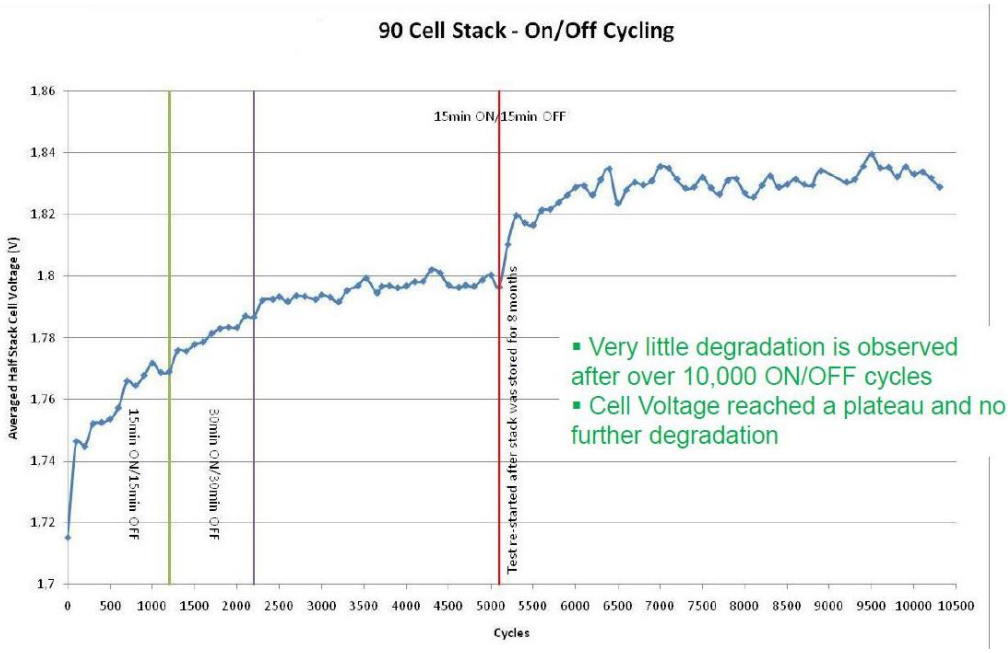

Figure 7.1 The effect of On/Off switching on the voltage of an alkaline electrolyser made by Hydrogenics [128]

They switched the electrolyser 1,200 times with a switching period of 15 minutes. They then continued the experiment with a switching period of 30 minutes for 1,000 cycles. For the rest of the experiment a switching period of 15 minutes was used; however, after 5,100 times of switching, the stack was stored for eight months, and the experiment was continued with an on/off switching period of 15 minutes. The figure shows that the voltage of the stack was increasing until the system experienced 6,000 switching operations, and after that point, no further degradation was observed. Hydrogenics claims that, even the degradation before this point (6,000 cycles), was not as a result of on/off switching, and it happens to the electrolyser as a result of aging

even without on/off cycles. The voltage rise due to corrosion of electrodes was gradually stabilised after 6,000 times of switching. However, the degradation continued at a very slow rate. From the result of this experiment, they have concluded that the performance of their electrolyser does not degrade as the result of On/Off switching or variability of its load due to the characteristics of novel materials used in their electrodes.

7.2 How to obtain the polarization curve of an alkaline electrolyser

It is possible to obtain a graph showing the relationship between the voltage and the current of an alkaline electrolysis cell stack by conducting a polarisation curve experiment at a specific temperature and pressure. The current of the stack should be increased or decreased step by step and the voltage of the stack should be recorded while the system keeps the pressure and temperature constant. The polarization curve can also be depicted by showing the relationship between the current and the power of the electrolyser cell stack [8].

7.3 The visit to Rjukan-EKA chemicals

On Thursday, 27th of October 2011, the author visited the Rjukan-EKA chemicals company where 4 units of 2.1 MW electrolysis plants made by NEL Hydrogen were operating. The company uses both hydrogen and oxygen from the electrolysis process to produce hydrogen-peroxide. The electricity is not very expensive in Norway (€0.097/kWh in 2013 [129]), so it is still beneficial to produce the hydrogen and oxygen onsite by electrolysis rather than buying it from other sources. Figure 7.2 shows these large scale (2.1 MW) alkaline electrolysers with their separation tanks.

The plants has been working for 9 years continuously with almost constant load. They only shut down the electrolyser for maintenance, e.g. for changing the system lye (i.e. KOH) every two years. The whole factory consumes 10-11 MW of electricity. The input voltage of the electrolyser transformer is 21 kV. The electrolyser rectifier has 3

phase input with nominal frequency of 50 Hz. The input rating of the AC voltage of the rectifier is 376 V, and its AC current input rating is 4800 A. The DC output voltage of the rectifier can change between 0-461 V, and its DC output current can change between 0 and 6,000A. The nominal DC voltage of the electrolyser stack is 450 V with the nominal DC current of 5,170 A.

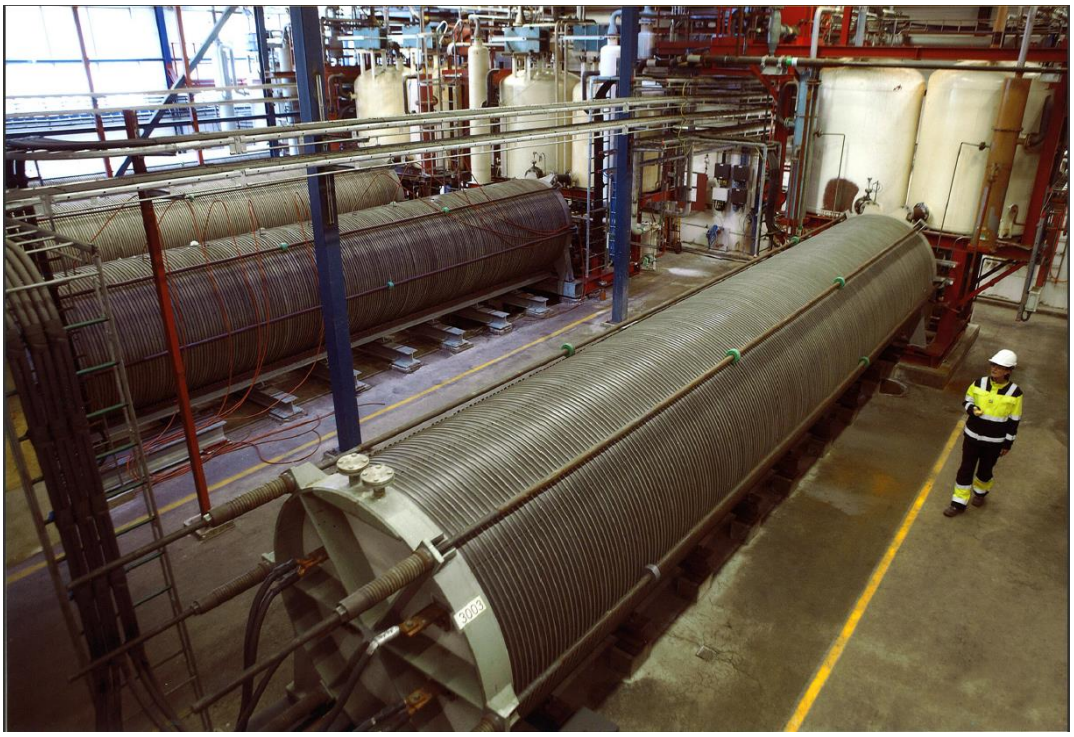

Figure 7.2 Large scale (2.1 MW) alkaline electrolysers with their separation tanks

During the visit, the electrolyser had these operating parameters:

- Working with 74.4% of operation capacity (74.4% of the nominal load)
- Hydrogen production rate: 344 Nm^3/h
- The current set-point: 3,602A
- DC current 3,600A
- DC voltage: 368.5V
- Total load:1,328 kW
- Impurity of oxygen in hydrogen: 0.05%
- Impurity of hydrogen in oxygen: 0.41%

There was a significant amount of heat coming from the electrolyser during its operation, which is dissipated to the open air. However, the company was planning to use the heat from the electrolyser to provide heat energy for the buildings around the factory.

The Uninterruptible Power Supply (UPS) system in the factory had many unexpected shut-down problems, which were probably due to the excess harmonics injected to the grid by the rectifiers in the system, but there was not any reported problem or complaint from the electrical power supplier regarding this harmonic issue.

7.4 Design of a system to inject variable power to an alkaline electrolyser using a PID controller

A power supply system has been designed to provide an open cell Alkaline electrolysis system with a variable power profile (such as a scaled-down version of an actual wind power profile) to investigate the impact of variation of electrolyser demand on the performance of electrodes over a long period of time. This system uses a LabVIEW based program that has a PID controller to control the load of the cell. A data acquisition system has also been designed to measure the cell physical parameters, like voltage, current and temperature, automatically. This data is used to find out the voltage efficiency of the cell.

If the electrolyser has a current controlled rectifier, and the operator decides to adjust the electrolyser load, then the control system should use the polarisation curve of the stack to calculate the corresponding current that makes the electrolyser absorb that specific amount of power, but if the operator uses a PID controller to directly control the load of the stack, then there would not be any need to use the I/V curve of the electrolyser to calculate the current to be injected into the electrolyser to absorb the required amount of power. This is an advantage of systems with direct input power control from a PID controller over systems with current controllers.

7.4.1 Details of the system used in the experiment

An open cell alkaline electrolyser was used in the experiment because we did not have a proper alkaline electrolyser available in our lab. The separation gap between the two electrodes was 8 mm. Nickel mesh was used as the cathode and anode electrodes for the open cell electrolyser. The active area of the mesh electrode was 7.56 cm^2. A Celgard 5550 membrane (25µm Micro porous Monolayer polypropylene membrane) was used to separate the oxygen and hydrogen sides of the electrolysis cell. KOH solution with mass concentration of 30% was used in the experiment. Figure 7.3 shows the overall view of the system designed to control the electrolyser load.

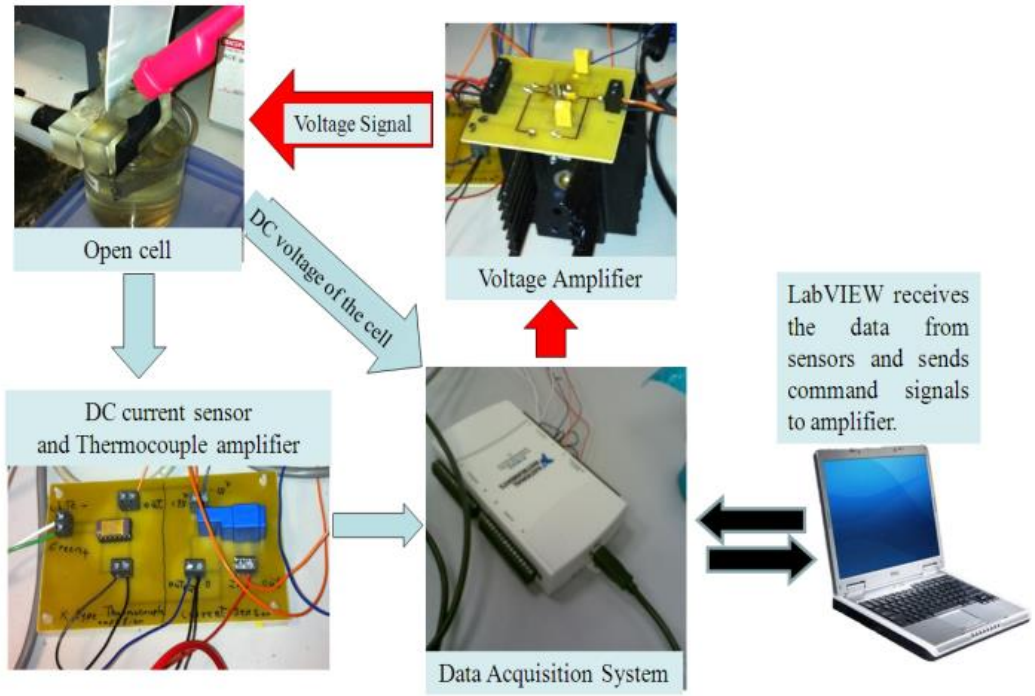

Figure 7.3 The overall view of the designed control and measurement system

A voltage amplifier with a gain of 20 was used to amplify the command signal from the data acquisition device and give the appropriate power to the open cell. This voltage amplifier is made of an OPA548 op-amp that is able to deliver continuous current of 3A for a steady-state condition. A current sensor (HY5P from LEM Company) was used to measure the current of the cell. A k-type thermocouple was also used to measure the temperature of the cell. A thermocouple amplifier (AD595CQ) was used to compensate for the cold junction of the thermocouple and

also to amplify the voltage from the thermocouple. Two power sources were used to supply the sensors and the amplifier respectively. A data acquisition device (USB NI6218) from National Instrument was used for the experiments.

A PID controller was designed in the LabVIEW environment to control the load of the electrolyser. The sampling frequency of the data acquisition system was set to 1 kHz, and the PID controller was also calculating its control signal with the same speed. Three analogue input ports of the data acquisition device were used to measure voltage, current and the temperature of the cell. One output port of the data acquisition device was used to give the control signal generated by the PID controller to the voltage amplifier.

Figure 7.4 shows the schematic of the control and measurement system. The PID controller uses a scaled down version of the wind power profile as a reference signal for its operation. The input of the PID controller is an error signal which is equal to the difference between the reference signal and the actual load of the cell.

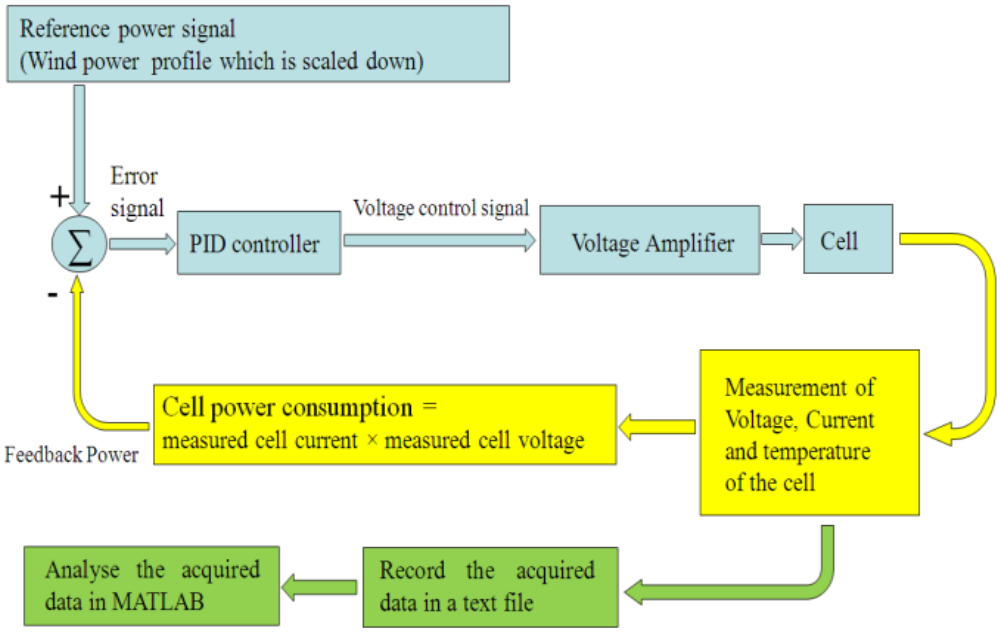

Figure 7.4 The schematic of the control and measurement system

The output of the PID controller is a control signal applied to the input of the voltage amplifier through an analogue output port of the *USB NI6218*. The coefficients of the PID controller were selected in a way that the system would remain stable and also the

load of the electrolyser would follow the power output of the wind turbine with an acceptable rise and settling time. The data collected from the data acquisition device was stored in a text file and analysed in the *MATLAB* environment using an m-file.

The wind data used in the system had a resolution of ten seconds and was taken from an actual wind farm located in China. The rated power of this wind turbine was 1.5MW. Figure 7.5 shows the original power of the wind turbine used in the experiment which lasted for five minutes.

This wind power profile is scaled down to become suitable for the small scale electrolyser. The nominal load of this small scale electrolyser is selected to be 2 W. This limitation was applied to prevent the voltage amplifier overheating.

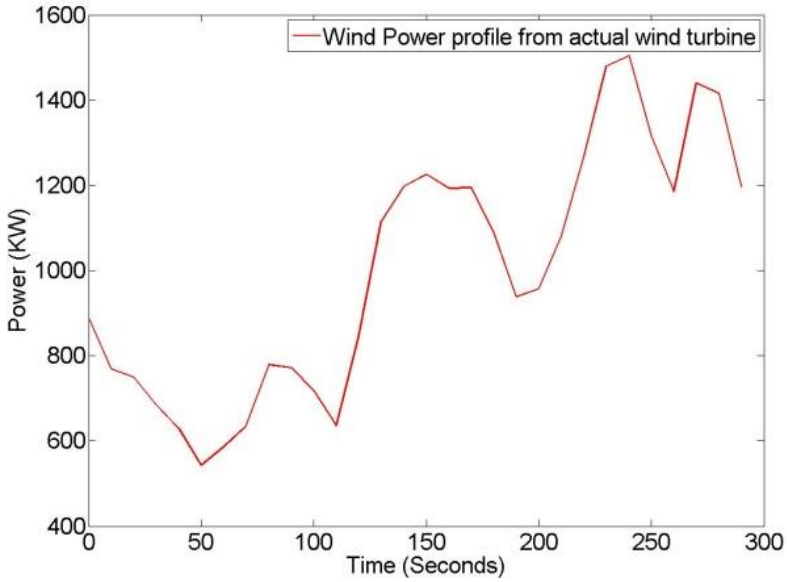

Figure 7.5 The original power of wind farm used during the five minute experiment

7.4.2 Results of the experiment and discussions

Figure 7.6 shows the voltage of the cell during the experiment of supplying the electrolyser with a variable wind power profile. The cell voltage changed between 2.27 to 2.67 Volts. It is clear that the voltage of the cell changed in a way that enabled the electrolyser to absorb the available wind power.

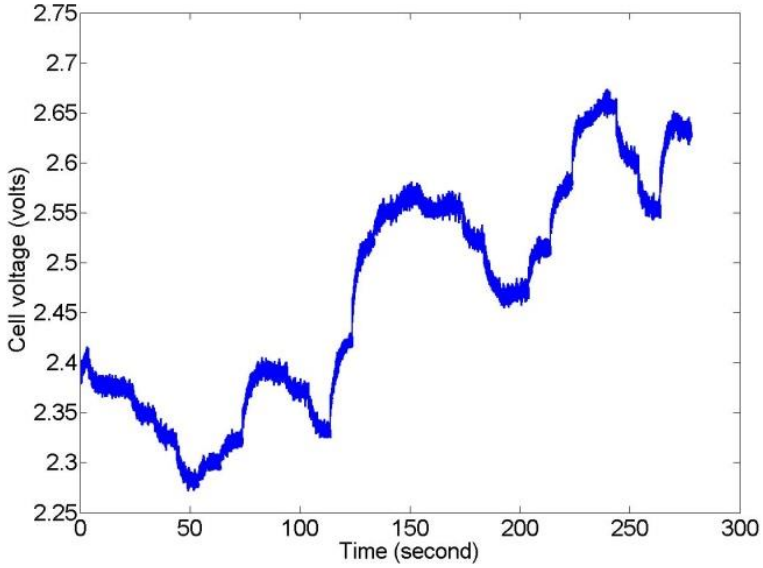

Figure 7.6 Voltage of the open cell during the experiment

Figure 7.7 shows the load of the cell compared to the scaled down power from the wind turbine. The electrolyser load was able to follow the power output of the wind turbine with an acceptable accuracy.

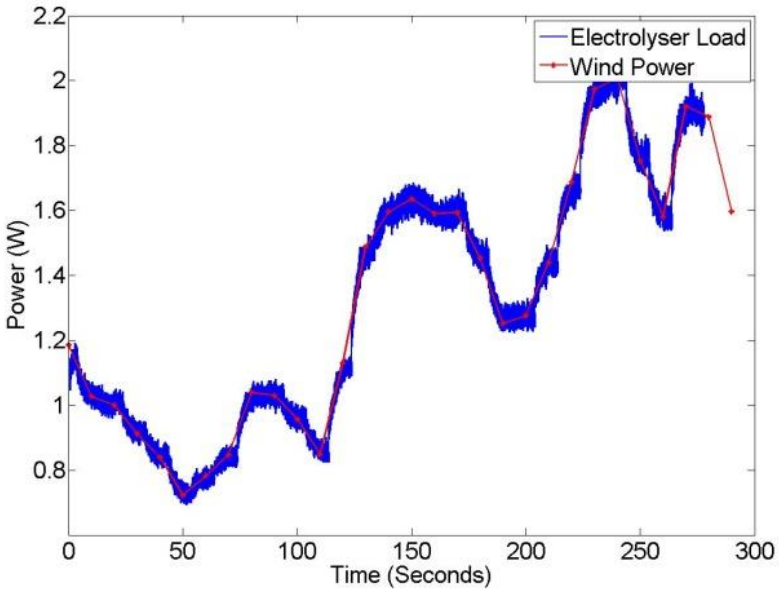

Figure 7.7 The load of the cell and the scaled down power output of the wind turbine during the experiment

It is worth mentioning that, in this case, the reference input signal of the PID controller was set to a value equal to the scaled down value of the power from the wind turbine. However, in general, it is possible to set this reference point equal to any value that the electrolyser is going to absorb as input power and the rest of the power from wind farm could be used by other loads in the grid. In other words, it is possible to give the electrolyser just the excess wind power that is not used by the other demands in the power system.

Equation 2.3 was used to find the voltage efficiency of the cell during the experiment. Figure 7.8 shows the voltage efficiency of the cell, which was 55-65% during the experiment.

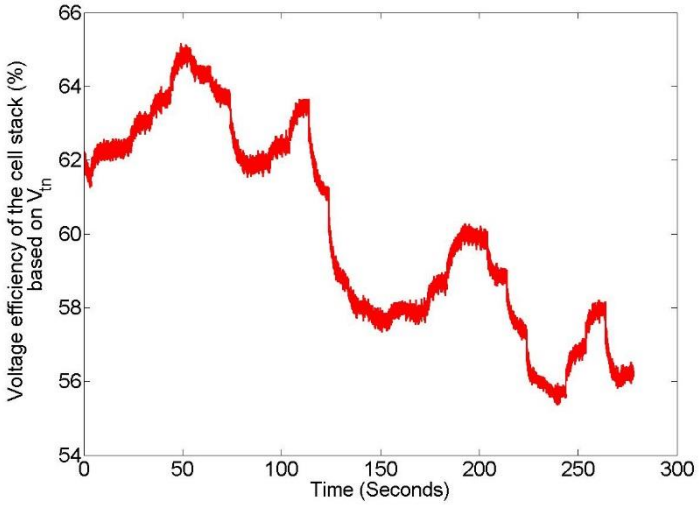

Figure 7.8 The voltage efficiency of the open cell during the experiment

Figure 7.9 shows the predicted voltage efficiency of the cell with respect to the load of the electrolyser. The efficiency of the cell was decreasing as the load of the cell increased from 0.72 W to 2.1 W.

During the test, the efficiency of the cell was not very good because no catalyst was used for the electrodes, and also the cell did not have a zero-gap configuration. In addition, the experiment was carried out in low room temperature of 23°C, which reduced the voltage efficiency noticeably.

As demonstrated in this experiment, it is not necessary to know the internal model (e.g. VI curve) of electrolyser to inject a specific amount of power to the cell stack. The electrolyser designers can simply use a PID controller to change the load of electrolyser with an acceptable precision.

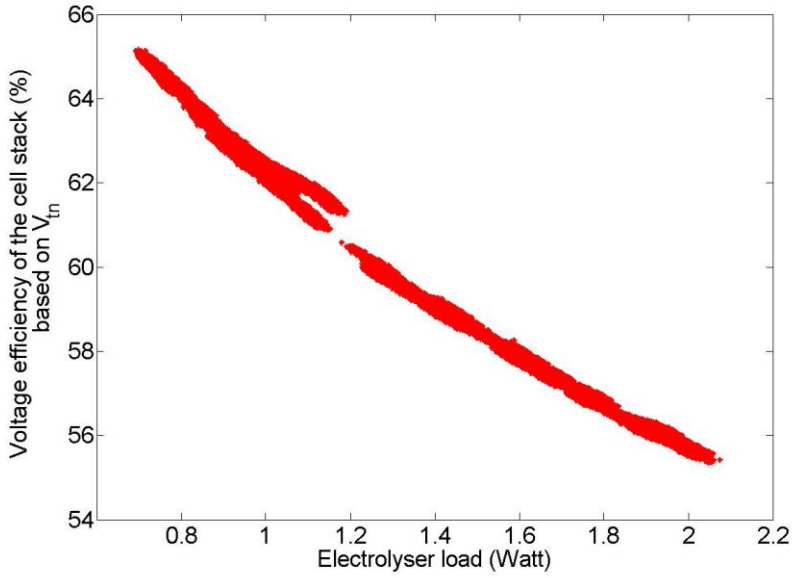

Figure 7.9 The voltage efficiency of the open cell with respect to the electrolyser load during the experiment

REFERENCES

[1] Wilson, I.A.G., McGregor, P.G., and Hall, P.J., Energy storage in the UK electrical network: Estimation of the scale and review of technology options, Energy Policy, Volume 38, Issue 8, August 2010, Pages 4099-4106, ISSN 0301-4215, DOI: http://dx.doi.org/10.1016/j.enpol.2010.03.036.

[2] Holladay, J.D., Hu, J., King, D.L., and Wang, Y., An overview of hydrogen production technologies, Catalysis Today, Volume 139, Issue 4, 30 January 2009, Pages 244-260, ISSN 0920-5861, DOI: http://dx.doi.org/10.1016/j.cattod.2008.08.039.

[3] Schlapbach, L. and Zuttel, A., Hydrogen-storage materials for mobile applications, Nature, Volume 414, Issue 6861, 15 Nov 2001, Pages 353-358, ISSN 0028-0836, DOI: 10.1038/35104634.

[4] Solomon, B.D. and Banerjee, A., A global survey of hydrogen energy research, development and policy, Energy Policy, Volume 34, Issue 7, May 2006, Pages 781-792, ISSN 0301-4215, DOI: http://dx.doi.org/10.1016/j.enpol.2004.08.007.

[5] Mazloomi, K. and Gomes, C., Hydrogen as an energy carrier: Prospects and challenges, Renewable and Sustainable Energy Reviews, Volume 16, Issue 5, June 2012, Pages 3024-3033, ISSN 1364-0321, DOI: http://dx.doi.org/10.1016/j.rser.2012.02.028.

[6] Züttel, A., Remhof, A., Borgschulte, A., and Friedrichs, O., Hydrogen: the future energy carrier, Philosophical transactions of the Royal Society A, Volume 368, Issue 1923, 21 June 2010, Pages 3329-42, DOI: 10.1098/rsta.2010.0113.

[7] World Energy Scenarios: Global Transport Scenarios 2050, World Energy Council, 2011, Available from: http://www.worldenergy.org/publications/2011/global-transport-scenarios-2050/ [Accessed 16/09/2014].

[8] Gandía, L.M., Oroz, R., Ursúa, A., Sanchis, P., and Diéguez, P.M., Renewable Hydrogen Production: Performance of an Alkaline Water Electrolyzer Working under Emulated Wind Conditions, Energy & Fuels, Volume 21, Issue 3, 01 May 2007, Pages 1699-1706, ISSN 0887-0624, DOI: 10.1021/ef060491u.

[9] Turner, J., Sverdrup, G., Mann, M.K., Maness, P.-C., Kroposki, B., Ghirardi, M., Evans, R.J., and Blake, D., Renewable hydrogen production, International Journal of Energy Research, Volume 32, Issue 5, 2008, Pages 379-407, ISSN 1099-114X, DOI: 10.1002/er.1372.

[10] Roy, A., Dynamic and transient modelling of electrolysers powered by renewable energy sources and cost analysis of electrolytic hydrogen, PhD Thesis, Loughborough University, 2006, Available from: https://dspace.lboro.ac.uk/dspace-jspui/handle/2134/10973 [Accessed 25 April 2014].

[11] Korpås, M. and Greiner, C.J., Opportunities for hydrogen production in connection with wind power in weak grids, Renewable Energy, Volume 33, Issue 6, June 2008, Pages 1199-1208, ISSN 0960-1481, DOI: http://dx.doi.org/10.1016/j.renene.2007.06.010.

[12] Ulleberg, Ø., Nakken, T., and Eté, A., The wind/hydrogen demonstration system at Utsira in Norway: Evaluation of system performance using operational data and updated hydrogen energy system modeling tools, International Journal of Hydrogen Energy, Volume 35, Issue 5, March 2010, Pages 1841-1852, ISSN 0360-3199, DOI: http://dx.doi.org/10.1016/j.ijhydene.2009.10.077.

[13] Thomas, C.E., Fuel cell and battery electric vehicles compared, International Journal of Hydrogen Energy, Volume 34, Issue 15, Aug 2009, Pages 6005-6020, ISSN 0360-3199, DOI: http://dx.doi.org/10.1016/j.ijhydene.2009.06.003.

[14] Offer, G.J., Howey, D., Contestabile, M., Clague, R., and Brandon, N.P., Comparative analysis of battery electric, hydrogen fuel cell and hybrid vehicles in a future sustainable road transport system, Energy Policy, Volume 38, Issue 1, Jan

2010, Pages 24-29, ISSN 0301-4215, DOI: http://dx.doi.org/10.1016/j.enpol.2009.08.040.

[15] Hydrogen Filling Stations Worldwide website [Online], Available from: http://www.netinform.net/h2/H2Stations/Default.aspx [Accessed 12 June 2013].

[16] Lantz, E., Wiser, R., and Hand, M., IEA Wind Task 26: The Past and Future Cost of Wind Energy, Work Package 2, The National Renewable Energy Laboratory (NREL) website, 2012, NREL/TP-6A20-53510, Available from: http://www.nrel.gov/docs/fy12osti/53510.pdf [Accessed 16/09/2014].

[17] 2012 UK greenhouse gas emissions, provisional figures and 2011 UK greenhouse gas emissions, final figures by fuel type and end-user, Department of Energy & Climate Change, Available from: https://www.gov.uk/government/uploads/system/uploads/attachment_data/file/175659/ghg_national_statistics_release_2012_provisional.pdf [Accessed 12 June 2013].

[18] Ozaki, M., Tomura, S., Ohmura, R., and Mori, Y.H., Comparative study of large-scale hydrogen storage technologies: Is hydrate-based storage at advantage over existing technologies?, International Journal of Hydrogen Energy, Volume 39, Issue 7, 25 February 2014, Pages 3327-3341, ISSN 0360-3199, DOI: http://dx.doi.org/10.1016/j.ijhydene.2013.12.080.

[19] Mathiesen, B.V. and Lund, H., Comparative analyses of seven technologies to facilitate the integration of fluctuating renewable energy sources, Renewable Power Generation, IET, Volume 3, Issue 2, June 2009, Pages 190-204, ISSN 1752-1416, DOI: 10.1049/iet-rpg:20080049.

[20] The Fuel Cell Technologies Office Multi-Year Research, Development, and Demonstration (MYRD&D) Plan, The US Energy Department website, 2015, Available from: http://energy.gov/eere/fuelcells/downloads/fuel-cell-technologies-office-multi-year-research-development-and-22 [Accessed 20 December 2015].

[21] Ulleberg, Ø., Modeling of advanced alkaline electrolyzers: a system simulation approach, International Journal of Hydrogen Energy, Volume 28, Issue 1, Jan 2003, Pages 21-33, ISSN 0360-3199, DOI: http://dx.doi.org/10.1016/S0360-3199(02)00033-2.

[22] Ursúa, A., Marroyo, L., Gubía, E., Gandía, L.M., Diéguez, P.M., and Sanchis, P., Influence of the power supply on the energy efficiency of an alkaline water electrolyser, International Journal of Hydrogen Energy, Volume 34, Issue 8, May 2009, Pages 3221-3233, ISSN 0360-3199, DOI: http://dx.doi.org/10.1016/j.ijhydene.2009.02.017.

[23] Jones, S., Evans, G., and Galvin, K., Bubble nucleation from gas cavities—a review, Advances in colloid and interface science, Volume 80, Issue 1, 28 Feb 1999, Pages 27-50, ISSN 0001-8686.

[24] Zeng, K. and Zhang, D., Recent progress in alkaline water electrolysis for hydrogen production and applications, Progress in Energy and Combustion Science, Volume 36, Issue 3, June 2010, Pages 307-326, ISSN 0360-1285, DOI: http://dx.doi.org/10.1016/j.pecs.2009.11.002.

[25] Ivy, J., Summary of electrolytic hydrogen production, Milestone Completion Report, National Renewable Energy Laboratory, 2004, NREL/MP-560-36734, Available from: http://www.nrel.gov/hydrogen/pdfs/36734.pdf [Accessed 12 June 2013].

[26] Marshall, A., Børresen, B., Hagen, G., Tsypkin, M., and Tunold, R., Hydrogen production by advanced proton exchange membrane (PEM) water electrolysers—Reduced energy consumption by improved electrocatalysis, Energy, Volume 32, Issue 4, April 2007, Pages 431-436, ISSN 0360-5442, DOI: http://dx.doi.org/10.1016/j.energy.2006.07.014.

[27] Carmo, M., Fritz, D.L., Mergel, J., and Stolten, D., A comprehensive review on PEM water electrolysis, International Journal of Hydrogen Energy, Volume 38, Issue

12, 22 April 2013, Pages 4901-4934, ISSN 0360-3199, DOI: http://dx.doi.org/10.1016/j.ijhydene.2013.01.151.

[28] Vie, P., Ulleberg, Ø., Fell , H., and Rasten, E. Development of a Prototype PEM-electrolyser for distributed renewable energy systems: testing under Emulated wind power conditions, WHEC2008-World Hydrogen Energy Conference, Brisbane, 15–19 June 2008.

[29] Shin, Y., Park, W., Chang, J., and Park, J., Evaluation of the high temperature electrolysis of steam to produce hydrogen, International Journal of Hydrogen Energy, Volume 32, Issue 10–11, July 2007, Pages 1486-1491, ISSN 0360-3199, DOI: http://dx.doi.org/10.1016/j.ijhydene.2006.10.028.

[30] Avālence website [Online], Available from: http://www.avalence.com/products/default.htm#p [Accessed 12 June 2013].

[31] Hydrogenics Company website [Online], Available from: http://www.Hydrogenics.com/ [Accessed 12 June 2013].

[32] NEL Hydrogen company website [Online], Available from: http://www.nel-Hydrogen.com/home/ [Accessed 12 June 2013].

[33] Proton OnSite company website [Online], Available from: http://www.protononsite.com/ [Accessed 12 June 2013].

[34] ITM Power website [Online], Available from: http://www.itm-power.com/ [Accessed 12 June 2013].

[35] Pure Energy Centre website [Online], Available from: http://www.pureenergycentre.com/pureenergycentre/index.php [Accessed 12 June 2013].

[36] AccaGen website [Online], Available from: http://www.accagen.com/products-and-services/products/electrolysers [Accessed 12 June 2013].

[37] ELT Elektrolyse Technik GmbH website [Online], Available from: http://www.elektrolyse.de/vkp/modules.php?name=Content&pa=showpage&pid=5 [Accessed 12 June 2013].

[38] Teledyne Energy Systems website [Online], Available from: http://www.teledynees.com/index.asp [Accessed 12 June 2013].

[39] Onda, K., Kyakuno, T., Hattori, K., and Ito, K., Prediction of production power for high-pressure hydrogen by high-pressure water electrolysis, Journal of Power Sources, Volume 132, Issue 1–2, 20 May 2004, Pages 64-70, ISSN 0378-7753, DOI: http://dx.doi.org/10.1016/j.jpowsour.2004.01.046.

[40] Ibrahim, S. and Cohen, S., Alkaline high pressure electrolysis, DOE hydrogen program review, 2005, Available from: http://www.hydrogen.energy.gov/pdfs/review05/pd26_ibrahim.pdf [Accessed 22/04/2014].

[41] Artuso, P., Gammon, R., Orecchini, F., and Watson, S.J., Alkaline electrolysers: Model and real data analysis, International Journal of Hydrogen Energy, Volume 36, Issue 13, July 2011, Pages 7956-7962, ISSN 0360-3199, DOI: http://dx.doi.org/10.1016/j.ijhydene.2011.01.094.

[42] Lebbal, M.E. and Lecœuche, S., Identification and monitoring of a PEM electrolyser based on dynamical modelling, International Journal of Hydrogen Energy, Volume 34, Issue 14, July 2009, Pages 5992-5999, ISSN 0360-3199, DOI: http://dx.doi.org/10.1016/j.ijhydene.2009.02.003.

[43] Zhou, T. and Francois, B., Modeling and control design of hydrogen production process for an active hydrogen/wind hybrid power system, International Journal of

Hydrogen Energy, Volume 34, Issue 1, Jan 2009, Pages 21-30, ISSN 0360-3199, DOI: http://dx.doi.org/10.1016/j.ijhydene.2008.10.030.

[44] Brossard, L., Bélanger, G., and Trudel, G., Behavior of a 3 kW electrolyser under constant and variable input, International Journal of Hydrogen Energy, Volume 9, Issue 1–2, 1984, Pages 67-72, ISSN 0360-3199, DOI: http://dx.doi.org/10.1016/0360-3199(84)90033-8.

[45] Bergen, A., Pitt, L., Rowe, A., Wild, P., and Djilali, N., Transient electrolyser response in a renewable-regenerative energy system, International Journal of Hydrogen Energy, Volume 34, Issue 1, Jan 2009, Pages 64-70, ISSN 0360-3199, DOI: http://dx.doi.org/10.1016/j.ijhydene.2008.10.007.

[46] Gammon, R., Roy, A., Barton, J., and Little, M., The Hydrogen and Renewable Integration (HARI) Projcct case study report for the International Energy Agency, 2006, Available from: http://www.ieahia.org/page.php?s=d&p=casestudies [Accessed 12 June 2013].

[47] Ete, A., Optimization of the HARI stand-alone energy system with TRNSYS, University of Strathclyde, 2006, Available from: http://www.esru.strath.ac.uk/Documents/MSc_2006/ete.pdf [Accessed 11 September 2014].

[48] Deshmukh, S.S. and Boehm, R.F., Mathematical modelling of performance of a grid connected solar-hydrogen system for residential applications, Journal of Energy and Climate Change, Volume 1, Issue 2, 2006, Pages 113-125.

[49] Kai, T., Uemura, Y., Takanashi, H., Tsutsui, T., Takahashi, T., Matsumoto, Y., Fujie, K., and Suzuki, M., A demonstration project of the hydrogen station located on Yakushima Island—Operation and analysis of the station, International Journal of Hydrogen Energy, Volume 32, Issue 15, Oct 2007, Pages 3519-3525, ISSN 0360-3199, DOI: http://dx.doi.org/10.1016/j.ijhydene.2007.02.015.

[50] Gazey, R., Salman, S.K., and Aklil-D'Halluin, D.D., A field application experience of integrating hydrogen technology with wind power in a remote island location, Journal of Power Sources, Volume 157, Issue 2, 3 July 2006, Pages 841-847, ISSN 0378-7753, DOI: http://dx.doi.org/10.1016/j.jpowsour.2005.11.084.

[51] Dynamic demand, Government Response to Clause 18 of the Climate Change and Sustainable, Energy Act, 2007, Available from: http://webarchive.nationalarchives.gov.uk/+/http://www.berr.gov.uk/files/file41011.pdf [Accessed 04/01/2013].

[52] Hamidi, V., Li, F., and Robinson, F. Responsive demand in networks with high penetration of wind power, Transmission and Distribution Conference and Exposition T&D. IEEE/PES, 21-24 April 2008, Pages 1-7.

[53] Strbac, G., Demand side management: Benefits and challenges, Energy Policy, Volume 36, Issue 12, Dec 2008, Pages 4419-4426, ISSN 0301-4215, DOI: http://dx.doi.org/10.1016/j.enpol.2008.09.030.

[54] Gross, R., Heptonstall, P., Anderson, D., Green, T., Leach, M., and Skea, J., The Costs and Impacts of Intermittency: An Assessment of the Evidence on the Costs and Impacts of Intermittent Generation on the British Electricity Network, UK Energy Research Centre, London, 2006, 22 April, Available from: http://www.uwig.org/0604_Intermittency_report_final.pdf [Accessed 10 December 2015].

[55] Pepermans, G., Driesen, J., Haeseldonckx, D., Belmans, R., and D'haeseleer, W., Distributed generation: definition, benefits and issues, Energy Policy, Volume 33, Issue 6, 4// 2005, Pages 787-798, ISSN 0301-4215, DOI: http://dx.doi.org/10.1016/j.enpol.2003.10.004.

[56] Strbac G., Ramsay S., and D., P., Integration of Distributed Generation into the UK Power System, 2007, Available from:

http://www.sedg.ac.uk/Publication/DGSEE%20Integration%20of%20DG%20Mar2007.pdf [Accessed 10 December 2015].

[57] Méndez, V.H., Rivier, J., Fuente, J.I.d.l., Gómez, T., Arceluz, J., Marín, J., and Madurga, A., Impact of distributed generation on distribution investment deferral, International Journal of Electrical Power & Energy Systems, Volume 28, Issue 4, May 2006, Pages 244-252, ISSN 0142-0615, DOI: http://dx.doi.org/10.1016/j.ijepes.2005.11.016.

[58] Lopes, J.A.P., Hatziargyriou, N., Mutale, J., Djapic, P., and Jenkins, N., Integrating distributed generation into electric power systems: A review of drivers, challenges and opportunities, Electric Power Systems Research, Volume 77, Issue 9, July 2007, Pages 1189-1203, ISSN 0378-7796, DOI: http://dx.doi.org/10.1016/j.epsr.2006.08.016.

[59] Liew, S.N. and Strbac, G., Maximising penetration of wind generation in existing distribution networks, Generation, Transmission and Distribution, IEE Proceedings-, Volume 149, Issue 3, May 2002, Pages 256-262, ISSN 1350-2360, DOI: 10.1049/ip-gtd:20020218.

[60] Atwa, Y.M. and El-Saadany, E.F., Optimal Allocation of ESS in Distribution Systems With a High Penetration of Wind Energy, Power Systems, IEEE Transactions on, Volume 25, Issue 4, November 2010, Pages 1815-1822, ISSN 0885-8950, DOI: 10.1109/TPWRS.2010.2045663.

[61] Zhao, H., Wu, Q., Hu, S., Xu, H., and Rasmussen, C.N., Review of energy storage system for wind power integration support, Applied Energy, Volume 137, January 2015, Pages 545-553, ISSN 0306-2619, DOI: http://dx.doi.org/10.1016/j.apenergy.2014.04.103.

[62] Barton, J.P. and Infield, D.G., Energy storage and its use with intermittent renewable energy, IEEE Transactions on Energy Conversion, Volume 19, Issue 2, 2004, Pages 441-448, ISSN 0885-8969, DOI: 10.1109/TEC.2003.822305.

[63] Ferreira, H.L., Garde, R., Fulli, G., Kling, W., and Lopes, J.P., Characterisation of electrical energy storage technologies, Energy, Volume 53, May 2013, Pages 288-298, ISSN 0360-5442, DOI: http://dx.doi.org/10.1016/j.energy.2013.02.037.

[64] Carpinelli, G., Celli, G., Mocci, S., Mottola, F., Pilo, F., and Proto, D., Optimal Integration of Distributed Energy Storage Devices in Smart Grids, Smart Grid, IEEE Transactions on, Volume 4, Issue 2, June 2013, Pages 985-995, ISSN 1949-3053, DOI: 10.1109/TSG.2012.2231100.

[65] National grid website [Online], Available from: http://www.nationalgrid.com/uk/Electricity/Balancing/services/ [Accessed 12 June 2013].

[66] Wilson, I.A.G., McGregor, P.G., Infield, D.G., and Hall, P.J., Grid-connected renewables, storage and the UK electricity market, Renewable Energy, Volume 36, Issue 8, Aug 2011, Pages 2166-2170, ISSN 0960-1481, DOI: http://dx.doi.org/10.1016/j.renene.2011.01.007.

[67] Gutiérrez-Martín, F., Confente, D., and Guerra, I., Management of variable electricity loads in wind – Hydrogen systems: The case of a Spanish wind farm, International Journal of Hydrogen Energy, Volume 35, Issue 14, July 2010, Pages 7329-7336, ISSN 0360-3199, DOI: http://dx.doi.org/10.1016/j.ijhydene.2010.04.181.

[68] Celli, G., Mocci, S., Pilo, F., and Loddo, M. Optimal integration of energy storage in distribution networks, PowerTech, 2009 IEEE Bucharest, June 28 2009-July 2 2009, Pages 1-7.

[69] Carpinelli, G., Mottola, F., Proto, D., and Russo, A. Optimal allocation of dispersed generators, capacitors and distributed energy storage systems in distribution networks, Modern Electric Power Systems (MEPS), 2010 Proceedings of the International Symposium, 20-22 Sept. 2010, Pages 1-6.

[70] Nick, M., Cherkaoui, R., and Paolone, M., Optimal siting and sizing of distributed energy storage systems via alternating direction method of multipliers, International Journal of Electrical Power & Energy Systems, Volume 72, November 2015, Pages 33-39, ISSN 0142-0615, DOI: http://dx.doi.org/10.1016/j.ijepes.2015.02.008.

[71] Yu, Z., Zhao Yang, D., Feng Ji, L., Ke, M., Jing, Q., and Kit Po, W., Optimal Allocation of Energy Storage System for Risk Mitigation of DISCOs With High Renewable Penetrations, Power Systems, IEEE Transactions on, Volume 29, Issue 1, 2014, Pages 212-220, ISSN 0885-8950, DOI: 10.1109/TPWRS.2013.2278850.

[72] Nick, M., Hohmann, M., Cherkaoui, R., and Paolone, M. Optimal location and sizing of distributed storage systems in active distribution networks, PowerTech (POWERTECH), 2013 IEEE Grenoble, 16-20 June 2013, Pages 1-6.

[73] Bamane, P.D., Kshirsagar, A.N., Raj, S., and Jadhav, H. Temperature dependent Optimal Power Flow using gbest-guided artificial bee colony algorithm, Computation of Power, Energy, Information and Communication (ICCPEIC), 2014 International Conference on, 16-17 April 2014, Pages 321-327.

[74] Zimmerman, R.D., Murillo-Sanchez, C.E., and Thomas, R.J. MATPOWER's extensible optimal power flow architecture, Power & Energy Society General Meeting, 2009. PES '09. IEEE, 26-30 July 2009, Pages 1-7.

[75] Lakervi, E. and Holmes, E.J. (2003) Electricity Distribution Network Design. Place Published, Institution of Engineering and Technology.

[76] Government GHG Conversion Factors for Company Reporting: Methodology Paper for Emission Factors, UK government website, 2013, Available from: https://www.gov.uk/government/uploads/system/uploads/attachment_data/file/224437/pb13988-emission-factor-methodology-130719.pdf [Accessed 4th September 2014].

[77] Kothari, R., Buddhi, D., and Sawhney, R.L., Comparison of environmental and economic aspects of various hydrogen production methods, Renewable and Sustainable Energy Reviews, Volume 12, Issue 2, February 2008, Pages 553-563, ISSN 1364-0321, DOI: http://dx.doi.org/10.1016/j.rser.2006.07.012.

[78] Elbaset, A. and Abdalla, O. Modelling and Control of a Wind Farm and Electrolyser System Connected to an Electrical Grid, The International Engineering Conference on Hot Arid Regions (IECHAR 2010), King Faisal University, KSA, 1-2 May 2010, Pages 71-77.

[79] Barton, J. and Gammon, R., The production of hydrogen fuel from renewable sources and its role in grid operations, Journal of Power Sources, Volume 195, Issue 24, December 2010, Pages 8222-8235, ISSN 0378-7753, DOI: http://dx.doi.org/10.1016/j.jpowsour.2009.12.100.

[80] Short, J.A., Infield, D.G., and Freris, L.L., Stabilization of Grid Frequency Through Dynamic Demand Control, IEEE Transactions on Power Systems, Volume 22, Issue 3, 2007, Pages 1284-1293, ISSN 0885-8950, DOI: 10.1109/TPWRS.2007.901489.

[81] Hydrogenics news release. (2011) Hydrogenics Successfully Completes Utility-Scale Grid Stabilization Trial with Ontario's Independent Electricity System Operator [Online], Hydrogenics website, Available from: http://www.hydrogenics.com/about-the-company/news-updates/2011/06/16/hydrogenics-successfully-completes-utility-scale-grid-stabilization-trial-with-ontario's-independent-electricity-system-operator [Accessed 11 August 2011].

[82] Vachirasricirikul, S., Ngamroo, I., and Kaitwanidvilai, S., Application of electrolyzer system to enhance frequency stabilization effect of microturbine in a microgrid system, International Journal of Hydrogen Energy, Volume 34, Issue 17, Sept 2009, Pages 7131-7142, ISSN 0360-3199, DOI: http://dx.doi.org/10.1016/j.ijhydene.2009.06.050.

[83] Li, X., Song, Y.-J., and Han, S.-B., Frequency control in micro-grid power system combined with electrolyzer system and fuzzy PI controller, Journal of Power Sources, Volume 180, Issue 1, 15 May 2008, Pages 468-475, ISSN 0378-7753, DOI: http://dx.doi.org/10.1016/j.jpowsour.2008.01.092.

[84] Miland, H., Glöckner, R., Taylor, P., Jarle Aaberg, R., and Hagen, G., Load control of a wind-hydrogen stand-alone power system, International Journal of Hydrogen Energy, Volume 31, Issue 9, Aug 2006, Pages 1215-1235, ISSN 0360-3199, DOI: http://dx.doi.org/10.1016/j.ijhydene.2005.09.005.

[85] NEL Hydrogen company website [Online], Available from: http://www.nel-Hydrogen.com/home/?pid=76 [Accessed 12 June 2013].

[86] Engineering Recommendation G5/4: Planning Levels for Harmonic Voltage Distortion and the Connection of Non-Linear Equipment to Transmission and Distribution Networks Energy Networks Association, 2001.

[87] Fell, H.J., Chladek, P., Wallevik, O., and Briskeby, S.T. Flexible Production of hydrogen from Sun and Wind: Challenges and Experiences, Proceedings of the 18th World Hydrogen Energy Conference (WHEC 2010), Essen, 16-21 May 2010, Pages 112-8.

[88] IHT Company website [Online], Available from: http://www.iht.ch/ [Accessed 12 June 2013].

[89] Rashid, M.H. (2004) Power Electronics Circuits, Devices, and Applications. Third Edition, Place Published, Pearson Prentice Hall, ISBN 978-0-12-382036-5.

[90] Electromagnetic compatibility (EMC) Part 3-2: Limits for harmonic current emissions, Standard IEC, The International Electrotechnical Commission (IEC), 2005.

[91] Foote, C., Djapic, P., Ault, G., Mutale, J., and Strbac, G., United Kingdom Generic Distribution System (UKGDS), Defining the Generic Networks, DTI Centre for Distributed Generation and Sustainable Electrical Energy, 2005, Available from: http://www.sedg.ac.uk/ [Accessed 14th December 2010].

[92] Metered half-hourly electricity demands [Online], National grid website, Available from: http://www.nationalgrid.com/uk/Electricity/Data/Demand+Data/ [Accessed 14 October 2015].

[93] Hill, D.C., McMillan, D., Bell, K.R.W., and Infield, D., Application of Auto-Regressive Models to U.K. Wind Speed Data for Power System Impact Studies, IEEE Transactions on Sustainable Energy, Volume 3, Issue 1, Jan 2012, Pages 134-141, ISSN 1949-3029, DOI: 10.1109/TSTE.2011.2163324.

[94] REpower Systems website [Online], Available from: http://www.repower.de/en/ [Accessed 12 June 2013].

[95] Historic System Prices [Online], The Balancing Mechanism Reporting System (BMRS) website, Available from: http://www.bmreports.com/bsp/SystemPricesHistoric.htm [Accessed 9 September 2014].

[96] Chunshu Rectifier Co. website [Online], Available from: http://chunshu.en.alibaba.com/productgrouplist-212892773/IGBT_switch_mode_rectifier.html [Accessed 12 June 2013].

[97] Alarcon-Rodriguez, A.D., A Multi-objective Planning Framework for Analysing the Integration of Distributed Energy Resources, Department of Electronic and Electrical Engineering, University of Strathclyde, 2009, Available from: [Accessed 6 October 2015].

[98] ITM power website [Online], ITM power website, Available from: http://www.itm-power.com/news-item/hydrogen-cost-structure-update [Accessed 6 October 2015].

[99] Kundur, P. (1993) Power System Stability and Control. Place Published, McGraw-Hill, ISBN 9780070359581, Pages 581–592.

[100] Grid Code, Frequency and Voltage Operating Range Working Group, National Grid website, 2010, Available from: http://www.nationalgrid.com/NR/rdonlyres/79DB4BE7-714C-490D-AF4E-1F21A9F795BA/39960/FreqVoltOprange_final29Jan10.pdf [Accessed 17/12/2012].

[101] Report of the investigation into the automatic demand disconnection following multiple generation losses and the demand control response that occurred on the 27 May 2008 National Grid website, 2008, Available from: http://www.nationalgrid.com/NR/rdonlyres/D680C70A-F73D-4484-BA54-95656534B52D/26917/PublicReportIssue1.pdf [Accessed 29 November 2010].

[102] The grid code, National grid website, 2013, Available from: http://www.nationalgrid.com/uk/Electricity/Codes/gridcode/gridcodedocs/ [Accessed August 2013].

[103] Wu, L. and Infield, D.G., Towards an Assessment of Power System Frequency Support From Wind Plant-Modeling Aggregate Inertial Response, IEEE Transactions on Power Systems, Volume 28, Issue 3, Aug 2013, Pages 2283-2291, ISSN 0885-8950, DOI: 10.1109/TPWRS.2012.2236365.

[104] Wu, L. and Infield, D. Assessing Emulated Inertial Response from Wind Generation in the GB Power System, Scientific Proceedings at European Wind Energy Association Annual Conference (EWEA 2013), Vienna, Austria 6th -8th Feb. 2013.

[105] UK Wind Energy Database (UKWED) [Online], RenewableUK website, Available from: http://www.renewableuk.com/en/renewable-energy/wind-energy/uk-wind-energy-database/index.cfm [Accessed 2 December 2015].

[106] Electricity Market Reform Delivery Plan, UK government website, 2013, Available from: https://www.gov.uk/government/uploads/system/uploads/attachment_data/file/268221/181213_2013_EMR_Delivery_Plan_FINAL.pdf [Accessed 5th Sept 014].

[107] Monthly Balancing Services Summary, March 2012 [Online], National Grid website, Available from: http://www.nationalgrid.com/uk/Electricity/Balancing/Summary/ [Accessed 14 June 2012].

[108] Wildash, D., Future System Requirements, UK National Grid website, 2012, Available from: http://occ.awlonline.com/bookbind/pubbooks/marieb-essentials/ [Accessed 14th June 2012].

[109] Frequency Response: UK National Grid website [Online], Available from: http://www.nationalgrid.com/uk/Electricity/Balancing/services/frequencyresponse/ [Accessed 14th June 2012].

[110] Weckx, S., D'Hulst, R., and Driesen, J., Primary and Secondary Frequency Support by a Multi-Agent Demand Control System, Power Systems, IEEE Transactions on, Volume 30, Issue 3, 2015, Pages 1394-1404, ISSN 0885-8950, DOI: 10.1109/TPWRS.2014.2340582.

[111] 2050 Pathways Analysis, Department of Energy and Climate Change (DECC) Web Site, 2010, Available from: http://www.decc.gov.uk/assets/decc/what%20we%20do/a%20low%20carbon%20uk/2050/216-2050-pathways-analysis-report.pdf [Accessed 14th June 2012].

[112] Kabouris, J. and Kanellos, F.D., Impacts of Large-Scale Wind Penetration on Designing and Operation of Electric Power Systems, IEEE Transactions on Sustainable Energy, Volume 1, Issue 2, 2010, Pages 107-114, ISSN 1949-3029, DOI: 10.1109/TSTE.2010.2050348.

[113] Post Assessment Tender Report September 2015, Services Reports, National grid website, 2015, Available from: http://www2.nationalgrid.com/UK/Industry-information/Electricity-transmission-operational-data/Report-explorer/Services-Reports/ [Accessed 5 November 2015].

[114] UK Petroleum Industry Association Website [Online], Available from: http://www.ukpia.com/industry_information/industry-overview.aspx [Accessed 4 Feb 2013].

[115] Helmolt, R.V. and Eberle, U., Fuel cell vehicles: Status 2007, Journal of Power Sources, Volume 165, Issue 2, 20 Mar 2007, Pages 833-843, ISSN 0378-7753, DOI: http://dx.doi.org/10.1016/j.jpowsour.2006.12.073.

[116] Kraushaar, J.J. and Ristinen, R.A. (2006) Energy and the Environment. Second Edition, Place Published, John Wiley & Sons, Inc., ISBN 978-0471739890.

[117] Weinert, J.X., A Near-Term Economic Analysis of Hydrogen Fueling Stations, Master's thesis, University of California, Davis, 2005, Reference Number: UCD-ITS-RR-05-04, Available from: http://its.ucdavis.edu/research/publications/publication-detail/?pub_id=46 [Accessed 25 April 2014].

[118] Fuel properties comparison [Online], US department of energy website, Available from: http://www.afdc.energy.gov/fuels/fuel_comparison_chart.pdf [Accessed 7 August 2015].

[119] Harrison, K., Martin, G., Ramsden, T., and Saur, G., Renewable electrolysis integrated system development and testing, 2009, Available from:

http://Hydrogen.energy.gov/pdfs/review09/pdp_17_harrison.pdf [Accessed 12 June 2013].

[120] Energy Trends: special feature article - Electricity generation and supply figures for Scotland, Wales, Northern Ireland and England, 2009 to 2012, 2013, Available from: https://www.gov.uk/government/organisations/department-of-energy-climate-change/series/electricity-statistics [Accessed 4th February 2013].

[121] World Total electricity installed Capacity [Online], The U.S. Energy Information Administration (EIA) website, Available from: http://www.eia.doe.gov/emeu/international/electricitycapacity.html [Accessed 4 February 2013].

[122] National Electricity Transmission System Seven Year Statement, National Grid website, 2011, Available from: http://www.nationalgrid.com/NR/rdonlyres/4AB92B80-499A-4D3A-84E4-BBE884CBBA55/49900/NETSSYS2011.pdf [Accessed 13 June 2013].

[123] Wu, L. and Infield, D. Delivering Combined Droop and Inertial Response from Wind Plant to the GB Power System, The 11th International Workshop on Large-Scale Integration of Wind Power into Power Systems as well as on Transmission Networks for Offshore Wind Power Plants, Lisbon, Portugal, 13th -15th Nov., 2012.

[124] RenewableUK website [Online], Available from: http://www.renewableuk.com/ [Accessed 13 June 2013].

[125] Microgen Database [Online], Sheffield Solar, University of Sheffield, Available from: http://www.solar.sheffield.ac.uk/panel-data/ [Accessed 13 August 2015].

[126] Economy 7 Tariffs explained [Online], Simply switch website, Available from: https://www.simplyswitch.com/energy/guides/what-is-an-economy-7-tariff/ [Accessed 20 October 2015].

[127] Polman, E.A., Laat, J.C.d., and Crowther, M., Reduction of CO2 emissions by adding hydrogen to natural gas, Apeldoorn, 2003, Available from: http://www.ieaghg.org/docs/General_Docs/Reports/Ph4-24%20Hydrogen%20in%20nat%20gas.pdf [Accessed 29 October 2015].

[128] Schmid, R., Electrolysis for grid balancing: Where are we?, Copenhagen, 2012, Available from: http://www.hydrogennet.dk/fileadmin/user_upload/PDF-filer/Aktiviteter/Kommende_aktiviteter/Elektrolysesymposium/Raymond_Schmid_Hygrogenics_120510_Copenhagen_Symposium_Final.pdf [Accessed 14 June 2012].

[129] Half-yearly electricity and gas prices, first half of year, 2011–13 [Online], Eurostat website, Available from: http://epp.eurostat.ec.europa.eu/statistics_explained/index.php/File:Half-yearly_electricity_and_gas_prices,_first_half_of_year,_2011%E2%80%9313_(EUR_per_kWh)_YB14.png [Accessed 9 September 2014].